Functional Characterisation of a *RECQL4* Mutation in Rothmund-Thomson Syndrome

Tianyi Wu

St. Catharine's College

University of Cambridge

May 2020

This dissertation is submitted for the degree of Doctor of Philosophy

Declaration

This thesis is the result of my own work and includes nothing which is the outcome of work done in collaboration except as declared in the preface and specified in the text.

It is not substantially the same as any that I have submitted or is being concurrently submitted for a degree, diploma, or other qualification at the University of Cambridge, any other university, or similar institution. I further state that no substantial part of my dissertation has already been submitted or is being concurrently submitted for any such degree, diploma, or other qualification at the University of Cambridge, any other university, or similar institution.

I further confirm that this dissertation does not exceed the limit of 60,000 words excluding figures, tables, legends, appendices, and references as set by the Degree Committee for Clinical Medicine and Clinical Veterinary Medicine.

Tianyi Wu

May 2020

Abstract

Functional Characterisation of a *RECQL4* Mutation in Rothmund-Thomson Syndrome

Tianyi Wu

Germline mutations affecting the RECQL4 DNA helicase cause Type II Rothmund-Thomson syndrome (RTS), a human disease characterised by defects in skeletal development and predisposition to specific types of cancer, including osteosarcoma (OS). RECQL4 has been implicated in multiple cellular functions that mediate accurate DNA replication and repair. How germline *RECQL4* mutations associated with Type II RTS affect these functions to cause disease remains unclear, in part due to the paucity of appropriate cellular models.

In this work, CRISPR/Cas9 gene editing was used to generate cell lines containing a prevalent RTS patient *RECQL4* mutation, the "Mut-2" c.2269C>T. The resulting Mut-2 clones exhibited greatly reduced RECQL4 protein levels, similar to decreases observed in RTS patient cells. Unexpectedly, the major effect of this predicted nonsense mutation was the upregulation of the use of an alternative splice site in exon 14 which skipped the premature stop codon and resulted in the deletion of 66 amino acids in the RECQL4 ATPase domain.

Despite the lower overall RECQL4 expression, single cell clones bearing the Mut-2 mutation showed mostly normal cell cycle distribution with a slight increase in population doubling times. When challenged with various DNA damaging agents, these Mut-2 clones exhibited increased sensitivities to DNA alkylators and topoisomerase inhibitors, and mild sensitivities to DNA crosslinkers and PARP inhibitors, a sensitivity profile suggestive of defects in DNA double-strand break (DSB) repair.

When further assayed using flow cytometric GFP reporters, the Mut-2 clones showed decreased DNA DSB repair capacities in the homologous recombination (HR) and microhomology mediated end joining (MMEJ) pathways, providing evidence that *RECQL4* disruption impacted replication-specific DNA DSB repair in particular. Additional RECQL4 reconstitution studies confirmed that the decreased HR repair was a result of structural changes to RECQL4 due to the Mut-2 mutation.

Finally, the formation of RAD51 foci—a commonly used marker of HR function—in the Mut-2 clones post-DNA DSB induction was investigated. Surprisingly, upon DNA DSB challenge, all Mut-2 clones were as proficient at forming RAD51 foci as parental HEK293. This suggested that the *RECQL4* Mut-2 mutation disrupted its function further downstream in the HR pathway than had been previously reported.

The work presented in this dissertation is a novel approach to studying the effects of clinical RTS *RECQL4* mutations. These studies have illuminated mechanisms of RECQL4 disruption in Type II RTS as well as the roles of the RECQL4 helicase in cellular DNA damage repair. Because about 30% of Type II RTS patients are diagnosed with osteosarcoma, a common and deadly primary malignancy of the bone, the results presented here could shed new light on potential mechanisms underlying osteosarcoma tumour development and ultimately suggest new avenues and strategies for targeted clinical intervention.

To mom and dad, with all my love and gratitude

Acknowledgements

I want to thank my supervisors, Dr. Paul Meltzer and Prof. Ashok Venkitaraman, for all their guidance, encouragement, patience, optimism, and faith in me. I truly appreciate the lengths to which you have gone to bat and came through for me time and time again.

Many thanks go to the UT Southwestern MSTP and the medical school administration as well as the NIH OxCam program for putting up with me and for being infinitely patient and understanding.

To members of the Venkitaraman Lab, especially MiYoung, Stephanie, and Stela, thank you for a wonderful sojourn in Cambridge and for everything you did to make me feel at ease far away from home.

A big shout out to the members of the Meltzer Lab, past and present, for all the help you have given me and for accepting me into the lab family. Nancy and John, without you two, I wouldn't have gotten nearly as far as I have. Marbin, Dave, Sanjit, Nancy Lee, Keith, Konrad, Sven, Katie, and Josh, you have all played a part in getting me to this point and I am glad to call you all my friends.

Thanks, in particular, go to Jack Zhu and Yonghong Wang, who were invaluable in helping me analyse my sequencing data. I know I am a demanding customer, thanks for putting up with my often urgent requests and questions.

A huge debt of gratitude is owed to Bob Walker. Thank you so much for all those library captures you did for me and for always being willing to listen to my ideas and helping me troubleshoot problems. Truly, without you, this project would not have been possible.

To my Cambridge friends, JJ, Frances, JMak, Dylan, Babak, Katie, Sebastian, Ray, Danilo, and Yasu, you made my stay in Cambridge unforgettable and I look forward to seeing you all again, wherever we end up.

To Sarah Clatterbuck Soper (and Toby, Nate, Cordelia, Liam, Arlo, Chase, Waffles, and Schuyler) and Ryan Young (and Emily, Kit, Harry, Komet, and Haley), what can I say? Words cannot describe how beyond grateful I am to you both that you have essentially adopted me into your families. You have been there with me through milestones and birthdays, failures and triumphs, the sunny days and the rainy days. Without you, there would have been no this, it is as simple as that.

Finally, to my family, Mom and Dad. You have been there from the very beginning and you have walked with me every step of the way from there to here. The biggest thank you I can give is to you for your unwavering support, your listening ears, your helping hands, and your loving hearts. Thank you for literally everything that I have and that I am. This work is dedicated to you.

Table of Contents

Declaration ii

Abstract iii

Acknowledgements vi

List of Figures xii

List of Tables xiii

List of Abbreviations xiv

Chapter 1 Introduction 1

1.1 Overview of RecQ family helicases and RECQL4 1

1.2 RECQL4 structure and function – N-terminal region 3

1.3 RECQL4 C-terminal region – is it a helicase? 6

1.3.1 Unwinding the mystery of RECQL4's missing helicase activity 7

1.3.2 Recent insights into RECQL4 C-terminal structure and helicase mechanism 9

1.4 RECQL4 in DNA Damage Repair 12

1.4.1 RECQL4 in ssDNA damage repair 15

1.4.1a Nucleotide Excision Repair (NER) 15

1.4.1b Base Excision Repair (BER) 16

1.4.2 RECQL4 in double-strand break repair 17

1.4.2a Non-homologous End Joining (NHEJ) 18

1.4.2b Homologous Recombination (HR) 19

1.4.2c Microhomology-mediated End Joining (MMEJ) 21

1.4.3 RECQL4, replication, and DNA damage repair 22

1.5 RECQL4 in human disease 23

1.5.1 RAPADILINO Syndrome 23

1.5.2 Baller-Gerold Syndrome 24

1.5.3 Overview of Rothmund-Thomson Syndrome 24

1.5.4 *RECQL4* mutations in Type II RTS 25

1.5.4a *RECQL4* c.1573delT 26

1.5.4b *RECQL4* c.2269C>T 26

1.6 Modelling *RECQL4* Disruption 29

1.6.1 *Recql4* mouse models 29
1.6.2 *RECQL4* cell line models 31
1.7 Specific Aims 32
Chapter 2 Cell Line Model Generation 34
2.1 Introduction 34
2.2 Materials and Methods 37
2.2.1 Cell Culture 37
2.2.2 CRISPR/Cas9 Editing of *RECQL4* 37
2.2.3 Sanger Sequencing 39
2.2.4 Western Blot 40
2.2.4a Lysate Sample Preparation 40
2.2.4b SDS-PAGE 40
2.2.4c Immunoblotting 40
2.2.5 RNAi Knockdown 42
2.2.6 Quantitative RT-PCR (RT-qPCR) 43
2.2.7 Enrichment of Sequencing Libraries with Custom *RECQL4* Baits 46
2.2.8 Next generation DNA-Seq and RNA-Seq analysis 47
2.2.8a DNA sequencing 47
2.2.8b RNA sequencing 48
2.3 Results 51
2.3.1 CRISPR/Cas9 editing of *RECQL4* in HEK293 51
2.3.2 Sanger sequencing identifies potential candidates 51
2.3.3 RECQL4 protein levels in candidate Mut-2 clones 53
2.3.4 Residual RECQL4 band is an alternative splicing variant 58
2.3.5 Next generation sequencing reveals the state of the *RECQL4* locus in candidate clones 63
2.4 Discussion 73
2.4.1 Mut-2 clones are hemizygous for *RECQL4* mutation 73
2.4.2 RECQL4 expression is drastically altered in Mut-2 clones 76
2.4.3 Mut-2 RECQL4 truncation is a minor protein product 77
2.4.4 Mut-2 upregulates alternative splicing of RECQL4 78
2.4.5 Mut-2 clones are viable models for functional studies of Mut-2 83

Chapter 3 Mut-2 Clones – Functional Characterisation 84
3.1 Introduction 84
3.1.1 DNA damaging agents 85
3.1.1a Replication stress inducers 85
3.1.1b Radiomimetics 86
3.1.1c DNA alkylators 87
3.1.1d DNA crosslinkers 89
3.1.1e Topoisomerase inhibitors 91
3.1.1f PARP inhibitors 92
3.1.2 Genetic reporters of DNA DSB repair pathways 96
3.1.3 Summary of findings 97
3.2 Materials and Methods 99
3.2.1 Cell Culture 99
3.2.2 Cell Cycle Staining 99
3.2.3 DNA Damage Repair GFP Reporter Assays 99
3.2.4 Etoposide Recovery Assay and p-Histone H3 staining 101
3.2.5 Immunofluorescence Staining 101
3.2.6 Incucyte Proliferation Assay 102
3.2.7 Lentivirus Production and Transduction 104
3.2.8 Plasmid Construction 105
3.2.9 Quantitative RT-PCR 106
3.2.10 RNAi Knockdown 106
3.2.11 Western Blot 106
3.3 Results 107
3.3.1 *RECQL4* Mut-2 mutation has a minor effect on growth characteristics in clones 107
3.3.2 Mut-2 clones showed increased sensitivity to certain classes of DNA damaging agents 107
3.3.3 Effects of etoposide in Mut-2 clones 119
3.3.4 Mut-2 clones showed defects in HR and MMEJ DNA DSB repair 123
3.3.5 The effects of RECQL4 overexpression on drug sensitivity in Mut-2 clones 126

3.3.6 Effects of RECQL4 overexpression on DNA DSB repair pathway function in Mut-2 clones 138
3.3.7 Mut-2 clones do not show defective RAD51 foci formation 139
3.4 Discussion 145
3.4.1 *RECQL4* Mut-2 mutation and cell proliferation characteristics 145
3.4.2 Sensitivity profile of Mut-2 clones to DNA damaging compounds pointed to DNA DSB repair defect 146
3.4.3 Etoposide treatment pointed to compromised replication-associated DNA DSB repair in Mut-2 clones 148
3.4.4 Mut-2 clones showed decreased DNA DSB repair by HR and MMEJ but not NHEJ 149
3.4.5 Reconstitution of RECQL4 expression in Mut-2 clones 150
3.4.6 Mut-2 clones did not exhibit impaired RAD51 foci formation 152
3.4.7 Final summary 153
Chapter 4 Final Discussion 154
4.1 Mut-2 clones are novel models for *RECQL4* Mut-2 mutation 154
4.2 Functional characterisation of Mut-2 clones 156
4.2.1 Mut-2 clones exhibited surprisingly normal growth phenotypes 156
4.2.2 Drug sensitivity profile of Mut-2 clones uncovered replication-specific DNA DSB repair defect 156
4.3 Limitations of the Mut-2 clones as models of RTS 158
4.4 Future directions 159
References 163

List of Figures

Figure 1.1 Comparison of RecQ family helicases 2

Figure 1.2 RECQL4 C-terminal domains 10

Figure 1.3 The role of RECQL4 in DNA damage repair 14

Figure 1.4 *RECQL4* mutations reported in Type II RTS patients 28

Figure 2.1 Next generation sequencing data analysis pipelines 50

Figure 2.2 Sanger Sequencing of isolated single cell clones 52

Figure 2.3 Western blot analyses of candidate *RECQL4* Mut-2 clones 57

Figure 2.4 The alternative splicing of the *RECQL4* exon 14-15 junction 62

Figure 2.5 Genomic structure of candidate clone 2.11 at the *RECQL4* Mut-2 target site 66

Figure 2.6 Genomic structure of candidate clone 2.14 at the *RECQL4* Mut-2 target site 68

Figure 2.7 Genomic structure of candidate clone 2.16 at the *RECQL4* Mut-2 target site 69

Figure 2.8 Genomic structure of candidate clone 2.88 at the *RECQL4* Mut-2 target site 71

Figure 2.9 Predicted structural effects of RECQL4 exon 14-15 alternative splicing 82

Figure 3.1 Chemical structures of DNA damaging agents 95

Figure 3.2 Plasmid constructs for GFP reporter assays 98

Figure 3.3 Growth characteristics of Mut-2 clones 110

Figure 3.4 Sensitivities of Mut-2 clones to various DNA damaging compounds 117

Figure 3.5 The effects of etoposide on the Mut-2 clones 120

Figure 3.6 Etoposide treatment and recovery in Mut-2 clones 122

Figure 3.7 DNA DSB repair pathway function in Mut-2 clones 125

Figure 3.8 Effects of RECQL4 overexpression on sensitivities to select compounds in Mut-2 clones 136

Figure 3.9 Effects of RECQL4 overexpression on DNA DSB repair capacity in Mut-2 clones 142

Figure 3.10 RAD51 foci formation in Mut-2 clones 144

List of Tables

Table 2.1 Western blot primary and secondary antibodies and their dilutions 41

Table 2.2 RECQL4 antibodies tested by western blot and dilutions used 42

Table 2.3 siRNA sequences and target regions 43

Table 2.4 TaqMan assay information 45

Table 2.5 RTS patient sample information..... 54

Table 3.1 DNA damaging compounds tested and stock concentrations used 104

Table 3.2 Sensitivities of the Mut-2 clones to different classes of DNA damaging agents.147

List of Abbreviations

4NQO	4-nitroquinoline 1-oxide
aa	Amino acid
alt-NHEJ	Alternative nonhomologous end joining
ANNOVAR	Annotate variation
AP site	Apurinic/apyrimidinic (abasic) site
APC/C	Anaphase-promoting complex/cyclosome
APH	Aphidicolin
ATCC	American Type Culture Collection
ATP	Adenosine triphosphate
BAC	Bacterial artificial chromosome
BCA	Bicinchoninic acid assay
BER	Base excision repair
BGS	Baller-Gerold Syndrome
BLM	Bleomycin or Bloom Syndrome helicase
Bps	Base pairs
BRASS	BReakpoint AnalySiS
BSA	Bovine serum albumin
BUS	Busulfan
BWA	Burrows-Wheeler Aligner
c-NHEJ	Canonical nonhomologous end joining
C-terminal	Carboxyl terminal
CβApr	Chicken beta actin promoter
CDDP	Cisplatin
CMVpr	Cytomegalovirus promoter
CP	Cyclophosphamide
CPT	Camptothecin
CRISPR	Clustered regularly interspaced short palindromic repeats
CTD	Carboxyl terminal domain
CTP	Cytidine triphosphate
D-loop	Displacement loop
DAPI	4’,6-diamidino-2-phenylindole
dbNSFP	Database of human Nonsynonymous Single nucleotide variations and their Functional Predictions and annotations
dbSNP	Single Nucleotide Polymorphism Database
DMEM	Dulbecco’s modified Eagle’s medium
DMSO	Dimethyl sulfoxide
DNA	Deoxyribonucleic acid
DNase	Deoxyribonuclease
dNTP	Deoxyribonucleoside triphosphate
DPBS	Dulbecco’s phosphate buffered saline
DSB	[DNA] Double-strand break
dsDNA	Double-stranded deoxyribonucleic acid
DTT	Dithiothreitol
E. coli	Escherichia coli

EBSS	Earle's balanced salt solution
ECL	Enhanced chemiluminescence
EDTA	Ethylenediaminetetraacetic acid
EdU	5-Ethynyl-2'-deoxyuridine
EMEM	Eagle's minimum essential medium
ETP	Etoposide
FA	Fanconi anaemia
FAM	Fluorescein amidite
FBS	Foetal bovine serum
FIJI	FIJI is just ImageJ
G1	Gap 1 phase
G2	Gap 2 phase
γH2AX	Phospho-histone H2AX (Serine 139)
GATK	Genome analysis toolkit
GFP	Green fluorescent protein
HDR	Homology-directed repair
HEK293	Human embryonic kidney 293
HEPES	4-(2-hydroxyethyl)-1-piperazineethanesulfonic acid
Hg19	Human genome assembly 19
Hg38	Human genome assembly 38
hr	Hour
HR	Homologous recombination
HRDC	Helicase and RNase D like C-terminal domain
HRP	Horseradish peroxidase
HU	Hydroxyurea
ICL	Interstrand crosslink
IDT	Integrated DNA Technologies
IgG	Immunoglobulin Gamma
KCl	Potassium chloride
kDa	kilodalton
KNIME	KoNstanz Information MinEr
LDS	Lithium dodecyl sulfate
M	Mitotic phase
MEM	Minimum essential medium
$MgCl_2$	Magnesium chloride
Min	Minute
MMC	Mitomycin C
MMEJ	Microhomology mediated end joining
MMS	Methyl methanesulfonate
MOPS	3-(N-morpholino)propanesulfonic acid
MRN	MRE11/RAD50/NBS1
mRNA	Messenger ribonucleic acid
N-terminal	Amino terminal
N3-MeA	3-methyladenine
N7-MeG	7-methylguanine
NaCl	Sodium chloride
NCS	Neocarzinostatin

NEB	New England Biolabs
NER	Nucleotide excision repair
NHEJ	Nonhomologous end joining
NHLBI	National Heart, Lung, and Blood Institute
NIH	National Institutes of Health
NMD	Nonsense mediated decay
NTS	Nuclear targeting sequence
NTS1	Nuclear targeting sequence 1
NTS2	Nuclear targeting sequence 2
OLA	Olaparib
OS	Osteosarcoma
PARP	Poly (ADP-ribose) polymerase
PBS	Phosphate buffered saline
PBST	Phosphate buffered saline with 0.1% Tween-20
PCR	Polymerase chain reaction
PES	Polyethersulfone
PMSF	Phenylmethylsulfonyl fluoride
PNK	Polynucleotide kinase
PVDF	Polyvinylidene fluoride
qPCR	Quantitative polymerase chain reaction
R4ZBD	RecQ4 zinc binding domain
R4ZBD-WH	RecQ4 zinc binding domain – winged helix
RAPADILINO	Syndrome characterised by RAdial aplasia/hypoplasia, PAtellar aplasia/hypoplasia and cleft/highly arched PAlate, DIarrhoea and DIslocated joints, LImb malformation and LIttle size, and slender NOse and NOrmal intelligence
RIPA	Radioimmunoprecipitation assay
RNA	Ribonucleic acid
RNAi	Ribonucleic acid interference
RNase	Ribonuclease
RQC	RecQ conserved domain
RT-qPCR	Reverse transcription – quantitative polymerase chain reaction
RTS	Rothmund-Thomson Syndrome
s	Seconds
S phase	Synthesis phase
S. cerevisiae	Saccharomyces cerevisiae
SDS	Sodium dodecyl sulfate
SDS-PAGE	Sodium dodecyl sulfate – polyacrylamide gel electrophoresis
SEM	Standard error of the mean
SF2	Superfamily 2
sgRNA	Single guide ribonucleic acid
siRNA	Small interfering ribonucleic acid
SSB	[DNA] Single-strand break
ssDNA	Single-stranded deoxyribonucleic acid
ssODN	Single-stranded oligodeoxyribonucleotide
SSPE	Sodium chloride – sodium phosphate – ethylenediaminetetraacetic acid
STAR	Spliced transcripts alignment to a reference

TBS	Tris buffered saline
TBST	Tris buffered saline with 0.1% Tween-20
TPM	Transcripts per million
TPT	Topotecan
UV	Ultraviolet
VEL	Veliparib
VIC	2'-chloro-7'phenyl-1,4-dichloro-6-carboxy-fluorescein
WT	Wild-type
X. laevis	Xenopus laevis

Chapter 1 Introduction

1.1 Overview of RecQ family helicases and RECQL4

RECQL4 is a member of the RecQ family of helicases in humans that also includes RECQL1, BLM, WRN, and RECQL5 (Kitao et al., 1998). Part of the SF2 helicase superfamily, human RecQ helicases are homologous to RecQ in *E. coli* and Sgs1 in *S. cerevisiae* and play important roles in the maintenance of genome stability (Fairman-Williams et al., 2010; Gorbalenya et al., 1989; Kitao et al., 1998). In particular, mutations in *BLM* and *WRN* lead to inherited cancer predisposition syndromes Bloom Syndrome and Werner Syndrome respectively (Ellis et al., 1995; Yu et al., 1996).

In humans, RecQ family helicases are characterised by the presence of seven shared conserved core helicase motifs that function in ATP-driven DNA unwinding as well as the zinc-binding RecQ conserved (RQC) domain (Ellis et al., 1995; Kitao et al., 1998; Puranam and Blackshear, 1994; Seki et al., 1994; Yu et al., 1996). In addition, both BLM and WRN also share the helicase and RNase D like C-terminal (HRDC) domain which functions in recruitment to sites of DNA damage (Samanta and Karmakar, 2012). However, unique among the RecQ family helicases, RECQL4 possesses neither the RQC nor the HRDC domains (Kaiser et al., 2017). Instead, RECQL4 is the sole member of the RecQ family of helicases and indeed the only protein thus far identified in humans to possess, on the N-terminus, a domain bearing homology to the yeast protein Sld2 which is essential in the initiation of DNA replication (Abe et al., 2011; Kamimura et al., 1998; Matsuno et al., 2006; Ohlenschläger et al., 2012; Sangrithi et al., 2005). Therefore, evolutionarily, RECQL4 can be thought of as a chimeric combination of two different protein domains, each performing distinct functions within the cell (Figure 1.1).

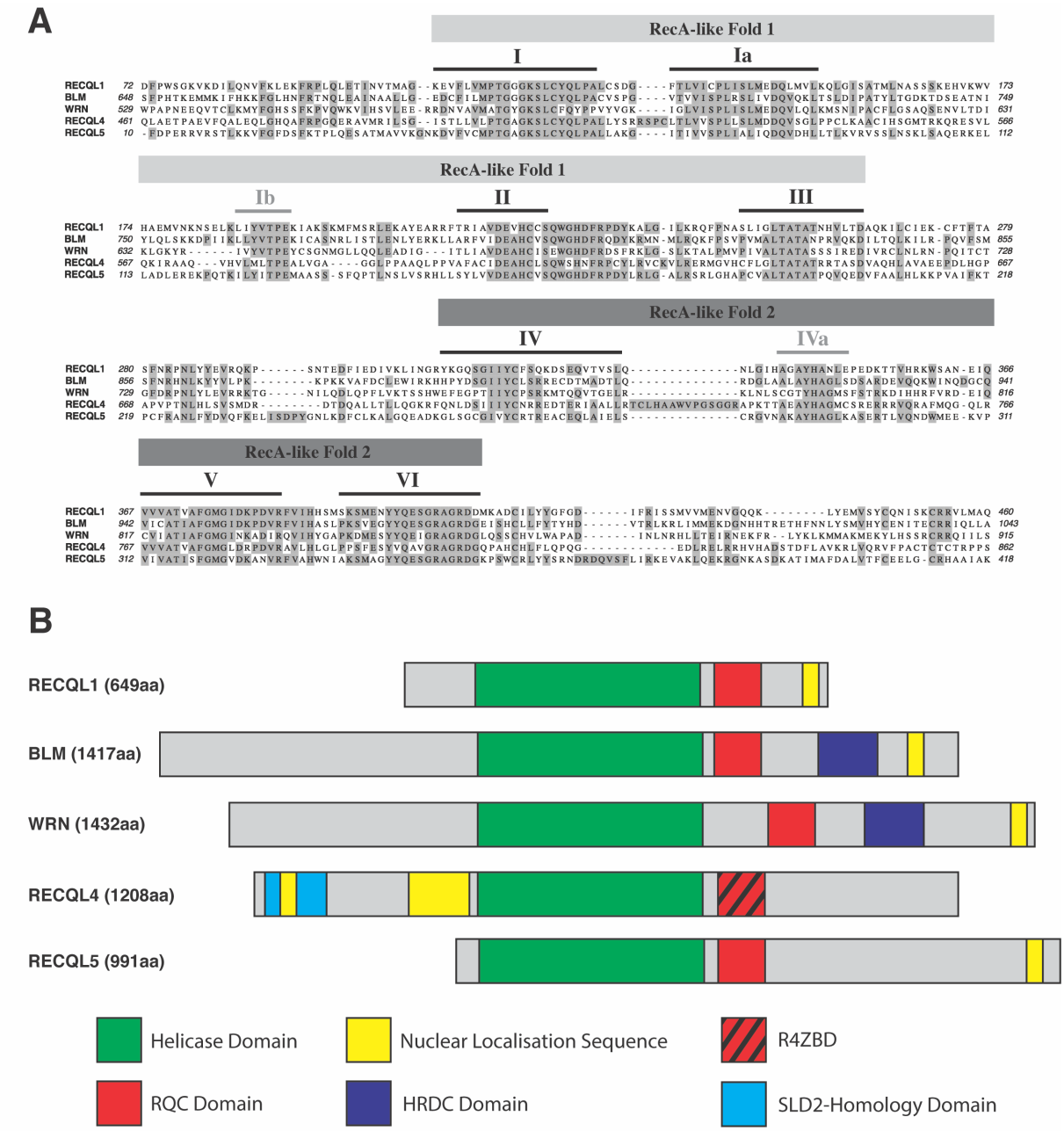

Figure 1.1 Comparison of RecQ family helicases

A. Protein sequence alignment of the helicase domains of the RecQ family helicases in humans. The seven conserved helicase motifs are denoted in black. RecA-like folds are denoted by grey boxes.

B. Structural comparison of RecQ family helicases in humans.

(Figure adapted from Kitao et al., 1998 and from Croteau et al., 2014. Amino acid sequence alignment done using MacVector)

1.2 RECQL4 structure and function – N-terminal region

RECQL4 is an approximately 150kDa protein composed of 1208 amino acids in a chimeric combination of two distinct protein domains (Kaiser et al., 2017; Kitao et al., 1998; Ohlenschläger et al., 2012). The N-terminal portion of RECQL4 comprises exons 1-8 (aa 1-494) and contains an Sld2-homology domain found only in RECQL4 in humans (Ohlenschläger et al., 2012). In *S. cerevisiae*, Sld2 and its interaction with Dpb11 is essential for the initiation of DNA replication (Kamimura et al., 1998). Similarly, the N-terminal domains of respective RECQL4 homologs are also required for DNA replication in *X. laevis* egg extracts and DT40 chicken cells. Furthermore, defects in DNA replication arising from depletion of homologs of RECQL4 in these systems can be rescued by expression of the N-terminal portion of the human RECQL4 protein (Abe et al., 2011; Matsuno et al., 2006; Sangrithi et al., 2005). In human cells, RECQL4's functions in the initiation of DNA replication has been demonstrated by studies showing its requirement in the recruitment of MCM10 and CTF4 to origins of replication (Im et al., 2015). In addition, RECQL4 has also been shown to interact with and play a role in the assembly of the CDC45-MCM2-7-GINS complex at replication origins (Im et al., 2009; Xu et al., 2009a). Similar to Sld2 and its interaction with Dpb11 in budding yeast, human RECQL4 also interacts with TOPBP1, the Dpb11 homolog in humans, through the region comprising the first 54aa of the N-terminal region (Ohlenschläger et al., 2012). Unlike in yeast, this interaction has been reported to be dispensable for DNA replication in human cells (Im et al., 2009). As the aforementioned repletion studies in *X. laevis* egg extracts and DT40 have speculated, the essential DNA replication functions of RECQL4 can be entirely assigned to its N-terminal region (exons 1-8, aa 1-494) (Abe et al., 2011; Matsuno et al., 2006; Sangrithi et al., 2005). Indeed, endeavours at generating mouse and human cell line models of RECQL4 mutants have shown

that the N-terminal portion of RECQL4 is both necessary and sufficient for viability thus providing a natural delineation of RECQL4 structure-function (Ichikawa et al., 2002; Kohzaki et al., 2012).

In addition to its functions in the initiation of DNA replication, the N-terminal region of RECQL4 also serves important roles in directing RECQL4 protein localisation and protein-protein interactions (Croteau et al., 2012a). Uniquely among RecQ family helicases, RECQL4 contains a mitochondrial localisation signal in the first 84aa that facilitates translocation of RECQL4-p53 complex to the mitochondria where it plays a critical role in maintaining of mitochondrial genome stability (De et al., 2012; Gupta et al., 2014). Equally important, the RECQL4 N-terminal region also contains two nuclear targeting sequences (NTS), NTS1 (aa 37-66) and NTS2 (aa 363-492), the latter of which functions as the main driver of RECQL4 nuclear import and retention (Burks et al., 2007).

Aside from its functions in organising the cellular compartmentalisation of RECQL4, the N-terminal region of RECQL4 also mediates a variety of protein recruitment and interactions many of which are critical to its role in DNA damage repair and genome stability. The nuclear targeting signal NTS2 promotes localisation of RECQL4 to sites of DNA double-strand breaks (DSBs) (Singh et al., 2010). Once there, RECQL4's N-terminal region has been shown to play roles in both of the major DNA DSB repair pathways—HR and NHEJ. RECQL4 N-terminal region interacts with the MRE11-RAD50-NBS1 (MRN) complex and mediates recruitment of CtIP, both early steps in HR (Lu et al., 2016). In addition, RECQL4's N-terminal region also interacts with the Ku70/80 complex which caps DNA break ends in NHEJ (Shamanna et al., 2014).

Alongside RECQL4's interactions with components of the DNA DSB repair pathways, RECQL4 has also been reported to play roles in other types of DNA damage repair and genome stability maintenance pathways. The N-terminal region has been shown to interact with

nucleotide excision repair (NER) factor XPA (Fan and Luo, 2008). Furthermore, RECQL4 also colocalises with APE1, FEN1, and Pol β in modulating activity of the base excision repair pathway (BER) (Schurman et al., 2009). Finally, RECQL4 has been reported to interact with fellow RecQ family member WRN and components of the shelterin complex TRF1, TRF2, and POT1 in the resolution of D-loop structures at telomeric ends (Ferrarelli et al., 2013; Ghosh et al., 2012). It should be noted however that further studies are needed to identify the region of the RECQL4 protein that participates in BER and telomeric maintenance. Elsewhere in the cell, RECQL4 has been reported to form complexes with p53 and Pol γ in an N-terminal region dependent manner to maintain mitochondrial genome stability (De et al., 2012; Gupta et al., 2014).

Besides serving as a site for various protein-protein interactions, reports indicate that RECQL4's N-terminal region also possesses various DNA substrate binding functions. Structurally, aside from a small homeodomain-like structure at the beginning of the protein, the N-terminal region is largely an intrinsically disordered domain. Studies report this region to have the ability to bind ssDNA, dsDNA, Y-shaped DNA substrates, and G4 quadruplexes in vitro, with particular affinity for the latter substrate. Functionally, RECQL4's N-terminal region appears to mediate DNA strand annealing and ATP-independent strand exchange in vitro though the cellular contexts for these activities remain unknown (Keller et al., 2014; Ohlenschläger et al., 2012).

In summary, RECQL4's N-terminal region serves two primary known functions. First, the Sld2-homology domain plays an essential role, through interactions with various replication factors and potentially DNA substrates, in the initiation of DNA replication and consequently cellular proliferation. Second, RECQL4's N-terminal region serves as an important site and signal for its targeting cellular localisation and protein-protein interactions

which are critical for its functions in DNA damage repair and the maintenance of genome integrity.

1.3 RECQL4 C-terminal region – is it a helicase?

Despite the fact that *RECQL4* was first discovered and cloned in humans more than two decades ago, until recently, the structure of the helicase domain and C-terminal region of the RECQL4 protein remained mostly uncharacterised. Initially, the identification of *RECQL4* as encoding a member of the RecQ family helicase was based on the presence of the seven conserved motifs of the core helicase domain that is a hallmark of the RecQ helicase family (Figure 1.1A) (Kitao et al., 1998). These seven motifs constituted two tandem RecA-like folds which are known to possess ATPase and ssDNA-binding functions and are variously termed the "motor" core of the helicase catalytic domain (Bernstein et al., 2003; Harmon and Kowalczykowski, 2001; Kaiser et al., 2017).

Aside from the core helicase domain however, RECQL4 was thought to lack other conserved features shared among members of the RecQ helicase family such as the RecQ conserved (RQC) and helicase and RNase-D C-terminal (HRDC) domains—features thought to be important for RecQ helicase function (Figure 1.1B) (Bernstein et al., 2003; Croteau et al., 2012a; Lu et al., 2014b; Mojumdar et al., 2017; Pike et al., 2009). In particular, based on studies of the structure of RECQL1, the RecA-like folds and the RQC domain together was thought to constitute the "catalytic core" of the helicase with the former providing the ssDNA-binding and ATPase functions and the latter containing a winged-helix domain that separates the DNA duplex through a β-hairpin mediated mechanism (Bernstein et al., 2003; Pike et al., 2009). The failure to identify a region with sequence homology to the RQC domain in RECQL4, when coupled with subsequent failure to experimentally detect RECQL4 DNA unwinding activity in

vitro (see below), initially raised doubts as to its predicted helicase function (Macris et al., 2006).

1.3.1 Unwinding the mystery of RECQL4's missing helicase activity

Despite RECQL4's initial identification as a member of the RecQ helicase family and the known functions of the other RecQ family helicases in DNA metabolism and genomic stability, RECQL4's biochemical functions were not immediately apparent when first discovered (Macris et al., 2006; Opresko et al., 2004; Sharma et al., 2006; Yin et al., 2004). Early biochemical characterisations of RECQL4 reported DNA-dependent ATPase activity, which was to be expected of the putative helicase (Yin et al., 2004). However, despite the ability to hydrolyse ATP, these studies found no evidence of DNA duplex unwinding by RECQL4 and only reported evidence of strand annealing activity on DNA substrates (Macris et al., 2006; Yin et al., 2004).

Xu and colleagues were the first to report helicase activity in RECQL4. By postulating that the known strand annealing activity of RECQL4 might act to mask helicase function, they reported finding RECQL4 to possess 3' -> 5' duplex unwinding activity when excess ssDNA was added to prevent re-annealing of the labelled duplex substrates (Xu and Liu, 2009). These findings were confirmed by subsequent studies which further characterised RECQL4 as a low processivity helicase that can unwind a 17mer duplex but not a 35mer substrate (Capp et al., 2009; Suzuki et al., 2009). Unexpectedly, Xu and colleagues reported that both the N-terminal region as well as the C-terminal helicase domains of RECQL4 possessed independent duplex unwinding activity and in fact found the former region to be a stronger helicase than the latter (Xu and Liu, 2009).

Based on the finding that RECQL4 was a low processivity helicase, Rossi and colleagues found that the excess ssDNA "sponge" was no longer required for helicase activity if short duplex substrates such as a 22mer forked duplex are used instead of the longer 30mer duplex

used by Xu et al. (Rossi et al., 2010; Suzuki et al., 2009; Xu and Liu, 2009). In fact, Rossi and colleagues reported RECQL4's DNA unwinding activity disappeared when using duplex substrates as short as 26bp in the absence of excess ssDNA. Further data suggested that RECQL4's competing annealing activity strengthens as substrate length increases, leading the authors to propose a model of RECQL4 function wherein duplex unwinding and strand annealing activities are in substrate length-dependent equilibrium (Rossi et al., 2010). This was proposed to explain the requirement for excess ssDNA in previous studies to prevent the masking of duplex unwinding by strand annealing when using longer duplex substrates (Rossi et al., 2010; Xu and Liu, 2009).

From there, Rossi and colleagues also tested RECQL4 helicase activity on a variety of DNA substrates and reported observable duplex unwinding only in the presence of forked (Y-shaped) DNA duplex substrates of varying lengths. No helicase activity was detected for DNA substrates resembling G4-quadruplexes, Holliday junction-like crosses, or straight duplexes. This led the authors to conclude that RECQL4 is a low processivity helicase with a preferred substrate of short, forked DNA duplexes (Rossi et al., 2010).

To address the unexpected results seen by Xu and colleagues of apparent duplex unwinding by both RECQL4 N-terminal region and the helicase domain fragments, Rossi and colleagues tested for helicase function with a RECQL4 K508M mutant containing a catalytically dead core helicase domain. This mutant not only failed to show any duplex unwinding activity but also showed strand annealing activity comparable to wild-type RECQL4. This demonstrated that RECQL4's helicase activity required the helicase domain and furthermore, that RECQL4 helicase and strand annealing activities are independent and separate (Rossi et al., 2010; Xu and Liu, 2009). It was possible that the RECQL4 N-terminal region duplex unwinding activity reported by Xu and colleagues was due to duplex destabilisation by protein

binding followed by strand exchange driven by RECQL4's strand annealing activity. Subsequent biochemical studies have shown that RECQL4's N-terminal region is sufficient for strand annealing and ATP-independent strand exchange activities providing further evidence for this explanation for the observations reported by Xu et al. (Keller et al., 2014; Rossi et al., 2010; Xu and Liu, 2009).

1.3.2 Recent insights into RECQL4 C-terminal structure and helicase mechanism

Recently, a new study of the RECQL4 C-terminal region has yielded insights into the constituent components of that portion of the protein, including the question of the missing RQC domain. Kaiser and colleagues elucidated the first ever detailed crystal structure of the RECQL4 helicase domain and C-terminal region and identified a previously unknown RecQ4 Zn^{2+}-binding domain (R4ZBD) downstream of the RecA-like folds of the helicase core. This new domain seemed to contain similar structures to those found in the canonical RQC domains of RecQ helicases such as a zinc-coordinating site (R4ZBD-Zn^{2+}) as well as portions with homology to winged-helix like structures in bacterial proteins (R4ZBD-WH) (Kaiser et al., 2017). The R4BZD connects to the helicase core via a series of bridging α-helices that constitutes part of a "backbone" for the protein domain. A C-terminal domain (CTD) comprising the final 92aa of RECQL4 was also functionally delineated at the end of the protein (Figure 1.2) (Kaiser et al., 2017).

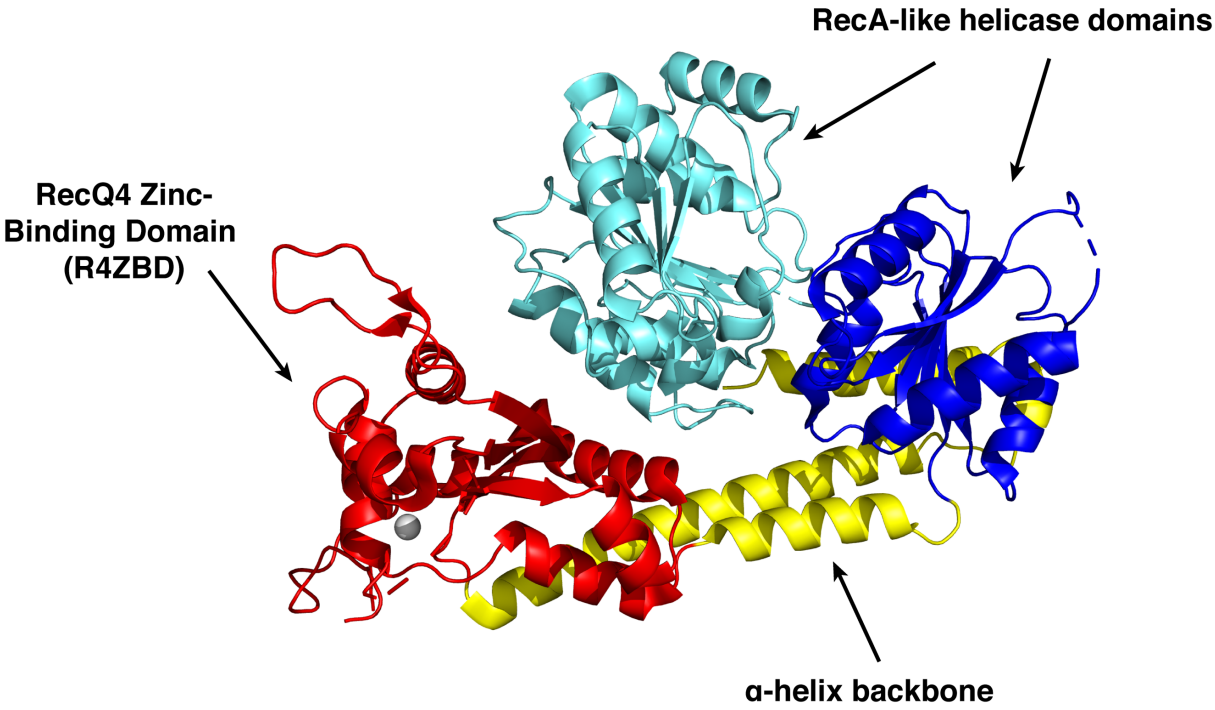

Figure 1.2 RECQL4 C-terminal domains
Figure depicts the structure of the C-terminal portion of RECQL4 from aa 449-1111 and highlights the different domains present. The tandem RecA-like folds 1 and 2 of the helicase ATPase domain are shown in cyan (RecA-like fold 1, aa 449-668) and blue (RecA-like fold 2, aa 669-819). The R4ZBD is shown in red (aa 837-1044). The α-helices comprising the "backbone" of the C-terminal region of RECQL4 are shown in yellow (aa 820-836 and aa 1045-1111). The grey sphere represents a Zn^{2+} ion.

(Figure was adapted from Kaiser et al., 2017 and made using PyMOL, PDB: 5LST)

Contrary to expectation, it does not appear that the R4ZBD-WH in RECQL4 contains the β-hairpin structure that is necessary for strand separation in RECQL1 (Kaiser et al., 2017; Pike et al., 2009). In addition, the spatial position of the R4ZBD-WH within the tertiary structure of the RECQL4 helicase domain also appears to argue against a strand-separation catalytic function based on comparisons to the structures of other RecQ helicases. Instead, mutational studies indicate that R4ZBD-WH is required for neither DNA binding nor helicase activity, leading to speculation that it may serve as a platform for substrate-specific DNA interaction or protein-protein interaction (Kaiser et al., 2017).

Downstream from the R4ZBD, Kaiser and colleagues identified a series of bridging α-helices that double back towards the second of the core helicase RecA-like folds and form a "backbone-like" structure for the protein (Figure 1.2). More importantly, their tertiary arrangement bears strong resemblance to the RQC Zn^{2+} binding domains found in other RecQ helicases. Fragment analysis of the region indicates that portions of these helices are critical for promoting protein stability. Lastly, Kaiser and colleagues demonstrated that the final 92aa C-terminal domain (CTD) at the end of the RECQL4 protein plays an important role in promoting helicase activity by increasing DNA binding affinity (Kaiser et al., 2017).

Altogether, these new insights into RECQL4 structure-function suggest a model for the mechanism of DNA unwinding by RECQL4 that is different from that of other RecQ helicases in humans. Rather, the newly proposed model is similar to one which has been proposed for bacterial RecQ helicase. The binding of ssDNA by the RecA-like folds, together with its ATPase-driven translocation along the DNA strand, is coupled to binding of dsDNA by the C-terminal domain (CTD). This induces a critical bending angle in the DNA substrate leading to melting of the duplex (Kaiser et al., 2017; Manthei et al., 2015). This model of RECQL4's helicase action and its predicted requirement for substrates containing both ssDNA and dsDNA could explain

the preference for forked substrates previously observed in biochemical studies of RECQL4 (Rossi et al., 2010; Xu and Liu, 2009). Further work is needed to assess the validity of this model.

1.4 RECQL4 in DNA Damage Repair

RecQ helicases are important for maintaining genomic stability, as evidenced by the premature aging and cancer predisposition phenotypes of the diseases to which they are linked (Bernstein et al., 2010; Croteau et al., 2014; Ellis et al., 1995; Kitao et al., 1999a; Lu et al., 2014b; Yu et al., 1996). However, as RECQL4's biochemical activity as a helicase has only recently been established, studies of its functions in DNA damage repair are just beginning to shed new insights into its roles in the cellular responses to DNA damage. Below, the current models and reports of RECQL4's DNA damage repair functions are briefly summarised (Figure 1.3).

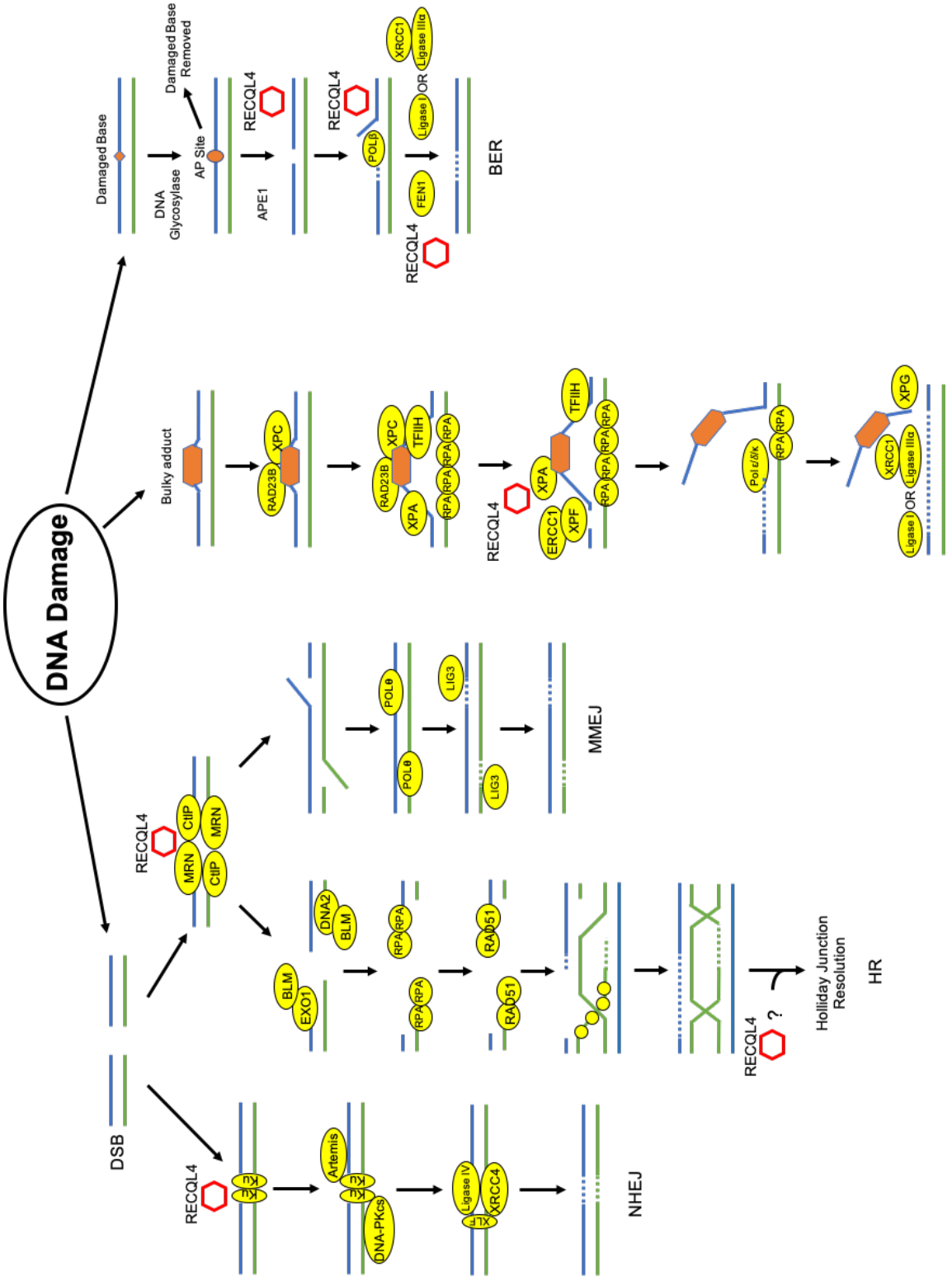
DNA Damage
Damaged Base
DNA Glycosylase
AP Site
Damaged Base Removed
APE1
RECQL4
POLβ
FEN1
XRCC1
Ligase IIIα
Ligase I
OR
BER
Bulky adduct
RAD23B
XPC
TFIIH
XPA
RPA
ERCC1
XPF
Pol ε/δ/κ
XPG
NER
DSB
Ku
Artemis
DNA-PKcs
Ligase IV
XRCC4
NHEJ
CtIP
MRN
DNA2
BLM
EXO1
RAD51
POLθ
LIG3
MMEJ
?
Holliday Junction Resolution
HR

Figure 1.3 The role of RECQL4 in DNA damage repair
The reported roles of RECQL4 in DNA damage repair pathways. RECQL4 is represented by red diamonds at points of reported protein interactions alongside its interaction partners. See detailed discussions of each pathway in Section 1.4.

(Figure adapted from Croteau et al., 2014; Schärer, 2013; Sfeir and Symington, 2017. Data on RECQL4's roles are from Fan and Luo, 2008; Lu et al., 2016; Schurman et al., 2009; Sedlackova et al., 2015; Shamanna et al., 2014)

1.4.1 RECQL4 in ssDNA damage repair

RECQL4 is involved in two major pathways in ssDNA damage repair – nucleotide excision repair (NER) and base excision repair (BER) (Figure 1.3) (Fan and Luo, 2008; Schurman et al., 2009). Their mechanisms are briefly discussed below along with the current understanding of RECQL4's functions in those pathways.

1.4.1a Nucleotide Excision Repair (NER)

NER removes bulky DNA adducts such as nucleotide dimers that result from insults such as UV irradiation or 4-nitroquinoline 1-oxide (4NQO) and DNA intrastrand crosslinks produced by compounds such as cisplatin, all of which can distort and weaken DNA structure and inhibit DNA metabolism (reviewed in Ikenaga et al., 1975 and Setlow and Setlow, 1972; Fichtinger-Schepman et al., 1985). Briefly, DNA lesions are recognised by either stalled RNA polymerase (transcription-coupled NER) or by XPC-RAD23B complex (globally) which recruits TFIIH to unwind a bubble around the lesion. The ssDNA in the newly formed bubble is stabilised by RPA and XPA, the latter of which recruits ERCC1-XPF to make a nick at the 5' end of the bubble upstream of the lesion. Repair synthesis is then carried out by pol ε (dividing cells) or pol δ/κ (non-dividing cells). The lesion-containing strand is finally nicked again at the 3' end of the bubble downstream of the lesion by XPG before the newly synthesised patch is ligated to the existing DNA by DNA Ligase I (dividing cells) or ligase IIIα and XRCC1 (non-dividing cells) to complete the repair process (reviewed in Schärer, 2013 and Spivak, 2015).

RECQL4 has been reported to interact with XPA to promote NER (Figure 1.3). However, though RECQL4 overexpression appears to increase NER-mediated removal of cyclobutane pyrimidine dimer—a UV radiation induced DNA adduct—it is unclear whether RECQL4 is required for NER (Fan and Luo, 2008). Additionally, the precise role and function of RECQL4 in NER remain to be elucidated.

Equally unclear are the effects of RECQL4 disruption on DNA damage repair via NER. RECQL4 deficiency and depletion have been shown to impair S-phase arrest after UV irradiation (Park et al., 2006). However, the viability of RECQL4-deficient cells—both RTS patient cells and *Recql4*-deficient mouse cells—after induction of NER-activating DNA damage is variable (Hoki et al., 2003; Jin et al., 2008; Shinya et al., 1993; Smith and Paterson, 1981). Furthermore, studies of NER activity in RTS patient cells--as measured by unscheduled DNA synthesis post-challenge—report no changes compared to normal controls to intermediate levels of repair between NER-competent and deficient controls (Grant et al., 2000; Shinya et al., 1993; Vasseur et al., 1999). It is likely that such variability arises from the specific mechanisms of RECQL4 disruption or deficiency studied as well as the assays used. Diverse and sometimes essential functions have been attributed to different regions of the RECQL4 protein (discussed above in Sections 1.2 and 1.3). Disruptions such as the varying RTS patient mutations, exon-specific deletions in *Recql4*-deficient mouse models, and RNAi-mediated RECQL4 knockdown should be expected to have differing effects on RECQL4 protein structure and/or abundance and therefore result in a spectrum of residual RECQL4 function.

1.4.1b Base Excision Repair (BER)

Base excision repair is responsible for the removal from DNA of damaged bases that result from challenges such as alkylation, oxidation, or deamination (Krokan and Bjørås, 2013). In addition, steps in BER have also been shown to function in the repair of DNA single-strand breaks (SSBs) (Caldecott, 2008). The major steps of BER include recognition and cleavage of damaged bases by DNA glycosylases to generate apurinic/apyrimidinic (AP) sites. The strand 5' of the AP site is then nicked by AP Endonuclease 1 (APE1) to allow for the binding of pol β and synthesis of new DNA to displace the damaged portions. Finally, the flap of displaced damaged strand is nicked by Flap Endonuclease 1 (FEN1) 3' of the lesion site allowing for

ligation of the newly synthesised DNA with existing DNA by DNA Ligase I or Ligase IIIα-XRCC1 (Figure 1.3) (reviewed in Krokan and Bjørås, 2013).

In BER, RECQL4 has been reported to localise with and stimulate the activities of APE1, pol β, and FEN1 (Figure 1.3) (Schurman et al., 2009). In support of these findings, oxidative stress has been shown to modulate RECQL4 nuclear localisation (Woo et al., 2006). In addition, some RTS patient cells accumulate more damage and show decreased viability compared to normal controls when exposed to oxidative challenge (Schurman et al., 2009; Werner et al., 2006). However, more studies are needed to determine whether RECQL4 is required for BER and what its precise functions are.

1.4.2 RECQL4 in double-strand break repair

DNA double-strand breaks (DSBs) are extremely detrimental to cells. Therefore, efficient mechanisms are in place to rapidly detect and repair DNA DSBs. The two major pathways for DNA DSB repair in cells are non-homologous end joining (NHEJ) and homologous recombination (HR) (reviewed in Jasin and Rothstein, 2013; Lieber, 2010). NHEJ joins break ends without requiring long stretches of sequence complementarity for templated repair synthesis while HR uses the presence of a homologous repair template such as a sister chromatid to faithfully reconstruct damaged sections of DNA. This gives rise to the model of NHEJ being the dominant DNA DSB repair pathway during G1 and early-S phases while HR takes over during late-S and G2 phases of the cell cycle when sister chromatid repair templates become available (Chapman et al., 2012; Jasin and Rothstein, 2013; Johnson and Jasin, 2000; Karanam et al., 2012; Lieber, 2010; Lieber et al., 2003; Saleh-Gohari and Helleday, 2004; Symington and Gautier, 2011). In addition to the two major pathways above, microhomology mediated end joining (MMEJ), in which break ends are joined through annealing of short homology regions near the break ends, is considered to be a backup DNA DSB repair

mechanism that complements the activities of HR and NHEJ (reviewed in Sfeir and Symington, 2017).

RECQL4 is known to have multiple roles in the cellular responses to DNA DSBs. Its N-terminal region, in particular the nuclear targeting signal NTS2, has been shown to be sufficient to localise RECQL4 to DNA DSBs at sites of laser micro-irradiation (Singh et al., 2010). In addition, engineered cells expressing only helicase-truncated RECQL4 show increased sensitivity to ionising radiation as well as delayed DNA DSB resolution and S-phase progression compared to isogenic controls expressing wild-type RECQL4 (Kohzaki et al., 2012). Below, the mechanisms of each of the DNA DSB repair pathways mentioned above are briefly discussed along with the reported functions of RECQL4 in each (Figure 1.3).

1.4.2a Non-homologous End Joining (NHEJ)

NHEJ is a non-template driven DNA DSB repair pathway generally thought to be active and dominant during G1 and early-S phases of the cell cycle (Karanam et al., 2012; Lieber et al., 2003). To briefly summarise, DNA DSB ends are recognised and bound by Ku70/80 heterodimers which act to bridge and align the ends with the help of the XRCC4-XLF complex and short sequence homologies present at the ends. The Ku-complex also serves as a scaffold for the recruitment of downstream NHEJ pathway components for end processing and ligation. Processing of break ends is not essential to NHEJ and depends on end structure. It can involve a variety of factors and steps such as resection of ssDNA overhands by DNA-PK/Artemis or filling in of gaps by polymerases such as Pol μ or Pol λ. Finally, the ends are re-ligated by XRCC4-Ligase IV complex which is recruited by the Ku-complex (Figure 1.3) (reviewed in Cannan and Pederson, 2016; Lieber, 2010; Lieber et al., 2003).

Given RECQL4's known recruitment to sites of DNA DSBs, several recent studies have reported association of RECQL4 with the Ku complex—a component of NHEJ—after DNA DSB

induction (Figure 1.3) (Shamanna et al., 2014; Singh et al., 2010). While RNAi-mediated depletion of RECQL4 appeared to result in decreased NHEJ activity *in vitro* and *in vivo*, the effect seemed mild and substantial NHEJ activity remained, suggesting that RECQL4 is not essential for NHEJ. In addition, observations by Shamanna and colleagues implicated the N-terminal portion (aa 1-447) of RECQL4 in interactions with the Ku complex—a region which is generally spared by RTS *RECQL4* mutations (discussed in Section 1.5.4, Figure 1.4) (Shamanna et al., 2014; Siitonen et al., 2008). This finding further raises the question of whether NHEJ function is expected to be impacted by RECQL4 disruption in clinically relevant contexts.

1.4.2b Homologous Recombination (HR)

The other major DNA DSB repair pathway in cells is HR, a templated repair pathway that uses sequence homology between break ends and a repair template such as a sister chromatid to repair DNA DSBs in an error-free manner (Cannan and Pederson, 2016; Johnson and Jasin, 2000). Given its template requirement, HR is generally thought to be the dominant DNA DSB repair pathway during the late-S and G2 phases of the cell cycle (Cannan and Pederson, 2016; Johnson and Jasin, 2000; Karanam et al., 2012; Lieber et al., 2003; Saleh-Gohari and Helleday, 2004). Briefly, HR repair of DNA DSBs begin with the assembly of the MRE11/RAD50/NBS1 (MRN) complex on the break ends. The MRN complex mediates recruitment of CtIP and BRCA1 which begins resection of the break ends to generate 3' ssDNA overhangs. Initial resection is then superseded by more extensive resection through the actions of EXO1 or BLM/DNA2 which generates long stretches of ssDNA that are bound and stabilised by RPA, the ssDNA-binding protein. RPA is eventually replaced by Rad51 with help from BRCA2 to form a strand invasion-competent nucleoprotein filament which invades the nearby repair template duplex to form a D-loop at the site of sequence homology. Once the D-loop is established, templated repair synthesis can begin on the first strand while the second

strand also anneals to the D-loop to complete the double Holliday junction structure. Finally, the double Holliday junction structure is resolved through single strand nicking to separate the two DNA molecules and the breaks are sealed by DNA ligase (Figure 1.3) (Cannan and Pederson, 2016; Jasin and Rothstein, 2013; San Filippo et al., 2008).

Recent studies have shed light on RECQL4's participation in HR, starting with observations of RECQL4 localisation after DNA DSB induction (Petkovic et al., 2005; Singh et al., 2010). A study by Petkovic and colleagues first suggested that RECQL4 may play a role in HR when they reported that RECQL4 colocalises with Rad51 foci and ssDNA when DNA DSBs were induced with ionising radiation (Petkovic et al., 2005). Subsequent studies into the kinetics of RECQL4 recruitment to DNA DSBs seem to point to a role for RECQL4 early in the DNA DSB repair process as data showed RECQL4's presence at DNA DSBs peaked and declined within the first hour after damage induction in contrast to the recruitment kinetics of other RecQ helicases such as BLM and WRN (Singh et al., 2010).

In parallel with the above localisation studies, mutational studies and fragment analysis of RECQL4 demonstrated that, while the RECQL4 N-terminal region is sufficient for RECQL4 localisation to DNA DSB sites, the helicase and C-terminal regions are also necessary for RECQL4 function in DNA DSB repair (Kohzaki et al., 2012; Singh et al., 2010). Human pre-B lymphocytic NALM-6 cells expressing only RECQL4 truncated before the helicase domain are more sensitive to ionising radiation (IR) than isogenic controls expressing wild-type RECQL4. Additionally, synchronised NALM-6 *RECQL4* truncation mutant cells show impaired S-phase progression post-IR treatment. These findings suggest that RECQL4 helicase function is important for HR, the dominant DNA DSB repair pathway active during S-phase (Karanam et al., 2012; Kohzaki et al., 2012; Saleh-Gohari and Helleday, 2004; Singh et al., 2010).

Most recently, Lu and colleagues uncovered a role of RECQL4 in the break end resection step of HR and found multiple independent functions for different regions of the protein. In their model, RECQL4 N-terminal region interacts with MRE11 of the MRN complex at break ends to stimulate MRE11 endonuclease activity and to recruit CtIP for the initiation of 5'->3' resection and the generation of the necessary 3' ssDNA overhang. They report that while the RECQL4 N-terminal region is sufficient to stimulate MRE11-mediated strand cleavage and for the recruitment of CtIP, RECQL4 helicase function is also required for DNA resection as the catalytically dead helicase K508M mutant fails to rescue DNA resection in RECQL4 depleted cells. The role and mechanism of helicase function in this context remain to be elucidated. Finally, Lu and colleagues show RECQL4 interacts with downstream resection factors EXO1 and BLM to stimulate extended DNA resection (Lu et al., 2016). Taken together, they suggest that these data show RECQL4 playing a critical role in the early stages of HR by promoting end resection of the DNA DSB break ends (Figure 1.3).

1.4.2c Microhomology-mediated End Joining (MMEJ)

While NHEJ and HR are the major pathways for DNA DSB repair in the cell, other alternative pathways exist as backup to complement them. One such pathway is microhomology-mediated end joining (MMEJ), also called alternative NHEJ (alt-NHEJ) to differentiate it from the canonical NHEJ (c-NHEJ) previously described (Cannan and Pederson, 2016; Sfeir and Symington, 2015). Similar to c-NHEJ, MMEJ is also a non-templated error-prone DNA DSB repair mechanism. However, unlike c-NHEJ, MMEJ is both Ku- and DNA-PK independent and relies on longer microhomology regions at the break ends for end alignment and strand annealing. To briefly summarise, MMEJ shares the initial DNA DSB end resection step with HR involving the MRE11/RAD50/NBS1 (MRN) complex along with CtIP and possibly BRCA1 (Truong et al., 2013). This exposes short regions of homology on the two ends which

may be internal to the ends. These regions of microhomology anneal, bringing the two ends together and generating non-homologous flaps. The non-annealed flaps are excised by endonucleases such as ERCC1-XPF to expose extension-competent ends. DNA polymerase pol θ is then recruited to fill in the gaps in the break region before the newly synthesised strands are sealed by DNA ligase I/III (Bennardo et al., 2008; Cannan and Pederson, 2016; Truong et al., 2013; Wang and Xu, 2017). It can be seen therefore, that the role played by RECQL4 in the initial stages of HR should also be present in the initial stages of MMEJ, namely interaction with MRE11 and recruitment of CtIP (Lu et al., 2016; Truong et al., 2013). At this time however, no direct evidence has implicated any other MMEJ-specific roles for RECQL4.

1.4.3 RECQL4, replication, and DNA damage repair

Having reviewed RECQL4's dual but hitherto separate roles in DNA replication and DNA damage repair, a natural question is to consider the extent to which these two functions are linked and the importance of such a relationship. Do RECQL4's repair functions favour replication-specific DNA damage? Previous data has shown that RECQL4 is preferentially expressed in proliferating cells, unsurprising considering its essential role in the initiation of DNA replication (Abe et al., 2011; Im et al., 2009, 2015; Kawabe et al., 2000; Kitao et al., 1998; Matsuno et al., 2006; Sangrithi et al., 2005; Xu et al., 2009b). A recent study further reports that RECQL4 function is regulated in a cell cycle dependent manner—phosphorylation at serines 89 and 251 of RECQL4 by CDK1/2 promotes its interaction with MRE11 and thus recruitment to DNA DSBs during S-phase. Additionally, phosphorylation of RECQL4 also stimulates its helicase activity and promotes the initiation of DNA resection and thus the HR pathway (Lu et al., 2017). Finally, from the above discussion of RECQL4's roles in DNA damage repair, replication associated DNA DSB repair (HR) is the only pathway which has been definitively shown to require RECQL4 helicase activity (Kohzaki et al., 2012; Lu et al., 2016).

Given that the helicase portion of RECQL4 is preferentially targeted in Type II RTS (discussed below), it is conceivable that the role of RECQL4 in cellular response to replication-associated DNA damage is particularly clinically relevant.

1.5 RECQL4 in human disease

The major human disease to which *RECQL4* mutations are linked is Type II Rothmund-Thomson Syndrome (discussed below) (Kitao et al., 1999a; Siitonen et al., 2008; Wang et al., 2003). However, Type II RTS is not the only disease associated with *RECQL4* mutations. Mutations in *RECQL4* have also been linked to RAPADILINO Syndrome and Baller-Gerold Syndrome (BGS), which will be briefly covered first (Van Maldergem et al., 2006; Mo et al., 2018; Siitonen et al., 2003, 2008).

1.5.1 RAPADILINO Syndrome

RAPADILINO Syndrome is an autosomal recessive disorder characterised by Radial aplasia/hypoplasia, patellar aplasia/hypoplasia and cleft or highly arched palate, diarrhoea and dislocated joints, little size and limb malformation, and slender nose and normal intelligence (Kääriäinen et al., 1989; Sharma et al., 2006; Siitonen et al., 2003). While RAPADILINO Syndrome shares some phenotypic overlap with RTS, poikiloderma and significantly increased risk of cancer is not found in the former (Siitonen et al., 2003). Genetically, the majority of RAPADILINO patients have the c.1390+2delT founder mutation with many being homozygotes (Siitonen et al., 2003, 2008). This mutation leads to an in-frame skipping of *RECQL4* exon 7 (aa 420-463) which should disrupt the nuclear targeting signal NTS2 and thus RECQL4 nuclear localisation (Burks et al., 2007). However, biochemical characterisation of this variant appears to point to a defect in helicase and ATPase activity despite the skipped region being outside the helicase domain (Croteau et al., 2012b). Other

mutations found in RAPADILINO patients appear to mostly target the helicase domain similar to those found in Type II RTS patients.

1.5.2 Baller-Gerold Syndrome

Baller-Gerold Syndrome (BGS) is an extremely rare autosomal recessive condition characterised by radial aplasia/hypoplasia and craniosynostosis (Baller, 1950; Gerold, 1959; Van Maldergem et al., 2006; Mo et al., 2018). Causal mutations in *RECQL4* were found in a subset of (BGS) patients, however the mutational spectrum is heterogeneous (Van Maldergem et al., 2006; Siitonen et al., 2008). BGS patients do not appear to have an increased risk of cancer though very few BGS patients have been diagnosed to date (Siitonen et al., 2008).

1.5.3 Overview of Rothmund-Thomson Syndrome

Rothmund-Thomson Syndrome (RTS) is an autosomal recessive inherited cancer predisposition syndrome characterised by a range of symptoms including poikiloderma, juvenile cataracts, skeletal abnormalities, short stature, premature aging, and increased incidence of mesenchymal malignancies such as lymphoma and osteosarcoma (Kitao et al., 1999b; Larizza et al., 2010; Mo et al., 2018; Vennos and James, 1995; Vennos et al., 1992). The disease is subdivided into two subtypes—Type I RTS, comprising around one third of RTS patients, manifests with poikiloderma and juvenile cataracts with no increased risk of osteosarcoma while Type II RTS, diagnosed in around two thirds of RTS patients, is characterised by poikiloderma, skeletal abnormalities, and increased risk of osteosarcoma (Larizza et al., 2010; Wang et al., 2003). In particular, the incidence rate of osteosarcoma in Type II RTS patients has been estimated to be roughly 30%, a much higher rate than that of sporadic osteosarcoma in the general population (Wang et al., 2001, 2003).

Genetically, sequencing studies of RTS patient cohorts have suggested a link between Type I RTS and germline mutations in the gene *ANAPC1*, which encodes a component of the

anaphase-promoting complex/cyclosome (APC/C) complex (Ajeawung et al., 2019). Type II RTS, on the other hand, has been linked to germline mutations in the *RECQL4* gene (Kitao et al., 1998, 1999a, 1999b; Lindor et al., 2000).

1.5.4 RECQL4 mutations in Type II RTS

The majority of disease-causing *RECQL4* mutations in humans are associated with Type II RTS (Kitao et al., 1999a; Lindor et al., 2000; Siitonen et al., 2008; Wang et al., 2003). As a cohort, Type II RTS *RECQL4* mutation is heterogeneous. However, a few insights can be gleaned from an overview of some of the published mutations (Figure 1.4). First, the preponderance of RTS *RECQL4* mutations occur after exon 8, sparing the essential N-terminal region. Furthermore, a majority of mutations fall between exons 9-14, which encodes the helicase domain, suggesting that helicase function is particularly targeted in Type II RTS. Second, very few RTS *RECQL4* mutations are missense mutations. The majority of RTS *RECQL4* mutations are predicted to be nonsense, frameshift, or missplicing mutations which ablate portions of the protein, particularly the helicase domain. It has been noted that the *RECQL4* gene contains many compact introns which approach the minimum threshold length necessary for efficient splicing. Based on this observation and the RTS *RECQL4* mutational spectrum, intronic mutations which adversely affect splicing efficiency have been proposed as a common mutational mechanism at the *RECQL4* locus (Kitao et al., 1999b; Siitonen et al., 2008; Wang et al., 2002). Third, the majority of RTS patients are compound heterozygous for *RECQL4* mutations. Finally, despite the breadth of the RTS *RECQL4* mutational spectrum, two mutations stand out as especially prevalent—c.1573delT and c.2269C>T. They will be discussed separately below (Figure 1.4) (Siitonen et al., 2008).

1.5.4a RECQL4 c.1573delT

RECQL4 c.1573delT is the most common *RECQL4* mutation found in Type II RTS patients. First identified by Kitao et al. as one of the original RTS *RECQL4* causal mutations, it is also known as “Mut-5” (Kitao et al., 1999b). It is a single base pair deletion in exon 9 predicted to result in frameshift and premature translation termination 32aa downstream. The resulting product should be a truncated 557aa peptide containing mostly the N-terminal region of the RECQL4 protein (Siitonen et al., 2008). It has been reported however, that in patient cells containing this mutation, no transcript can found with this mutation, possibly due to nonsense-mediated decay (Beghini et al., 2003). Tellingly, *RECQL4* c.1573delT is found exclusively in the context of compound heterozygosity in RTS patients. Thus, this mutation may represent an extremely deleterious non-productive functional knockout allele.

1.5.4b RECQL4 c.2269C>T

RECQL4 c.2269C>T is the second most common *RECQL4* mutation found in Type II RTS patients. Also first identified by Kitao et al. as one of the original RTS *RECQL4* causal mutations, it was originally named by the authors as “Mut-2” (Kitao et al., 1999b). It is a single base pair substitution in exon 14 which results in a premature stop codon. The resulting protein product is predicted to be truncated in the middle of the second RecA-like fold of the core helicase domain and thus have a severe impact on helicase activity (Siitonen et al., 2008). Interestingly however, a recent study of a very similar nonsense mutation, *RECQL4* c.2272C>T, instead found upregulation of alternative splicing in exon 14 leading to the in-frame skipping of the final 66aa of exon 14 (aa 756-821). The deleted segment also includes the premature stop codons introduced by both the c.2269C>T and c.2272C>T mutations and allows production of an almost full-length protein (Colombo et al., 2014). The results of this study will be further

discussed in Chapter 2 (Section 2.3.4). It is unknown at this time whether *RECQL4* c.2269C>T has the same effect on RECQL4 splicing and protein structure.

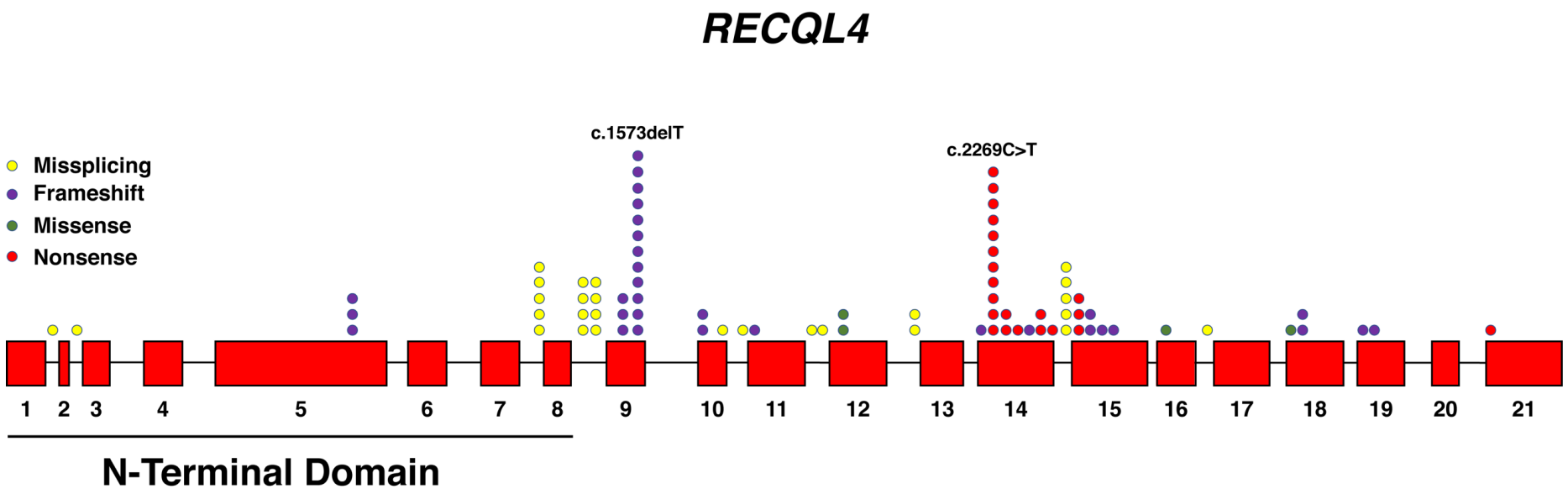

Figure 1.4 *RECQL4* mutations reported in Type II RTS patients
Type II RTS patient mutations are categorised by predicted effect. The vast majority of mutations occur after exon 8, thus sparing the essential N-terminal domain. In addition, the majority of the mutations fall within the helicase domain (exons 9-14).

(Data from Colombo et al., 2014 and Siitonen et al., 2008)

1.6 Modelling *RECQL4* Disruption

A variety of approaches have been taken to study the functional effects of *RECQL4* disruption in disease. Below I will briefly outline studies of *RECQL4* using mouse models, engineered human cell lines, and RTS patient cells.

1.6.1 Recql4 mouse models

Ichikawa and colleagues made the first attempt to generate a *Recql4*-disrupted mouse model when they attempted to create mice with *Recql4* exon 5-8 deletion. In their study, homozygous exon 5-8 deletion was embryonic lethal and no mice survived to birth (Ichikawa et al., 2002).

Hoki et al. established the first mouse model of Type II RTS by deleting *Recql4* exon 13, part of the core helicase domain. Homozygous *Recql4* Δ13 mice in their study showed growth retardation with 40% mortality immediately after birth and 95% within 2 weeks of birth. Furthermore, these mice showed accelerated hair loss and skin aging along with skeletal hypoplasia. However, unlike the poikiloderma seen in some Type II RTS patients, *Recql4* Δ13 mice do not show inflammation of the skin (Hoki et al., 2003).

Mann and colleagues established another model of RTS when they created a *Recql4* exon 9-13 deletion mouse. The targeting construct in this study truncates the Recql4 protein immediately after exon 8, leaving only the N-terminal region of Recql4 intact. In contrast to Hoki's model, Mann et al. did not observe the significant mortality seen in the previous model. The Mann model mice showed skeletal malformations and skin phenotypes consistent with RTS. However, significant palatal defects were also reported, which is more consistent with RAPADILINO Syndrome. Mann also reported increased genomic instability in these *Recql4*-truncated mice and increased risk of cancer on a sensitised background (Mann et al., 2005).

More recently, Lu and colleagues explored the effect of helicase deletion on *in vivo* cell proliferation. They report that deletion of Recql4 helicase domain leads to increased signs of DNA damage as well as senescence, resulting accelerated aging phenotypes such as hair loss and bone marrow failure (Lu et al., 2014a).

In order to further study the skeletal-specific effects of *Recql4* disruption, Lu and colleagues generated a *Recql4*$^{fl/fl}$*;Prx1-Cre*$^{+}$ conditional RECQL4 knockout mouse. Consistent with RTS, they report significant skeletal phenotypes such as limb malformations as well as growth plate proliferation defects in these mice. Activation of p53 is associated with *Recql4* disruption and inactivation of p53 rescues the skeletal phenotype seen in this model (Lu et al., 2015).

Finally, Walkley and colleagues generated a series of mouse models starting first with a conditional exon 9-10 deletion *Recql4* knockout (Smeets et al., 2014). Mice in which Recql4 was lost showed defective haematopoiesis that was rescued by expression of a helicase-dead Recql4 variant suggesting that the phenotype observed was not due to disruptions of Recql4's helicase function (Smeets et al., 2014). When the same conditional deletion of *Recql4* was restricted to the osteoblastic lineage, proliferation and differentiation defects, skeletal hypoplasia, and skeletal malformation were observed only when Cre expression was initiated in osteoblastic progenitors, indicating a requirement for Recql4 in early osteoblastic proliferation and bone formation. Deletion of *Recql4* in mature osteoblasts and osteocytes, however, showed no observable phenotype. In both cases, no elevated incidence of OS was found (Ng et al., 2015).

In their latest study, Walkley and colleagues generated a series of mice harbouring point mutations in *Recql4* including a helicase-dead mutation (K525A) and a small panel of mutations (M789K, G522Efs, R347*) that are genetically equivalent to select RTS patient

RECQL4 mutations. Interestingly, mice harbouring missense point mutations, including the helicase-dead mutation, were notable in their lack of detectable phenotype whether in viability, growth characteristics, haematopoiesis, skeletal development, sensitivity to DNA damaging agents, or OS incidence. In contrast, mice carrying truncation mutations which grossly impacted Recql4 protein structure exhibited defects in haematopoiesis similar to *Recql4* knockout mice described previously (Castillo-Tandazo et al., 2019). This dichotomy of phenotypic differences resulting from the nature of the underlying mutations seems to be consistent with the observation that missense point mutations in *RECQL4* are uncommon in Type II RTS patients, in whom the vast majority of Type II RTS *RECQL4* mutations are predicted to have large impacts on protein structure (Siitonen et al., 2008). It also calls into question the utility of models based on the former.

Taken together, mouse models established thus far recapitulate various aspects of Type II RTS. However, none of them have been able to completely model the disease and its range of phenotypic features in their entirety, most notably, the noted predisposition to cancers such as osteosarcoma.

1.6.2 RECQL4 cell line models

Modelling Type II RTS in human cell lines have generally taken two approaches – using patient derived cells or modifying the endogenous *RECQL4* locus in a normal cell line (Jin et al., 2008; Kohzaki et al., 2012; Singh et al., 2010; Yin et al., 2004). RTS patient fibroblasts have provided convenient and clinically relevant models for studying the effects of RECQL4 deficiency. However, they present two challenges that prevent effective data interpretation. First, matched normal fibroblasts are generally not available as controls. Normal human fibroblasts are usually used instead, however these controls cannot guarantee that any results seen are solely due to *RECQL4* mutations. Second, as mentioned previously, with very few

exceptions, RTS patients are generally compound heterozygotes at the *RECQL4* loci. Thus, any study of fibroblasts from RTS patients are likely assessing the effects of a heterogeneous mix of *RECQL4* mutations, possibly with different effects. These factors may partially account for the fact that assessments of RTS patient fibroblast sensitivity to various genotoxic agents in different studies often yield conflicting results and interpretations (Jin et al., 2008).

A second approach to cell-based modelling of RECQL4 function is direct modification of the endogenous *RECQL4* loci through gene editing techniques in normal human cell lines. Thus far, Kohzaki and colleagues have presented the best example of this approach through their engineering and characterisation of RECQL4 helicase-truncated NALM-6 cell lines (Kohzaki et al., 2012). However, at this time, no such models exist based on clinically relevant *RECQL4* mutations which would enable finer-grained studies of RECQL4 structure-function relationships as well as RTS disease pathogenesis.

1.7 Specific Aims

The overall goal of this study is to dissect the functional consequences of a prevalent clinical Type II RTS *RECQL4* mutation—c.2269C>T or "Mut-2". Current models for and approaches to studying Type II RTS are unsuitable for the purposes of this study. Therefore, I have the following three specific aims:

1. Use CRISPR/Cas9 gene editing to generate human cell lines containing a common RTS patient mutation (*RECQL4* c.2269C>T, "Mut-2"), with the expectation that these cell lines will represent a viable and faithful model of RECQL4 dysfunction in Type II RTS.
2. Characterise the effect of this mutation on RECQL4 protein structure and expression by analysing RECQL4 mRNA transcript and protein abundance.
3. Investigate the phenotype of these cell lines in terms of growth characteristics, sensitivity to genotoxic challenges, and DNA damage repair capacity and function.

Recent studies have yielded new insights into the functions and mechanisms of RECQL4's helicase activity (Kohzaki et al., 2012; Lu et al., 2016, 2017). Their findings will serve as a springboard in the following chapters to better understand how *RECQL4* mutations in Type II RTS affect DNA damage repair.

Chapter 2 Cell Line Model Generation

2.1 Introduction

RECQL4 was first identified as a member in the human RecQ helicase family in 1998 (Kitao et al., 1998). Shortly thereafter, germline mutations in *RECQL4* were identified as the cause for what is now known as Type II RTS (Kitao et al., 1999a, 1999b; Lindor et al., 2000). Early efforts to study RECQL4 function in the context of human disease made use of various mouse models of *RECQL4* mutation or deletion (Castillo-Tandazo et al., 2019; Hoki et al., 2003; Ichikawa et al., 2002; Lu et al., 2014a, 2015; Mann et al., 2005; Ng et al., 2015; Smeets et al., 2014). However, efforts at generating mouse models of RTS have been complicated by the essential role of RECQL4 in viability (Ichikawa et al., 2002). Furthermore, no mouse model thus far has been able to adequately recapitulate the phenotype of Type II RTS, including skin abnormalities, skeletal malformation, and most importantly, increased susceptibility to osteosarcoma.

Another approach to studying the functions of RECQL4 was to use cell line models to avoid the complexities of animal models or to study targets whose disruption may not be viable in animal models. Such studies have variously used RTS patient cells (Jin et al., 2008; Lee et al., 2018; Schurman et al., 2009), engineered knock-in RECQL4 mutants (Kohzaki et al., 2012), or exogenous RECQL4 knockdown and/or overexpression systems (Lu et al., 2016; Singh et al., 2010). However, each of these approaches also has its own disadvantages. Studies using engineered RECQL4 mutant cell lines or exogenous RECQL4 overexpression/knockdown did not reflect clinically relevant changes and engineering mutant cell lines was often a laborious and time-consuming process. On the other hand, studies of RTS patient-derived cells must confront the challenges of maintaining cells that are often difficult to culture and to

manipulate. Furthermore, the vast majority of RTS patients have been identified as *RECQL4* compound heterozygotes, making dissections of structure-function relationships between individual *RECQL4* mutations and their effects difficult.

With the recent advances in targeted genome editing using CRISPR/Cas9 a new approach with much higher efficiency than those previously available is now possible. By simultaneously expressing a custom guide RNA targeted to a genomic region of interest, the Cas9 protein, and supplying a short exogenous homologous repair template (the ssODN), the bacterial immune defence system CRISPR/Cas9 can be harnessed to instead seek out the targeted region in the host genome, induce a specific DNA DSB at that location, and trigger the host's endogenous repair processes to modify the target sequence based on the supplied ssODN template. This enables rapid, inexpensive, and highly efficient genomic editing in a way that has not been possible before (Cho et al., 2013; Cong et al., 2013; Jinek et al., 2013; Mali et al., 2013; Ran et al., 2013; Wiedenheft et al., 2012).

To better study the effects of a clinically relevant *RECQL4* mutation in the context of RTS, CRISPR/Cas9 gene editing was used to knock-in a *RECQL4* mutation previously identified in RTS patients. The mutation chosen was the *RECQL4* c.2269C>T mutation, a putative nonsense mutation predicted to truncate the RECQL4 protein in exon 14 which is also commonly identified in literature as "Mut-2" (Kitao et al., 1999a). This mutation was chosen for two main reasons. First, it is one of the most prevalent *RECQL4* mutations identified in RTS patients, especially among RTS patients diagnosed with osteosarcoma (Siitonen et al., 2008). Second, at least one RTS patient homozygous for *RECQL4* c.2269C>T has been reported, which indicates viability of and relevance for a homozygous cell line model (Wang et al., 2003).

HEK293 was chosen as the target cell line for several reasons. HEK293 is a commonly used cell line—including in previous studies of RECQL4—which may facilitate comparison of

study results with previously published data (Chi et al., 2012; Lu et al., 2016; Mo et al., 2018; Ohlenschläger et al., 2012; Park et al., 2006; Petkovic et al., 2005; Stepanenko and Dmitrenko, 2015; Yokoyama et al., 2019). HEK293, despite its complex karyotype, is diploid at the *RECQL4* locus and has been reported to be karyotypically stable under normal maintenance conditions (Bylund et al., 2004; Lin et al., 2014; Stepanenko and Dmitrenko, 2015). And finally, HEK293 is easy to maintain and to experimentally manipulate.

As expected, the resulting CRISPR/Cas9-edited *RECQL4* Mut-2 containing cell lines showed a complete loss of wild-type RECQL4. Additionally, overall RECQL4 protein levels were also markedly decreased. Rather than the predicted truncation effect of the *RECQL4* c.2269C>T nonsense mutation, however, the majority of the *RECQL4* Mut-2 cell lines actually expressed increased levels of an alternatively spliced transcript of RECQL4. This transcript partially rescued the expected protein truncation by skipping the exonic region containing the premature stop codon, a novel and unforeseen outcome of the *RECQL4* Mut-2 mutation. Finally, next generation DNA and RNA sequencing revealed that these cell line models are, in fact, hemizygous for the targeted mutation, giving an in-depth look into the fidelity and outcomes of the CRISPR/Cas9 gene editing process. In summary, the cell lines described in this chapter are viable models which recapitulate the genetic and protein level findings associated with *RECQL4* mutation in Type II RTS patients (Colombo et al., 2014; De et al., 2012; Gupta et al., 2014; Petkovic et al., 2005; Siitonen et al., 2008; Werner et al., 2006; Yin et al., 2004; Yokoyama et al., 2019). They will be useful for further studies of clinically relevant RECQL4 structure-function relationships in the context of Type II RTS (see Chapter 3).

2.2 Materials and Methods

2.2.1 Cell Culture

HEK293 (ATCC) was cultured in DMEM (ThermoFisher), with 4.5mg/ml glucose and L-glutamine, supplemented by 10% foetal bovine serum (ThermoFisher) and 100U/ml Penicillin-Streptomycin (ThermoFisher).

Healthy donor and RTS patient fibroblasts were obtained from the Coriell Institute for Medical Research and, with the exception of AG18371, maintained in EMEM, with EBSS and L-glutamine (Lonza), supplemented by 15% FBS and 100U/ml Pen-Strep. AG18371 fibroblasts were maintained in MEM Alpha, with L-glutamine, ribonucleosides, and deoxyribonucleosides (ThermoFisher), supplemented by 15% FBS and 100U/ml Pen-Strep.

2.2.2 CRISPR/Cas9 Editing of RECQL4

CRISPR/Cas9 editing of *RECQL4* was carried out as described previously (Ran et al., 2013) and adapted by MiYoung Lee (University of Cambridge). Principal steps are briefly outlined below.

Constructs and Cloning

sgRNA was designed using the Zhang Lab online sgRNA design tool (crispr.mit.edu) and a 250bp context sequence flanking the mutation site (hg38, Chr8:144,513,288-537). The candidate sgRNA with the highest score whose target sequence included the Mut-2 mutation site (hg38, Chr8:144,513,412) was chosen and forward and reverse oligos were ordered from Integrated DNA Technologies (IDT).

Name	Sequence, 5'-3'
Mut2_sg1F	CACCGGTACAGCGAGCCTTCATGC
Mut2_sg1R	AAACGCATGAAGGCTCGCTGTACC
U6-Fwd	GAGGGCCTATTTCCCATGATTCC

The sgRNA oligo pair was phosphorylated using T4 PNK (NEB) at 37°C for 30 minutes and annealed at 95°C for 5min followed by a 5°C/min ramp down to 25°C. The annealed sgRNA was cloned into PX459 with FastDigest BbsI (ThermoFisher) and T7 Ligase (NEB). The ligation reaction was treated with Plasmid-Safe exonuclease (Lucigen) before transformation. Successful insertion was confirmed via Sanger sequencing using the U6-Fwd primer. pSpCas9(BB)-2A-Puro (PX459) was a gift from Feng Zhang (Addgene plasmid #48139; http://n2t.net/addgene:48139; RRID:Addgene_48139).

The cloned PX459-Mut2 sgRNA construct was based on the V1.0 PX459 backbone which contained a R166H mutation in the puromycin resistance gene that was reported to decrease its efficacy. Therefore, the original puromycin gene was replaced with the puromycin gene from pLVX-TetOne-Puro (Clontech) to generate PX459 v2.5. The puromycin gene insert was amplified with the primer set Puro1F and Puro2R using the Herculase II Fusion DNA Polymerase (Agilent). The PX459 backbone without the puromycin gene was amplified with the primer set Puro1R and Puro2F, also using the Herculase II Fusion DNA Polymerase. The two fragments were then ligated using the In-Fusion HD Cloning Kit (TaKaRa).

Name	Sequence, 5'-3'
Puro1F	GTACAAGCCCACGGTGCGCCTC
Puro2R	CACCGGGCTTGCGGGTCATG
Puro1R	GAGGCGCACCGTGGGCTTGTAC
Puro2F	CATGACCCGCAAGCCCGGTG

The CRISPR/Cas9 HDR template (Mut2_ssODN_NEW2) was designed as a 181bp sense ssODN comprising 90bp homology arms on either side of the target mutation site and the target mutation itself and synthesised as a PAGE-purified ultramer (IDT) (hg38, Chr8:144,513,322-502).

Name	Sequence, 5'-3'
Mut2_ssODN_NEW2	CATCTGCCTGTCTTCCCCAAAGGTCGTGCCCCCAAAACCACAG CCGAGGCCTACCACGCGGGCATGTGCAGCCGGGAACGGCGG CGGGTATAGCGAGCCTTCATGCAGGGCCAGTTGCGGGTGGTG GTGGCCACGGTGGCCTTTGGGATGGGGCTGGACCGGCCAGAT GTGCGGGCTGTGC

CRISPR/Cas9 Genome Editing

HEK293 cells were plated in 6-well plates at 70-90% confluency the day before transfection and co-transfected with 1.2µg PX459-sgRNA construct and 2.4µl 10µM ssODN using Lipofectamine 2000 (ThermoFisher). The transfected cells were selected with 2µg/ml puromycin (ThermoFisher) for 3 days and then replated into 96-well plates at a density of 0.5 cells/well. Colonies were isolated starting at 2 weeks for further screening.

2.2.3 Sanger Sequencing

Genomic DNA was isolated from cultured cells using QuickExtract DNA Extraction Solution (Lucigen) according to manufacturer's protocol. 5µl of gDNA template was used to amplify an 968bp amplicon flanking the CRISPR/Cas9 target region (hg38, Chr8:144,512,798-144,513,765) using Herculase II Fusion DNA Polymerase with 3% DMSO (Agilent) and the primer set Mut2_F4 and RTS2 2R8.

Name	Sequence, 5'-3'
Mut2_F4	ACACGCCGACCCCTCCTCACTC
RTS2 2R8	CGCGGGGACAGCCCCTCCAC

The PCR product was purified using the DNA Clean & Concentrator ZR-96 kit (Zymo Research). The purified product was Sanger sequenced with the Mut2_F4 primer and BigDye v3.1 by the NIH CCR Genomic Core. The electropherograms were analysed in SnapGene (GSL Biotech) to determine mutation status at the target site.

2.2.4 Western Blot

2.2.4a Lysate Sample Preparation

Cultured cells were trypsinised and washed once with cold PBS. Cell pellets were lysed in ice cold RIPA buffer (50mM Tris pH8.0, 0.5% sodium deoxycholate, 0.1% SDS, 150mM NaCl, 2mM EDTA, 1% Triton X-100) supplemented with 1mM PMSF, 1X Halt Protease Inhibitor Cocktail (ThermoFisher), and 500U Benzonase (Millipore). The lysates were sonicated for 5s at 30% power and cleared of debris by centrifugation.

The lysates were quantified by Pierce BCA Protein Assay Kit (ThermoFisher) using the manufacturer's microplate procedure and read on a BMG FluoStar Optima plate reader in absorbance mode with 570nm excitation filter. 120µg of protein lysate were diluted in a total volume of 40µl with ice cold RIPA buffer supplemented with 1mM PMSF, 1X Halt Protease Inhibitor Cocktail (ThermoFisher), 1X NuPAGE LDS Sample buffer (ThermoFisher), and 20mM DTT. The sample was denatured at 100°C for 10 minutes and then centrifuged at max speed for 1min.

2.2.4b SDS-PAGE

60ug each of lysate samples were run via SDS-PAGE on NuPAGE Bis-Tris 4-12% mini/midi protein gels in 1X MOPS running buffer (ThermoFisher) at 150V/200V for 55 minutes. The samples were then transferred at 20V/1.5 hours onto a 0.45µm PVDF membrane (Millipore) using a Novex semi-dry blotter in 2X NuPAGE Transfer Buffer supplemented with 10% methanol and 1X NuPAGE Antioxidant (ThermoFisher).

2.2.4c Immunoblotting

Post-transfer, the membrane was blocked in 5% BSA (Fisher Scientific) in TBS-0.1% Tween20 (TBST) for 1 hour at room temperature. The membrane was then incubated overnight at 4°C (RECQL4) or 1 hour at room temperature (β-actin) with anti-RECQ4 (1:1000,

Cell Signaling #2814) or anti-β-actin-HRP (C4, 1:10,000, Santa Cruz sc-47778 HRP) antibodies diluted in blocking solution. Blots were washed 3X with TBST and RECQL4 blots were incubated for 1 hour at room temperature with anti-rabbit IgG-HRP secondary antibody (1:2000, Cell Signaling #7074). The blots were then washed 3X with TBST before treatment with SuperSignal West Femto ECL (RECQL4) or SuperSignal West Pico PLUS ECL (β-actin) (ThermoFisher) and imaged with Bio-Rad ChemiDoc imaging system. Images were quantified using FIJI.

Table 2.1 Western blot primary and secondary antibodies and their dilutions

Target	Primary	Secondary	ECL
RECQL4	Anti-RECQL4 (Cell Signaling #2814, 1:1000)	Anti-Rabbit IgG HRP (Cell Signaling #7074, 1:2000)	SuperSignal West Femto
β-actin	Anti-β-actin HRP (Clone C4, Santa Cruz sc-47778 HRP, 1:10,000)		SuperSignal West Pico PLUS

A total of nine commercially available anti-RECQL4 antibodies (see table below) were tested via western blot using whole cell lysates from parental HEK293. Cell Signaling #2814 yielded the best results when considering both sensitivity and specificity. Due to the generally low RECQL4 abundance in HEK293 and its derivatives, the much more sensitive SuperSignal West Femto ECL was used as standard protocol despite increased non-specific signal.

Table 2.2 RECQL4 antibodies tested by western blot and dilutions used

Tested Anti-RECQL4 Antibody	Dilution
ABBIOTEC #200164	1:500
Abcam #ab192375	1:500, 1:1000
Atlas #HPA025821	1:250, 1:500
Cell Signaling #2814	1:1000, 1:2000
LSBio #LS-C340948	1:1000
LSBio #LS-C409066	1:1000
NovoPro #114676	1:1000, 1:3000
Novus Biologicals #25470002	1:1000, 1:2000
Santa Cruz (N-17) #sc-16924	1:500

2.2.5 RNAi Knockdown

ON-TARGETplus siRNAs for RECQL4 were obtained from Dharmacon, resuspended according to manufacturer's protocol in 1X siRNA buffer (60mM KCl, 6mM HEPES pH7.5, 0.2mM $MgCl_2$) to a concentration of 20µM, and pooled in equimolar proportions to obtain a final concentration of 20µM.

ON-TARGETplus Non-targeting Control siRNA and ON-TARGETplus UPF1 siRNA were obtained from Dharmacon as pools and resuspended in 1X siRNA buffer to a final concentration of 50µM (sequences listed below).

Cells were plated in 6-well plates at a confluency of 50-70% a day before transfection. Cells were transfected with 80pmol siRNA per well using Lipofectamine RNAiMAX according to manufacturer's protocol. Cells were harvested for analysis 72 hours post-transfection.

Table 2.3 siRNA sequences and target regions

Name	Sequence	Target Region
siRECQL4 #1 (J-010559-05)	CCUAGAUCCUGGCUGGUUA	RECQL4 Exon 5
siRECQL4 #2 (J-010559-06)	GCGACCACCUAUACCCAUU	RECQL4 Exon 16
siRECQL4 #3 (J-010559-07)	GAAAAUACCUGCACCUGAG	RECQL4 Exon 21
siRECQL4 #4 (J-010559-08)	CAAUACAGCUUACCGUACA	RECQL4 Exon 15
siUPF1 Pool	CAGCGGAUCGUGUGAAGAA, CAAGGUCCCUGAUAAUUAU, GCAGCCACAUUGUAAAUCA, GCUCGCAGACUCUCACUUU	UPF1 Exon 16, UPF1 Exon 8, UPF1 Exon 4, UPF1 Exon 1
Non-targeting Pool	UGGUUUACAUGUCGACUAA, UGGUUUACAUGUUGUGUGA, UGGUUUACAUGUUUUCUGA, UGGUUUACAUGUUUUCCUA	N/A

2.2.6 Quantitative RT-PCR (RT-qPCR)

Total RNA was isolated from cells. Briefly, cells were trypsinised, pelleted, and lysed in TriZOL reagent (ThermoFisher). Total RNA was extracted with chloroform and precipitated with 70% ethanol. The precipitated RNA was bound to RNeasy mini columns (Qiagen), digested with DNase I on column (Qiagen), washed and eluted. The purified total RNA was quantified by Nanodrop.

100ng of total RNA was added to each 20µl RT-qPCR reaction along with a TaqMan assay for RECQL4 (FAM) and GAPDH endogenous control (VIC) (target sequences in table below). The RT-qPCR reactions were run using TaqMan RNA-to-C_T *1-Step* Kit (ThermoFisher) according to manufacturer instructions on a Bio-Rad CFX96 Real-Time qPCR system. Samples were generally run in at least triplicate.

Analysis of RT-qPCR data was done using the $\Delta\Delta C_t$ method by normalising C_t values from individual wells first to the duplexed GAPDH endogenous control to obtain ΔC_t values.

ΔC_t values for replicate sample wells were then averaged and normalised to the average parental HEK293 ΔC_t value to obtain $\Delta\Delta C_t$ values. Fold changes were then calculated using the following formula:

$$Fold\ Change = 2^{-\Delta\Delta C_t}$$

The results were plotted in Graphpad Prism.

Table 2.4 TaqMan assay information

TaqMan Assay ID	Forward Primer	Probe	Reverse Primer	Notes
Hs00171627_m1		TGGATGACCAGGTGTCTGGCCTGCC (FAM)		RECQL4 Exon 9-10 Junction
Hs00355454_g1		AGCCCCAGGGCGAAGACCTGCGAGA (FAM)		RECQL4 Exon 14-15 Canonical Splice Junction
APAACYZ (RTS_DEL14_NEW) [Custom Assay]	CATGTGCAGCCGGGAAC	CGGCGGCGGGGCGAAGACCTGCGAG (FAM)	TCGGCGTGCACATGTCT	RECQL4 Exon 14-15 Alternate Splice Junction
Hs99999905_m1		GGGCGCCTGGTCACCAGGGCTGCTT (VIC)		GAPDH Exon 2-3 Junction

2.2.7 Enrichment of Sequencing Libraries with Custom RECQL4 Baits

Total RNA and genomic DNA for sequencing was prepared from cultured cells using method described above (total RNA) and DNeasy Blood & Tissue Kit (genomic DNA) according to manufacturer's protocols (Qiagen). Next generation sequencing libraries were then prepared from total RNA using SMARTer Stranded Total RNA-Seq Kit – Pico Input Mammalian (TaKaRa) and from genomic DNA using KAPA HyperPrep Kit (Roche).

BAC construct containing *RECQL4* genomic sequence (hg19, Chr8:145,676,350-145,800,825) was obtained from BACPAC Genomics, Inc. (Clone CTD-2230H11) as template for bait preparation. Briefly, the BAC was sheared on a Covaris S2 to a mean size of 400bps (Duty Cycle=5%, Intensity=5, Cycles/Burst=200, Time=55s). The fragments were end-repaired and A-tailed using KAPA Hyper Prep Kit (Roche). BBt adapter (Ishihara et al., 2017, see note below) was ligated and adapter-conjugated fragments were purified with SPRIselect beads (Beckman Coulter) before amplification with T7/T3 primer set (see below) using KAPA HiFi HotStart Ready Mix (Roche). The amplified bait library was purified twice with SPRIselect beads before RNA bait preparation.

Name	Sequence, 5'-3'
BBt Adapter Sense	P-CCCTATAGTGAGTCGTATTAGATCATTAACCCTCACTAAAGGGAT
BBt Adapter Anti-sense	P-TCCCTTTAGTGAGGGTTAATGATCTAATACGACTCACTATAGGGT
T7 Primer	TAATACGACTCACTATAGGG
T3 Primer	GCAATTAACCCTCACTAAAGG

Note: BBt adapter was made by combining sense and anti-sense oligos in equimolar proportions and annealing through denaturing in 1L boiling water for 5 minutes followed by cooling to room temperature on the bench.

Biotinylated RNA capture baits were prepared from the purified bait library by in vitro transcription using the MAXIscript T7 Transcription Kit (ThermoFisher) with biotin-14-CTP analogue (ThermoFisher) replacing 40% of the unlabelled CTP. The transcribed products were purified with TURBO DNase digestion and NucAway Spin Columns (ThermoFisher) and SUPERase In RNase Inhibitor (ThermoFisher) was added.

Separately, total RNA and genomic DNA sequencing libraries were combined with blocking mix consisting of human Cot-1 DNA, salmon sperm DNA (ThermoFisher), and xGen Universal Blockers – TS Mix (IDT) and concentrated in a speed-vac. The blocked library mixtures were then denatured and combined with the RNA baits mixture. The library/bait mixtures were finally combined with hybridisation buffer (10X SSPE, 10mM EDTA, 10X Denhardt's buffer, 2.5% SDS) and incubated for 48 hours at 65 °C.

The hybridised libraries were bound to Dynabead Streptavidin T1 magnetic beads (ThermoFisher), washed, and minimally PCR amplified (9 cycles) on bead with KAPA HiFi HotStart Ready Mix and Illumina library amplification primers. The enriched and amplified libraries were then purified twice with SPRIselect beads. The purified libraries were finally sequenced by paired-end sequencing on Illumina MiSeq instruments using Illumina MiSeq Micro Kit v2 (300 cycles).

2.2.8 Next generation DNA-Seq and RNA-Seq analysis

Analyses of next generation DNA and RNA sequencing data were performed by Jack Zhu (NIH) and Yonghong Wang (NIH). The analysis pipelines used are briefly outlined below and diagrammed in Figure 2.1.

2.2.8a DNA sequencing

Processing and analysis of DNA sequencing data was performed on one of two locally available Linux clusters using home-brew, snakemake-based pipelines that mainly followed

the Best Practices workflow recommended by the Broad Institute (http://www.broadinstitute.org/gatk/guide/best-practices, Figure 2.1A) (DePristo et al., 2011; Köster and Rahmann, 2012). Briefly, raw sequencing reads were mapped to human genome build 19 (Hg19) by Burrows-Wheeler Aligner (BWA, version 0.7.17). This was followed by local realignment using the GATK suite (version 3.8.1). Duplicated reads were then marked using Picard tools (version 2.17.11, http://broadinstitute.github.io/picard/) (Li and Durbin, 2009; McKenna et al., 2010).

Somatic variant calling on paired mutant-parental HEK293 samples was done using either the standalone Strelka somatic variant caller (version 2.9.0) or a tandem Manta (version 1.6.0) /Strelka (Chen et al., 2015; Saunders et al., 2012). Structural variants were identified by Delly (version 0.8.1) and BRASS (version 6.1.2) using paired mutant-parental HEK293 samples (Nik-Zainal et al., 2016; Rausch et al., 2012).

The SnpEff (version 4.3t), ANNOVAR (version 2018-04-16), and VariantAnnotator (GATK version 3.8.1) were then used to annotate and predict the effects of variants with multiple annotation databases, including dbNSFP (version Hg19-dbNSFP2.9.1), dbSNP (NCBI, build 147), ESP6500 (NHLBI Exome Sequencing Project, ESP6500SI-V2-SSA137.updatedRsIds.snps_indels.vcf), etc. (Cingolani et al., 2012; Liu et al., 2013; Wang et al., 2010).

2.2.8b RNA sequencing

The RNA sequencing data processing pipeline is shown in Figure 2.1B. Briefly, RNA sequencing reads were aligned to human genome build 19 (Hg19) using STAR aligner (version 2.6.1c) (Dobin et al., 2012). STAR-Fusion (version 1.5.0) was used to detect fusion transcript reads (Haas et al., 2017). Salmon RNA-seq software (version 0.14.1) was applied directly to the FASTQ files to generate transcripts-per-million (TPM) quantification for genes and

transcript models included in the GENCODE release 25 at the gene and transcript levels (Harrow et al., 2012; Patro et al., 2017). Sashimi plots were generated using Integrative Genomics Viewer (version 2.8.0) (Robinson et al., 2011, 2017; Thorvaldsdóttir et al., 2012).

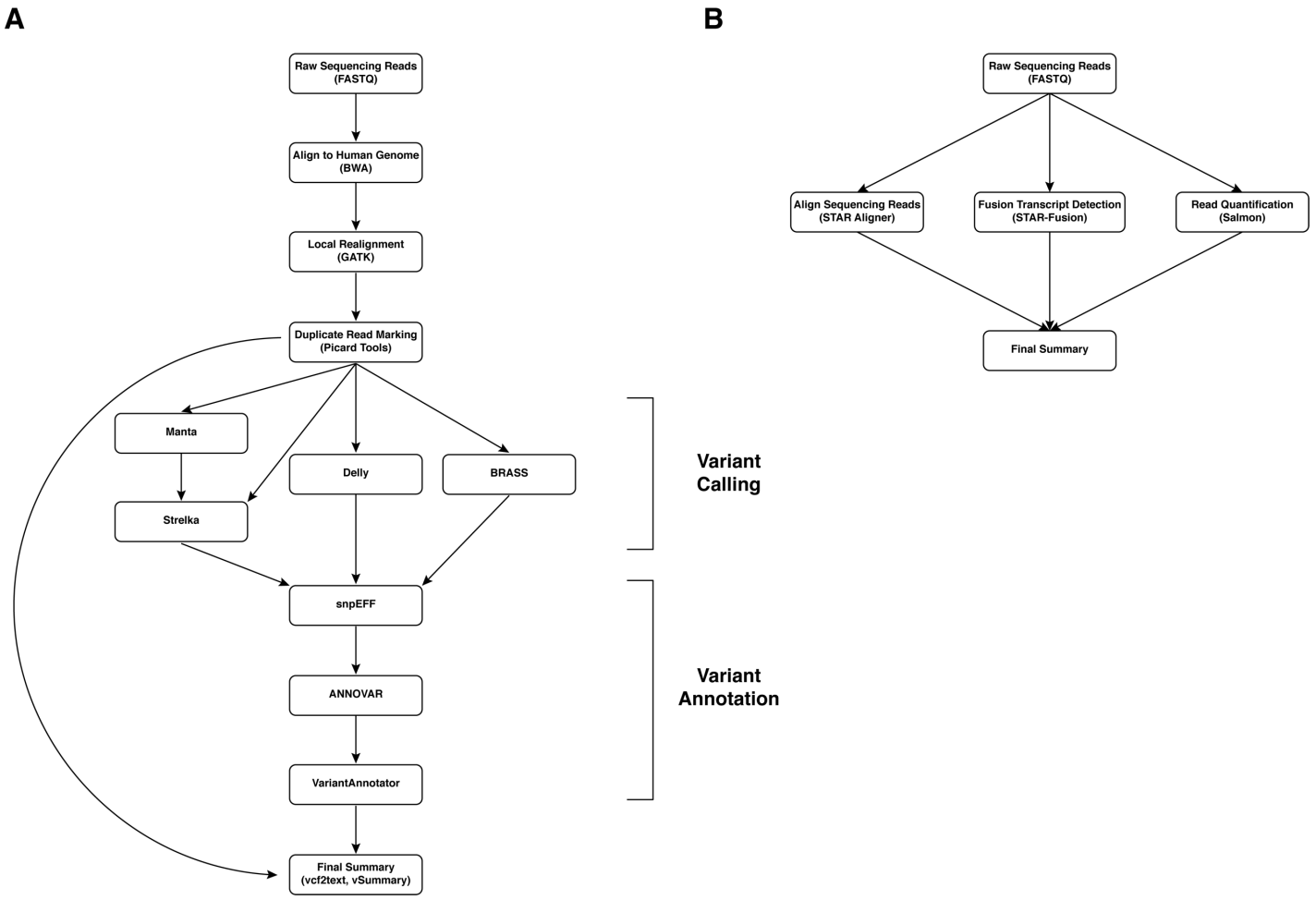

Figure 2.1 Next generation sequencing data analysis pipelines

A. Analysis pipeline for DNA-Seq data. Details discussed above in Section 2.2.8a.

B. Analysis pipeline for RNA-Seq data. Details discussed above in section 2.2.8b.

Figure was adapted from original made by Jack Zhu (NIH)

2.3 Results

2.3.1 CRISPR/Cas9 editing of RECQL4 in HEK293

Based on a 250bp genomic context sequence (hg38, Chr8:144,513,288-144,513,537) flanking the target mutation (*RECQL4* c.2269C>T), a list of candidate sgRNAs was designed using the online tool from the Zhang Lab (crispr.mit.edu, Ran et al., 2013a). The final sgRNA was chosen from the candidate list using the criteria that the target sequence must include the target mutation site (hg38, Chr8:144,513,412) while maximising the "on-target" score. The sgRNA chosen targeted a 20bp region (hg38, Chr8:144,513,397-144,513,416) with the Cas9 induced DNA DSB occurring between Chr8:144,513,399-144,513:400 (hg38). Using this sgRNA, the CRISPR/Cas9 process generated 69 viable single-cell clones for further screening.

2.3.2 Sanger sequencing identifies potential candidates

Initial screening of single-cell clones was performed using Sanger sequencing of PCR products from the region containing the targeted mutation and identified four candidates which were potentially homozygous for *RECQL4* c.2269C>T at the targeted position (Figure 2.2C). Sanger sequencing results for parental HEK293 (wild-type *RECQL4*) and potential heterozygous clones (2.57 and 2.68) are also shown for comparison (Figure 2.2A and B).

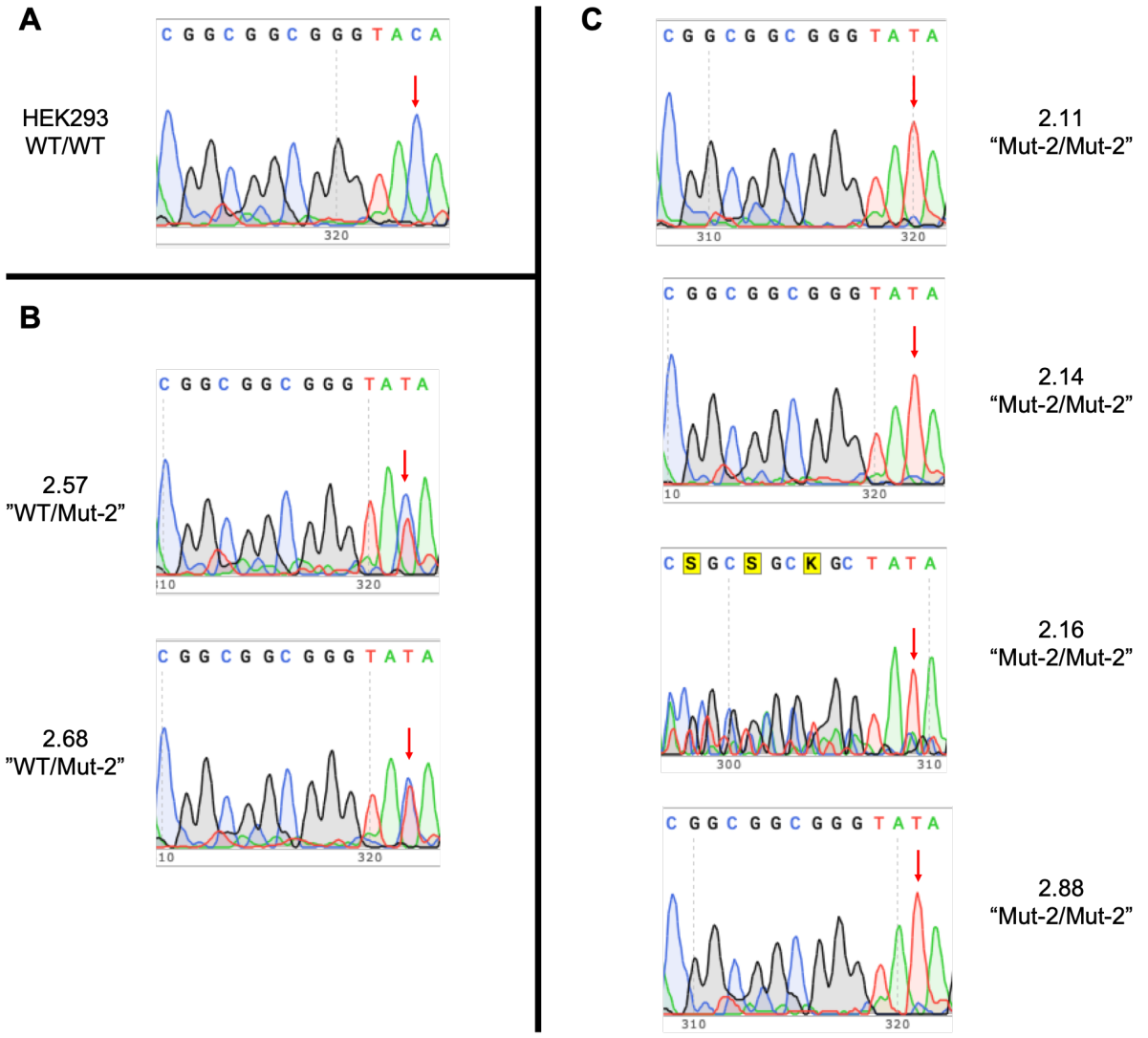

Figure 2.2 Sanger Sequencing of isolated single cell clones
Electropherograms from Sanger sequencing of parental HEK293 (Part A) candidate Mut-2 clones (Parts B-C). The target site of interest is located at Chr8:144,513,412 (hg38, red arrows). The desired mutation is a C>T transition.

A. Parental HEK293 showing wild-type *RECQL4* (C) at the target site.
B. Clones showing WT/Mut-2 heterozygosity (C/T) at the target site.
C. Clones showing only Mut-2 sequence (T) at the target site, potentially homozygous.

All data shown are representative of at least 2 independent experiments except for HEK293 WT/WT (Part A) and 2.16 (Part C) which were each sequenced once.

2.3.3 RECQL4 protein levels in candidate Mut-2 clones

The CRISPR/Cas9 gene editing process produced several candidate single-cell clones carrying either heterozygous or homozygous *RECQL4* Mut-2 mutations (Figure 2.2C). The next step was to determine whether predicted changes in the RECQL4 protein could be detected both qualitatively and quantitatively in the candidate clones bearing homozygous *RECQL4* Mut-2 mutations. Whole cell lysates isolated from parental HEK293 cells and the four putative "homozygous" Mut-2 *RECQL4* clones were blotted for RECQL4 using western blot (Figure 2.3A). If these cell lines were truly homozygous for the knock-in *RECQL4* Mut-2 mutation, then no signal matching the size of wild-type RECQL4 (150kDa) and the concurrent appearance of a smaller truncation RECQL4 protein product (predicted 82kDa) would be expected in the corresponding samples.

Indeed, the wild-type RECQL4 protein (150kDa) completely disappeared in all four of the candidate clones as anticipated (Figure 2.3A, red arrow). When average RECQL4 expression in the candidate clones relative to parental HEK293 was compared to a panel of RTS patient fibroblasts (AG03587, AG05013, AG18371) and healthy donor fibroblasts (GM00010, GM01603, GM05386, GM06166), the average reduction in wild-type RECLQ4 signal was comparable, though none of the RTS patient samples is known to harbour the *RECQL4* Mut-2 mutation (Figure 2.3B and C, see table below for RTS patient sample information). Surprisingly, however, a faint residual band could be observed running slightly smaller than the wild-type RECQL4 band (slightly lower than 150kDa). In order to ascertain whether this residual band was a non-specific artefact of this particular RECQL4 antibody, RNAi-mediated knockdown of RECQL4 on the parental HEK293 and the four candidate clones was done using a pool of four RECQL4 siRNAs and the results compared with cells treated with a pool of non-targeting siRNA (Figure 2.3D). As positive control, substantial knockdown of

wild-type RECQL4 could be observed in parental HEK293 treated with siRECQL4 as compared to non-targeting siRNA treated cells. In the candidate clones, the previously seen residual band also decreased in intensity with siRECQL4-mediated knockdown, suggesting that this band represented a form of RECQL4.

Table 2.5 RTS patient sample information

RTS Patient Sample	Sex	Age (at sampling)	Known *RECQL4* Mutations
AG03587	Male	7	Unknown
AG05013	Male	10	g.2492del2 ("Mut-3"*), IVS12AS G>T ("Mut-4"*)
AG18371	Male	12	g.2746del11

*Mutation nomenclature is from Kitao et al., 1999a

A

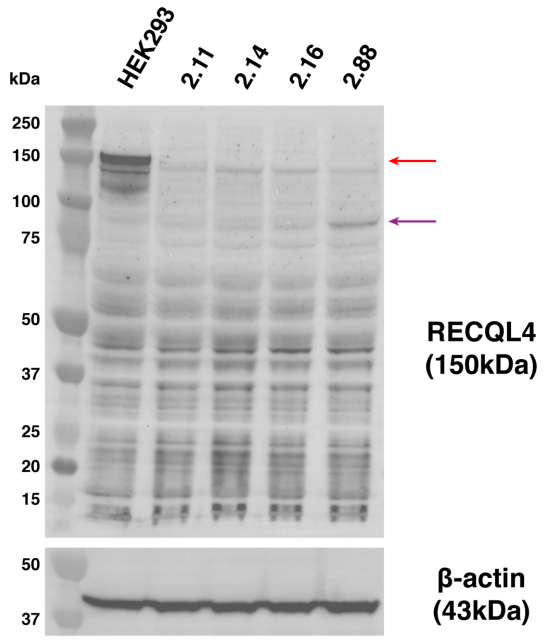
HEK293
2.11
2.14
2.16
2.88
kDa
250
150
100
75
50
37
25
20
15
50
37
RECQL4
(150kDa)
β-actin
(43kDa)

B

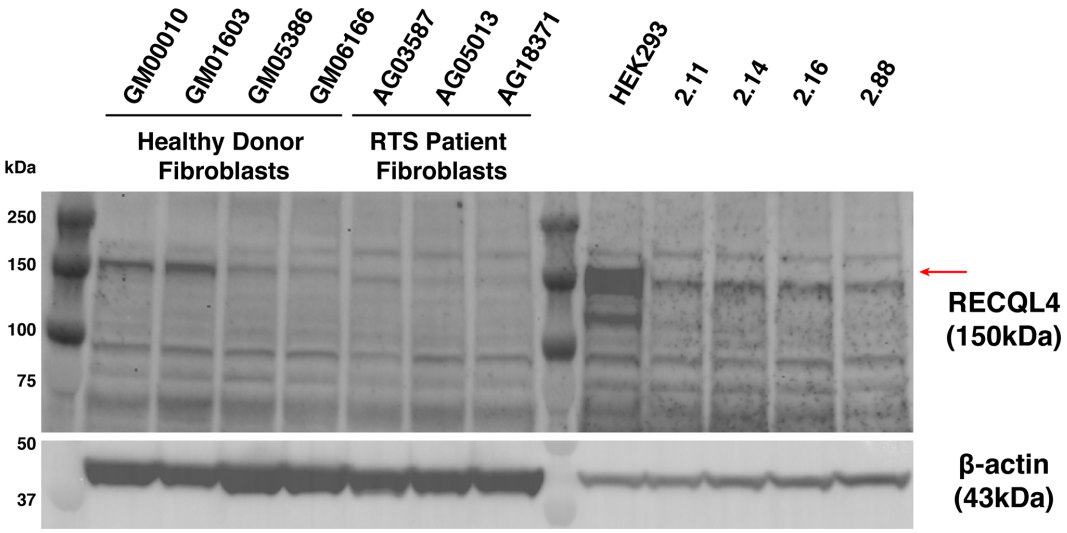
GM00010
GM01603
GM05386
GM06166
AG03587
AG05013
AG18371
HEK293
2.11
2.14
2.16
2.88
Healthy Donor
Fibroblasts
RTS Patient
Fibroblasts
kDa
250
150
100
75
50
37
RECQL4
(150kDa)
β-actin
(43kDa)

C

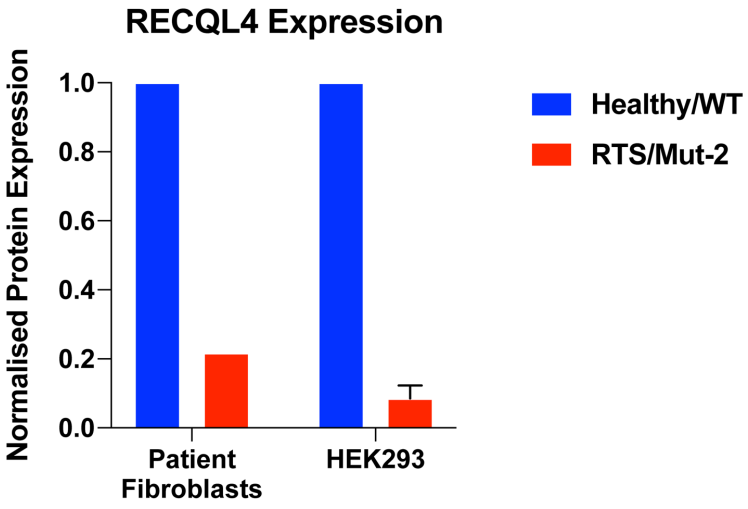
RECQL4 Expression
Normalised Protein Expression
1.0
0.8
0.6
0.4
0.2
0.0
Patient
Fibroblasts
HEK293
Healthy/WT
RTS/Mut-2

D

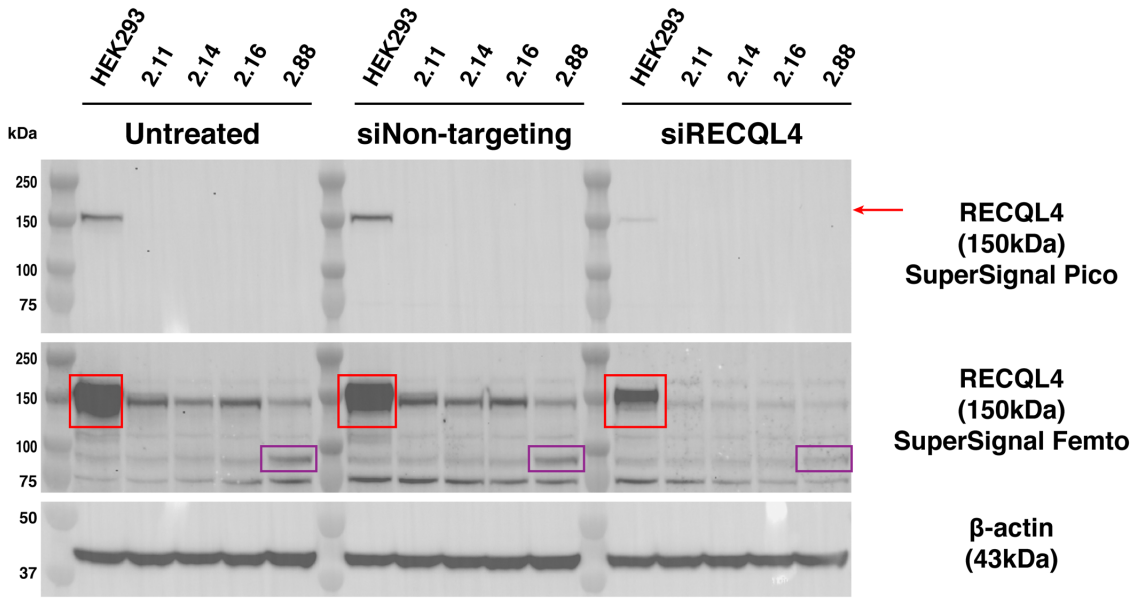
HEK293
2.11
2.14
2.16
2.88
HEK293
2.11
2.14
2.16
2.88
HEK293
2.11
2.14
2.16
2.88
kDa
Untreated
siNon-targeting
siRECQL4
250
150
100
75
RECQL4
(150kDa)
SuperSignal Pico
250
150
100
75
RECQL4
(150kDa)
SuperSignal Femto
50
37
β-actin
(43kDa)

E

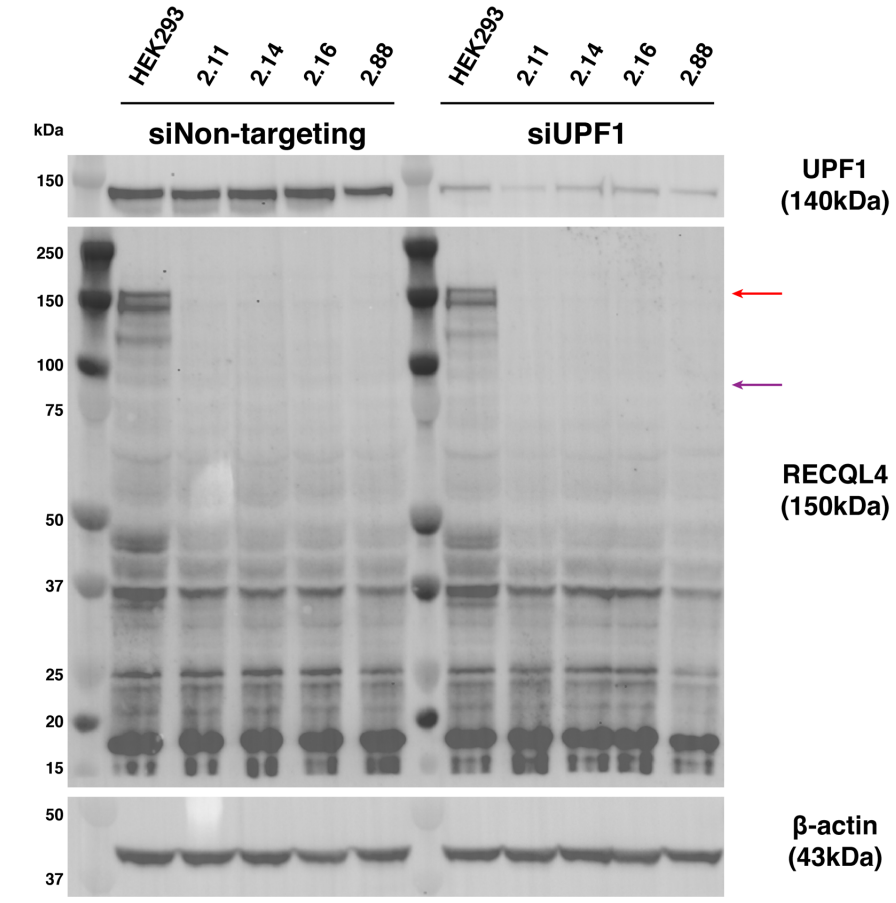
HEK293
2.11
2.14
2.16
2.88
HEK293
2.11
2.14
2.16
2.88
kDa
siNon-targeting
siUPF1
150
UPF1
(140kDa)
250
150
100
75
50
37
25
20
15
RECQL4
(150kDa)
50
37
β-actin
(43kDa)

Figure 2.3 Western blot analyses of candidate *RECQL4* Mut-2 clones
Red arrows show the position of the wild-type RECQL4 (150kDa). Purple arrows show the approximate predicted position of the RECQL4 Mut-2 truncation product (82kDa).

A. RECQL4 blot of parental HEK293 and candidate Mut-2 clones. Lanes with candidate Mut-2 clones show lack of wild-type RECQL4 (red arrow) along with a faint residual band slightly below the wild-type RECQL4 band. Western blot shown is representative of at least ten independent experiments.
B. Comparison of RECQL4 expression in a panel of healthy donor and RTS patient fibroblasts with that of parental HEK293 and candidate Mut-2 clones show similar magnitudes of reduction in RECQL4 abundance. Data for RTS patient samples match those previous reported by others (De et al., 2012; Gupta et al., 2014; Petkovic et al., 2005; Werner et al., 2006; Yin et al., 2004; Yokoyama et al., 2019). Data for Mut-2 clones is representative of what was observed from multiple experiments. Western blot shown is from one experiment.
C. Quantification of average RECQL4 expression in Part B by densitometry analysis show similar magnitudes of reduction in RECQL4 abundance. Quantification in RTS patient samples was done on one blot from one experiment. Quantification of Mut-2 clones was done on blots from five independent experiments and is typical of what is seen. Error bars show standard error of the mean (SEM).
D. RNAi in parental HEK293 and candidate Mut-2 clones using non-targeting siRNA pool and RECQL4 siRNA pool. Known wild-type RECQL4 (red boxes, parental HEK293), the residual band previously seen in Parts A-B (next to red boxes, slightly lower than 150kDa in the candidate Mut-2 clones), and the possible RECQL4 Mut2 truncation product (purple boxes) all show decreased intensity with siRECQL4 but not with siNon-targeting pool. RECQL4 blot shown is of an identical region on the same blot developed in succession with two difference ECL reagents. SuperSignal Femto is the increased-sensitivity femtogram-level ECL reagent. Red box indicates wild-type RECQL4. Purple box indicates possible RECQL4 Mut-2 truncation product. Western blot shown is representative of at least four independent experiments.
E. RNAi in parental HEK293 and candidate Mut-2 clones using siNon-targeting pool or siUPF1 pool shows no increased signal in the region (75kDa-100kDa) predicted to contain the RECQL4 Mut-2 truncation product when UPF1 expression is decreased. Western blot shown is representative of two independent experiments.

In addition to the disappearance of the wild-type RECQL4 band on western blot, the appearance of a truncated protein product (82kDa) was also expected as the *RECQL4* c.2269C>T Mut-2 mutation is predicted to be a nonsense truncation mutation. However, in the majority of the candidate clones (2.11, 2.14, 2.16), no new band was observed at the predicted size of 82kDa. The sole exception was in candidate clone 2.88 where a stronger band was present at the expected location (Figure 2.3A, purple arrow). While it might be reasonable to expect the truncation RECQL4 product to be present in all four candidate clones, siRNA-mediated knockdown was nevertheless performed to determine whether this band, which was only present in candidate clone 2.88, could be a form of RECQL4 as well. As shown, the band in question did respond to siRECQL4-mediated knockdown, which suggested that it might be the truncation product from the *RECQL4* Mut-2 mutation (Figure 2.3D).

Nonsense mediated decay (NMD) is a cellular mRNA surveillance mechanism whereby mRNA transcripts containing premature terminal codons in the reading frame are targeted for degradation (Hug et al., 2016). Since Mut-2 is predicted to be a nonsense mutation, transcripts containing Mut-2 could be targets for NMD and its inhibition by knockdown of UPF1, a protein required for NMD, could result in increased abundance of the predicted RECQL4 truncation product (Figure 2.3E). Treatment of candidate Mut-2 clones with siUPF1 failed to show any detectable increase in RECQL4 signal in the approximate size range predicted (82kDa) for the truncation product.

2.3.4 Residual RECQL4 band is an alternative splicing variant

While siRNA-mediated RECQL4 knockdown clearly suggested that the residual protein band seen running slightly smaller than wild-type RECQL4 (150kDa) on western blot of the candidate Mut-2 is a form of RECQL4 protein (Figure 2.3D), it is unclear what the origin of this form is given that the only predicted product from a Mut-2 *RECQL4* allele is a truncated protein

of 82kDa. However, a recent study of Type II RTS in a family of patients uncovered a very similar putative nonsense mutation (*RECQL4* c.2272C>T) located close to the site of the Mut-2 mutation (*RECQL4* c.2269C>T) (Colombo et al., 2014). Colombo and colleagues observed that rather than solely expressing the RECQL4 transcript containing the truncation mutation, cells from these RTS patients also upregulated usage of an alternate splice site in exon 14 upstream of the mutation. This alternative splicing resulted in the skipping of the last 198bp of RECQL4 exon 14 and consequently an in-frame deletion of the last 66aa in exon 14. More importantly, the deleted region also contained the nonsense mutation, thus removing its effects and enabling the production of a non-truncated protein of almost the same size as wild-type RECQL4. Colombo and colleagues attributed these changes in RECQL4 splicing to the disruption by the c.2272C>T mutation of predicted recognition motifs for the exonic splicing enhancers SF2/ASF and SRp55 (Figure 2.4A).

Due to the similar nature and location of the target Mut-2 mutation to the one found by Colombo, et al. and the fact that it also lies within the predicted exonic splicing enhancer recognition motifs (Figure 2.4A), the same splicing alterations could be happening in the candidate Mut-2 clones. To test this, a custom TaqMan assay spanning the predicted alternate splicing junction was designed. Pre-designed TaqMan assays that spanned the canonically spliced exon 14-15 junction and the exon 9-10 junction outside the affect region were also obtained. RT-qPCR was performed on total RNA isolated from parental HEK293 and the four candidate Mut-2 clones (Figure 2.4B). The exon 9-10 spanning TaqMan assay showed that in the candidate Mut-2 clones, RECQL4 transcript levels remained relatively unchanged to slightly decreased (Figure 2.4B, far left). However, transcripts containing the canonically spliced exon 14-15 junction (and thus the target Mut-2 mutation) had decreased by at least 50% in all candidate clones (Figure 2.4B, centre left). When assayed for the alternatively

spliced transcript (ΔEx14), large increases of the alternate transcript were seen in three of the four candidate clones (2.11, 2.14, 2.16) (Figure 2.4B, centre right). Candidate clone 2.88 alone seemed to show a decrease in the alternate transcript as well as the canonical transcript (Figure 2.4B, centre two panels). Finally, the ratio of the alternate transcript to the canonical transcript was examined as a control for variation between cell lines (Figure 2.4B, far right). The candidate clones which upregulated the alternate transcript had very much increased ratios of alternative-to-canonical transcripts. The exception was candidate clone 2.88 whose ratio was similar to that of parental HEK293. The RT-qPCR results confirmed the hypothesis that one of the major effects of the *RECQL4* c.2269C>T Mut-2 mutation was to upregulate an alternative splice variant that skips over the premature stop codon rather than production of the predicted truncation RECQL4 product.

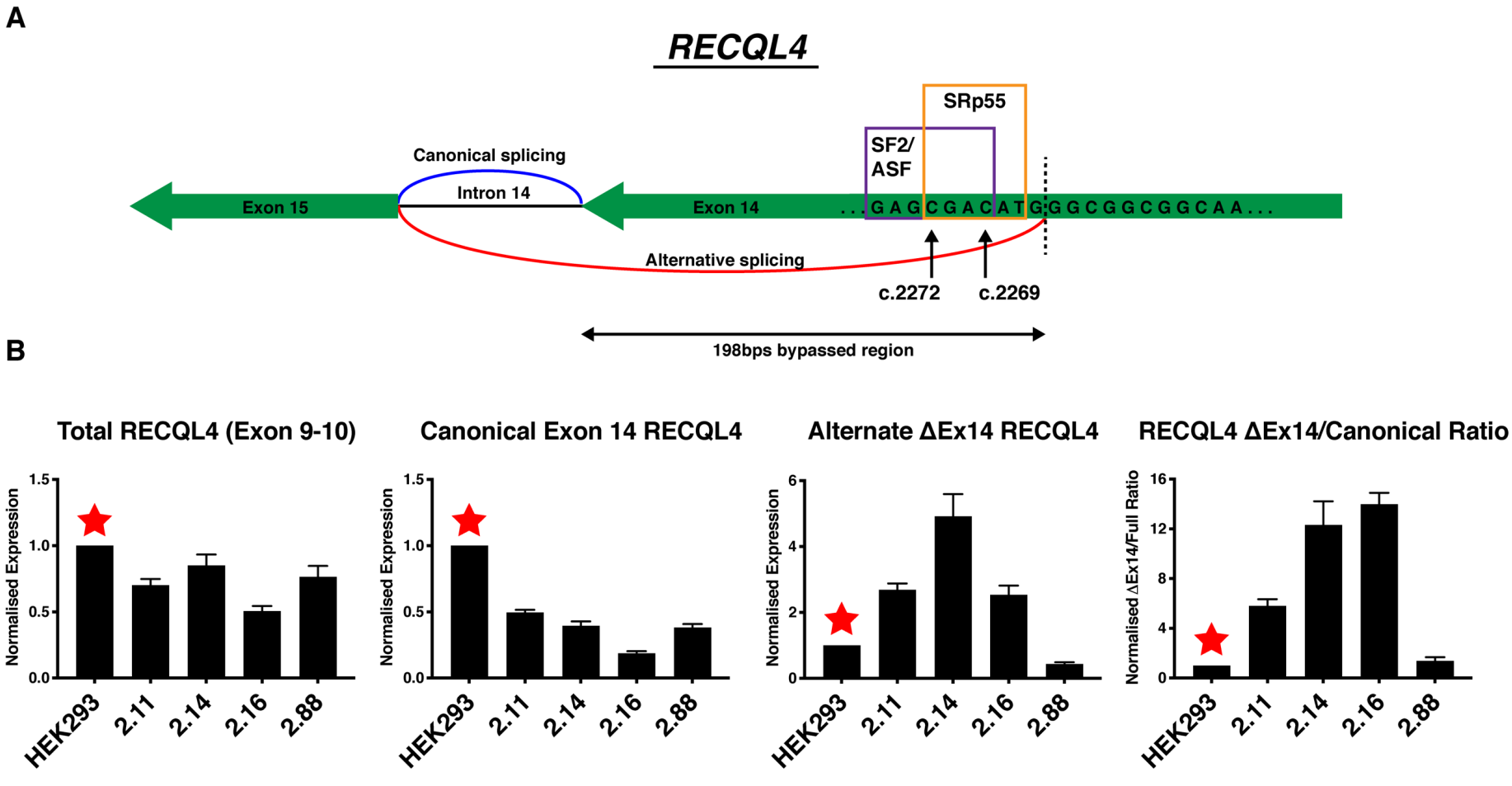
A
RECQL4
SRp55
SF2/
ASF
Canonical splicing
Intron 14
Exon 15
Exon 14
. . . G A G C G A C A T G G C G G C G G C A A . . .
Alternative splicing
c.2272
c.2269
198bps bypassed region
B
Total RECQL4 (Exon 9-10)
Canonical Exon 14 RECQL4
Alternate ΔEx14 RECQL4
RECQL4 ΔEx14/Canonical Ratio
Normalised Expression
Normalised ΔEx14/Full Ratio
HEK293
2.11
2.14
2.16
2.88

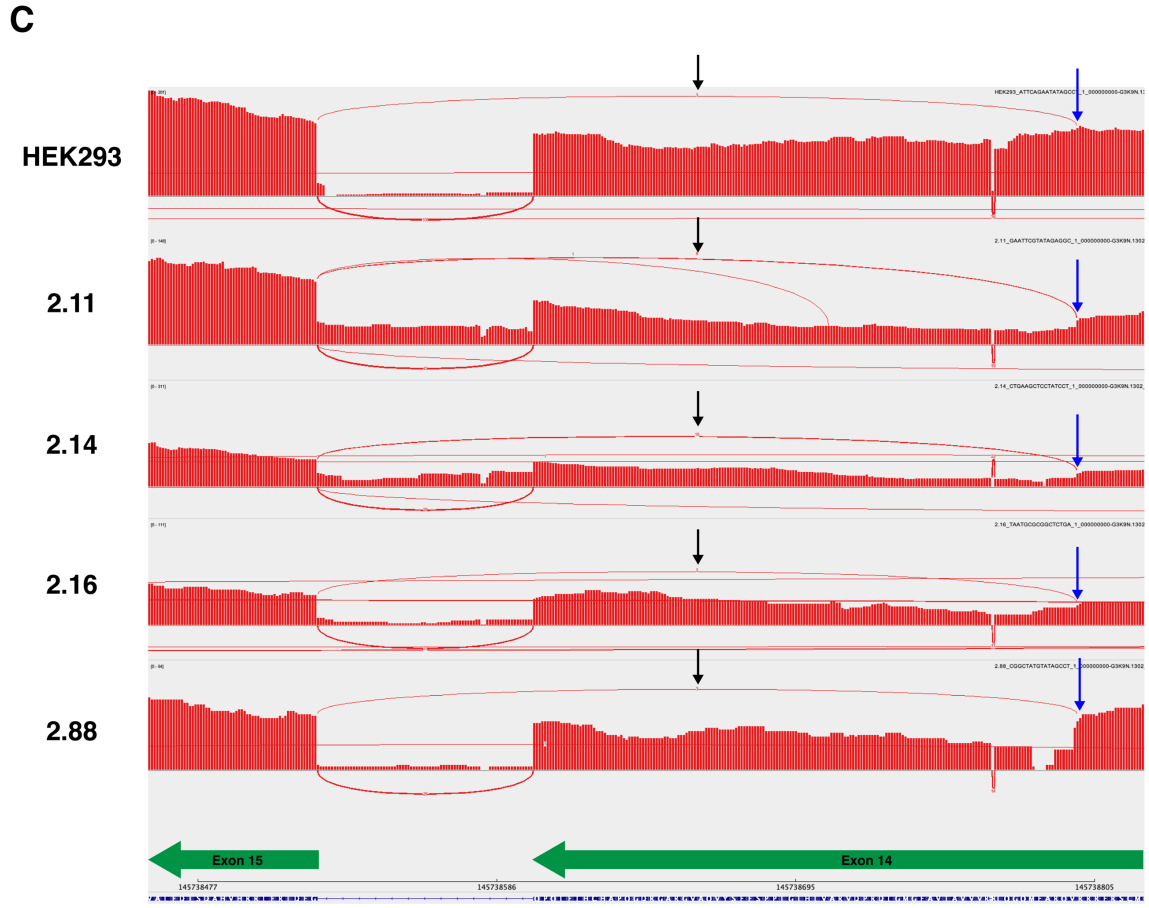

Figure 2.4 The alternative splicing of the *RECQL4* exon 14-15 junction

A. Alternative splicing in *RECQL4* exon 14 as identified in study by Colombo, *et al*. Predicted recognition motifs for SF2/ASF and SRp55 are outlined in purple and orange boxes respectively, with nucleotide positions of mutations shown. The target Mut-2 mutation is c.2269C>T, the location of the mutation originally found by Colombo and colleagues is denoted by c.2272 as reference. The green arrows indicate direction of transcription. (Figure adapted from Colombo, *et al.*, 2014).

B. RT-qPCR TaqMan assays for RECQL4 transcripts in parental HEK293 and the candidate Mut-2 clones, all data are normalised to that of the respective parental HEK293 in each plot (red stars). Total RECQL4 transcript levels as indicated by exon 9-10 TaqMan assay are slightly decreased in the candidate Mut-2 clones (far left). Levels of RECQL4 transcripts canonically spliced at exon 14-15 are decreased by at least 50% in all candidate Mut-2 clones compared to parental HEK293 (centre left). All candidate Mut-2 clones except for 2.88 show increases in levels of RECQL4 transcripts using the alternative exon 14-15 splice site (centre right). The ratios of alternatively spliced to canonically spliced RECQL4 transcript are greatly increased in all candidate Mut-2 clones except in 2.88 (far right). Data presented is the average from at least five independent experiments. Error bars show SEM.

C. RNA-Seq of parental HEK293 and candidate Mut-2 clones confirms the presence and structure of the alternatively spliced RECQL4 transcript as shown in the sashimi plots. The blue arrows indicate the location of the alternative splice site while the black arrows indicate the alternative splicing event. The green arrows at the bottom indicate direction of transcription. Data shown is typical of two independent sequencing experiments.

2.3.5 Next generation sequencing reveals the state of the RECQL4 locus in candidate clones

After screening the four candidate Mut-2 clones via Sanger sequencing and assaying for RECQL4 protein level and transcript levels, the final confirmation of the status of these candidate clones came from in-depth studies of genomic DNA and total RNA using next generation sequencing.

The following work was performed by Robert Walker (NIH) with bioinformatic analyses performed by Jack Zhu (NIH) and Yonghong Wang (NIH). Next generation sequencing libraries were enriched for the *RECQL4* genomic region and transcripts via in vitro transcribed RNA baits spanning the region Chr8:145,676,350-145,800,825 (hg19) and sequenced on the Illumina MiSeq platform (see Methods Section 2.2.7 above).

Outlined below are the detailed structures of the *RECQL4* alleles and derivatives around the Mut-2 target region in each of the candidate clones as well as status of any associated RNA transcripts as verified using bioinformatic tools (see Methods Section 2.2.8 above) and manual curation. The structures of the *RECQL4* alleles and derivatives could only be definitively distinguished and elucidated in the regions where significant, dense, and/or small-scale variations existed—usually the region surrounding the Mut-2 target in this study. This is a technical limitation of the Illumina short-read sequencing technology coupled with the enrichment of the sequencing libraries during sample preparation (see Methods Section 2.2.7 above). Due to these two factors, isolated mutations and/or structural variations and those outside the region of enrichment generally cannot be attributed to specific alleles or derivatives and, in the latter case, are usually undetectable.

Clone 2.11 (Figure 2.5)

- One *RECQL4* allele contained the desired Mut-2 C>T mutation at position Chr8:145,738,796 (hg19) as well as a 1bp base T insertion at the sgRNA cut site between positions Chr8:145,738,783-784 (hg19).
- A second derivative consisted of a non-reciprocal translocation between the C-terminal portion of *WNT7A* and the C-terminal portion of *RECQL4*. The portion of *WNT7A* downstream and inclusive of position Chr3:13,878,176 (hg19) was joined with the portion of *RECQL4* downstream and inclusive of position Chr8:145,738,793 (hg19). There was an intervening 49bp sequence between the two arms of the translocation consisting of a 4bp random insertion and a 45bp inserted segment from the Cas9 gene from the PX459 CRISPR/Cas9 construct.
- A third *RECQL4* derivative showed deletion of the segment Chr8:145,738,784-793 (hg19) inclusive and its replacement with a series of short tandem duplications of mostly adjacent segments of the *RECQL4* gene along with repetitive genomic sequences of unknown origin. Within this replacement section, starting at the upstream end, there is a 69bp inverted duplication of Chr8:145,738,714-783 (hg19), followed by a 34bp duplication of Chr8:145,738,797-831 (hg19), followed by another non-inverted 69bp duplication of Chr8:145,738,714-783 (hg19). The segment ended with a section of repetitive genomic sequences of indeterminate origin and length with the downstream end joined back to the C-terminal portion of *RECQL4* at Chr8:145,738,783 (hg19).

Figure 2.5 indicates that the endpoints of the *RECQL4* fragment in Derivative 2 and 3 are uncertain. With the aforementioned caveats in mind, two lines of indirect evidence suggest that the C-terminal portion of *RECQL4* downstream of the sgRNA cut site is present in

its entirety in three copies, indicating duplication of at least that region (Figure 2.5). First, though Derivative 2 contains only C-terminal portions of *RECQL4* and *WNT7A* and thus is expected to be promoterless, one unique RNA sequencing read spanning the breakpoint was detected by RNA-Seq. It may be reasonable to speculate that this transcript was the product of transcription read-through from the adjacent *MFSD3* locus, which is transcribed in the direction opposite to that of *RECQL4*. This would imply that the region is intact on Derivative 2. Second, the lack of structural variation in the C-terminal portion of *RECQL4* in the genomic DNA sequencing data is strong evidence against the disruption of the C-terminal regions of *RECQL4* on any of the alleles or derivatives.

Since parental HEK293 is diploid at the *RECQL4* locus, one question raised by the presence of three copies of the C-terminal region of *RECQL4* is whether 2.11 is indeed a single-cell clone rather than a mixed cell population. To address this concern, candidate clone 2.11 was subcloned and genomic DNA and total RNA from 11 subclones were also sequenced. 10 of the 11 subclones were found to contain all three *RECQL4* alleles/derivatives, strongly supporting the conclusion that candidate 2.11 is a single-cell clone that contains a duplication of the C-terminal region of *RECQL4* downstream of the sgRNA cut site.

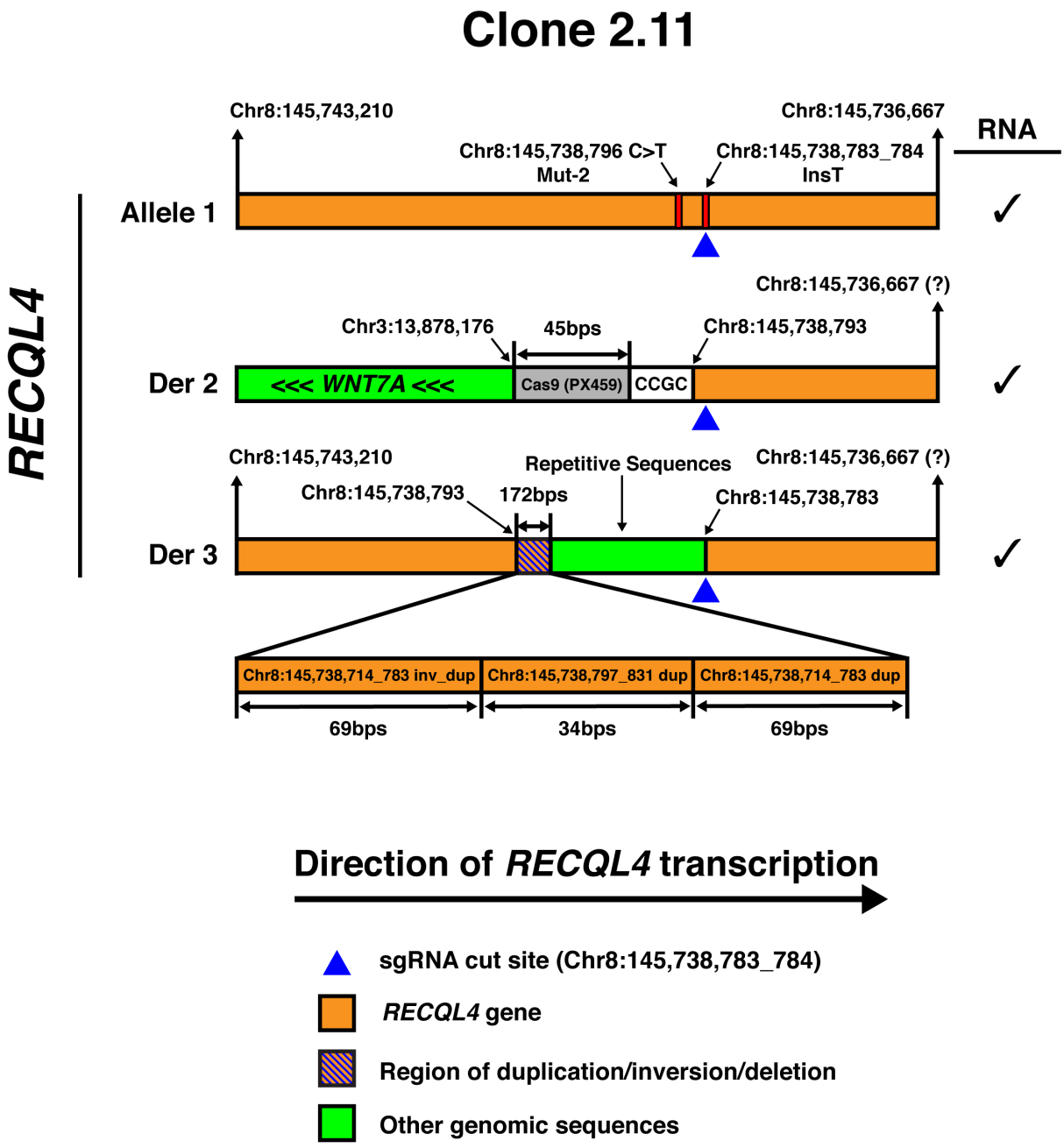

Figure 2.5 Genomic structure of candidate clone 2.11 at the *RECQL4* Mut-2 target site
Due to the orientation of the *RECQL4* gene on chromosome 8, it is shown with genome coordinates ***decreasing*** from left to right so that the direction of transcription is from left to right. (<<<) indicates the ordinary direction of transcription of the *WNT7A* gene fragment. Question marks (?) indicate uncertainty regarding the location of the end point of the fragment in question (see above). Check marks under RNA indicate whether RNA transcripts from the particular allele or derivative were found in RNA-Seq data. See detailed descriptions are above. Data is from two independent sequencing experiments.

Clone 2.14 (Figure 2.6)

- One *RECQL4* allele contained the desired Mut-2 C>T mutation at position Chr8:145,738,796 (hg19) as well as a 1bp base C deletion at position Chr8:145,738,788 (hg19).
- A second derivative consisted of a translocation of the N-terminal portion of the *RECQL4* gene with portions of the PX459 CRISPR/Cas9 construct. The breakpoint in the *RECQL4* gene was after position Chr8:145,738,802 (hg19). There was a 65bps intervening segment between the *RECQL4* arm and the PX459 arm which consisted of an inverted segment of the *RECQL4* gene from Chr8:145.738,714-779 (hg19). A 24bps segment of the *RECQL4* gene from Chr8:145,738,780-803 (hg19) had been deleted.
- A third derivative consisted of a translocation of the C-terminal portion of the *RECQL4* gene with the end of the q arm of chromosome 11. The breakpoint in chromosome 11 was located before Chr11:74,383,190 (hg19) and the breakpoint in *RECQL4* was found to be at the sgRNA cut site (hg19, Chr8:145,738,783_784).

While RNA-Seq data showed transcripts from all three allele/derivatives of *RECQL4* in candidate clone 2.14, the majority came from allele 1 with very few reads from Derivatives 2 and 3. Since the translocation partner of Derivative 3 is an intergenic region on Chr11, it is expected to be promoterless. RNA transcripts from this derivative may have come from transcription read-through from the adjacent *MFSD3* locus.

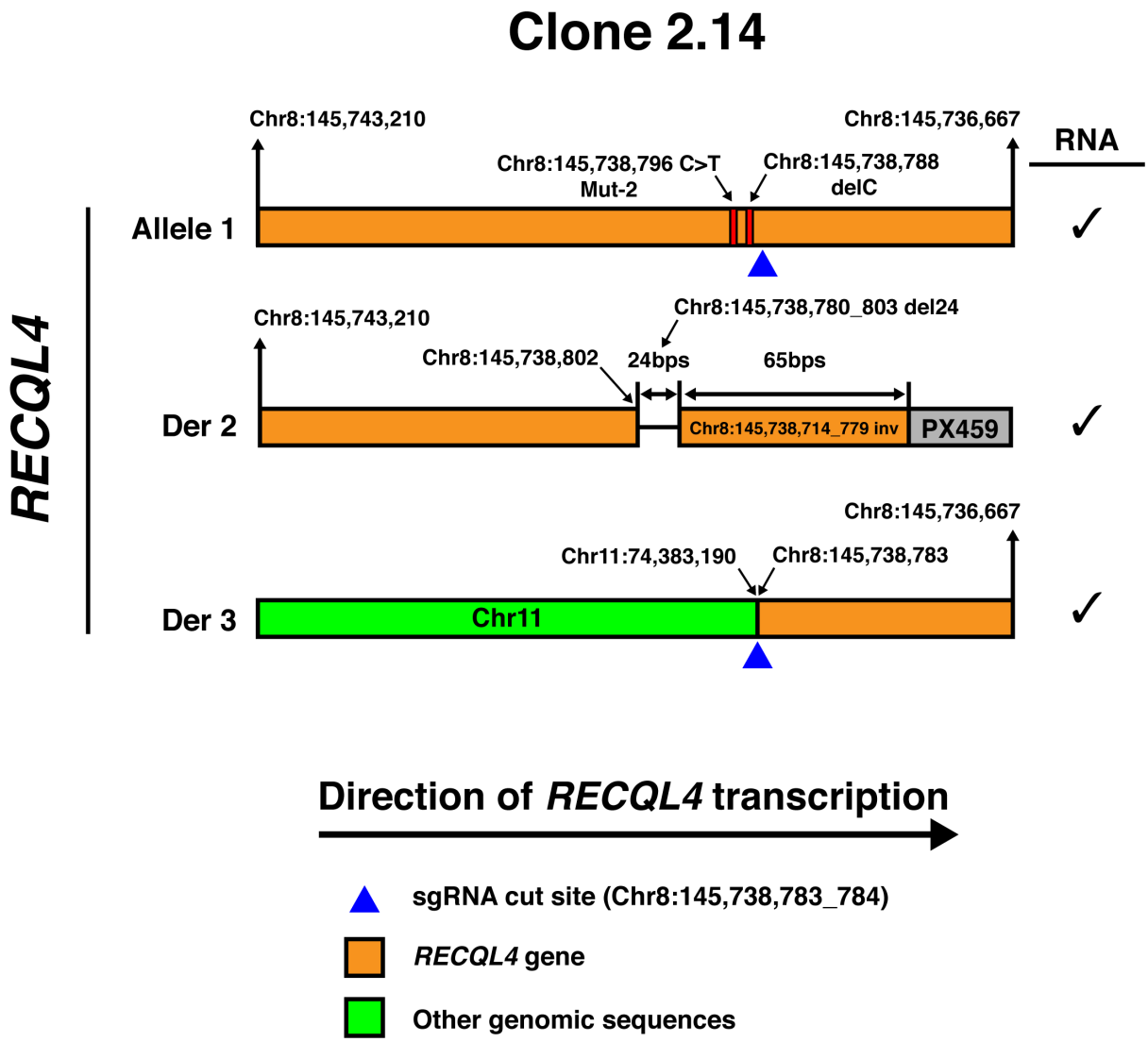

Figure 2.6 Genomic structure of candidate clone 2.14 at the *RECQL4* Mut-2 target site
Figure layout and notation are generally same as Figure 2.5 above. Where sgRNA cut site falls within a deleted region (Der 2), the corresponding notation has been omitted. (<<<) marks an inverted fragment of *RECQL4*. Detailed descriptions are above. Data is from two independent sequencing experiments.

Clone 2.16 (Figure 2.7)

- One *RECQL4* allele contained the desired Mut-2 C>T mutation at position Chr8:145,738,796 (hg19) as well as a 1bp base T insertion at the sgRNA cut site between positions Chr8:145,738,783-784 (hg19). The majority
- The second *RECQL4* allele contained a large deletion between intron 12 and intron 18 from Chr8:145,737,490-145,739,191 (hg19) inclusive. There was also a 1bp base T insertion at the breakpoint junction.

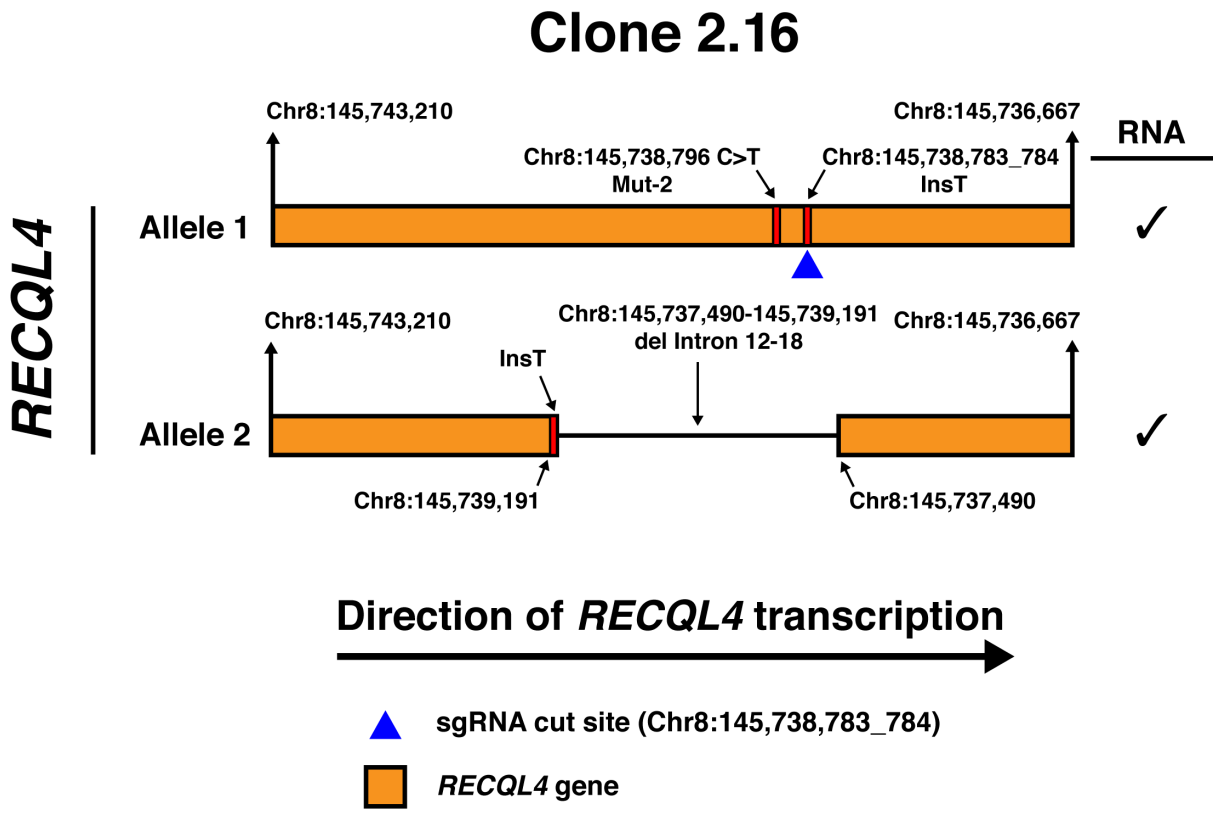

Figure 2.7 Genomic structure of candidate clone 2.16 at the *RECQL4* Mut-2 target site
Figure layout and notation are generally same as Figure 2.5 above. Detailed descriptions are above. Data is from two independent sequencing experiments.

Clone 2.88 (Figure 2.8)

- One *RECQL4* allele contained the desired Mut-2 C>T mutation at position Chr8:145,738,796 (hg19) as well as an 8bps deletion adjacent to the sgRNA cut site between positions Chr8:145,738,784-791 (hg19) inclusive.
- A derivative contained a translocation joining the N-terminal portion of the *RECQL4* gene with a portion of the PX459 CRISPR/Cas9 construct within the ampicillin resistance gene. The breakpoint in the *RECQL4* gene was located before Chr8:145,738,799 (hg19).
- A second derivative comprised a reciprocal translocation joining the C-terminal portion of the *RECQL4* gene also with a portion of the PX459 CRISPR/Cas9 construct. The breakpoint in the *RECQL4* gene was located after Chr8:145,738,685 (hg19).

In candidate 2.88, transcript from Derivative 2 accounted for almost half of the transcript reads mapped to the *RECQL4* locus at the Mut-2 target site, suggesting significant transcription activity from Derivative 2. This was likely because the C-terminal translocation partner on Derivative 2 was the N-terminal portion of the ampicillin resistance gene from the PX459 CRISPR/Cas9 construct. Therefore, most of the Derivative 2 transcripts sequenced may have come from transcription driven by the ampicillin resistance cassette promoter on the translocation partner and in the opposite direction of the normal transcription at the *RECQL4* locus. Transcripts from Derivative 3 were, once again, possibly due to transcription read-through from the adjacent *MFSD3* locus.

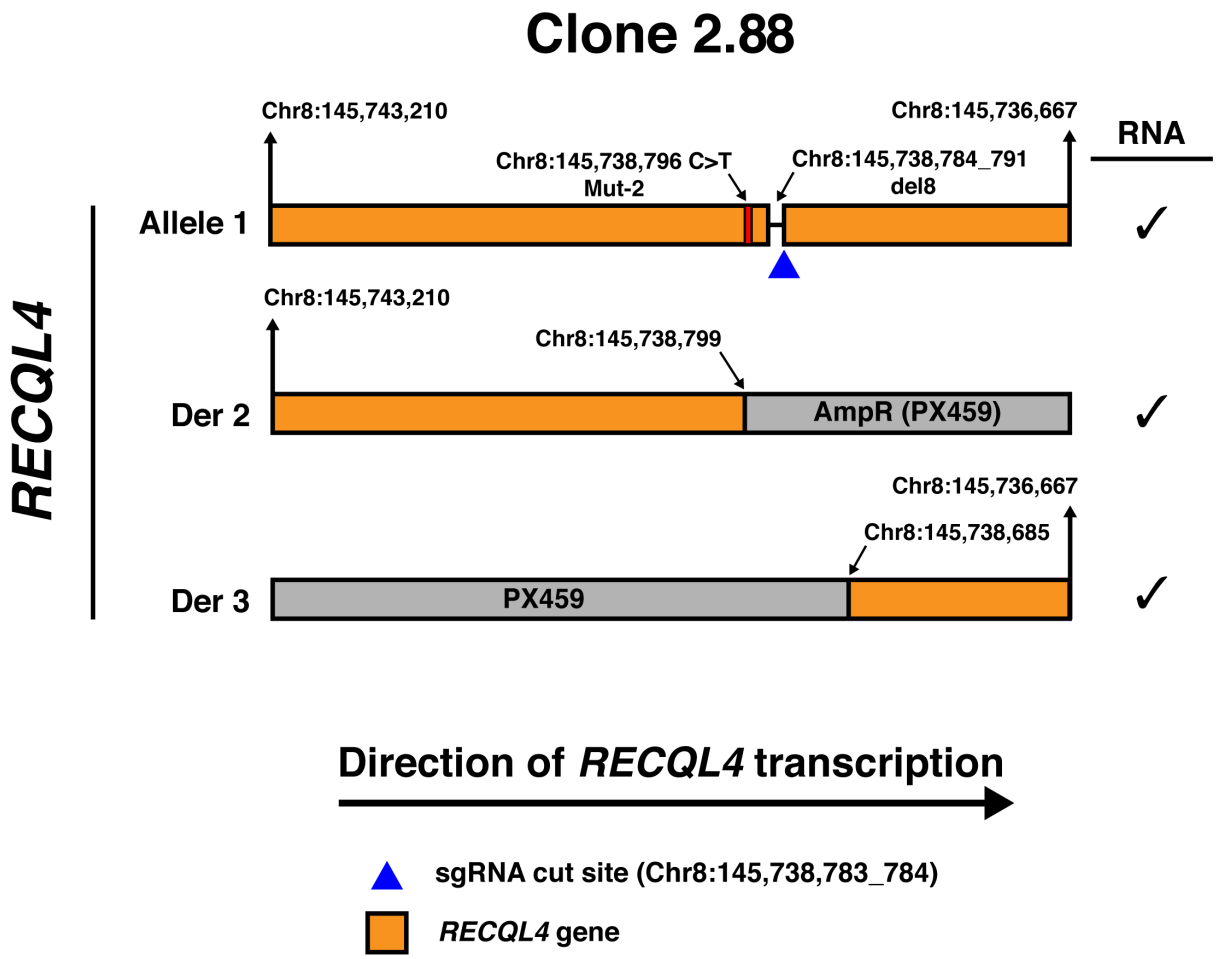

Figure 2.8 Genomic structure of candidate clone 2.88 at the *RECQL4* Mut-2 target site
Figure layout and notation are generally same as Figure 2.5 above. Detailed descriptions are above. Data is from two independent sequencing experiments.

These sequencing data illuminated several important insights in the Mut-2 candidate clones. First, in all four candidate clones, there was only one allele in each which bears the *RECQL4* Mut-2 target mutation. Furthermore, in each case, that Mut-2 bearing allele had a small indel mutation—usually a 1bp insertion or deletion (8bp deletion for clone 2.88)—downstream of the target site near the Cas9 targeted cut site (implications are further discussed below in Chapter 2 Section 2.4.1). Regarding the second *RECQL4* allele, in all cases, it had been disrupted by complex structural rearrangements such as long-range deletions, translocations, indels, and tandem duplications/inversions. Interestingly, several translocation partners appeared to be derived from the transiently transfected CRISPR/Cas9 construct (PX459) which was not linearised prior to transfection.

RNA-Seq of the candidate Mut-2 clones confirmed both the absence of wild-type RECQL4 transcript as well as the presence of both the canonically and the alternatively spliced RECQL4 transcripts seen in previous RT-qPCR TaqMan assays (Figure 2.4B and C). Despite the fact that the alternatively spliced transcript was more abundant in the Mut-2 clones as compared to parental HEK293, the canonically spliced transcript remained the most abundant form seen in absolute quantity. All forms and structural variants of *RECQL4* identified by DNA-Seq were also observed in the RNA as confirmation.

Overall, next generation sequencing of genomic DNA and total RNA provided definitive insights into the genomic structure of the candidate Mut-2 clones. Sequence data had shown that rather than homozygous clones as first believed, these Mut-2 candidates clones were, in actuality, functionally hemizygous *RECQL4* Mut-2 clones.

2.4 Discussion

2.4.1 Mut-2 clones are hemizygous for RECQL4 mutation

One of the original aims of the CRISPR/Cas9 gene editing was to generate homozygous knock-in of an RTS patient *RECQL4* mutation into a target cell line. Indeed, aside from the fact that it is one of the most prevalent RTS mutations, another reason that the *RECQL4* c.2269C>T Mut-2 was also originally chosen as the target mutation was because there were documented cases of RTS patients with homozygous *RECQL4* Mut-2 alleles, providing support for the technical feasibility of the endeavour (Siitonen et al., 2008; Wang et al., 2003).

The initial Sanger sequencing clone screens identified four candidate Mut-2 clones whose electropherograms showed only the desired C>T transition, which appeared to suggest Mut-2 homozygosity (Figure 2.2C). However, this conclusion was crucially based on an assumption of the degree of the fidelity of the CRISPR/Cas9 knock-in process, in particular, the assumption that the process would leave the *RECQL4* locus grossly intact post-repair. As further discussed below, more in-depth sequencing studies have subsequently revealed this assumption to be invalid in the case of the candidate Mut-2 clones.

Targeted next generation sequencing of the *RECQL4* locus in the candidate clones revealed two principal findings. First, there was only one *RECQL4* allele in each of the candidate clones which carried the desired c.2269C>T Mut-2 mutation. Furthermore, in all cases, that mutant allele also contained small indel mutations (1-8bps) around the sgRNA target site (Figure 2.5-8). Normally these mutations would be predicted to cause deleterious frameshifts that disrupt proper translation. However, in the case of these Mut-2 candidate clones, all mutations occurred downstream of the Mut-2 mutation—which results a premature terminal codon—and within the 198bps region that is skipped in the alternatively spliced transcript (see below). Thus, these indel mutations were predicted to have no

functional effect in either the canonically spliced RECQL4 transcript or the alternatively spliced variant and the *RECQL4* Mut-2 alleles on which they resided were still expected to be functionally equivalent to those found in patients with the *RECQL4* Mut-2 mutation.

The second finding was that in all candidate Mut-2 clones, the second *RECQL4* allele had been disrupted by complex structural rearrangements that severely disrupted the *RECQL4* gene. Most commonly, the *RECQL4* gene was involved in translocations with other chromosomes or with the exogenous transiently transfected PX459 CRISPR/Cas9 construct. Other structural variants also included large scale deletions and short-range inversion/duplications (Figure 2.5-7). While RNA-Seq identified transcripts from all these derivative fragments, most of them were not predicted to yield any viable protein product. It was possible that many of these transcripts might have resulted from transcription read-through from adjacent genes. Indeed, western blot for RECQL4 in these candidate clones failed to show any signal that could potentially be their protein product (see below, Figure 2.3A and D).

Overall, next generation sequencing revealed a much more complex genomic landscape at the *RECQL4* locus in the candidate Mut-2 clones than the initial Sanger sequencing-based screens had indicated. Contrary to initial expectations, the CRISPR/Cas9 editing of *RECQL4* was more error prone than anticipated, particularly in the non-Mut-2 bearing *RECQL4* derivatives in the candidate clones. These findings recalled a recent report that large scale disruptions frequently occurred as a result of Cas9 DNA DSB induction, though Kosicki and colleagues did not investigate CRISPR/Cas9 repair fidelity in the context of a targeted knock-in genomic edit with exogenously supplied repair template (Kosicki et al., 2018). Cas9-induced DNA DSBs are generally thought to be repaired through either NHEJ or HDR (homology-directed repair), with the latter being the error-free repair mechanism. For

precise targeted gene editing such as that attempted in this study, however, HDR is essential and therefore NHEJ activity should be minimised (Liu et al., 2019; Ran et al., 2013; Ryu et al., 2019). Sequencing results from the candidate Mut-2 clones suggested that HDR efficiency during the CRISPR/Cas9 process was sub-optimal. Future work using CRISPR/Cas9 gene editing to study *RECQL4* mutations should consider the various available methods to inhibit or suppress NHEJ-mediated repair in favour of HDR (Liu et al., 2019).

Given the aforementioned findings from next generation sequencing of the candidate Mut-2 clones, they could reasonably be considered to be functionally hemizygous for *RECQL4* Mut-2 rather than the homozygous *RECQL4* Mut-2 cells lines they were originally thought to be. Despite this, however, these clones still presented a viable model for further study for two reasons. First, the impetus behind the original proposal to generate these CRISPR/Cas9 edited Mut-2 clones was to obtain model systems that only expressed the mutant RECQL4 protein product of interest. In this respect, these Mut-2 clones fulfilled that criterion by only possessing one functional *RECQL4* allele—the one that carried the Mut-2 mutation.

Secondly, the hemizygous status of these Mut-2 clones likely better modelled the spectrum of genotypes seen in RTS patients. In particular, the majority of reported RTS patients were compound heterozygous for *RECQL4* mutations. Furthermore, among those who carried at least one *RECQL4* Mut-2 allele (and thus bore the closest resemblance to the Mut-2 clones), most patients possessed a second *RECQL4* allele that contained a more severe mutation disrupting translation much earlier in the protein (Siitonen et al., 2008). A good example of this scenario was a patient (FCP-129) who was found to have the c.1573delT ("Mut-5") frameshift truncation in exon 9 on the second *RECQL4* allele (Wang et al., 2003). Transcript containing this mutation had been reported as undetectable in RTS patients (Beghini et al., 2003). Additionally, multiple attempts as part of this study to generate clones

bearing only the *RECQL4* Mut-5 mutation were also unsuccessful (data not shown), suggesting that this mutation, by itself, may be incompatible with cell viability. Thus, Mut-5 could be thought of as a severely deleterious, possibly functionally null *RECQL4* mutation. A significant number of reported RTS patients with the Mut-2 allele had, as the second *RECQL4* allele, similar truncation or frameshift mutations in exon 9 (Siitonen et al., 2008). Based on these observations, it might be reasonable, therefore, to consider the hemizygous Mut-2 clones as functional models for RTS patients such as these.

2.4.2 RECQL4 expression is drastically altered in Mut-2 clones

Having determined the genomic status of the Mut-2 candidate clones at the *RECQL4* Mut-2 target site, the effects of these genetic changes on RECQL4 protein expression and abundance were then examined. First and foremost, the presence of wild-type RECQL4 (150kDa) disappeared completely in the candidate Mut-2 clones as expected (Figure 2.3A). However, more surprising was the fact that overall RECQL4 abundance was greatly reduced in the Mut-2 clones. This finding established that much lower levels of RECQL4 expression was sufficient to sustain the essential functions of RECQL4 in cell viability (Abe et al., 2011; Sangrithi et al., 2005). This was previously proposed by Abe, *et al.*, who reported that after induction of conditional *RECQL4* knockout in chicken DT40 cells, normal rates of cell proliferation continued to be observed for at least 1-2 more divisions during which RECQL4 levels were shown to be close to the threshold of detection if not below (Abe et al., 2011). The next chapter will investigate whether or how this reduction in RECQL4 expression impacts the growth characteristics of these clones.

RECQL4 protein levels in the Mut-2 candidate clones relative to parental HEK293 were also compared to levels found in RTS patient cells. Previous studies have shown that RTS patient fibroblasts had greatly reduced, or even undetectable, levels of RECQL4 (De et al.,

2012; Gupta et al., 2014; Petkovic et al., 2005; Werner et al., 2006; Yin et al., 2004; Yokoyama et al., 2019). The same reduction in RECQL4 levels in these RTS patient fibroblasts (AG03587, AG05013, and AG18371) was observed relative to the average RECQL4 levels seen in healthy human donor fibroblasts (GM00010, GM01603, GM05386, and GM06166), confirming published results. More importantly, the candidate Mut-2 clones showed a similar level of reduction in RECQL4 levels compared to parental HEK293 as seen in RTS patient fibroblasts relative to healthy donor fibroblasts (Figure 2.3B and C). In contrast to this, several previous studies which investigated the effects of specific point mutations that affected RECQL4 helicase function did so in the context of equal or overexpression of mutant RECQL4 (Castillo-Tandazo et al., 2019; Lu et al., 2016). This demonstrated that these clones represented a more reasonable model for RTS patient cells in terms of RECQL4 abundance.

2.4.3 Mut-2 RECQL4 truncation is a minor protein product

When the c.2269C>T "Mut-2" mutation was first identified in the initial cohort of *RECQL4* mutations linked to Type II RTS, it was classified as a nonsense truncation mutation based on sequence prediction (Kitao et al., 1999a). Indeed, in RNA-Seq data, the RECQL4 transcript carrying the Mut-2 mutation was a major, if not the predominant, RECQL4 transcript in the Mut-2 clones (Figure 2.4C). However, when blotting for RECQL4 protein by western blot, there was no detectable difference in signal intensity at the predicted size of the truncation protein (82kDa) between the majority of the candidate Mut-2 clones (2.11, 2.14, and 2.16) and the parental HEK293. The only clone that showed a detectably increased signal at that position was clone 2.88. This band was confirmed by RECQL4 siRNA-mediated knockdown to be a form of RECQL4 and most likely that of the truncation protein (Figure 2.3D).

Since Mut-2 is a putative nonsense mutation, it was possible that degradation of the truncation transcript by nonsense mediated decay (NMD) played a role in the lack of

detectable truncation product in the other three clones. Therefore, NMD inhibition was performed by siRNA-mediated knockdown of UPF1, a protein which is required for NMD. However, this did not lead to the detection of or an increase in the levels of the truncation product in the Mut-2 candidate clones. Subsequently, both transcript-specific RT-qPCR and RNA-Seq of the Mut-2 clones demonstrated that canonically spliced *RECQL4* transcripts bearing the truncation mutation was actually a major product of transcription from the Mut-2 allele in the clones (Figure 2.4B and C). These findings suggested that an NMD-mediated process might not be a major contributing factor to the lack of a truncation RECQL4 product.

In their study of the structure of the RECQL4 helicase domain, Kaiser, *et al.*, reported that the C-terminal α-helices in RECQL4 which resembled the RQC Zn^{2+} binding domain in other RecQ family helicases were important for protein stability (Kaiser et al., 2017). Therefore, it was possible that the Mut-2 truncation product was unstable and rapidly degraded in the Mut-2 clones. This could explain the lack of the RECQL4 truncation product in the majority of the Mut-2 clones despite the seemingly abundant presence of the corresponding transcript in the RNA-Seq data. Future work using proteasome inhibitors, perhaps in conjunction with NMD inhibition, would be needed to further investigate this.

In summary, in the majority of the Mut-2 candidate clones, the truncation product, if made, was undetectable and only a minor product. Only in 2.88 was the truncation RECQL4 product observed at a detectable level (further discussed below).

2.4.4 Mut-2 upregulates alternative splicing of RECQL4

If the predicted truncation product was not the major RECQL4 protein product in the Mut-2 clones, then what was? Since at least some portion of RECQL4's N-terminal portion is required for viability, another possibility must exist. Although the wild-type RECQL4 band was completely absent in the Mut-2 candidate clones, there were residual bands in each of the

clones that ran slightly smaller than the wild-type RECQL4 (150kDa). These bands responded to RECQL4 siRNA-mediated knockdown, which indicated that they were a form of RECQL4 (Figure 2.3D).

Recently, Colombo and colleagues reported a very similar *RECQL4* c.2272C>T mutation in an RTS patient family. The results of their study were discussed above in Chapter 2 Results Section 2.3.4. Since the mutation studied by Colombo and colleagues was so similar to Mut-2, which also lay within the predicted SF/ASF and SRp55 recognition motifs, the possibility of the alternatively spliced transcript being present in the candidate Mut-2 clones was studied using transcript-specific TaqMan RT-qPCR assays. While all four candidate clones downregulated canonical exon 14-15 splicing, three of them (2.11, 2.14, and 2.16) also upregulated the usage of the aforementioned alternate splice site. The only clone that failed to do so was 2.88 though the alternative transcript was still detected at a lower level. As a result, the first three clones had greatly increased ratios of the alternate transcript to the canonical transcript as compared to parental HEK293 (Figure 2.4B). The presence of this splice variant in the Mut-2 clones was then confirmed by RNA-Seq (Figure 2.4C).

In accordance with the study by Colombo and colleagues, the aforementioned alternative splicing was found to be physiological and the same transcript was also detected in parental HEK293 by both TaqMan RT-qPCR as well as RNA-Seq (Colombo et al., 2014). However, it was both interesting and important to note that the use of the alternative splicing removed the Mut-2 mutation from the resulting mRNA transcript and prevented the truncation of the protein. In effect, this alternative splicing of RECQL4 provided a way for cells to “rescue” the Mut-2 truncation mutation and produce a protein that is nearly full-length. Furthermore, it preserved the C-terminal portions of the RECQL4 protein, which includes the

C-terminal α-helices that have been reported to be important for protein stability (Kaiser et al., 2017).

Given these insights, the lack of increased alternative splice site use in clone 2.88 may provide a clue regarding the reason that the Mut-2 truncation RECQL4 product was solely observed in this particular clone (Figure 2.3A). Absent a mechanism to generate a potentially more stable and non-truncated RECQL4 protein, it was likely that clone 2.88 was more dependent on expression of the Mut-2 truncation RECQL4 product as its primary means of maintaining the essential levels of RECQL4 protein needed for viability. Thus, the truncation product was found at a detectable level only in this particular clone. The other three clones appeared to preferentially use the alternative splicing mechanism described above instead and therefore did not need to rely on the expression of the Mut-2 truncation RECQL4 product (Figure 2.3A and D and Figure 2.4B). It was tempting to further speculate that this clear preference for alternative splicing as a rescue mechanism in the case of RECQL4 truncation could be due to the predicted decrease in the stability of the Mut-2 truncation product and thus the anticipated increase in transcription and translation—and the attendant necessary resources required—on the part of the cell to maintain the minimal RECQL4 levels needed for viability.

Finally, based on known structures of the RECQL4 helicase domain, what would be the predicted effects of the deletion of the 66aa in exon 14? While it is difficult to predict what the structural effects of the deletion would be, some functional effects could be predicted given what is known about the structure-function relationships in the RECQL4 helicase domain (Fairman-Williams et al., 2010; Kitao et al., 1998). The 66aa skipped by the alternately spliced variant of RECQL4 made up the latter half the second RecA-like fold of the RECQL4 helicase core, covering conserved motifs V and VI (Figure 2.9). Among the crucial functions ascribed to

this region were the binding and hydrolysis of ATP, essential for proper helicase function (Fairman-Williams et al., 2010). Thus, it would be reasonable to predict that the alternately spliced form of RECQL4 would show impaired helicase function due to inability to bind and hydrolyse ATP.

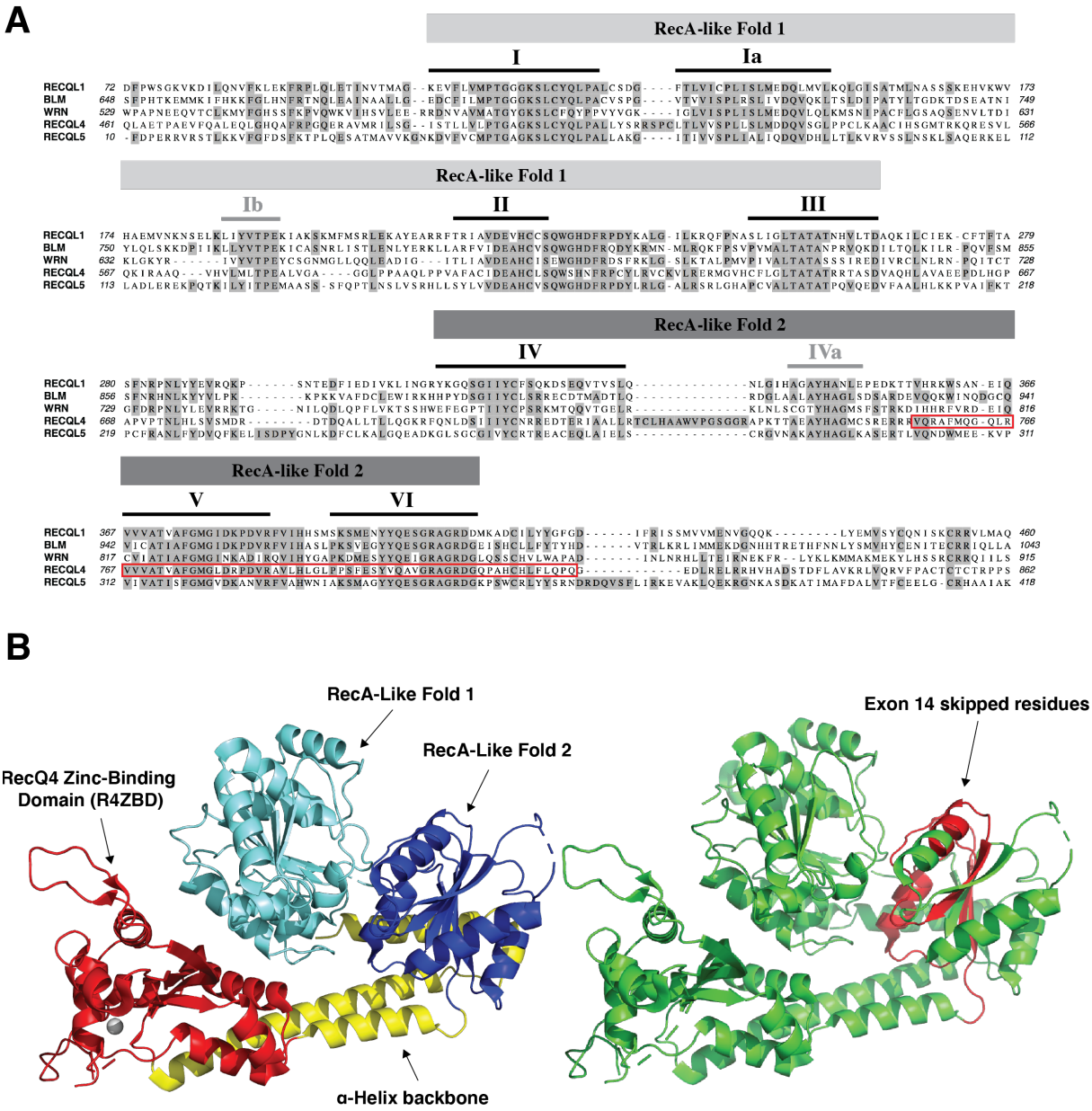

Figure 2.9 Predicted structural effects of RECQL4 exon 14-15 alternative splicing

A. Protein sequence alignment of the helicase core of the RecQ family helicases in humans. The seven conserved helicase motifs are denoted in black. RecA-like folds are denoted in grey boxes. Red box indicates the exon 14 skipped residues.

B. RECQL4 C-terminal region domain structure (left, details in Figure 1.2 legend) and the location of the exon 14 skipped residues (right, red).

(Figures adapted from Kitao et al., 1998 and Kaiser et al., 2017. Amino acid sequence alignment in A done using MacVector. Structures in B were drawn in PyMOL, PDB: 5LST)

2.4.5 Mut-2 clones are viable models for functional studies of Mut-2

This chapter described the generation of four HEK293-derived cells lines carrying the *RECQL4* c.2269C>T Mut-2 RTS mutation as models to study the effects of *RECQL4* mutation in Type II RTS. Studies characterising the genomic structure of the *RECQL4* Mut-2 sites in these four candidate clones have demonstrated that they are functionally hemizygous Mut-2 mutants which closely modelled the genotypes observed in RTS patients. RECQL4 protein expression in these candidate Mut-2 clones—in terms of abundance as well as structure—closely matched what had been previously reported by various studies of RTS patient samples. Taken together, these four Mut-2 clones are novel and viable models for further functional studies of the RTS *RECQL4* Mut-2 mutation.

Chapter 3 Mut-2 Clones – Functional Characterisation

3.1 Introduction

Since its first identification as a member of the RecQ helicase family in humans, RECQL4 has been proposed to function in the maintenance of genomic stability (Kitao et al., 1998). Mutations in two other members of the RecQ helicase family—*BLM* and *WRN*—had previously been identified as the underlying causes for the progeroid cancer predispositions Bloom Syndrome (BS) and Werner Syndrome (WS), respectively. Both BS and WS are marked by genomic instability (Chaganti et al., 1974; Ellis et al., 1995; German, 1969; German et al., 1965; Hoehn et al., 1975; Salk et al., 1981a, 1981b; Vijayalaxmi et al., 1983; Yu et al., 1996). Soon thereafter, mutations in *RECQL4* itself were implicated in a subset of patients with RTS, another progeroid cancer predisposition syndrome, further strengthening the case for RECQL4's role in protecting against DNA damage (Kitao et al., 1999a; Lindor et al., 2000).

Since then, studies have used many models—RTS patient cells, mouse models, and engineered cells lines—to investigate the effects of *RECQL4* disruption on genome stability and DNA damage repair in the face of various challenges, yielding generally inconsistent results (Castillo-Tandazo et al., 2019; Jin et al., 2008; Kohzaki et al., 2012). The previous chapter detailed efforts to generate cell line models for the study of the prevalent RTS *RECQL4* c.2269C>T "Mut-2" mutation. Here, the first aim then was to characterise the response of these HEK293 Mut-2 clones to a broad panel of DNA damaging agents. The resulting sensitivity profile could then be used to pinpoint common DNA damage repair pathways that are frequently activated by those agents to which the Mut-2 clones show increased sensitivity and guide further mechanistic studies of the effects of the *RECQL4* Mut-2 mutation. Below, the

genotoxic agents used are briefly outlined along with their mechanisms of action, effects, and the repair pathways they activate. Chemical structures can be found in Figure 3.1.

3.1.1 DNA damaging agents

3.1.1a Replication stress inducers

Although many agents indirectly lead to replication stress, the two agents discussed here cause replication stress as their principal effect by interfering with the function of the DNA polymerase. Hydroxyurea (HU, Figure 3.1A) is a ribonucleotide reductase inhibitor which inhibits the production of deoxyribonucleotides (dNTPs) from ribonucleotides. As dNTPs are the monomers from which DNA is synthesised, the depletion of the dNTP pool by HU leads to inhibition of DNA synthesis, accumulation of short stretches of single-stranded DNA (ssDNA), and replication fork stalling (Krakoff et al., 1968; Reichard, 1988; Sogo et al., 2002). Aphidicolin, on the other hand, is a direct inhibitor of DNA polymerase α, leading to replication fork stalling, the decoupling of the DNA polymerase enzyme from the advancing DNA helicase, and the production of long stretches of ssDNA (Baranovskiy et al., 2014; Krokan et al., 1981; Loenn and Loenn, 1988).

Fork stalling is a major cause of replication stress and prolonged replication fork stalling leads to replication fork collapse and the formation of deleterious DNA DSBs (Cortez, 2015; Liao et al., 2018; Petermann et al., 2010a). Inducers of replication stress such as hydroxyurea and aphidicolin promote the production and accumulation of ssDNA which is rapidly bound and protected by RPA (Chen et al., 2013; Liao et al., 2018; Loenn and Loenn, 1988; Sogo et al., 2002; Wold and Kelly, 1988). At the same time, RPA binding also activates the ATR-Chk1 pathway and the S-phase checkpoint to suppress further origin firing and prevent the depletion of the cellular RPA pool (Petermann et al., 2010b; Shechter et al., 2004; Syljuåsen et al., 2005; Toledo et al., 2013; Zou and Elledge, 2003). This process stabilises

existing stalled replication forks, allowing for replication restart once the replication stress has been resolved, while also preventing formation of new stalled replication forks (Liao et al., 2018). Under conditions of prolonged replication fork stalling however, initial replication fork stabilisation transitions to fork reversal involving regression of the stalled replication fork mediated by SMARCAL1 (Bétous et al., 2012). This leads to the formation of a 4-way junction through annealing of the leading and lagging synthesis strands and formation of a nucleoprotein filament in an HR-independent process mediated by RAD51 and BRCA2 (Higgins et al., 1976; Mijic et al., 2017; Petermann et al., 2010a; Schlacher et al., 2011; Sogo et al., 2002; Zellweger et al., 2015). Fork reversal functions to protect the stalled replication forks from degradation by nucleases such as MRE11 or MUS81 while providing a substrate for replication fork restart (Bryant et al., 2009; Kolinjivadi et al., 2017; Pepe and West, 2013; Schlacher et al., 2011; Thangavel et al., 2015; Ying et al., 2012).

Despite the above mechanisms of stalled replication fork stabilisation and protection, sustained replication stress ultimately leads to accumulation of DSBs as a result of fork collapse (Petermann et al., 2010a). These DSBs are then repaired by HR, the DSB repair pathway active during S-phase (Johnson and Jasin, 2000; Petermann et al., 2010a). While it is known that the number of DSBs increases with duration of replication stress, the frequency of such breaks in human cells is unclear (Cortez, 2015; Petermann et al., 2010a). It is thought that DSBs resulting from prolonged replication stress and replication fork collapse are infrequent events even when cells are challenged with replication stress inducers (Cortez, 2015).

3.1.1b Radiomimetics

Radiomimetic agents, as their name suggests, comprise a class of compounds that mimic the effects of ionising radiation through the generation of free radicals leading to DNA

DSBs (D'Andrea and Haseltine, 1978; Dedon and Goldberg, 1992). Bleomycin (Figure 3.1B) is one such compound. Though its precise mechanism of action remains unclear, bleomycin is thought to generate DNA DSBs through activation by a metal ion such as Fe^{2+} to produce free radical intermediates (D'Andrea and Haseltine, 1978; Dedon and Goldberg, 1992; Hecht, 2000; Povirk et al., 1989).

Neocarzinostatin (NCS, Figure 3.1B), another radiomimetic used in these studies, is a two-part compound comprising an active chromophore non-covalently interacting with and stabilised by an apoprotein (Gottschalk et al., 1991; Napier et al., 1979). The active chromophore is responsible for the generation of DNA DSB-causing free radicals (Dedon and Goldberg, 1992; Ohtsuki and Ishida, 1980; Shiloh et al., 1983). What makes NCS a useful yet difficult compound to work with are its extremely short half-life and rapidly inactivation by light (Burger et al., 1978; Gottschalk et al., 1991; Maeda and Takeshita, 1975). But, if properly handled, NCS can be used to deliver a concentrated yet temporally isolated pulse of genotoxic challenge to the target cells, allowing for increased temporal resolution of its downstream effects. However, this advantage is tempered by the fact that the instability of NCS introduces an element of variability in the dose of challenge delivered even when handled with the utmost care.

DNA DSBs generated by radiomimetics are repaired by NHEJ, HR, and MMEJ in a cell-cycle dependent fashion (Karanam et al., 2012). The mechanisms of these pathways were previously discussed in Chapter 1 (Section 1.4.2).

3.1.1c DNA alkylators

DNA alkylators are agents that attack DNA by adding alkyl side groups to nucleotides. These bulky adducts can distort the DNA helix and disrupt proper base pairings. If left unrepaired, bulky DNA adducts can interfere with processes involving the DNA such as

transcription and DNA replication, leading to further stress and DNA damage such as DSBs (Wyatt and Pittman, 2006).

Methyl methanesulfonate (MMS, Figure 3.1C) is a DNA methylator whose predominant adduct product is 7-methylguanine (N7-MeG) with 3-methyladenine (N3-MeA) being the major minor product (Beranek, 1990; Drabløs et al., 2004; Wyatt and Pittman, 2006). Interestingly, MMS has, for many years, been considered to be a DNA DSB-producing radiomimetic compound due to studies that showed increased sensitivity of HR-deficient yeast to MMS treatment (Johzuka and Ogawa, 1995; Krogh and Symington, 2004; Tsubouchi and Ogawa, 1998). The current understanding of the cellular responses to MMS treatment, however, paints a more complex picture. Recent work has shown that MMS does not directly give rise to DNA DSBs (Lundin et al., 2005). Rather, DNA nucleotide adducts produced by MMS are predominantly repaired in the first instance by the base excision repair (BER) pathway (discussed in Chapter 1 Section 1.4.1). However, the nucleotide adducts themselves and those undergoing reactions such as depurination as well as intermediates of the BER repair pathway can present challenges to concurrent processes such as DNA replication, leading to stalled or collapsed replication forks and DNA DSBs. These breaks are then repaired by pathways such as NHEJ and HR (discussed in Chapter 1). Further evidence of the involvement of replication in the generation of DNA DSBs in MMS-treated cells is the fact that cells deficient in HR, a repair pathway active during S and G2 phases, are much more sensitive to MMS treatment than those deficient in NHEJ (Kondo et al., 2010; Lundin et al., 2005; Nikolova et al., 2010; Thompson and Hinz, 2009; Wyatt and Pittman, 2006).

Busulfan (BUS, Figure 3.1C) is another DNA alkylator used in these studies. It comprises two molecules of MMS joined by a short alkyl chain. Unlike MMS, however, busulfan is a bifunctional alkylator in which both ends of the molecular can separately attack different

nucleotides on the DNA. This can lead to three different outcomes—the production of monoadducts from a single alkylation event or the production of DNA intra- and interstrand crosslinks between nucleotides on the same or opposite DNA strands. Thus, busulfan can also be properly classified as a DNA crosslinker (discussed below) in addition to a DNA alkylator, with intrastrand crosslinks being the major product (Casorelli et al., 2012; Kondo et al., 2010; McNeill et al., 2009). However, since busulfan's structure and its mechanism of action are so similar to those of MMS, its effects are discussed in this section.

As mentioned above and seen in Figure 3.1C, the active ends of busulfan are essentially identical to MMS and thus, the nucleotide adduct products formed are also very similar—mainly N7-MeG and N3-MeA—and are generally repaired by the BER repair pathway in the same fashion (Casorelli et al., 2012; Iwamoto et al., 2004; Ponti et al., 1991). The repair of intrastrand crosslinks produced by busulfan, however, is mostly handled by the mismatch repair pathway (MMR) (Casorelli et al., 2012). In brief, adducts are recognised by MutSα (1-2nt) or MutSβ (1-15nt) which then recruit MutL and ExoI to nick and unwind the DNA strand flanking the adduct. The newly revealed ssDNA left behind is then quickly coated with the ssDNA-binding protein RPA before DNA polymerase δ/ε are recruited to fill in the gap and the newly synthesised DNA is sealed by DNA ligase I (Hsieh and Zhang, 2017; Li, 2008).

In the case of busulfan treatment, as with MMS, both the adducts themselves as well as the intermediates of their repair pathways can interfere with processes such as replication, leading to replication stress, fork stalling/collapse, DNA DSBs, and the activation of downstream repair pathways (Casorelli et al., 2012; Kondo et al., 2010).

3.1.1d DNA crosslinkers

DNA crosslinkers are compounds that form crosslinking bridges between nucleotides on the same DNA strand (intrastrand crosslinks) and on opposite DNA strands (interstrand

crosslinks, ICLs). The proportion of these products formed and thus the major repair pathways activated are compound dependent.

Cisplatin (CDDP, Figure 3.1D) is an inorganic platinum compound whose major products are 1,2-d(GpG) and 1,2d(ApG) intrastrand DNA crosslinks formed at the N7 atoms of guanine and adenine bases with N^7G:N^7G ICLs as a minor product (Fichtinger-Schepman et al., 1985; Vesela et al., 2017). Cyclophosphamide (CP, Figure 3.1D), on the other hand, forms a product mix that is mostly the opposite of cisplatin, with N^7G:N^7G ICLs being the major product and N^7G and N^7A intrastrand crosslinks and monoadducts being minor products (Vesela et al., 2017). Mitomycin C is an alkaloid that also forms N^7G:N^7G ICLs, but preferentially at 5'-CpG-3' sites (Ahn et al., 2004; Bass et al., 2013; Weng et al., 2010).

The repair of intrastrand crosslinks caused by crosslinking agents involves the nucleotide excision repair (NER) pathway (discussed in Chapter 1 Section 1.4.1) (Huang and Li, 2013; Thompson and Hinz, 2009; Vesela et al., 2017). The repair of ICLs, however, is much more complex and involves components of multiple DNA damage repair pathways coordinated by the Fanconi anaemia (FA) pathway (Deans and West, 2011; Huang and Li, 2013; Moldovan and D'Andrea, 2009). Briefly, ICLs blocking the replication fork are recognised by FANCM during S-phase which activates the FA pathway and recruits a large multi-protein FA core complex to the lesion. The FA core complex functions as a ubiquitin ligase to activate FANCD2/FANCI. This activation sequence then initiates the downstream ICL repair processes. First, the region flanking the ICL is nicked by MUS81-EME1 and ERCC1-XPF to generate a DNA DSB intermediate and a DNA adduct containing the ICL. REV1-mediated translesion synthesis then replicates past the ICL. The ICL itself is removed and repaired by the NER pathway. In parallel, the DNA DSB intermediate generated by the initial DNA nicks is repaired by HR. Indeed, mutants deficient in HR are extremely sensitive to DNA crosslinkers and reactivation

of recombination has been shown to be a mechanism for cellular resistance to these agents (Ahn et al., 2004; Basu and Krishnamurthy, 2010; Borst et al., 2008; Casorelli et al., 2012; Deans and West, 2011; Huang and Li, 2013; McHugh et al., 2000; Moldovan and D'Andrea, 2009; Moynahan et al., 2001; Rocha et al., 2018; Thompson and Hinz, 2009; Vesela et al., 2017; Weng et al., 2010). Interestingly, though cisplatin appears to generate very similar intrastrand crosslinks as busulfan (discussed above), mismatch repair (MMR) seems to be important in mediating cisplatin's cytotoxic effects rather than as a repair pathway as seen in busulfan (Vesela et al., 2017).

3.1.1e Topoisomerase inhibitors

Topoisomerases are enzymes which transiently induce DNA nicks (topoisomerase I) or DSBs (topoisomerase II) in DNA in order to relax DNA supercoiling as a result of processes such as transcription and DNA replication. Topoisomerase inhibitors then are agents which stabilise the transient topoisomerase-DNA break complex to generate longer-lasting DNA breaks (Champoux, 1978; Hande, 1998; Koster et al., 2007).

Camptothecin and its close analogue topotecan (CPT, TPT, Figure 3.1E) are both topoisomerase I inhibitors which stabilise the TOP1-DNA nick complex (Koster et al., 2007; Zhao et al., 2012). The resulting ssDNA nicks then lead to the generation of S-phase specific DNA DSBs when replication forks collide with the stabilised complex and collapse. The DNA DSBs generated as a result of camptothecin and topotecan treatment are therefore preferentially repaired through HR, the repair mechanism that is active during S-phase (Karanam et al., 2012; Saleh-Gohari et al., 2005; Tripathi et al., 2016; Zhao et al., 2012).

Etoposide (ETP, Figure 3.1E), on the other hand, is a topoisomerase II inhibitor that directly generates DNA DSBs by stabilising the TOP2-DNA DSB complex (Hande, 1998; Zhao et al., 2012). This also means that, unlike topoisomerase I inhibitors above, the DNA DSBs

generated by etoposide are not S-phase specific and neither are the subsequently activated repair pathways (Hande, 1998; Quennet et al., 2010; Zhao et al., 2012). However, the repair of etoposide generated DNA DSBs does differ from that of other DNA DSBs in two ways. First, the topoisomerase II protein complex must first be removed from the break ends in order for repair to proceed. This process is mediated by the MRN (Mre11, Rad50, Nbs1) complex and CtIP in a recombination-independent manner (Aparicio et al., 2016; Quennet et al., 2010). Second, it has been reported that prolonged etoposide treatment leads to G2/M arrest in cells which, as a consequence of the cell cycle phase, would likely affect the choice of repair pathway as compared to immediately after treatment (Schonn et al., 2010).

3.1.1f PARP inhibitors

In recent years, increased sensitivity to inhibitors of poly-ADP ribose polymerase (PARP) such as olaparib (OLA, Figure 3.1F) and veliparib (VEL, Figure 3.1F) has become a hallmark of cells that are deficient in HR (D'Andrea, 2018). Three mechanisms have been proposed for this sensitivity. The first mechanism proposes a synthetic lethality between HR deficiency and the inhibition of PARP, which is important in promoting DNA SSB repair (D'Andrea, 2018; Fisher et al., 2007). The resulting accumulated DNA SSBs are converted to DNA DSBs in collisions with replication forks. These deleterious breaks are normally then repaired by HR. Thus HR-deficient cells are unable to effect these repairs and exhibit increased sensitivity to PARP inhibition (D'Andrea, 2018).

A second model for explaining the sensitivity of HR mutants to PARP inhibition proposes that PARP inhibitors physically trap PARP at lesions such as DNA SSBs and SSB intermediates arising during BER. A previous study has reported that PARP inhibition leads to accumulation of SSB intermediates during BER whereas PARP depletion via siRNA treatment had the opposite effect, suggesting that the presence of PARP is necessary to mediate the

effect of PARP inhibitors (Ström et al., 2010). Additional findings from another study show that PARP inhibitors are more toxic than siRNA-mediated PARP depletion when cells are challenged with MMS treatment. Furthermore, PARP inhibitors increase PARP chromatin binding upon MMS treatment implicating DNA-PARP adducts in mediating the cytotoxic effects of MMS (Murai et al., 2012). This model of PARP inhibitor action posits that DNA-PARP adducts block access to the lesion for further repair and must be removed by an HR-dependent process before replication forks can proceed. Thus HR-deficient cells will be unable to dislodge these adducts, suffering fork collapse and deleterious downstream consequences (D'Andrea, 2018; Murai et al., 2012).

A final model for the activity of PARP inhibitors proposes that HR-deficient cells are more reliant on the backup MMEJ process for the repair of DNA DSBs during DNA replication. This pathway is dependent on PARP and DNA polymerase θ. PARP inhibition would therefore render both DNA DSB repair pathways inoperative in HR mutants, leading to the accumulation of unrepaired breaks and the attendant negative consequences (Ceccaldi et al., 2015; D'Andrea, 2018).

A

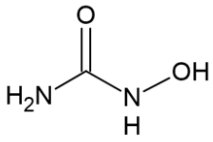

Hydroxyurea

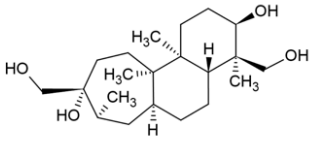

Aphidicolin

B

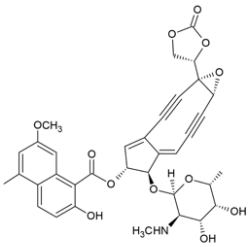

Neocarzinostatin

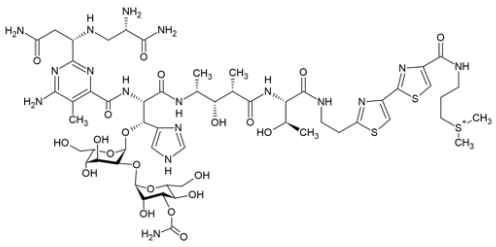

Bleomycin

C

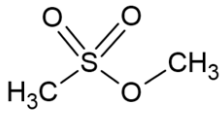

Methyl methanesulfonate

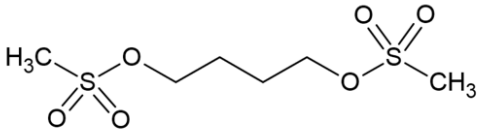

Busulfan

D

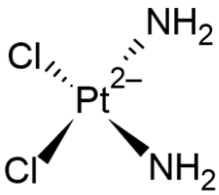

Cisplatin

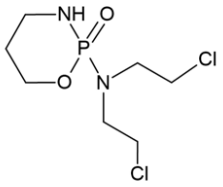

Cyclophosphamide

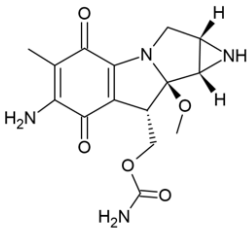

Mitomycin C

E

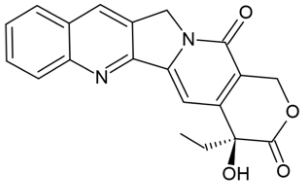

Camptothecin

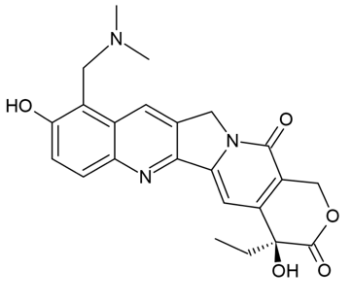

Topotecan

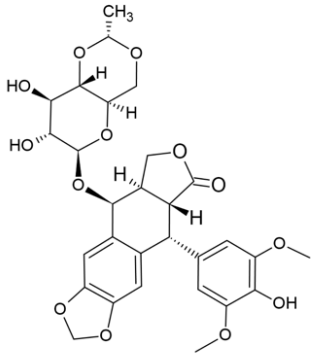

Etoposide

F

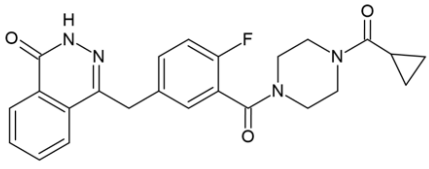

Olaparib

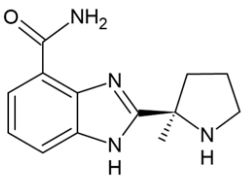

Veliparib

Figure 3.1 Chemical structures of DNA damaging agents
A. Replication stress inducers: hydroxyurea (HU) and aphidicolin (APH)
B. Radiomimetics: neocarzinostatin (NCS) and bleomycin (BLM)
C. DNA alkylators: methyl methanesulfonate (MMS) and busulfan (BUS)
D. DNA crosslinkers: cisplatin (CDDP), cyclophosphamide (CP), and mitomycin C (MMC)
E. Topoisomerase inhibitors: camptothecin (CPT), topotecan (TPT), and etoposide (ETP)
F. PARP inhibitors: olaparib (OLA) and veliparib (VEL)
(All figures drawn using ACD/ChemSketch)

3.1.2 Genetic reporters of DNA DSB repair pathways

While data from drug sensitivity assays might be helpful in implicating defects in DNA damage repair pathways, they might also be affected by confounding factors such as changes in proliferation rates that do not affect DNA damage repair (further discussion later in Chapter 3). Therefore, the functional status of the DNA DSB repair pathways (HR, NHEJ, and MMEJ) in the Mut-2 clones were also directly interrogated using GFP reporter constructs, a widely used assay modality in the study of DNA damage repair pathways. All three GFP reporter constructs used in this study were previously published (Figure 3.2), therefore, their mechanisms of action will be only briefly discussed below (Kostyrko and Mermod, 2016; Pierce et al., 1999; Seluanov et al., 2010).

The HR GFP reporter used was pDRGFP (Figure 3.2). It consists of a non-functional GFP expression cassette inactivated by a small deletion and insertion of an *I-SceI* restriction site (SceGFP) along with a downstream GFP fragment containing the deleted portion (iGFP). When cleaved by *I-SceI*, GFP expression can only be reconstituted when the break ends are repaired by HR using the downstream iGFP fragment as template without crossing over (Pierce et al., 1999).

The NHEJ GFP reporter used was based on a GFP expression construct (GFP-Pem1) in which the GFP cassette was interrupted by a Pem1 intron that is expected to be spliced out during transcription (Figure 3.2). The reporter was constructed by inserting an adenoviral exon (Ad) within the Pem1 intron which would disrupt the GFP reading frame and render the GFP non-functional if left in. The Ad exon was flanked by inverse tandem *I-SceI* sites which when cleaved would liberate the Ad exon while avoiding the generation of regions of microhomology at the break ends. The resulting break, when repaired by NHEJ would

reconstitute the intact Pem1 intron which would again be spliced out during transcription to generate functional GFP (Seluanov et al., 2010).

The MMEJ reporter was constructed based on work reported by Kostyrko and Mermod (Figure 3.2) (Kostyrko and Mermod, 2016). Using site-directed mutagenesis, a 9bp region segment within the GFP ORF was duplicated to generate tandem regions of microhomology with an *I-SceI* site inserted in between. When cleaved by *I-SceI*, the annealing of the break ends at the regions of microhomology and subsequent MMEJ-based repair would reconstitute functional GFP.

3.1.3 Summary of findings

The drug sensitivity data in generated in this chapter strongly implicated DNA DSB repair as pathways which are negatively impacted by the *RECQL4* Mut-2 mutation. This is consistent with the many reports of RECQL4's role in these pathways as previously discussed in Chapter 1 (Kohzaki et al., 2012; Lu et al., 2016; Shamanna et al., 2014; Singh et al., 2010).

Furthermore, GFP reporter construct assays showed that while the Mut-2 clones did not have a defect in NHEJ, they showed deficiencies in both HR and MMEJ, which would support a model for RECQL4 dysfunction leading to replication-specific DNA DSB repair defects. Additional GFP reporter assays using RECQL4 reconstituted cells suggested that the structural changes caused by *RECQL4* Mut-2 specifically affected HR efficiency.

Finally and most surprisingly however, staining for RAD51 in Mut-2 clones showed that RAD51 foci formation was not impaired in the Mut-2 clones, suggesting that *RECQL4* Mut-2 mutation affected HR at a point further downstream in the pathway than would be expected based on findings from other studies (Lu et al., 2016).

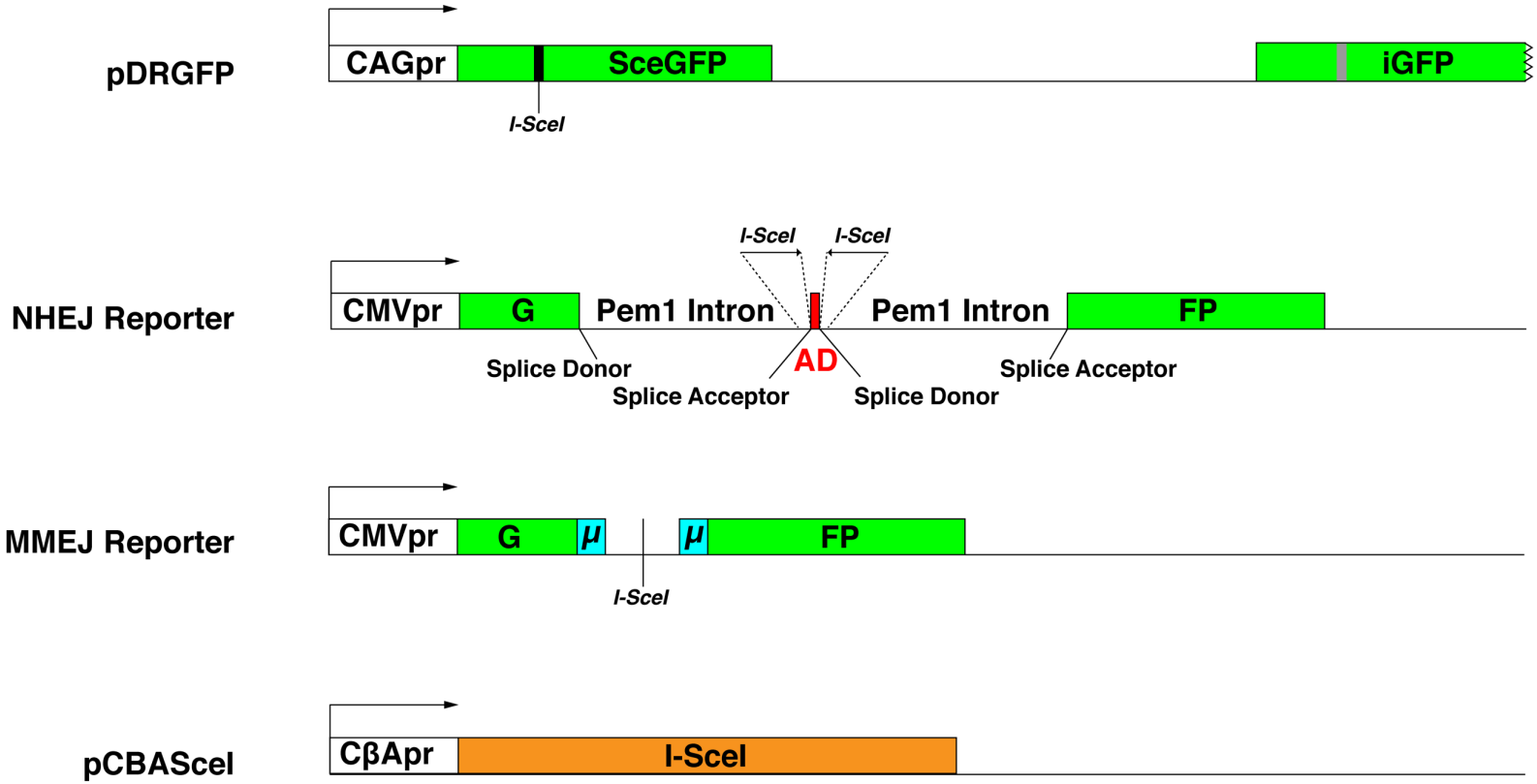

Figure 3.2 Plasmid constructs for GFP reporter assays

GFP reporter constructs for HR (pDRGFP), NHEJ, and MMEJ as well as I-SceI expression construct. The black box in SceGFP and the grey box in iGFP in pDRGFP represent the region of indel/*I-SceI* site and the repair template region respectively. The red box in the NHEJ reporter represents the intervening adenoviral exon. The blue boxes in the MMEJ reporter represent the tandemly duplicated regions of microhomology.

3.2 Materials and Methods

3.2.1 Cell Culture

HEK293 (ATCC) and derivatives and 293T/17 (ATCC) were cultured as described previously. When appropriate, media was supplemented with 2µg/ml puromycin and/or 15µg/ml blasticidin HCl (ThermoFisher) for selection and maintenance.

3.2.2 Cell Cycle Staining

Cells were labelled with 20µM EdU for 30min. Post-treatment, labelled cells were harvested and fixed, permeabilised, and processed with the Click-iT EdU Alexa Fluor 488 Flow Cytometry Kit (ThermoFisher) according to manufacturer's protocol. Cells were then stained with 1X FxCycle Far Red (ThermoFisher) supplemented with 100µg/ml RNase A (ThermoFisher) according to manufacturer's protocol. Post-staining, cells were assayed via flow cytometry on a Sony SA3800 using 488nm and 638nm excitation lasers and analysed in FlowJo (BD).

3.2.3 DNA Damage Repair GFP Reporter Assays

pCBASceI I-SceI expression construct was a gift from Maria Jasin (Addgene plasmid #26477; http://n2t.net/addgene:26477; RRID:Addgene_26477). pDRGFP HR reporter was a gift from Maria Jasin (Addgene plasmid #26475; http://n2t.net/addgene:26475; RRID:Addgene_26475). NHEJ reporter was a gift from Vera Gorbunova.

MMEJ reporter was constructed as outlined in Kostyrko & Mermod, 2016 by mutating the pEGFP-N1 backbone (Clontech) using PrimeSTAR HS DNA polymerase with GC buffer and In-Fusion HD cloning kit (TaKaRa). PCR and sequencing primers used are listed below:

Name	Sequence, 5'-3'
MMEJ-GFP_F2	ACGACGGCAACTACAAGACCCGCGCCGAGTAGGGATAACAGGGTAATCGC GCCGAGGTGAAGTTCGAGGGC
MMEJ-GFP_R2	GGTCTTGTAGTTGCCGTCGTCCTTGAAGAAGATGGTG
MMEJ-GFP_Seq3	CCACCTACGGCAAGCTGACCCTGAAG

pmC4.10CMV mCherry expression construct was made by Bryn Hardwick (University of Cambridge), briefly, mCherry was cloned into the pGL4.10[luc2] backbone (Promega) in place of luciferase using EcoRV and XbaI. The CMV promoter from pcDNA3.1 (Invitrogen) was then inserted between the NheI and EcoRV sites. The EcoRV site was destroyed in this step.

Cells were plated in triplicate at 50% confluency in a total volume of 100µl in 96-well plates (Corning) and allowed to adhere overnight. The next day, the cells were transfected with a total of 200ng DNA consisting of the GFP reporter construct, pCBASceI, and pmC4.10CMV in a ratio of 6:3:1 using Lipofectamine 2000 (ThermoFisher). Cells were assayed for GFP and mCherry expression 48 hours post-transfection on a Sony SA3800 flow cytometer using the 488nm and 561nm excitation lasers.

Data analysis was performed using FlowJo (BD). The number of GFP positive cells for each sample was normalised to the total number of cells positive for GFP and/or mCherry in that sample. Data from replicate wells were then averaged and background subtraction performed by subtracting the average GFP positive fraction from corresponding control wells transfected without pCBASceI. Average fraction GFP positive for each cell line and assay was then normalised to the average fraction GFP positive for the appropriate parental HEK293 control to calculate the normalised fraction GFP positive.

3.2.4 Etoposide Recovery Assay and p-Histone H3 staining

Cells were plated in poly-L-lysine coated flasks in media supplemented with 200nM etoposide or 0.1% DMSO and incubated overnight. At the start of the experiment (0hr), media was aspirated, cells were washed once with 1x DPBS, and fresh media was added. Cells were harvested every 2 hours from 0hr to 8hr and fixed and permeabilised in 70% ethanol at 4°C overnight.

For γH2AX and cell cycle staining, cells were stained using Alexa Fluor 488 FlowCellect Histone H2A.X Phosphorylation Assay Kit (Millipore) and then with 1X FxCycle Far Red supplemented with 100µg/ml RNase A (ThermoFisher) according to manufacturer's instructions. For phospho-Histone H3 and cell cycle staining, approximately 1 million cells were resuspended in 100µl of DPBS with 5µl Alexa Fluor 647 anti-Histone H3 Phospho (Ser10) (BioLegend) and 1X FxCycle Violet (ThermoFisher) and incubated on ice for 1hr.

Stained cells were assayed by flow cytometry on a Sony SA3800 using 405nm (FxCycle Violet), 488nm (Alexa Fluor 488), and 638nm (FxCycle Far Red, Alexa Fluor 647) excitation lasers. Data analysis was done in FlowJo (BD).

3.2.5 Immunofluorescence Staining

Cells were seeded at a density of 1.0-1.5×10^4 per well in 15-well angiogenesis µ-Slides (Ibidi) pre-coated overnight with 0.01% poly-L-lysine. Post-treatment, cells were harvested for immunofluorescence staining by aspirating media and fixing in 4% formaldehyde for 10 minutes at room temperature. Cells were then rinsed 3X with DPBS and permeabilised with 0.5% Triton X-100 for 10 minutes at room temperature. Cells were rinsed again with 3X DPBS and blocked for 1 hour at room temperature with rotation in 20% donkey serum diluted in PBS-0.1% Tween 20 (PBST). Post-block, cells were stained overnight in primary antibodies for γH2AX (Millipore, clone JBW301, 1:1000) and RAD51 (Abcam, ERP4030(3), 1:1000) diluted in

PBST with 5% donkey serum. Cells were then washed 3X with PBST and incubated for 1 hour at room temperature with rotation in secondary antibody mix comprising Alexa Fluor 488 donkey anti-mouse IgG and Alexa Fluor 594 donkey anti-rabbit IgG (Jackson ImmunoResearch, 1:1000) diluted in PBST with 5% donkey serum. Cells were again washed 3X with PBST and mounted with ProLong Diamond Antifade Mountant with DAPI (ThermoFisher) and allowed to cure overnight. Stained cells were imaged on a Zeiss LSM780 confocal microscope using a 63X objective and resulting images analysed in FIJI and KNIME with the image processing extensions software package.

3.2.6 Incucyte Proliferation Assay

Cells were trypsinised, counted on a Countess II cell counter (ThermoFisher), and plated in triplicates in 384-well black, clear-bottom plates (Corning) at a density of 1020 cells per well in a total volume of 30µl and allowed to adhere overnight. Appropriate drugs were diluted in media to a concentration of 2X and 30µl were added to each set of triplicate wells. Control wells were supplemented with the same volume of either fresh media or media containing 0.2% DMSO (vehicle). The plates were incubated and read in the Incucyte Zoom (Essen Bioscience) with phase-contrast images (1/well) taken every 4 hours with a 10X lens. Images were analysed using the Incucyte Zoom software for confluency using a custom HEK293 image definition derived from a training set of HEK293 images showing various levels of confluency. The assay endpoint was set as when the untreated or vehicle (DMSO) treated negative control wells initially reached 100% confluency.

Dose response analysis for each cell line was performed by averaging the confluency values of the replicate wells for each treatment condition (dose) at the assay endpoint. Normalisation was done by dividing the averages for all treatment conditions by the average

of the untreated or vehicle (DMSO) treated negative control wells for the corresponding cell line at the assay endpoint. The results were plotted using Graphpad Prism.

IC_{50} analyses were performed using GraphPad Prism on the dose response data calculated above. The averaged dose response data for each cell line and compound across all independent experiments was fitted to a custom sigmoidal, 4 parameter model with the "top" and "bottom" parameters set at 1 and 0 respectively using least squares regression that considered each independent experiment as sets of individual data points. The model used was:

$$Y = \frac{1}{1 + \left(\frac{IC_{50}}{X}\right)^{H}}$$

where Y is the response (proliferation) and X is the dose. H is the "HillSlope" calculated by Prism. The presence of outliers was reported alongside asymmetrical 95% confidence intervals. The results were plotted using Graphpad Prism.

Doubling times were calculated for each experiment by taking the time (in hours) and confluency (%) measurements closest to 40% and 60% confluency: (T_{40}, C_{40}) and (T_{60}, C_{60}) and applying the following formula:

$$\text{Doubling Time} = \frac{T_{60} - T_{40}}{log_2 \frac{C_{60}}{C_{40}}}$$

Doubling times were then plotted using Graphpad Prism.

The following table lists the compounds used, the source from which they were obtained, the solvent used for each, and their respective stock solution concentrations:

Table 3.1 DNA damaging compounds tested and stock concentrations used

Name	Source	Solvent	Stock Concentration
Aphidicolin (ready made solution)	Sigma	DMSO	1mg/ml, stored at -30°C
Bleomycin	Selleckchem	DMSO	10mg/ml, stored at -80°C
Busulfan	Sigma	DMSO	200mM, made fresh
(S)-(+)-camptothecin	Sigma	DMSO	10mM, stored at -30°C
Cisplatin	Millipore	PBS	1mg/ml, made fresh
Cyclophosphamide monohydrate	Sigma	PBS	100mM, made fresh
Etoposide	Sigma	DMSO	5mM, stored at -30°C
Hydroxyurea	Sigma	PBS	200mM, made fresh
Methyl methansulfonate (11.8M)	Sigma	PBS	200mM, diluted fresh
Mitomycin C	Sigma	PBS	1mg/ml, stored at 4°C
Neocarzinostatin (ready made solution)	Sigma	20mM MES buffer	~0.5mg/ml, stored at 4°C
Olaparib	Selleckchem	DMSO	100mM, stored at -80°C
Topotecan	Sigma	DMSO	5mM, stored at -30°C
Veliparib	Selleckchem	DMSO	100mM, stored at -80°C

3.2.7 Lentivirus Production and Transduction

2nd generation lentiviral packaging plasmids psPAX2 and pMD2.G were gifts from Didier Trono (Addgene plasmid #12260; http://n2t.net/addgene:12260; RRID:Addgene_12260; Addgene plasmid #12259; http://n2t.net/addgene:12259; RRID:Addgene_12259).

The day before transfection, 293T/17 cells were seeded onto 15cm tissue culture dishes (ThermoFisher) at 50% confluence and allowed to adhere overnight. The next day, cells were transfected with a total of 60µg DNA consisting of the lentiviral construct, psPAX2, and

pMD2.G in a ratio of 3:2:1 using Lipofectamine 2000 (ThermoFisher). Viral supernatant was harvested at 48hr and 72hr post-transfection, filtered with 0.45µm PES syringe filters, buffered with 5mM HEPES Buffer pH7.4, and mixed with Lenti-X Concentrator (Clontech) at a ratio of 3:1 and incubated at 4℃ overnight. The viral supernatant was concentrated by centrifugation at 1500 x g for 45 minutes at 4℃, the supernatant aspirated and the pellet resuspended in 1ml complete media.

Cells were transduced with lentivirus via spinoculation in 6-well plates. Concentrated lentivirus was added directly to the media along with 15µg/ml polybrene and the plates were centrifuged at 2500rpm for 90 minutes at 30℃. Afterwards, the media was left on the cells overnight before being replaced the next day with fresh media.

3.2.8 Plasmid Construction

The lentiviral RECQL4 expression construct EX-U0228-Lv246 and the corresponding empty vector control EX-NEG-Lv246 were obtained from Genecopoeia. The exon 14 skipping RECQL4 variant was constructed from the Genecopoeia plasmid by site-directed mutagenesis using Herculase II Fusion DNA Polymerase (Agilent) and In-Fusion HD Cloning Kit (Clontech) and verified by Sanger sequencing. The primers used are:

Name	Sequence, 5'-3'
RTSdel66_F	ggtcttcgccCCGCCGCCGTTCCCGGCTG
RTSdel66_R	acggcggcgGGGCGAAGACCTGCGAGAGCTGCGC
Lv246_F (Sequencing)	TTGAACTATGCGCTCGGG
Lv246_R (Sequencing)	CTGGAATAGCTCAGAGGC

"delGFP" or "ΔGFP" versions of the above three constructs without GFP were constructed via site-directed mutagenesis using Herculase II Fusion DNA Polymerase (Agilent)

and In-Fusion HD Cloning Kit (Clontech) and verified by Sanger sequencing. The primers used are:

Name	Sequence, 5'-3'
Lv246_delGFP_F	AGCGGCCGCGATCCCGC
Lv246_delGFP_R	ggggcgggatcgcggccgctGGTGGCGACCGGTATGGCGC
Lv246_F2 (Sequencing)	GCCTCTGAGCTATTCCAG

3.2.9 Quantitative RT-PCR

RT-qPCR was performed according to procedures outlined previously in Chapter 2 using the same TaqMan assays.

3.2.10 RNAi Knockdown

siRNA pools were obtained from Dharmacon. RNAi knockdown was performed as outlined previously in Chapter 2. Cells were harvested at 48 hours post-transfection for downstream assays.

Name	Sequence
siRAD51 Pool	UAUCAUCGCCCAUGCAUCA, CUAAUCAGGUGGUAGCUCA, GCAGUGAUGUCCUGGAUAA, CCAACGAUGUGAAGAAAUU
Non-targeting Pool	UGGUUUACAUGUCGACUAA, UGGUUUACAUGUUGUGUGA, UGGUUUACAUGUUUUCUGA, UGGUUUACAUGUUUUCCUA

3.2.11 Western Blot

Western blot procedures and antibodies used were as outlined previously in Chapter 2 (see Methods Section 2.2.4 and Table 2.1).

3.3 Results

3.3.1 RECQL4 Mut-2 mutation has a minor effect on growth characteristics in clones

The first functional studies compared the growth characteristics of the Mut-2 clones to those of the parental HEK293. In order to study their unperturbed cell cycle distributions, normally cycling cell populations were transiently pulsed with the nucleotide analogue EdU for 30 minutes followed by fixation and total DNA content staining. EdU/DNA dual-stained cells were then analysed by flow cytometry. The Mut-2 clones did not differ significantly from parental HEK293 in cell cycle phase distribution under normal cycling conditions (Figure 3.3A and B). Next, their growth kinetics were compared using the Incucyte proliferation assay. The growth curves of the Mut-2 clones also did not appear significantly different compared with parental HEK293 when in the exponential growth phase. The growth curves of the Mut-2 clones did, however, show increased duration of the initial lag phase and delayed entry into exponential growth (Figure 3.3D). The population doubling times of the Mut-2 clones were calculated based on time points taken from around the 50% confluency point in the exponential growth phase. Compared to parental HEK293, there were increases in population doubling times for all Mut-2 clones that were statistically significant though not drastic—approximately on the order of 20-30% higher doubling times were found (Figure 3.3C and D).

3.3.2 Mut-2 clones showed increased sensitivity to certain classes of DNA damaging agents

Having determined that the Mut-2 clones did not differ significantly from parental HEK293 in their growth characteristics (Figure 3.3), their sensitivity to a panel of various classes of DNA damaging agents was next investigated as discussed in the introduction above (Figure 3.1 and Figure 3.4). Compared with parental HEK293, the Mut-2 clones showed noticeably increased sensitivity to DNA alkylators (Figure 3.4E and F), DNA crosslinkers (Figure 3.4G and H, particularly CP and MMC), topoisomerase inhibitors (Figure 3.4I and J), and

moderate sensitivity to the PARP inhibitor olaparib (Figure 3.4K and L). There was also a trend of increased sensitivity of the Mut-2 clones to the DNA crosslinker cisplatin (Figure 3.4G and H) and to the PARP inhibitor veliparib (Figure 3.4K and L), however, the differences appear to be very slight. In contrast, there was no noticeable difference in sensitivity between the Mut-2 clones and the parental HEK293 to inducers of replication stress (Figure 3.4A and B) and radiomimetics (Figure 3.4C and D).

There was one clone (2.16) which stood out as being especially sensitive to every compound tested, including those to which the other three clones showed no increased sensitivity. This suggested that this phenotype might be a clone-specific outlier phenomenon (more details to follow).

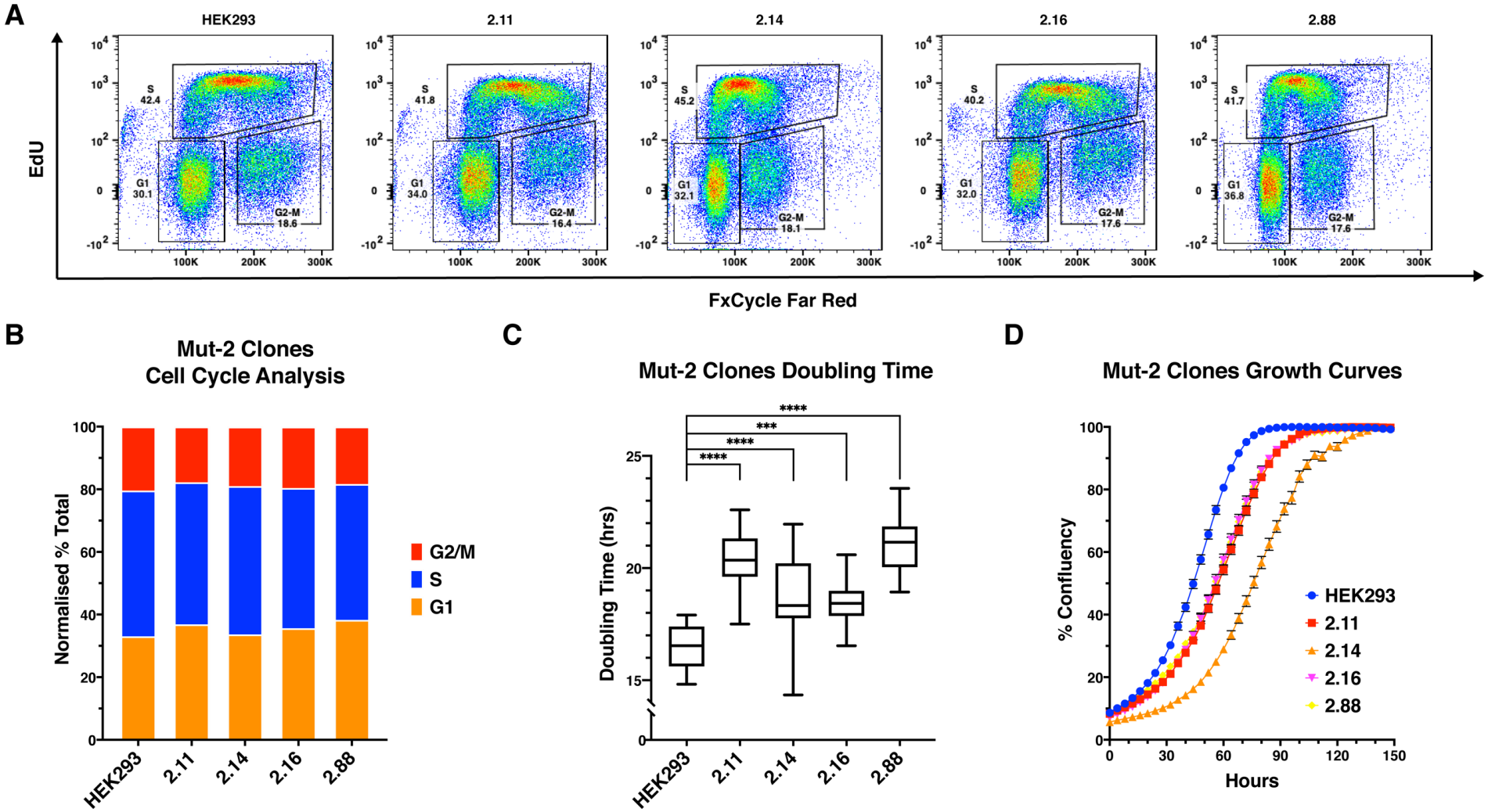
A
HEK293
2.11
2.14
2.16
2.88
EdU
FxCycle Far Red
S
G1
G2-M
B
Mut-2 Clones
Cell Cycle Analysis
Normalised % Total
G2/M
S
G1
C
Mut-2 Clones Doubling Time
Doubling Time (hrs)
D
Mut-2 Clones Growth Curves
% Confluency
Hours

Figure 3.3 Growth characteristics of Mut-2 clones

A. Flow cytometric cell cycle analyses show similar cell cycle distributions in both parental HEK293 and Mut-2 clones. Cells have been transiently pulsed with the nucleotide analogue EdU to mark active DNA synthesis and stained for total DNA content (FxCycle Far Red). Dual-stained cells are gated for G1, S, and G2/M based on total DNA content (FxCycle Far Red, x-axis, linear scale) and presence of active DNA synthesis (EdU, y-axis, bi-exponential scale). Each dot on the density plot represents one cell. Cells are further coloured based on density on the plot with red being the densest regions and blue being the least dense regions with each plot showing at least 50,000 cells. Data shown is typical of at least 3 independent experiments.

B. Normalised stacked bar plot summarising the cell cycle distribution flow cytometry data shown in Part A. The size of each section of each bar is normalised to the sum of the percentages shown in the gates in Part A for each cell line. Data shown is based on one experiment.

C. The doubling times (in hours) of the Mut-2 clones are higher than that of parental HEK293, indicating slower growth rate. The box-and-whisker plot shows distribution of doubling times for parental HEK293 and each Mut-2 clone from 20 independent experiments. Doubling times are calculated for each individual experiment using the formula given in Methods Section 3.2.6 above and Incucyte confluency readings taken every 4hrs during proliferation time courses. (*** = $p < 0.001$, **** = $p < 0.0001$).

D. Growth curves of the Mut-2 clones and parental HEK293 show grossly similar growth kinetics during the exponential growth phase. The Mut-2 clones, particularly 2.14, show prolonged lag phase before entry into exponential growth. Growth curves are plotted as percent confluency measured by the Incucyte vs. time since start of the experiment. Timepoints are generally taken every 4hrs and 0hr is the day after cell plating. Data shown is the average of 18 independent experiments. Error bars show SEM.

A

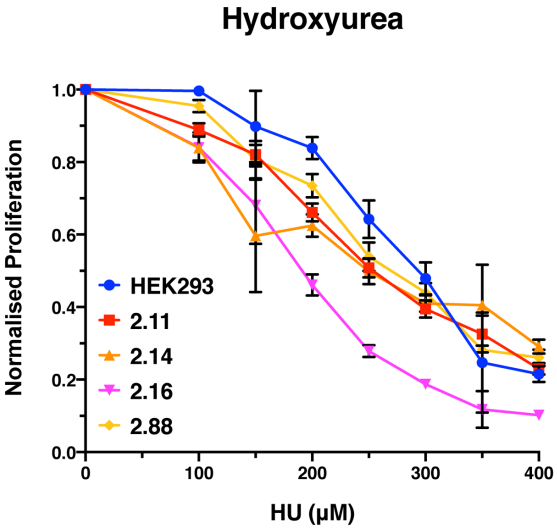
Hydroxyurea
Normalised Proliferation
1.0
0.8
0.6
0.4
0.2
0.0
0
100
200
300
400
HU (μM)
HEK293
2.11
2.14
2.16
2.88

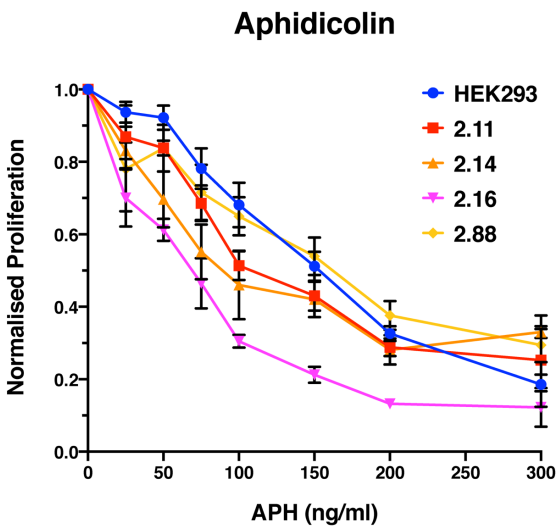
Aphidicolin
Normalised Proliferation
1.0
0.8
0.6
0.4
0.2
0.0
0
50
100
150
200
250
300
APH (ng/ml)
HEK293
2.11
2.14
2.16
2.88

B

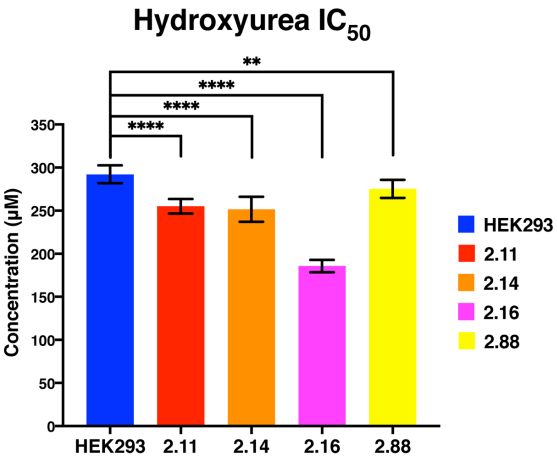
Hydroxyurea IC50
**
****
****
****
Concentration (μM)
350
300
250
200
150
100
50
0
HEK293
2.11
2.14
2.16
2.88

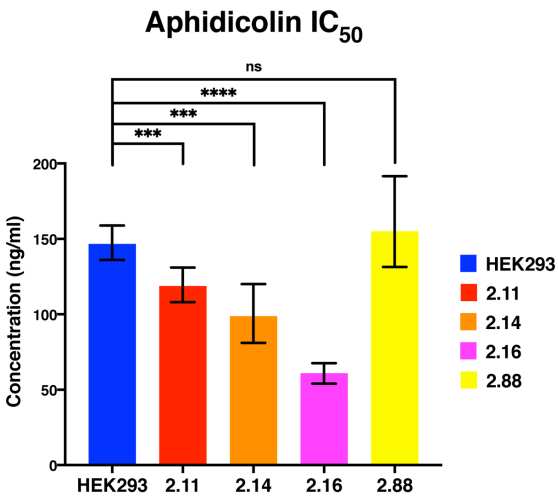
Aphidicolin IC50
ns
****
***
***
Concentration (ng/ml)
200
150
100
50
0
HEK293
2.11
2.14
2.16
2.88

C

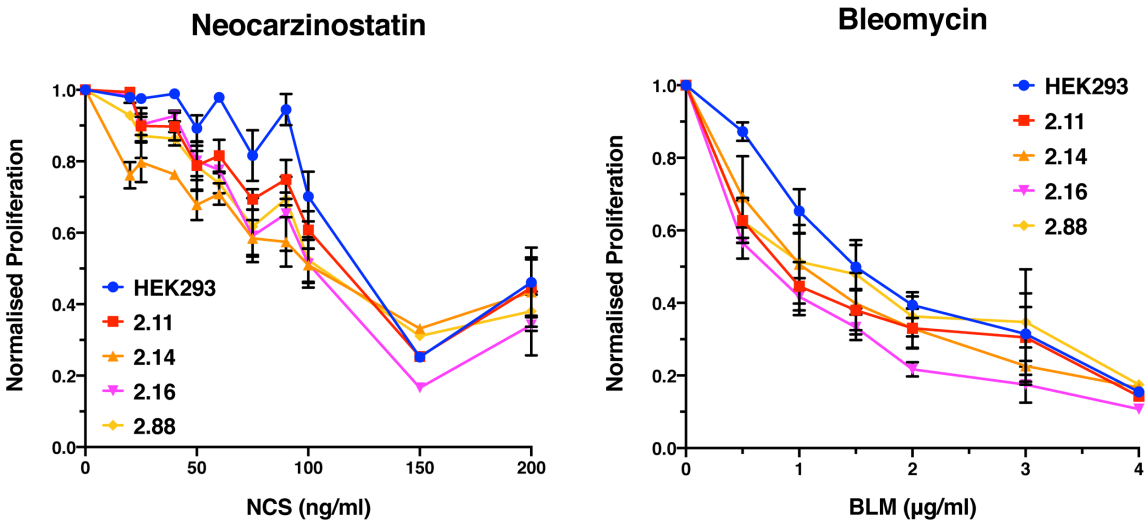
Neocarzinostatin
Normalised Proliferation
NCS (ng/ml)
HEK293
2.11
2.14
2.16
2.88
Bleomycin
Normalised Proliferation
BLM (µg/ml)
HEK293
2.11
2.14
2.16
2.88

D

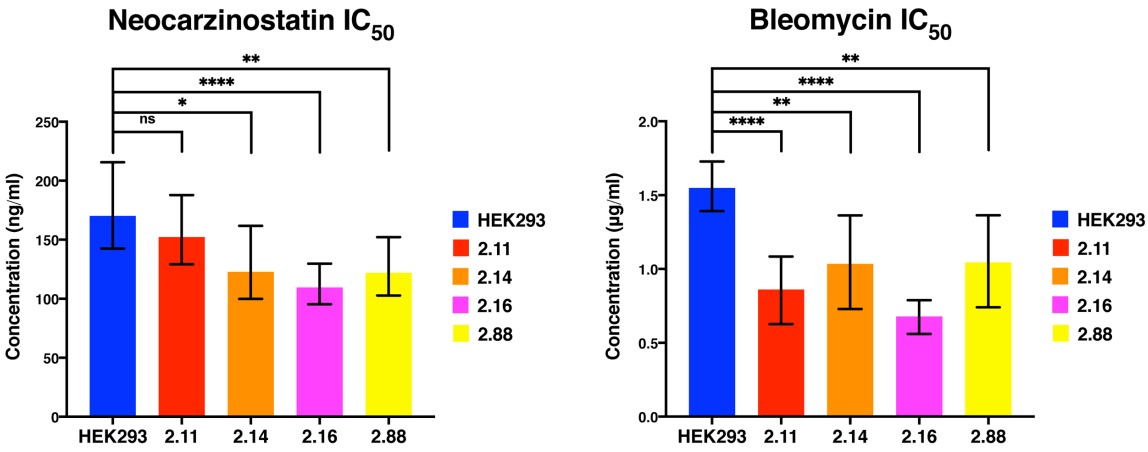
Neocarzinostatin IC50
Concentration (ng/ml)
ns
*
****
**
HEK293
2.11
2.14
2.16
2.88
Bleomycin IC50
Concentration (µg/ml)
****
**
****
**
HEK293
2.11
2.14
2.16
2.88

E

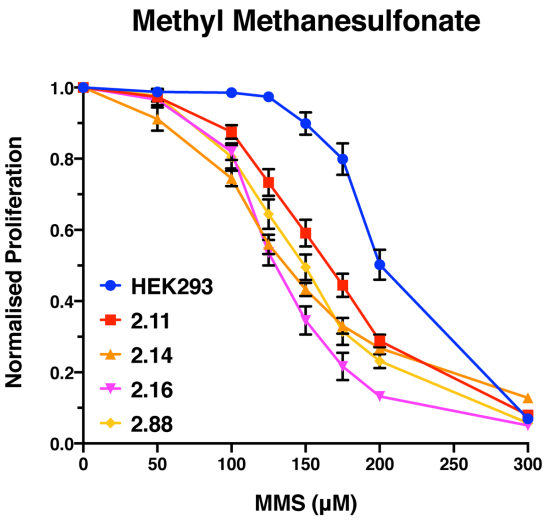
Methyl Methanesulfonate
Normalised Proliferation
1.0
0.8
0.6
0.4
0.2
0.0
0
50
100
150
200
250
300
MMS (μM)
HEK293
2.11
2.14
2.16
2.88

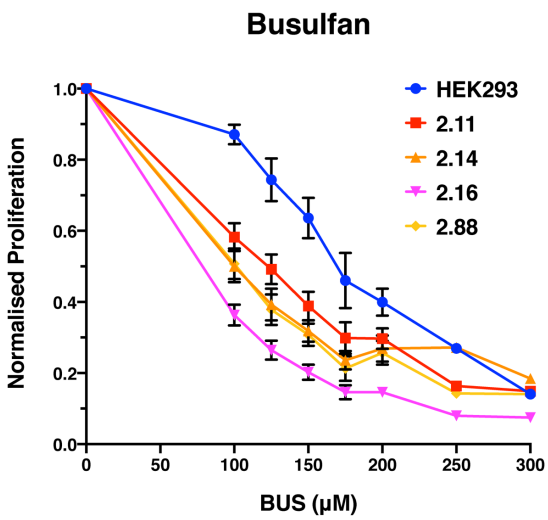
Busulfan
Normalised Proliferation
1.0
0.8
0.6
0.4
0.2
0.0
0
50
100
150
200
250
300
BUS (μM)
HEK293
2.11
2.14
2.16
2.88

F

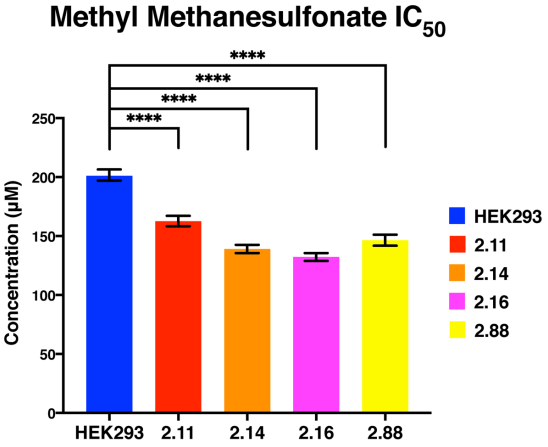
Methyl Methanesulfonate IC50
****
****
****
****
Concentration (μM)
250
200
150
100
50
0
HEK293
2.11
2.14
2.16
2.88

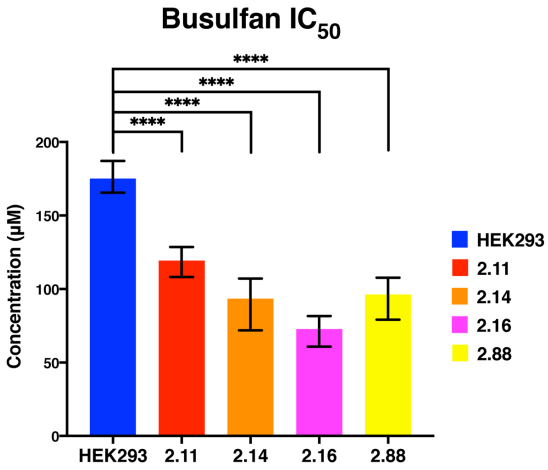
Busulfan IC50
****
****
****
****
Concentration (μM)
200
150
100
50
0
HEK293
2.11
2.14
2.16
2.88

G

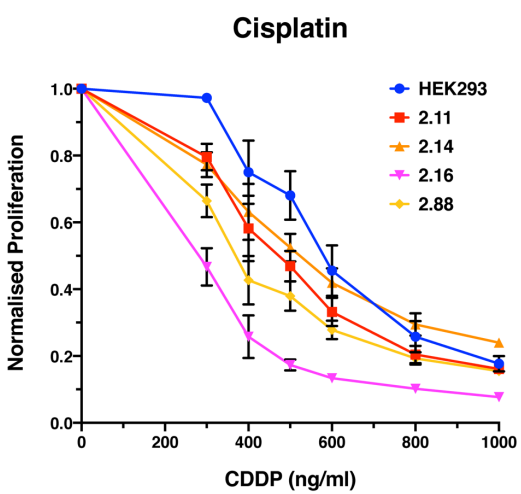
Cisplatin
Normalised Proliferation
CDDP (ng/ml)
HEK293
2.11
2.14
2.16
2.88

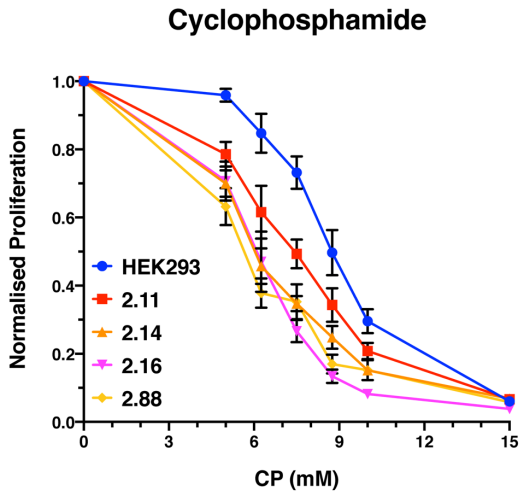
Cyclophosphamide
Normalised Proliferation
CP (mM)
HEK293
2.11
2.14
2.16
2.88

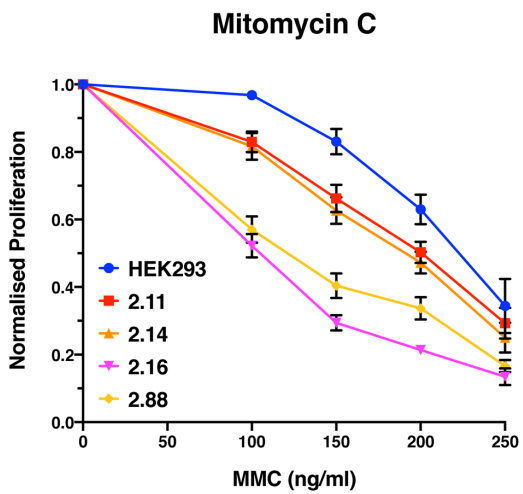
Mitomycin C
Normalised Proliferation
MMC (ng/ml)
HEK293
2.11
2.14
2.16
2.88

H

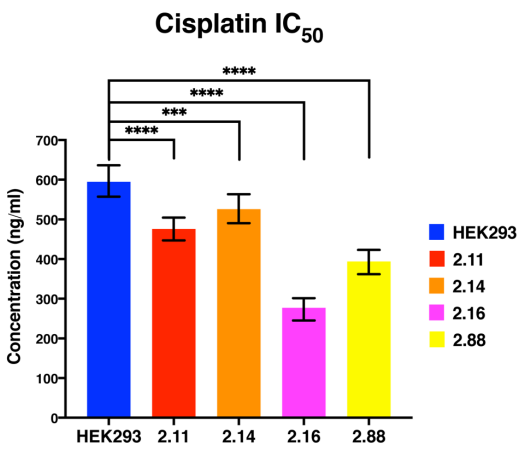
Cisplatin IC50
Concentration (ng/ml)
HEK293
2.11
2.14
2.16
2.88

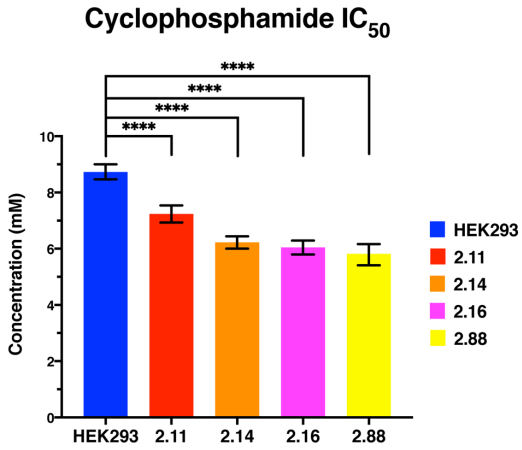
Cyclophosphamide IC50
Concentration (mM)
HEK293
2.11
2.14
2.16
2.88

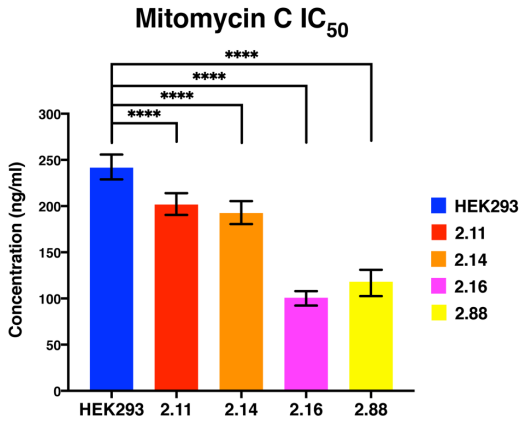
Mitomycin C IC50
Concentration (ng/ml)
HEK293
2.11
2.14
2.16
2.88

I

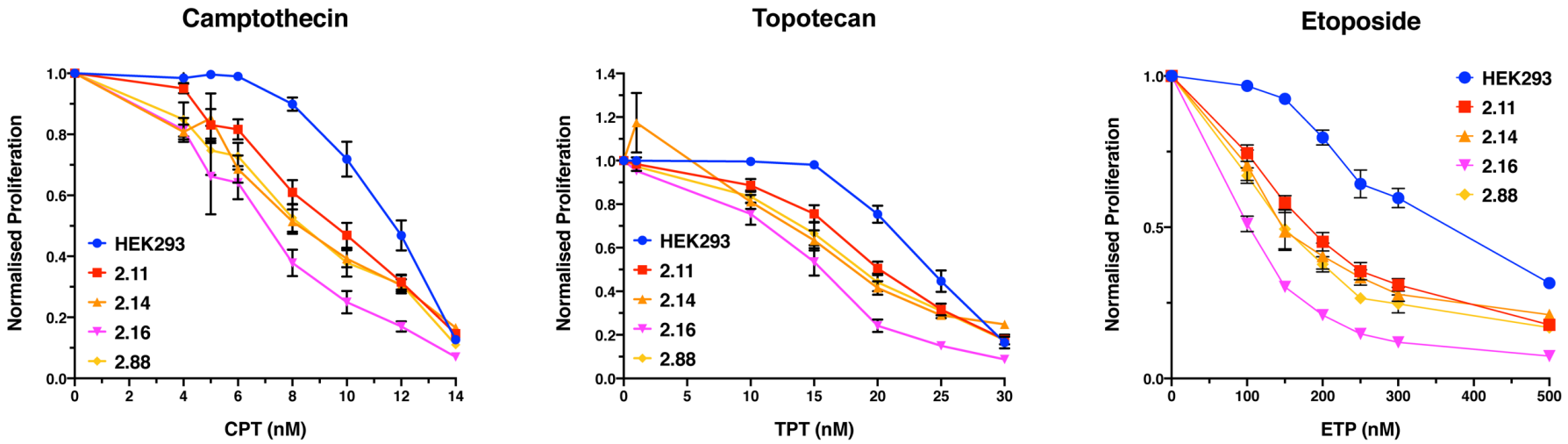
Camptothecin
Normalised Proliferation
CPT (nM)
HEK293
2.11
2.14
2.16
2.88
Topotecan
Normalised Proliferation
TPT (nM)
HEK293
2.11
2.14
2.16
2.88
Etoposide
Normalised Proliferation
ETP (nM)
HEK293
2.11
2.14
2.16
2.88

J

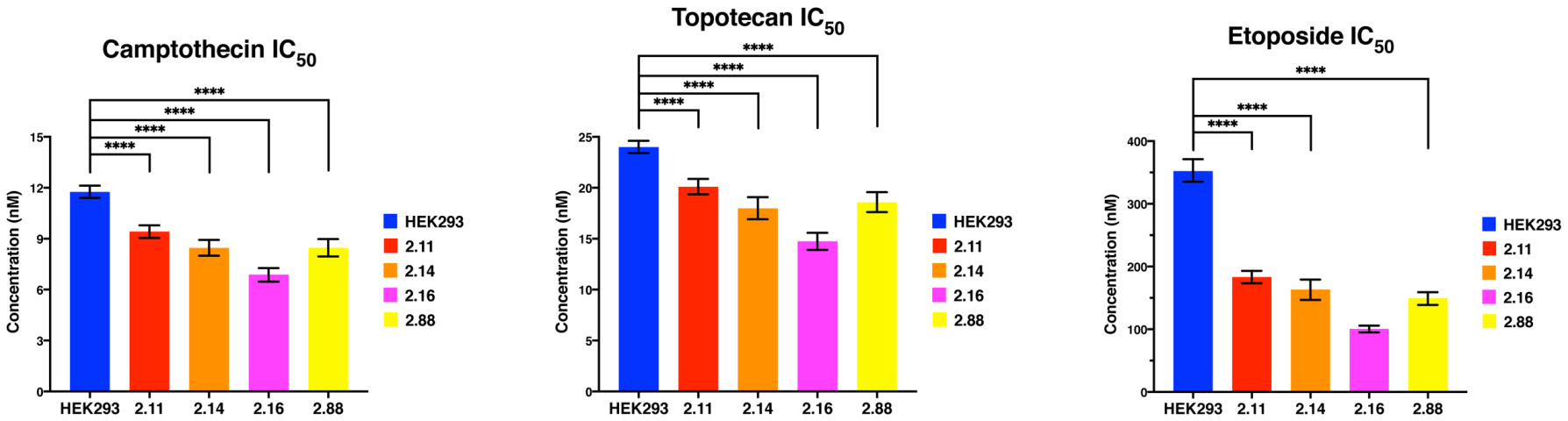
Camptothecin IC50
Concentration (nM)
HEK293
2.11
2.14
2.16
2.88
****
Topotecan IC50
Concentration (nM)
HEK293
2.11
2.14
2.16
2.88
****
Etoposide IC50
Concentration (nM)
HEK293
2.11
2.14
2.16
2.88
****

K

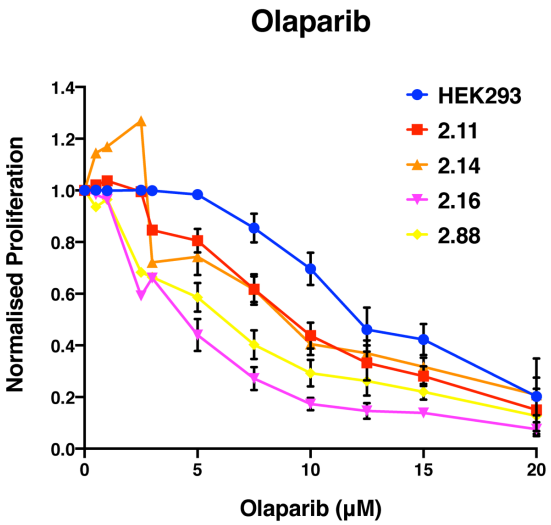
Olaparib
Normalised Proliferation
Olaparib (μM)
HEK293
2.11
2.14
2.16
2.88

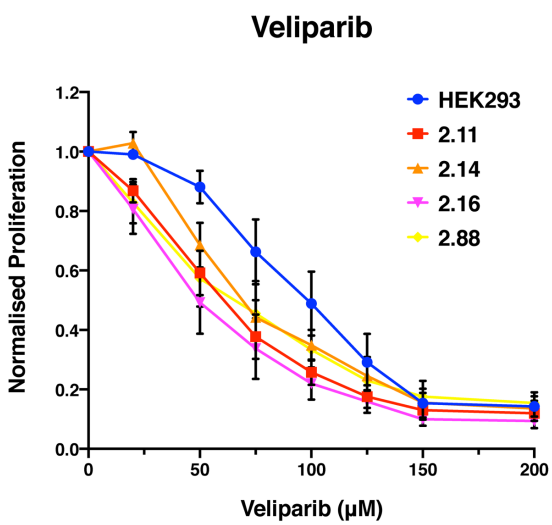
Veliparib
Normalised Proliferation
Veliparib (μM)
HEK293
2.11
2.14
2.16
2.88

L

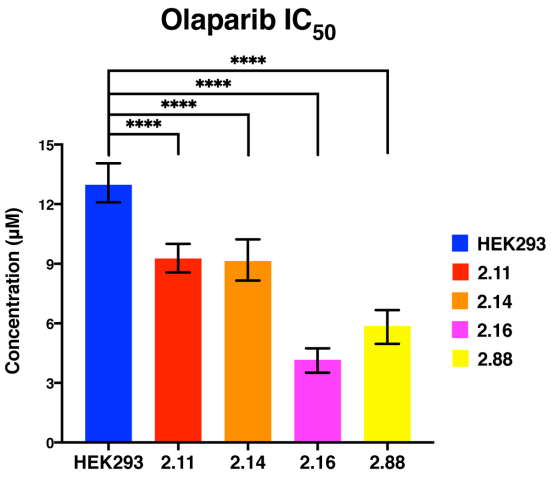
Olaparib IC50
Concentration (μM)
****
HEK293
2.11
2.14
2.16
2.88

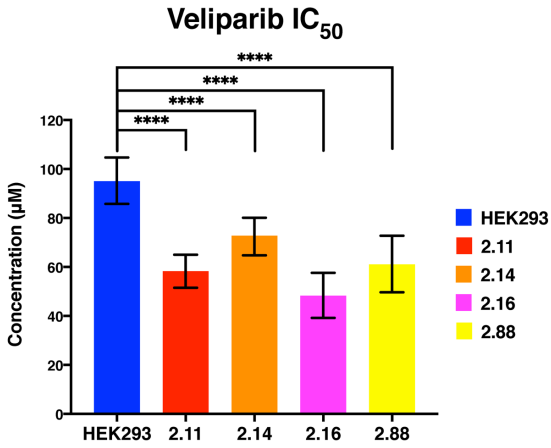
Veliparib IC50
Concentration (μM)
****
HEK293
2.11
2.14
2.16
2.88

Figure 3.4 Sensitivities of Mut-2 clones to various DNA damaging compounds
Dose response curve plots in Parts A, C, E, G, I, and K show normalised proliferation (as a fraction of the appropriate untreated or vehicle treated control) vs. treatment dose for parental HEK293 and each of the Mut-2 clones for the compound indicated in the title. Each plot shows an average of multiple experiments (exact numbers for each compound given below). Error bars represent SEM. Proliferation is measured by confluency using the Incucyte Zoom instrument. Each treatment condition was generally tested in triplicate for every experiment. Detailed assay setup and analysis methods are given above in Methods Section 3.2.6.

Bar graphs in Parts B, D, F, H, J, and L show IC_{50} values calculated using Graphpad Prism. Error bars show asymmetrical 95% confidence intervals reported by Prism's model fitting algorithm. Details on the curve-fitting model, the parameters, and the settings used are also given above in Methods Section 3.2.6. Statistical significance was determined using extra sum-of-squares F test. (* = $p < 0.05$, ** = $p < 0.01$, *** = $p < 0.001$, **** = $p < 0.0001$, ns = not significant).

The number of independent experiments performed for each compound is as follows:
HU = 18, APH = 7, NCS = 9, BLM = 6, MMS = 18, BUS = 13, CDDP = 12, CP = 9, MMC = 14, CPT = 17, TPT = 15, ETP = 12, OLA = 9, VEL = 6.

A. Dose response curves for the majority of Mut-2 clones (2.11, 2.14, 2.88) do not show substantially different sensitivities to replication stress inducers (HU and APH) compared to those for parental HEK293. Clones 2.16 is the exception, showing increased sensitivity to both HU and APH compared to parental HEK293.
B. IC_{50} values for HU and APH in the Mut-2 clones and parental HEK293 show very mild to no decreases in IC_{50} in the Mut-2 clones compared to those calculated for parental HEK293. As expected from Part A, IC_{50} values for clone 2.16 are substantially lower compared to those calculated for parental HEK293.
C. Dose response curves for the Mut-2 clones do not show substantially different sensitivities to radiomimetics (NCS and BLM) compared to those for parental HEK293.
D. IC_{50} values for NCS in the Mut-2 clones and parental HEK293 show very mild to no decreases in IC_{50} in the Mut-2 clones compared to those calculated for parental HEK293. IC_{50} values for BLM show slightly greater though more variable sensitivities in the Mut-2 clones relative to parental HEK293.
E. Dose response curves for the Mut-2 clones show significantly increased sensitivities to DNA alkylators (MMS and BUS) compared to those for parental HEK293.
F. IC_{50} values for MMS and BUS are substantially decreased in the Mut-2 clones relative to those for parental HEK293 showing the greater sensitivities of the former to DNA alkylators.
G. Dose response curves for the Mut-2 clones show mildly increased sensitivities to DNA crosslinkers (CDDP, CP, and MMC) compared to those for parental HEK293. Clone 2.16 is the exception, showing substantially increased sensitivities to CDDP and MMC compared to parental HEK293.
H. IC_{50} values for CDDP, CP, and MMC are decreased in the Mut-2 clones relative to those calculated for parental HEK293, consistent with their mildly increased sensitivities seen in the dose response curves in Part G. Also consistent with observations from Part G, CDDP and MMC IC_{50} values for clone 2.16 are substantially lower than those of the other Mut-2 clones.

I. Dose response curves for the Mut-2 clones show significantly increased sensitivities to inhibitors of both topoisomerase I (CPT and TPT) and topoisomerase II (ETP) compared to those for parental HEK293.
J. IC_{50} values for all three topoisomerase inhibitors (CPT, TPT, and ETP) are substantially decreased in the Mut-2 clones relative to those for parental HEK293.
K. Dose response curves for the Mut-2 clones show mildly increased sensitivities to PARP inhibitors (OLA and VEL) compared to those for parental HEK293.
L. IC_{50} values for OLA and VEL are decreased in the Mut-2 clones relative to those calculated for parental HEK293, consistent with their mildly increased sensitivities seen in the dose response curves in Part K.

3.3.3 Effects of etoposide in Mut-2 clones

The effects of etoposide, one of the compounds tested above to which the Mut-2 clones showed the particular sensitivity, were further studied. As expected, Mut-2 clones and parental HEK293 treated overnight with etoposide showed increased staining for γH2AX, a marker of DNA DSBs (Figure 3.5B) (Rogakou et al., 1998, 1999). Furthermore, consistent with a previous report, etoposide treatment appeared to arrest cells in G2/M when stained for DNA content (Figure 3.5A) (Schonn et al., 2010). However, when stained for phospho-histone H3, a specific marker for mitosis that correlates with chromosome condensation, etoposide-treated cells showed decreased p-Histone H3 staining, suggesting that the cell cycle arrest was before M phase, possibly in late-S/G2 (Figure 3.5C) (Gurley et al., 1978; Juan et al., 1998).

After etoposide treatment, cells were allowed to recover and samples were harvested periodically from 0-8 hours and assayed for DNA content and γH2AX levels. Compared to parental HEK293, Mut-2 clones showed delayed cell cycle restart and progression through mitosis as quantitatively measured by analysis of DNA content for G2/M cell fraction and also visually observed by reappearance of the G1 peak (Figure 3.6A and B). Furthermore, Mut-2 clones also showed delayed resolution of γH2AX signalling over the recovery period (Figure 3.6C).

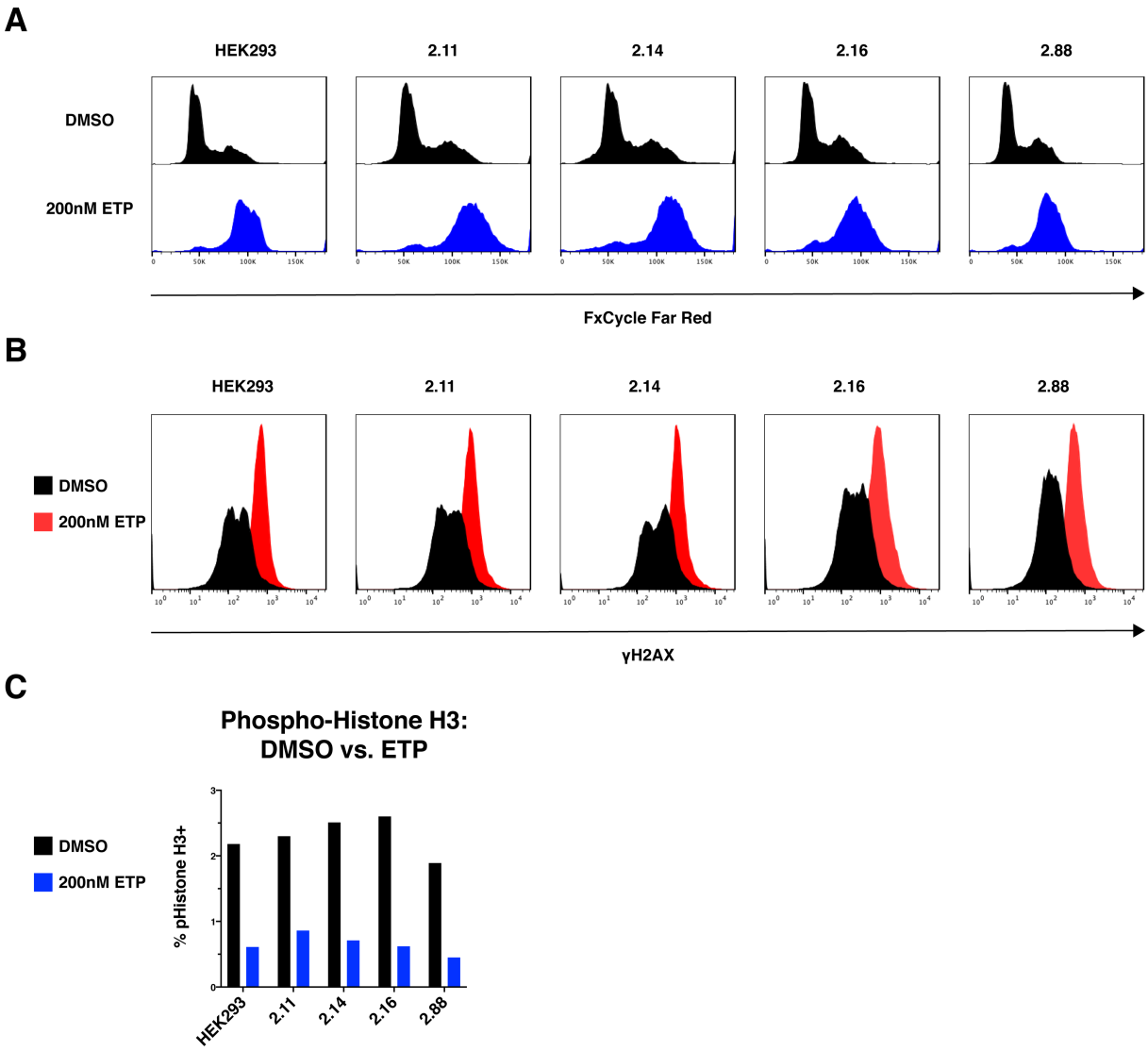

Figure 3.5 The effects of etoposide on the Mut-2 clones

A. Etoposide causes arrest at G2/M phase as shown by total DNA content (FxCycle Far Red). Histogram plots show linearly plotted total DNA content (x-axis). Each plot shows comparison of the corresponding cell line treated overnight with 0.1% DMSO (top, black) or 200nM ETP (bottom, blue). At least 18,000 cells were analysed by flow cytometry for each cell line and condition.

B. Overnight etoposide treatment leads to increased γH2AX staining in both the Mut-2 clones and the parental HEK293. Histogram plots show γH2AX staining plotted on log scales (x-axis). Cells were treated overnight with 0.1% DMSO (black) or 200nM ETP (red). At least 18,000 cells were analysed by flow cytometry for each cell line and condition.

C. Cell cycle arrest caused by etoposide decreases phospho-histone H3 staining in Mut-2, suggesting a pre-mitosis arrest in late-S/G2. Plot shows percentage of cells positive for phospho-histone H3 for each cell line after overnight treatment with 0.1% DMSO (black bars) or 200nM ETP (blue bars). At least 20,000 cells were analysed by flow cytometry for each cell line.

Data in A-B is representative of five independent experiments. Data in C is representative of three independent experiments.

A

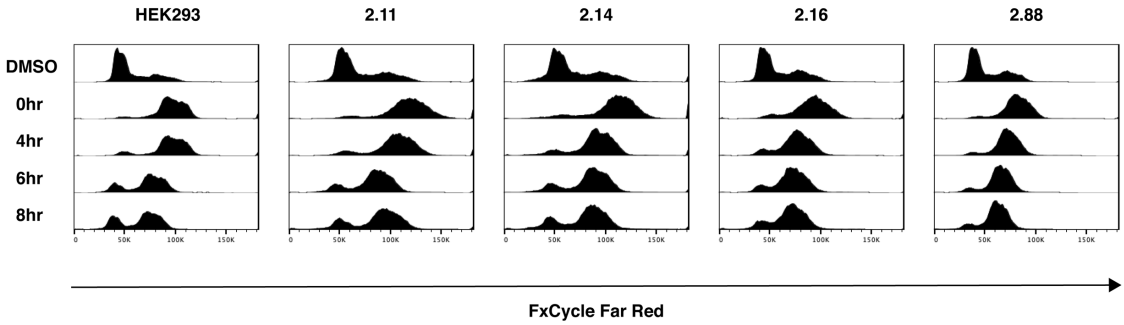
HEK293
2.11
2.14
2.16
2.88
DMSO
0hr
4hr
6hr
8hr
FxCycle Far Red

B

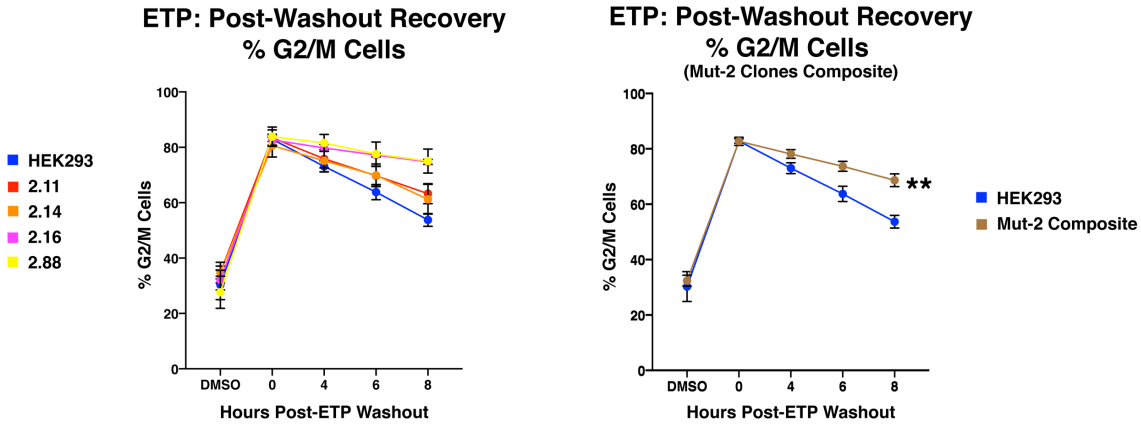
ETP: Post-Washout Recovery
% G2/M Cells
HEK293
2.11
2.14
2.16
2.88
% G2/M Cells
Hours Post-ETP Washout
ETP: Post-Washout Recovery
% G2/M Cells
(Mut-2 Clones Composite)
**
HEK293
Mut-2 Composite

C

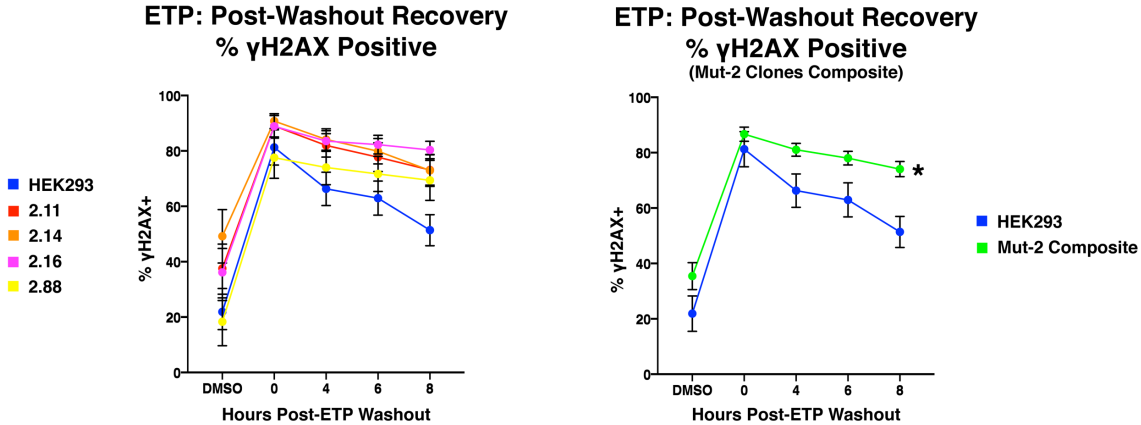
ETP: Post-Washout Recovery
% γH2AX Positive
HEK293
2.11
2.14
2.16
2.88
% γH2AX+
Hours Post-ETP Washout
ETP: Post-Washout Recovery
% γH2AX Positive
(Mut-2 Clones Composite)
*
HEK293
Mut-2 Composite

Figure 3.6 Etoposide treatment and recovery in Mut-2 clones
A. Cell cycle analyses of etoposide recovery using total DNA content (FxCycle Far Red) show delayed progression through M-phase and delayed reappearance of the G1 cell population in the Mut-2 clones compared with parental HEK293. Plots show stacked histograms of total DNA content staining linearly plotted on the x-axis. Hours indicate time after ETP washout. DMSO samples were assayed at the same time as the 0hr time point. At least 16,000 cells were analysed by flow cytometry for each cell line and condition.
B. Cell cycle progression during etoposide recovery as measured by the percentage of G2/M cells as determined by total DNA content. Mut-2 clones show slower decreases in G2/M cell population over time compared with parental HEK293. Curves for individual cell lines are shown on the left and composite plot showing the average of the Mut-2 clones is on the right. The flow cytometer was set to acquire 20,000 events for each cell line and condition in every experiment.
C. Mut-2 clones show slower decrease in γH2AX staining compared with parental HEK293. Curves for individual cell lines are shown on the left and composite plot showing the average of the Mut-2 clones is on the right. The flow cytometer was set to acquire 20,000 events for each cell line and condition in every experiment.

Statistical significance for the differences between the slopes of the composite curves in B and C were determined using extra sum-of-squares F test (* = $p < 0.05$ and ** = $p < 0.01$)

Data shown in A is representative of five independent experiments. Data shown in B-C is from five independent experiments. Error bars in B and C show SEM.

3.3.4 Mut-2 clones showed defects in HR and MMEJ DNA DSB repair

Based on the mechanisms of DNA damage repair activated by the DNA damaging agents used above, the pattern of sensitivity of the Mut-2 clones relative to parental HEK293 was suggestive of defective DNA DSB repair, particularly defective HR. Flow cytometry-based GFP reporter constructs were used to directly assay the functional status of HR, NHEJ, and MMEJ pathways in the Mut-2 clones. These constructs could be cleaved by a separately expressed restriction enzyme, *I-SceI*, and subsequently repaired using the specified pathway to reconstitute a functional GFP expression cassette. Critically, only correct DNA DSB repair by the particular pathway for which the reporter was designed would result in functional GFP expression. The details of these constructs and their mechanism of action are discussed in the Chapter 3 introduction above (Section 3.1.2, Figure 3.2).

In these GFP reporter assays, the Mut-2 clones showed 30-60% decreases in HR and MMEJ capacity. Additionally, the majority of clones (2.11, 2.14, and 2.88) did not show defective NHEJ (Figure 3.7B). The only exception was clone 2.16, which in the drug testing above showed clone-specific sensitivity to all compounds tested (Figure 3.4). Here, clone 2.16 not only showed the greatest decline in HR and MMEJ repair efficiency, but also showed a decrease in NHEJ repair capacity. This further strengthened the case for clone 2.16 being a clone-specific outlier.

A

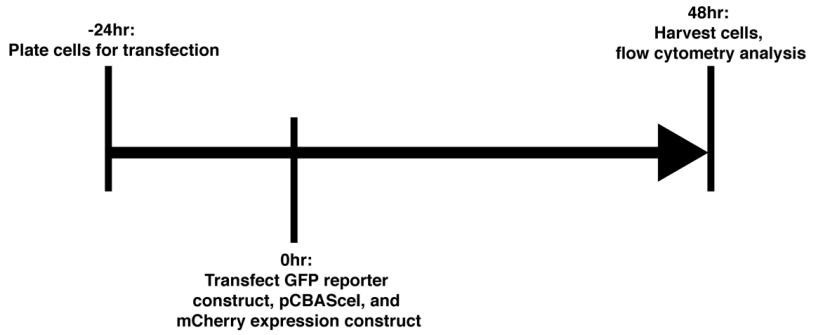
-24hr:
Plate cells for transfection
48hr:
Harvest cells,
flow cytometry analysis
0hr:
Transfect GFP reporter
construct, pCBAScel, and
mCherry expression construct

B

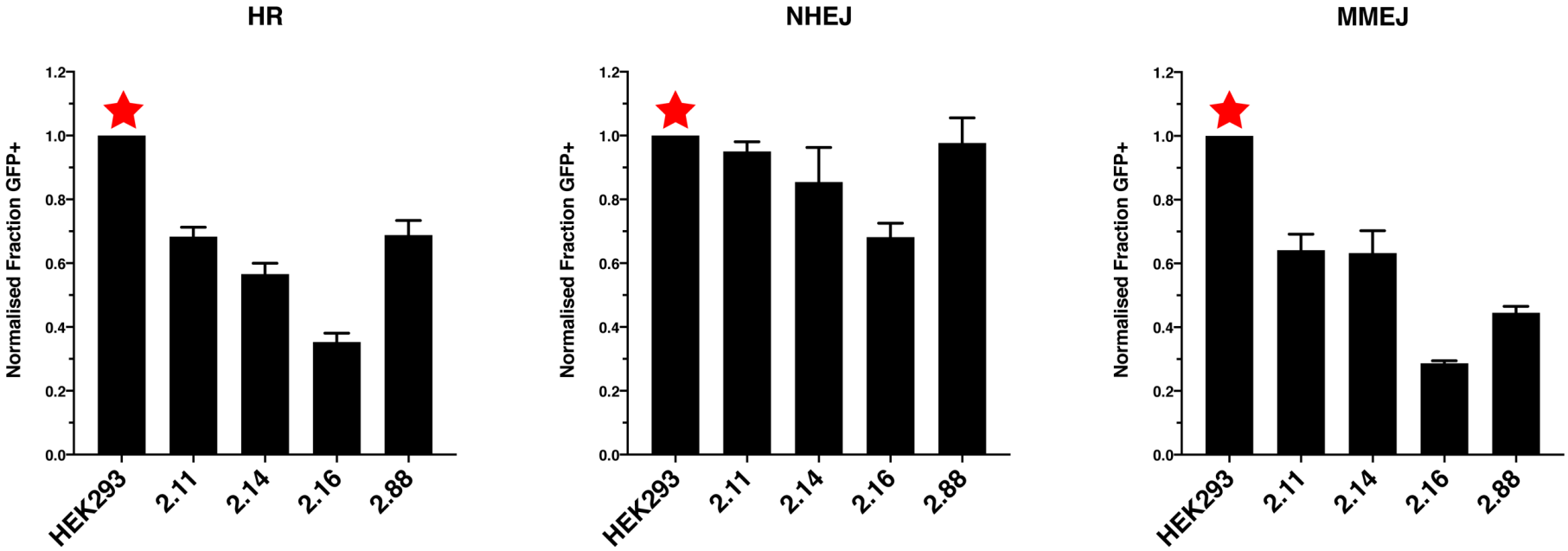
HR
NHEJ
MMEJ
Normalised Fraction GFP+
0.0
0.2
0.4
0.6
0.8
1.0
1.2
HEK293
2.11
2.14
2.16
2.88

Figure 3.7 DNA DSB repair pathway function in Mut-2 clones

A. Experimental timeline for the GFP reporter assays.

B. Capacity of DNA DSB repair pathways (HR, NHEJ, MMEJ) in parental HEK293 and Mut-2 clones as assayed by flow cytometric GFP reporter assays. Compared with parental HEK293, all Mut-2 clones show decreased rates of repair by HR and MMEJ. While the majority of Mut-2 clones (2.11, 2.14, and 2.88) show normal levels of NHEJ repair compared with parental HEK293, clone 2.16 is the exception in showing decreased rates of repair by NHEJ. All data are normalised to parental HEK293 (red star) in each respective reporter assay. The flow cytometer was set to acquire 20,000 events for each sample in every experiment. Data shown is the average of at least 7 independent experiments. Error bars show SEM.

3.3.5 The effects of RECQL4 overexpression on drug sensitivity in Mut-2 clones

To confirm that the sensitivities of the Mut-2 clones to the various compounds tested above (Figure 3.4) were indeed due to the *RECQL4* Mut-2 mutation, RECQL4 was overexpressed in the Mut-2 clones and the parental HEK293 by transduction with a GFP-containing empty lentiviral expression vector (EX-NEG-Lv246, Genecopoeia), the same vector expressing wild-type RECQL4, or the same vector expressing the cDNA of the alternatively spliced RECQL4 ΔEx14. Transduced cells were selected using puromycin and overexpression of the two variants of RECQL4 were confirmed both at the transcript and protein levels via RT-qPCR and western blot (Figure 3.8A and B).

These sets of cells were then tested with a selected panel of compounds used previously (HU, MMS, and ETP). As expected, the RECQL4-reconstituted cells showed no significant difference when compared with the empty vector controls when treated with HU, which did not produce increased sensitivity in the original Mut-2 clones (Figure 3.8C-E, Figure 3.4A). Unexpectedly however, the majority of the clones (2.11, 2.14, and 2.88) overexpressing both variants of RECQL4 showed rescue effects when treated with MMS and ETP relative to equivalent parental HEK293 and the empty vector controls (Figure 3.8F-K). Furthermore, cells overexpressing RECQL4 ΔEx14 were actually better at rescuing the effects of the drug treatments than wild-type RECQL4 in some cases (Figure 3.8H and K). The only exception to this rescue phenotype was clone 2.16, which showed little to no rescue effect in any drug treatment. This once again reinforced that the broad sensitivities seen previously in clone 2.16 (Figure 3.4) were possibly due to as yet undetermined clone-specific effects unrelated to the *RECQL4* Mut-2 mutation.

Since the Incucyte Zoom measured proliferation using confluency as a readout, it was possible that the rescue effects seen above by both variants of RECQL4 could be due to

increased proliferative potential as a result of increased levels of RECQL4 and RECQL4's role in DNA replication (Abe et al., 2011; Matsuno et al., 2006; Sangrithi et al., 2005). If this was indeed the case, then any defect in DNA damage repair might be masked by increased growth rate. Indeed, when measured by doubling time, both sets of Mut-2 cells overexpressing RECQL4 showed faster doubling times compared with parental HEK293 and empty vector controls (Figure 3.8L). Cells overexpressing RECQL4 ΔEx14, in particular, showed a greater magnitude of decrease in doubling times, which might explain their showing greater "rescue" effect (Figure 3.8E, H, K, and L).

A

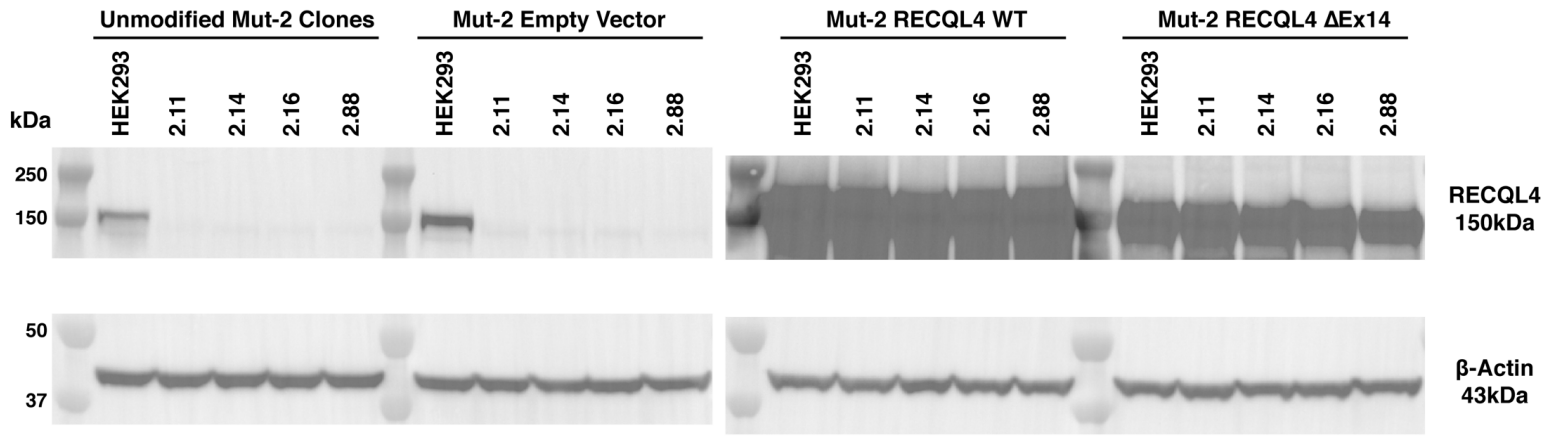
Unmodified Mut-2 Clones
Mut-2 Empty Vector
Mut-2 RECQL4 WT
Mut-2 RECQL4 ΔEx14
HEK293
2.11
2.14
2.16
2.88
kDa
250
150
50
37
RECQL4
150kDa
β-Actin
43kDa

B

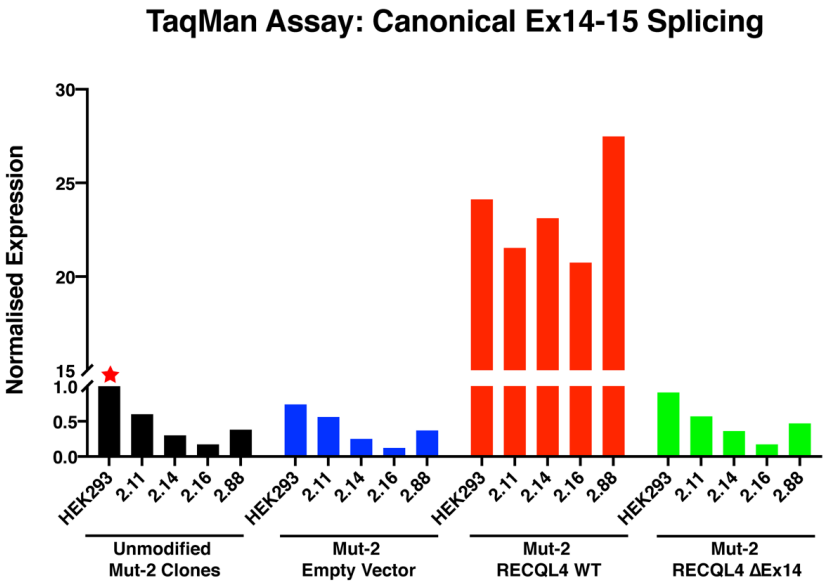
TaqMan Assay: Canonical Ex14-15 Splicing
Normalised Expression
30
25
20
15
1.0
0.5
0.0
HEK293
2.11
2.14
2.16
2.88
Unmodified Mut-2 Clones
Mut-2 Empty Vector
Mut-2 RECQL4 WT
Mut-2 RECQL4 ΔEx14

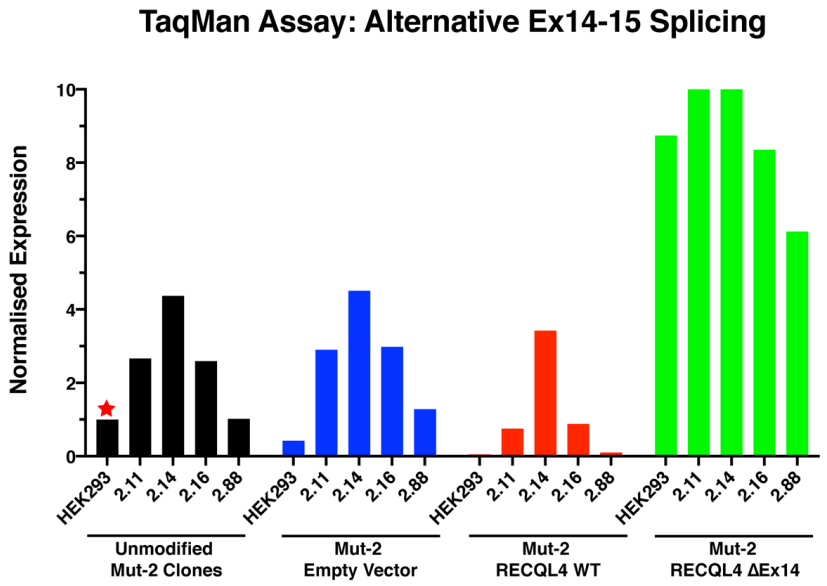
TaqMan Assay: Alternative Ex14-15 Splicing
Normalised Expression
10
8
6
4
2
0
HEK293
2.11
2.14
2.16
2.88
Unmodified Mut-2 Clones
Mut-2 Empty Vector
Mut-2 RECQL4 WT
Mut-2 RECQL4 ΔEx14

C

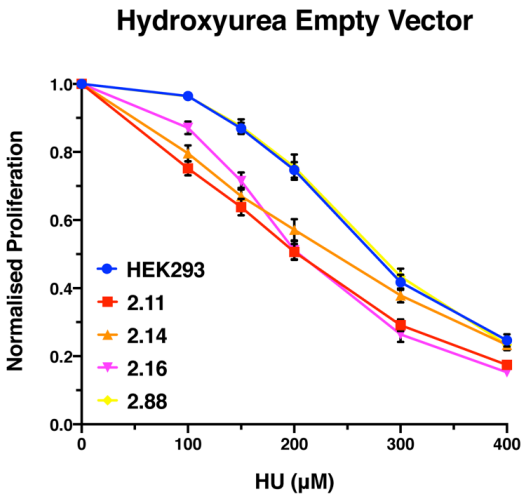
Hydroxyurea Empty Vector
Normalised Proliferation
HU (μM)
HEK293
2.11
2.14
2.16
2.88

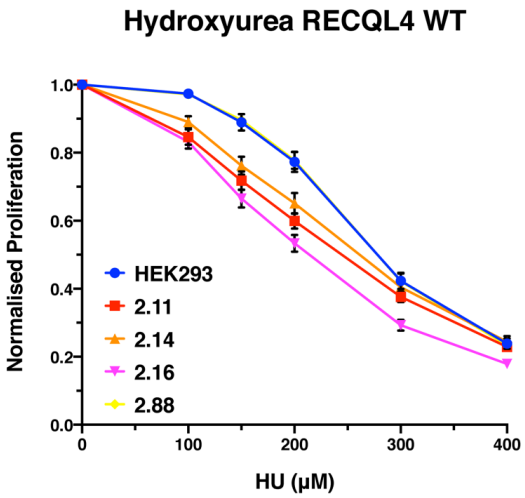
Hydroxyurea RECQL4 WT
Normalised Proliferation
HU (μM)
HEK293
2.11
2.14
2.16
2.88

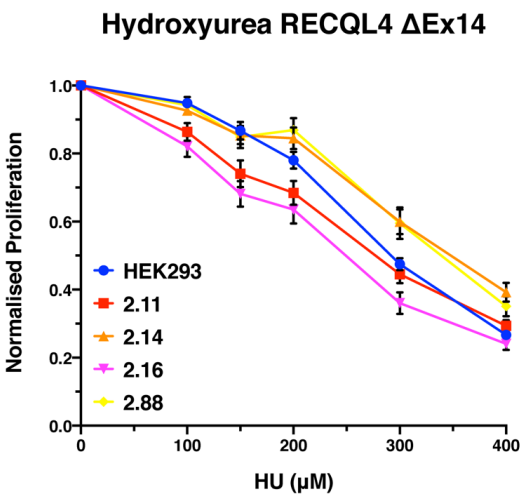
Hydroxyurea RECQL4 ΔEx14
Normalised Proliferation
HU (μM)
HEK293
2.11
2.14
2.16
2.88

D

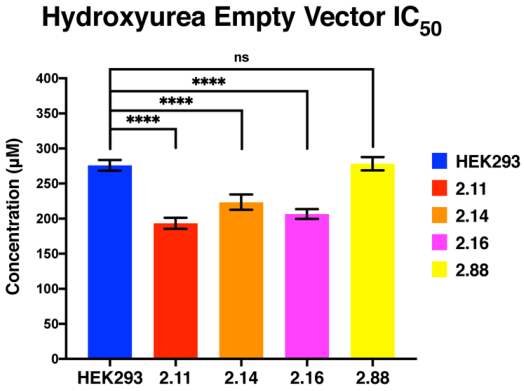
Hydroxyurea Empty Vector IC50
Concentration (μM)
ns
****
****
****
HEK293
2.11
2.14
2.16
2.88

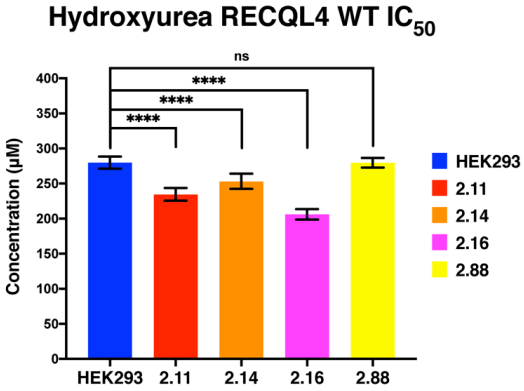
Hydroxyurea RECQL4 WT IC50
Concentration (μM)
ns
****
****
****
HEK293
2.11
2.14
2.16
2.88

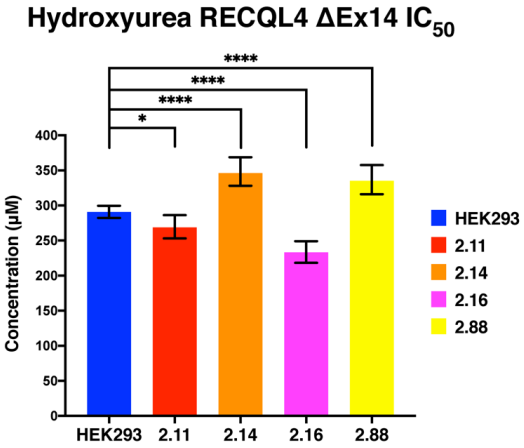
Hydroxyurea RECQL4 ΔEx14 IC50
Concentration (μM)
****
****
****
*
HEK293
2.11
2.14
2.16
2.88

E

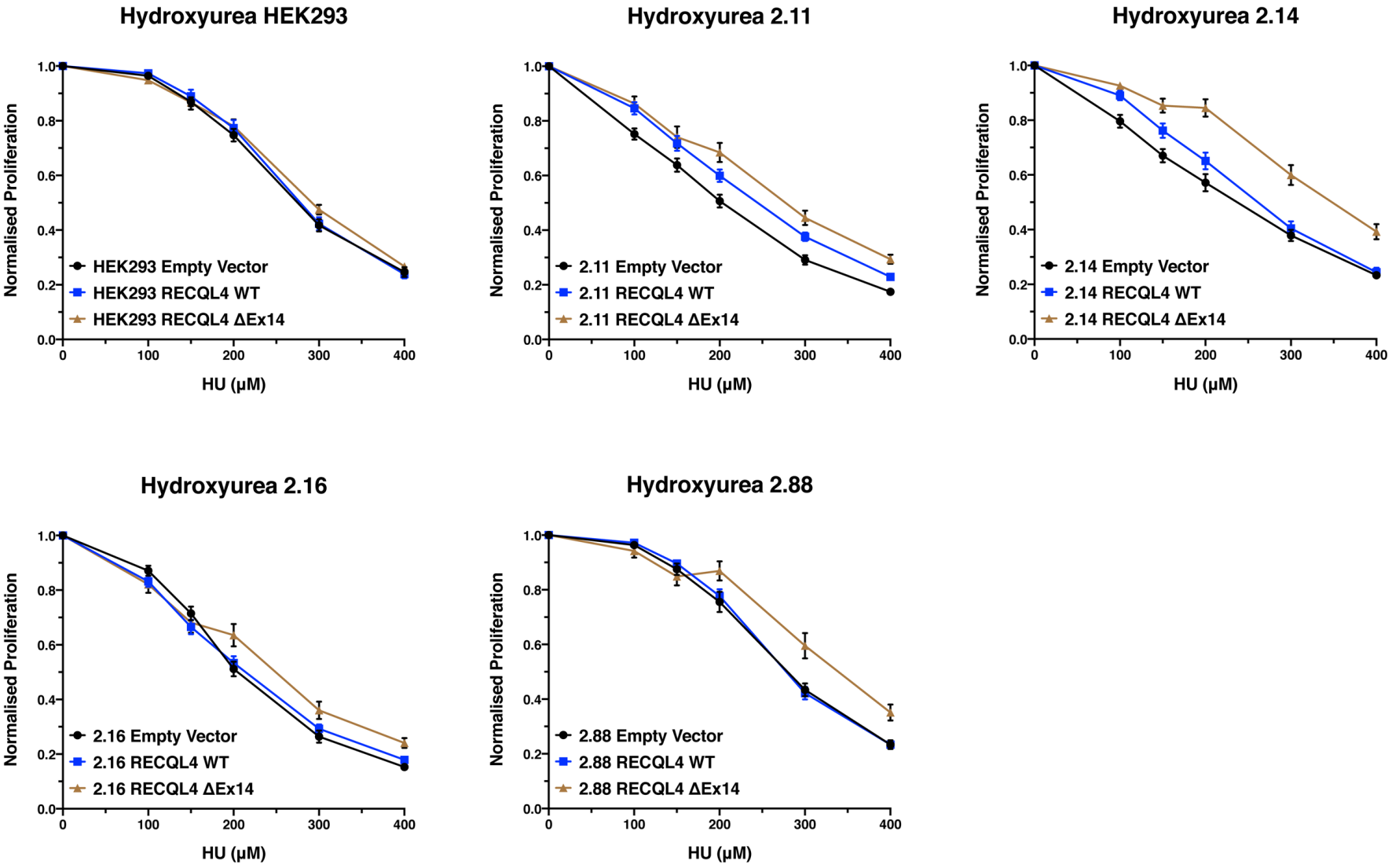
Hydroxyurea HEK293
Normalised Proliferation
HU (μM)
HEK293 Empty Vector
HEK293 RECQL4 WT
HEK293 RECQL4 ΔEx14
Hydroxyurea 2.11
2.11 Empty Vector
2.11 RECQL4 WT
2.11 RECQL4 ΔEx14
Hydroxyurea 2.14
2.14 Empty Vector
2.14 RECQL4 WT
2.14 RECQL4 ΔEx14
Hydroxyurea 2.16
2.16 Empty Vector
2.16 RECQL4 WT
2.16 RECQL4 ΔEx14
Hydroxyurea 2.88
2.88 Empty Vector
2.88 RECQL4 WT
2.88 RECQL4 ΔEx14

F

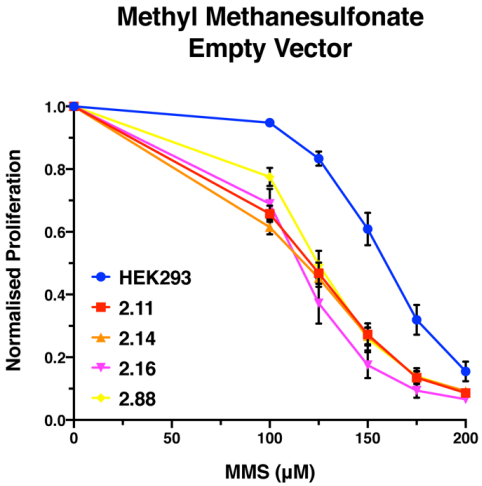
Methyl Methanesulfonate
Empty Vector
Normalised Proliferation
MMS (μM)
HEK293
2.11
2.14
2.16
2.88

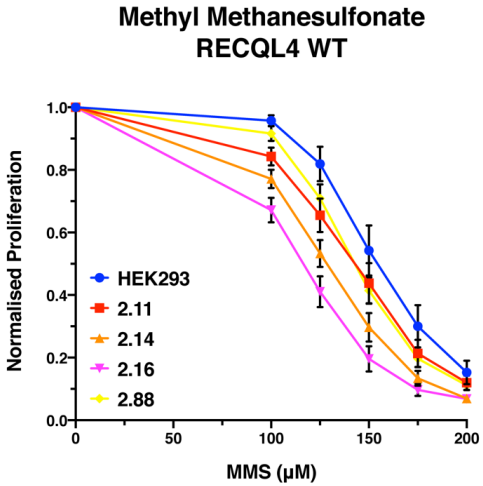
Methyl Methanesulfonate
RECQL4 WT
Normalised Proliferation
MMS (μM)
HEK293
2.11
2.14
2.16
2.88

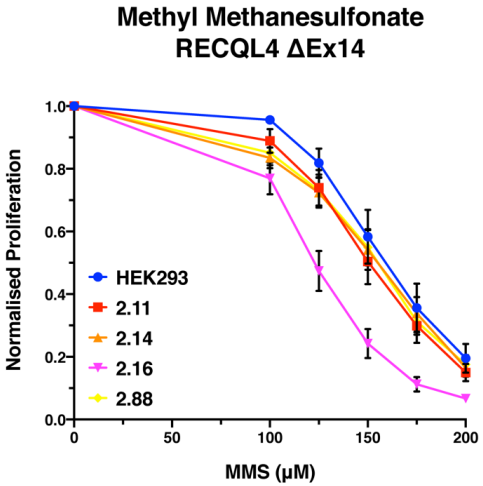
Methyl Methanesulfonate
RECQL4 ΔEx14
Normalised Proliferation
MMS (μM)
HEK293
2.11
2.14
2.16
2.88

G

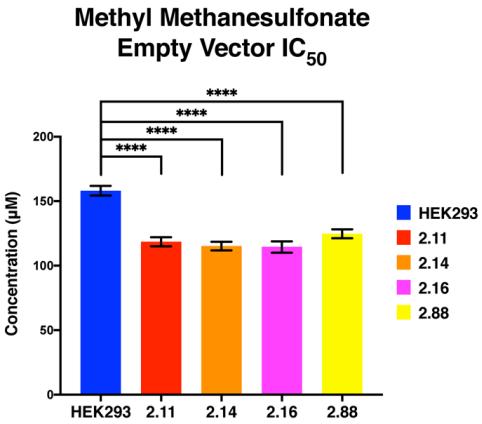
Methyl Methanesulfonate
Empty Vector IC50
Concentration (μM)
HEK293
2.11
2.14
2.16
2.88

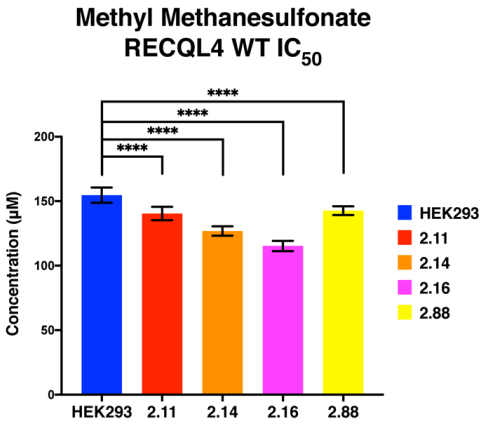
Methyl Methanesulfonate
RECQL4 WT IC50
Concentration (μM)
HEK293
2.11
2.14
2.16
2.88

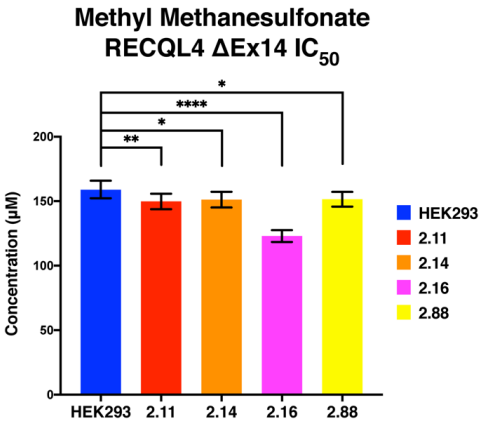
Methyl Methanesulfonate
RECQL4 ΔEx14 IC50
Concentration (μM)
HEK293
2.11
2.14
2.16
2.88

H

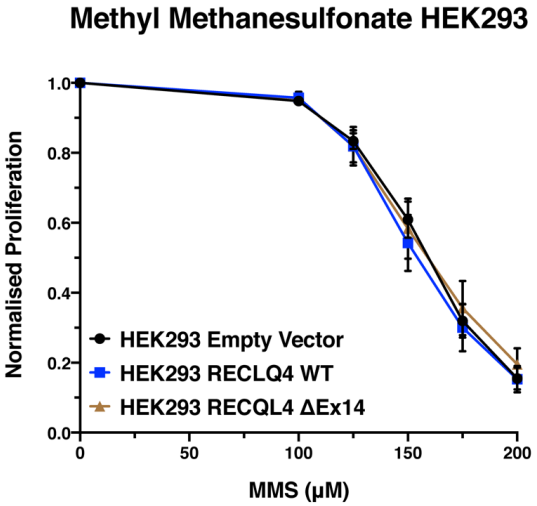
Methyl Methanesulfonate HEK293
Normalised Proliferation
1.0
0.8
0.6
0.4
0.2
0.0
0
50
100
150
200
MMS (μM)
HEK293 Empty Vector
HEK293 RECLQ4 WT
HEK293 RECQL4 ΔEx14

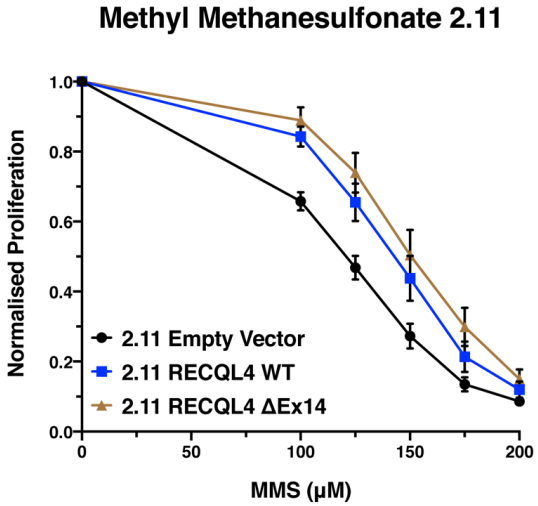
Methyl Methanesulfonate 2.11
Normalised Proliferation
1.0
0.8
0.6
0.4
0.2
0.0
0
50
100
150
200
MMS (μM)
2.11 Empty Vector
2.11 RECQL4 WT
2.11 RECQL4 ΔEx14

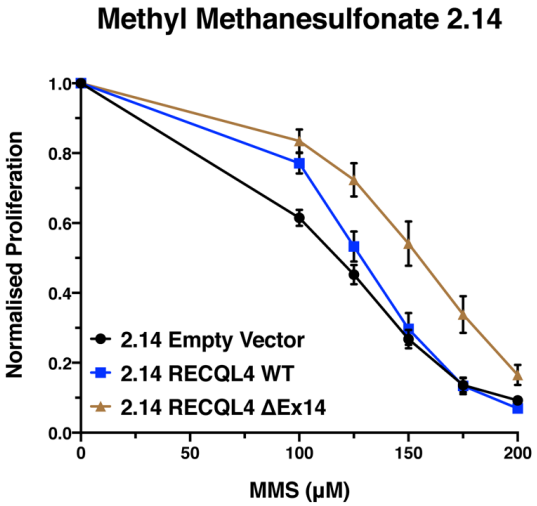
Methyl Methanesulfonate 2.14
Normalised Proliferation
1.0
0.8
0.6
0.4
0.2
0.0
0
50
100
150
200
MMS (μM)
2.14 Empty Vector
2.14 RECQL4 WT
2.14 RECQL4 ΔEx14

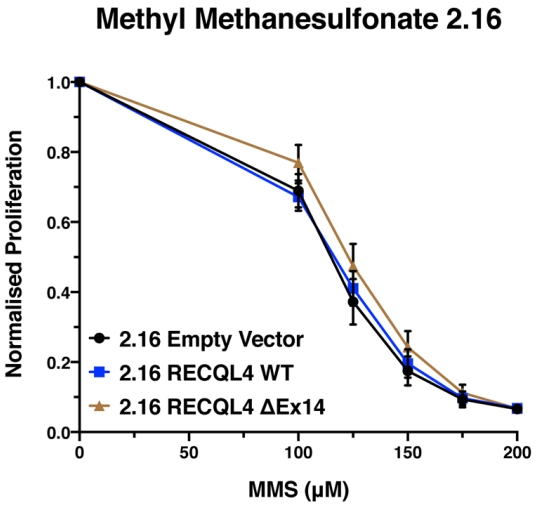
Methyl Methanesulfonate 2.16
Normalised Proliferation
1.0
0.8
0.6
0.4
0.2
0.0
0
50
100
150
200
MMS (μM)
2.16 Empty Vector
2.16 RECQL4 WT
2.16 RECQL4 ΔEx14

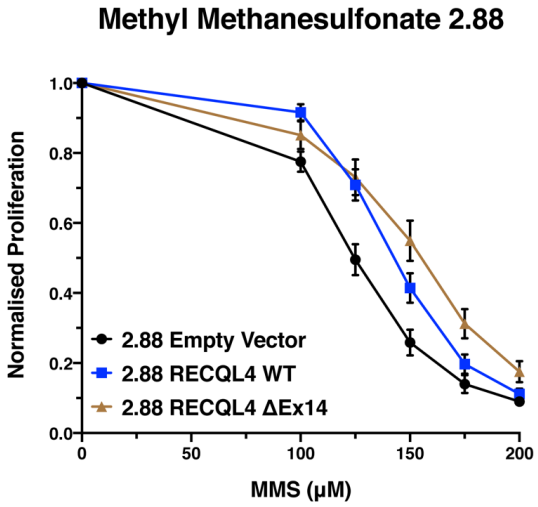
Methyl Methanesulfonate 2.88
Normalised Proliferation
1.0
0.8
0.6
0.4
0.2
0.0
0
50
100
150
200
MMS (μM)
2.88 Empty Vector
2.88 RECQL4 WT
2.88 RECQL4 ΔEx14

I

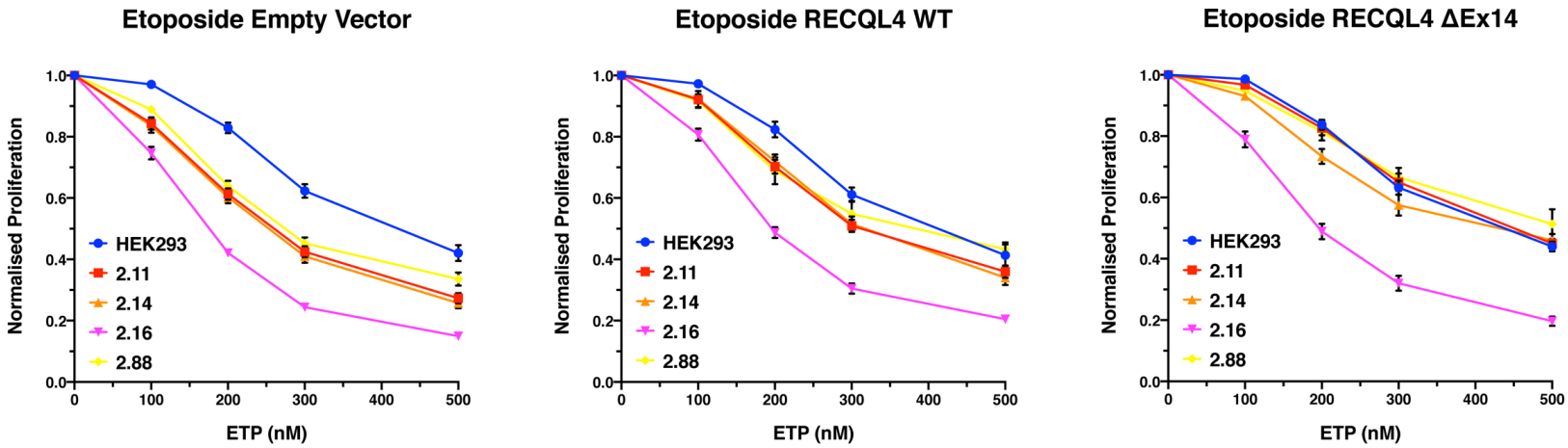
Etoposide Empty Vector
Etoposide RECQL4 WT
Etoposide RECQL4 ΔEx14
Normalised Proliferation
ETP (nM)
HEK293
2.11
2.14
2.16
2.88

J

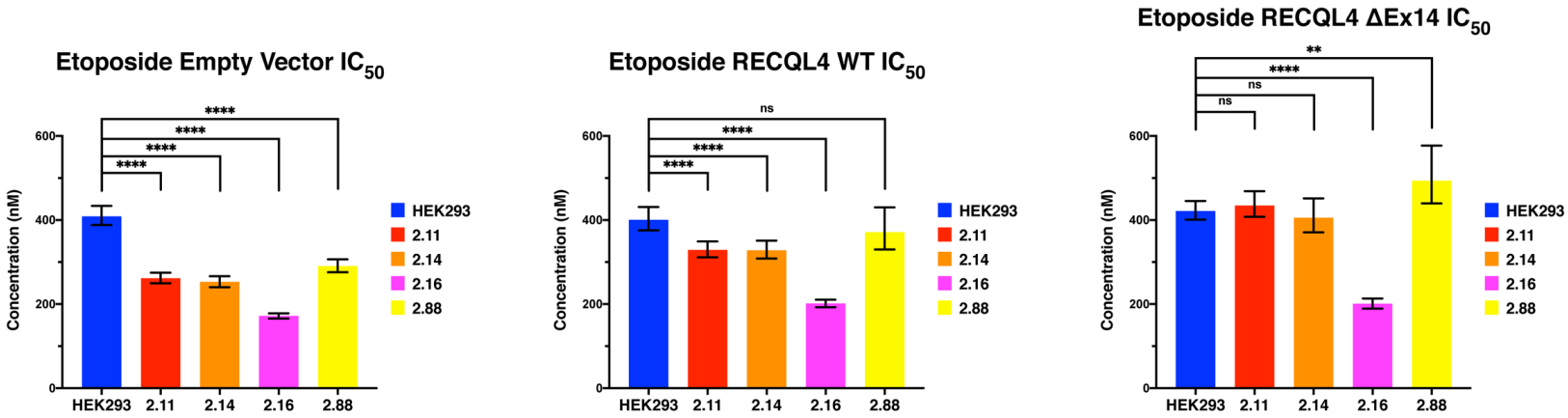
Etoposide Empty Vector IC50
Etoposide RECQL4 WT IC50
Etoposide RECQL4 ΔEx14 IC50
Concentration (nM)
HEK293
2.11
2.14
2.16
2.88
ns
**
****

K

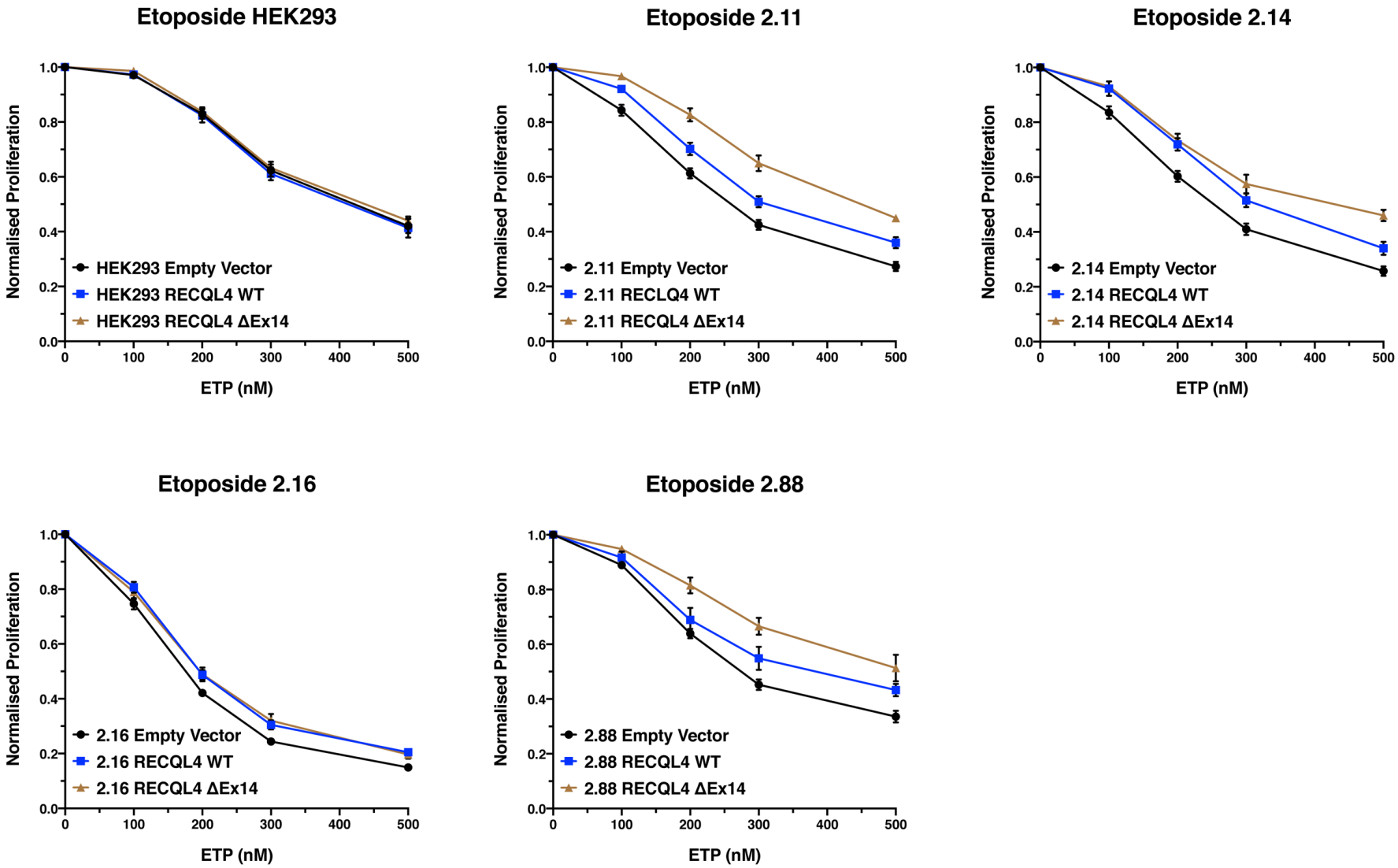
Etoposide HEK293
Normalised Proliferation
ETP (nM)
HEK293 Empty Vector
HEK293 RECQL4 WT
HEK293 RECQL4 ΔEx14
Etoposide 2.11
2.11 Empty Vector
2.11 RECLQ4 WT
2.11 RECQL4 ΔEx14
Etoposide 2.14
2.14 Empty Vector
2.14 RECQL4 WT
2.14 RECQL4 ΔEx14
Etoposide 2.16
2.16 Empty Vector
2.16 RECQL4 WT
2.16 RECQL4 ΔEx14
Etoposide 2.88
2.88 Empty Vector
2.88 RECQL4 WT
2.88 RECQL4 ΔEx14

L

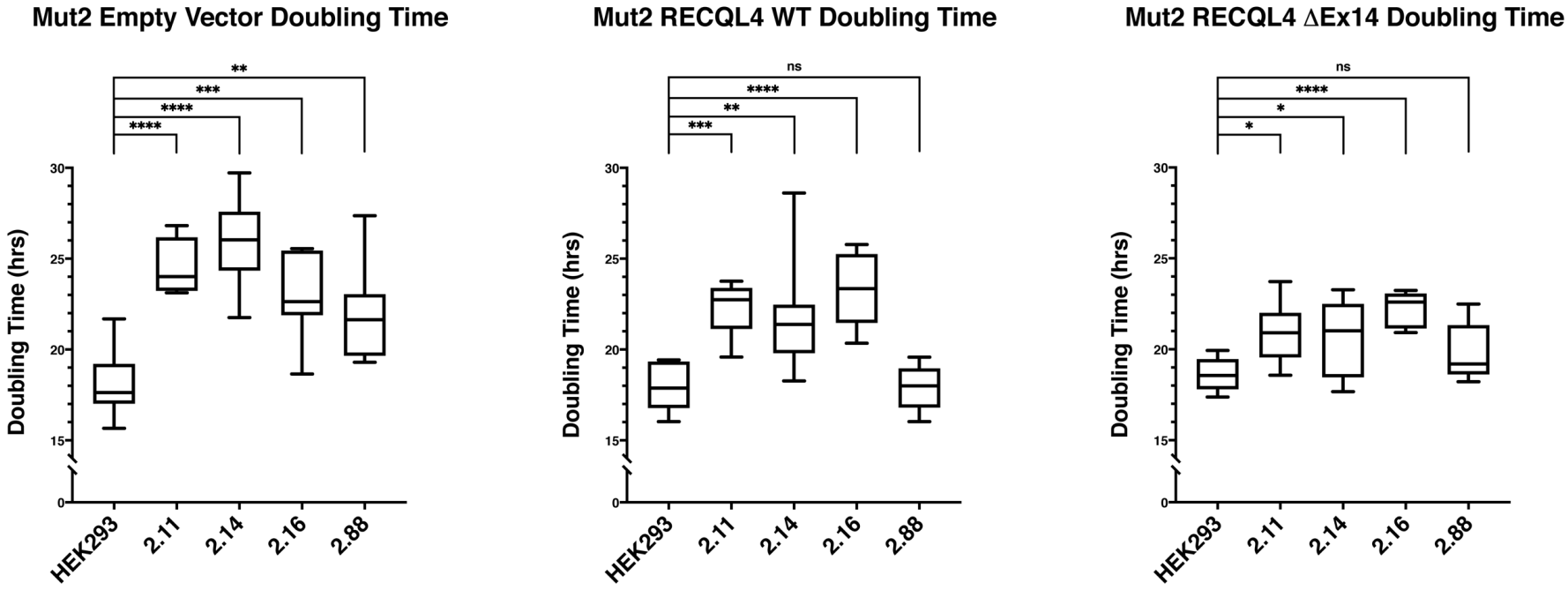
Mut2 Empty Vector Doubling Time
Doubling Time (hrs)
30
25
20
15
0
**
***
****
****
HEK293
2.11
2.14
2.16
2.88
Mut2 RECQL4 WT Doubling Time
Doubling Time (hrs)
ns
****
**
***
Mut2 RECQL4 ΔEx14 Doubling Time
Doubling Time (hrs)
ns
****
*
*

Figure 3.8 Effects of RECQL4 overexpression on sensitivities to select compounds in Mut-2 clones

Dose response curve plots in Parts C, F, and I show normalised proliferation (as a fraction of the appropriate untreated or vehicle treated control) vs. treatment dose for parental HEK293 and each of the Mut-2 clones. The RECQL4 variant expressed in each set of cells and the compound with which they were treated are indicated in the title. See more details in Figure 3.4 legend above

Dose response curve plots in Parts E, H, and K group curves based on cell line with each plot showing curves for a single cell line containing empty vector or expressing wild-type or ΔEx14 variant of RECQL4. The curves shown are the same as those shown in Parts C, F, and I.

Each dose response curve is an average of 14 independent experiments. Error bars represent SEM. Proliferation is measured by confluency using the Incucyte Zoom instrument. Each treatment condition was generally tested in triplicate for every experiment. Detailed assay setup and analysis methods are given above in Methods Section 3.2.6.

Bar graphs in Parts D, G, and J show IC_{50} values for the corresponding plots in Parts C, F, and I, calculated using Graphpad Prism. Error bars show asymmetrical 95% confidence intervals reported by Prism's model fitting algorithm. Details on the curve-fitting model, the parameters, and the settings used are also given above in Methods Section 3.2.6. Statistical significance was determined using extra sum-of-squares F test. (* = $p < 0.05$, ** = $p < 0.01$, *** = $p < 0.001$, **** = $p < 0.0001$, ns = not significant).

A. Western blot of RECQL4 in unmodified Mut-2 clones, Mut-2 clones with empty expression vector, Mut-2 clones overexpressing wild-type RECQL4, and Mut-2 clones overexpressing RECQL4 ΔEx14. Latter two sets of cells show greatly increased RECQL4 expression compared with unmodified or empty vector Mut-2 clones. Samples are divided between two blots with the former two sets of cells on the first blot and the latter two sets of cells on the second blot. Images shown are of the two blots developed simultaneously under identical conditions and exposure lengths in order to show the dynamic range of the RECQL4 protein abundance between the different sets of cells. Western blot shown is representative of two independent experiments.
B. RT-qPCR of RECQL4 transcripts from cells from Part A using TaqMan assays specific for the canonical RECQL4 exon 14-15 splice junction and the alternate exon 14-15 splice junction. Mut-2 clones with either wild-type or ΔEx14 RECQL4 show overexpression of appropriate form of RECQL4. Red stars indicate the samples used for normalisation in each assay. Data shown is from one experiment.
C-E. The overall sensitivity profiles of the sets of cells (Mut-2 clones and parental HEK293) containing empty expression vector, wild-type RECQL4, and RECQL4 ΔEx14 to hydroxyurea (HU) do not differ substantially from each other as seen in the dose response curves (C) and the IC_{50} values (D). Some clones (2.11 and 2.14) do show increased proliferation in cells overexpressing RECQL4 (E).
F-H. The overall sensitivity profiles of the same set of cells as Parts C-E above when treated with MMS show that, in the majority of the Mut-2 clones (2.11, 2.14, and 2.88), the increased sensitivities of the Mut-2 clones relative to parental HEK293 in the empty vector control set is rescued by overexpression of either forms of RECQL4 (F and H). The only exception is clone

2.16 where the rescue effect is not observed. This rescue effect is apparent when curves are grouped based on cell line (H).

I-K. The overall sensitivity profiles of the same set of cells as Parts C-H above when treated with ETP show that, in the majority of the Mut-2 clones (2.11, 2.14, and 2.88), the increased sensitivities of the Mut-2 clones relative to parental HEK293 in the empty vector control set is rescued by overexpression of either forms of RECQL4 (I and J). Once again, clone 2.16 is an exception where the rescue effect is not readily apparent. However, all four clones do show rescue effects when plots are grouped by cell line (K). The magnitude of the difference in clone 2.16, however, is smaller than those seen in the other three Mut-2 clones, explaining why the rescue effect is not apparent in plots in Parts I and J.

L. Distributions of doubling times for the cells above as measured by Incucyte proliferation assay. In general, the differences in doubling times between the parental HEK293 and the Mut-2 clones are decreased in the sets of cells overexpressing RECQL4. Consistent with this finding, the statistical significances of the differences are also reduced in the majority of the clones (2.11, 2.14, and 2.88). (* = $p < 0.05$, ** = $p < 0.01$, *** = $p < 0.001$, **** = $p < 0.0001$, ns = not significant). Data shown is from 9 independent experiments.

3.3.6 Effects of RECQL4 overexpression on DNA DSB repair pathway function in Mut-2 clones

Since overexpressing the two RECQL4 variants in the Mut-2 clones could have impacted cell proliferation characteristics and thus masked any effect on DNA damage repair pathway function in the Incucyte proliferation assay (Figure 3.8), versions of the RECQL4 overexpression cells were generated that do not constitutively express GFP as part of the expression construct. These ΔGFP versions of the expression constructs were derived from the original Genecopoeia backbones with the GFP expression cassette removed. By doing so, these new ΔGFP cells could then be used for directly measuring DNA DSB repair capacity via the flow cytometry-based GFP reporter assays used above (Figure 3.2 and Figure 3.7). After puromycin selection, RECQL4 overexpression was confirmed once again via RT-qPCR and western blot for transcript and protein levels (Figure 3.9A and B).

In the HR GFP reporter assay, all four Mut-2 clones that overexpressed wild-type RECQL4 showed significantly increased HR repair capacity when compared with corresponding empty vector controls. On the other hand, those cells that overexpressed RECQL4 ΔEx14 did not show any increase in HR repair capacity, with 2 clones (2.14 and 2.88) actually showing a decrease in HR repair function when compared with empty vector control (Figure 3.9C, left).

In the NHEJ reporter assay, neither sets of cells overexpressing RECQL4 variants showed any significant increase in NHEJ repair capacity compared to empty vector controls. Clones 2.14 and 2.88 overexpressing RECQL4 ΔEx14, however, showed decreased NHEJ repair function (Figure 3.9C, middle).

In the MMEJ reporter assay, the majority of clones (2.11, 2.14, and 2.88) did not show increased MMEJ repair capacity when overexpressing either of the RECQL4 variants. Once again, clones 2.14 and 2.88 overexpressing RECQL4 ΔEx14 showed decreased MMEJ repair

function. Interestingly, clone 2.16 overexpressing wild-type RECQL4 showed increased MMEJ repair capacity though this also reinforced its putative status as an outlier clone (Figure 3.9C, right).

3.3.7 Mut-2 clones do not show defective RAD51 foci formation

RAD51 is an important component of the HR pathway and the formation of RAD51 foci as part of the strand-invading nucleoprotein filament is a commonly used marker of HR status and function (Cruz et al., 2018; Gachechiladze et al., 2017; Graeser et al., 2010; Jasin and Rothstein, 2013; Vierstraete et al., 2017). To further delineate the mechanism of the effect of *RECQL4* Mut-2 on HR function, RAD51 foci formation in Mut-2 clones after overnight etoposide treatment was investigated. Z-stack images were acquired on a Zeiss 780 confocal microscope and processed into maximum-intensity projections using an ImageJ script. RAD51 foci quantification was done using a custom KNIME pipeline which was validated using cells transfected with either siNon-targeting control or siRAD51 and then treated with either DMSO or etoposide (Figure 3.10C).

Surprisingly, after etoposide treatment, all Mut-2 clones increased formation of RAD51 foci to a similar extent as parental HEK293 (Figure 3.10A and B). All Mut-2 clones showed roughly double the number of RAD51 foci after overnight etoposide treatment which was comparable to the absolute level and the magnitude of increase of RAD51 foci seen in parental HEK293 after etoposide treatment (Figure 3.10B).

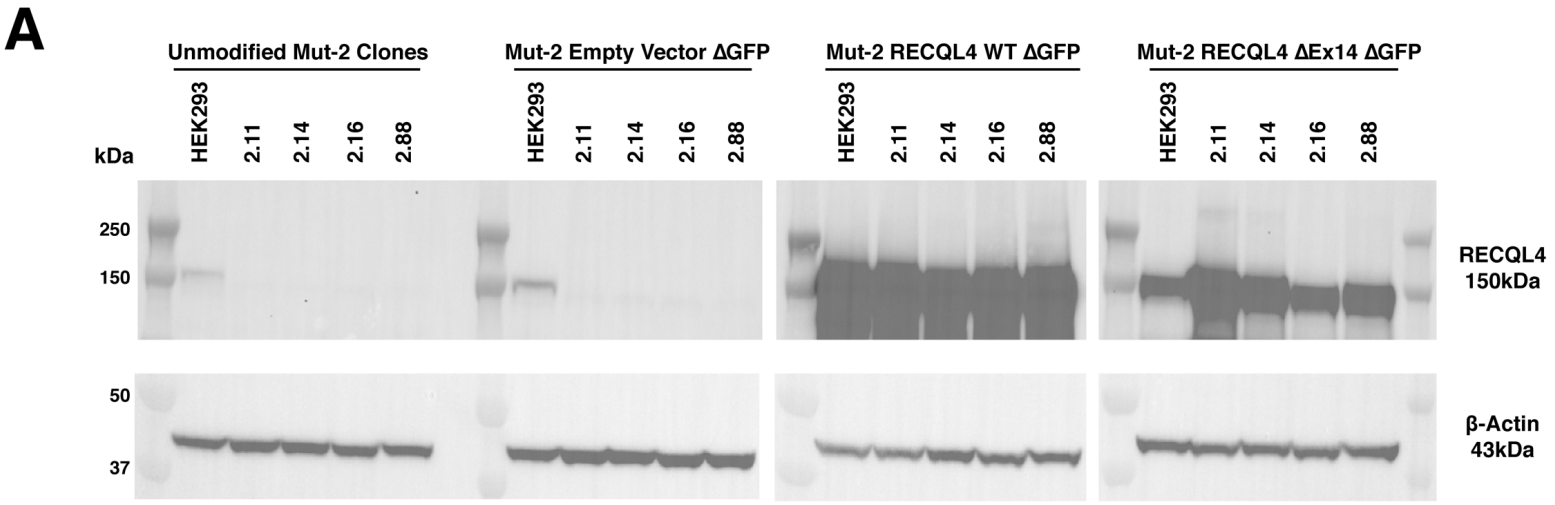
A
Unmodified Mut-2 Clones
Mut-2 Empty Vector ΔGFP
Mut-2 RECQL4 WT ΔGFP
Mut-2 RECQL4 ΔEx14 ΔGFP
HEK293
2.11
2.14
2.16
2.88
kDa
250
150
50
37
RECQL4
150kDa
β-Actin
43kDa

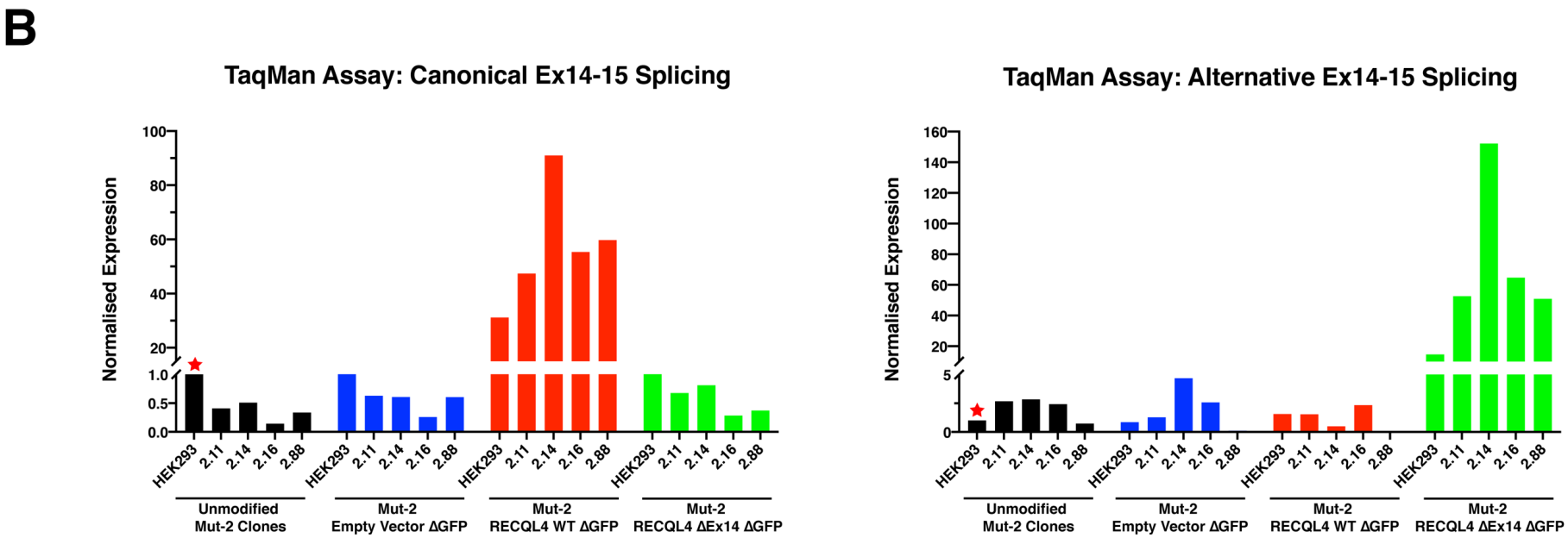
B
TaqMan Assay: Canonical Ex14-15 Splicing
TaqMan Assay: Alternative Ex14-15 Splicing
Normalised Expression
HEK293
2.11
2.14
2.16
2.88
Unmodified
Mut-2 Clones
Mut-2
Empty Vector ΔGFP
Mut-2
RECQL4 WT ΔGFP
Mut-2
RECQL4 ΔEx14 ΔGFP

C

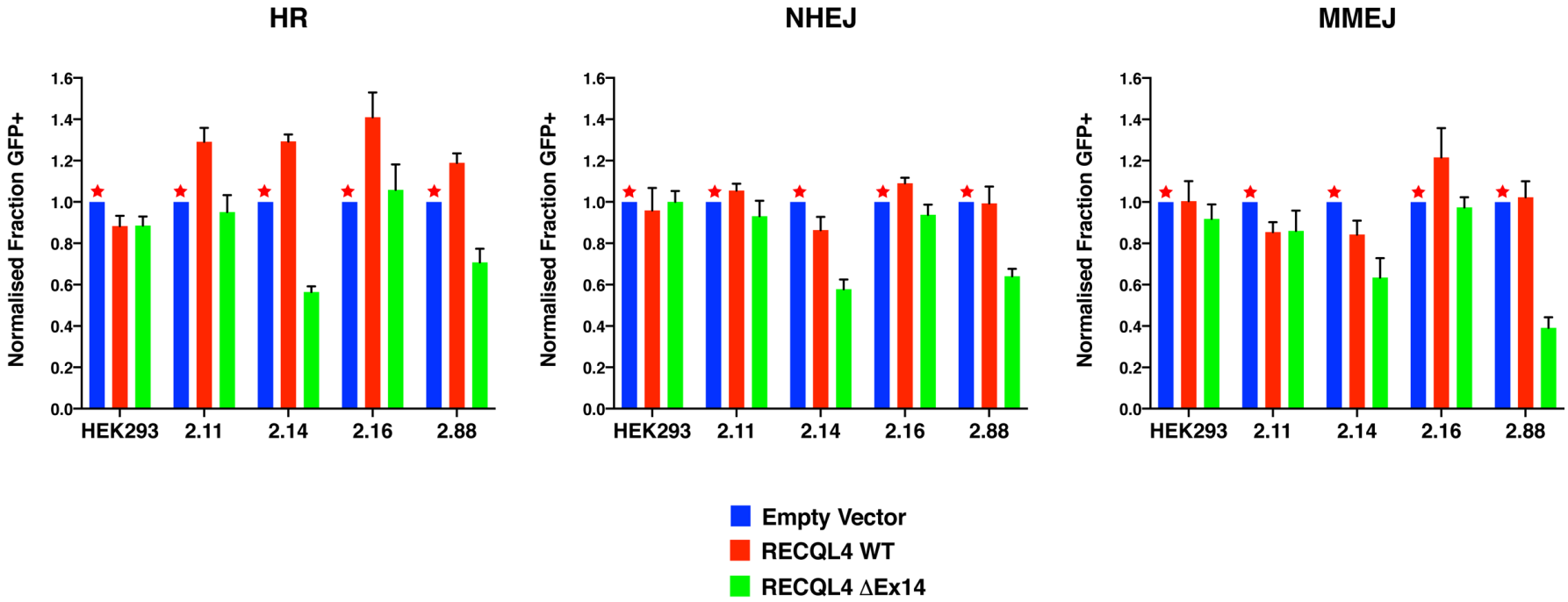
HR
NHEJ
MMEJ
Normalised Fraction GFP+
0.0
0.2
0.4
0.6
0.8
1.0
1.2
1.4
1.6
HEK293
2.11
2.14
2.16
2.88
Empty Vector
RECQL4 WT
RECQL4 ΔEx14

Figure 3.9 Effects of RECQL4 overexpression on DNA DSB repair capacity in Mut-2 clones
A-B. Validation by western blot and RT-qPCR of sets of cells (Mut-2 clones and parental HEK293) transduced with ΔGFP versions of the expression constructs used previously. Exposures of the western blots were chosen as in Figure 3.8A. See legend for Figure 3.8 Parts A-B above for more details. Data in Parts A-B are from one experiment each.
C. GFP reporter assays for HR, NHEJ, and MMEJ in the cells described in Parts A-B above. Each set of bars was normalised to the corresponding empty vector control within each cell line (red stars). Only the overexpression of wild-type RECQL4 results in increased rates of HR repair in the Mut-2 clones. The same effect on HR is not seen in those cells overexpressing the RECQL4 ΔEx14 variant. No consistent rescue effect is seen in either set of cells when assayed for NHEJ and MMEJ repair. Data shown is the average from 10 independent experiments. Error bars in C show SEM.

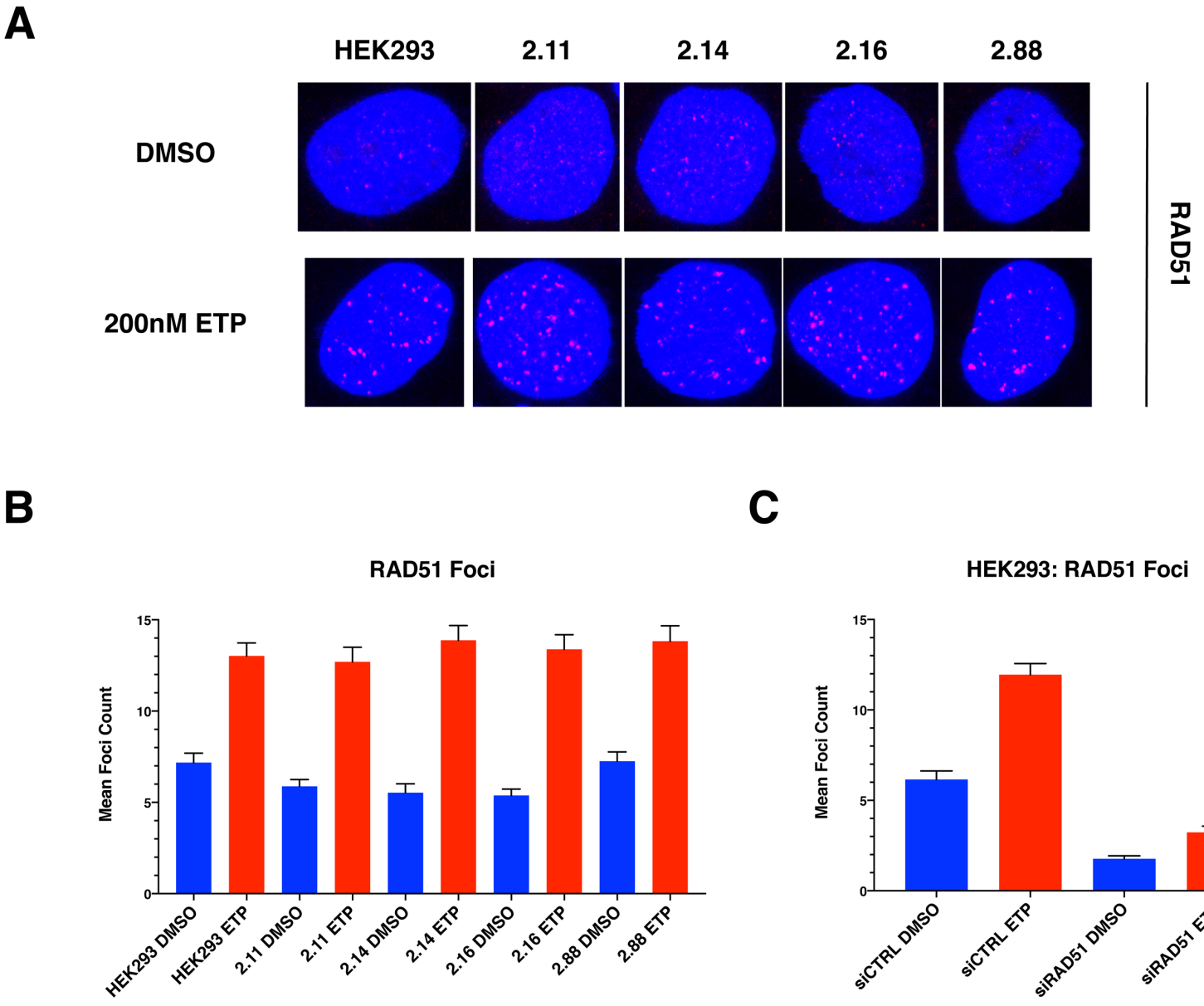
A
HEK293
2.11
2.14
2.16
2.88
DMSO
200nM ETP
RAD51
B
RAD51 Foci
Mean Foci Count
15
10
5
0
HEK293 DMSO
HEK293 ETP
2.11 DMSO
2.11 ETP
2.14 DMSO
2.14 ETP
2.16 DMSO
2.16 ETP
2.88 DMSO
2.88 ETP
C
HEK293: RAD51 Foci
Mean Foci Count
15
10
5
0
siCTRL DMSO
siCTRL ETP
siRAD51 DMSO
siRAD51 ETP

Figure 3.10 RAD51 foci formation in Mut-2 clones

A. Confocal images showing parental HEK293 and Mut-2 clones after overnight treatment with 0.1% DMSO or 200nM etoposide and staining with anti-RAD51 (red) and DAPI (blue). All cells show increased RAD51 foci formation with ETP treatment as would be expected with increased HR repair activity.

B. Quantification of RAD51 foci in cells from Part A. Mut-2 clones show increases in RAD51 foci formation upon ETP treatment (red bars) of the same magnitude as that seen in parental HEK293.

C. RAD51 foci quantification in cells transfected with siNon-targeting control or siRAD51 and then treated with 0.1% DMSO or 200nM etoposide. Cells treated with siRAD51 show substantially fewer RAD51 foci compared with those treated with siNon-targeting pool when both are treated with ETP.

Images and data shown in A-B are representative (the images) and from one experiment where at least 200 cells were imaged from each cell line and each treatment condition. Data and images are also representative of two independent experiments. Data shown in C is from one experiment where at least 200 cells were imaged for each treatment condition and siRNA used. Error bars in B and C show SEM.

3.4 Discussion

3.4.1 RECQL4 Mut-2 mutation and cell proliferation characteristics

Data previously shown in Chapter 2 demonstrated that RECQL4 expression in the Mut-2 clones were drastically reduced compared with parental HEK293—a decrease which was consistent with that found in RTS patient cells relative to comparable cells from healthy donors (Figure 2.3A-C). Since RECQL4 has a known essential role in the initiation of DNA replication and thus cell proliferation, one important goal in this study was to determine the effects of knocking in the *RECQL4* Mut-2 mutation—both in terms of the impact on RECQL4 protein structure and in terms of the changes in RECQL4 expression level—on the growth characteristics of the Mut-2 clones (Abe et al., 2011; Matsuno et al., 2006; Sangrithi et al., 2005).

Based on growth curves generated using Incucyte proliferation assays, the Mut-2 clones did not appear to greatly differ from parental HEK293 during the exponential growth phase, however a slightly prolonged initial lag phase was observed leading to temporal shifting of the Mut-2 growth curves and delayed entry into exponential growth (Figure 3.3D). When population doubling times during the exponential growth phase were calculated, the median doubling times of the Mut-2 clones were approximately 10-30% higher (range: 10.8-27.9%) compared to parental HEK293, a statistically significant increase (Figure 3.3C). Dual EdU/DNA content staining of normally dividing cells populations, however, showed that the distribution of cell cycle phases in the Mut-2 clones did not differ noticeably from that found in parental HEK293 which suggested that observed changes in doubling times were not cell cycle phase-dependent (Figure 3.3A and B).

To separate the structural effects of the Mut-2 mutation on RECQL4 protein from the effects of decreased overall RECQL4 protein levels in the Mut-2 clones, the growth rates of

Mut-2 clones overexpressing either wild-type RECQL4 or RECQL4 ΔEx14, the major RECQL4 protein product produced by the Mut-2 allele in the clones, were compared with corresponding parental HEK293s and also cells transduced with the empty vector control (Figure 3.8F). Overexpression of both forms of RECQL4 decreased doubling times in the Mut-2 cells compared to empty vector control cells. Interestingly, the RECQL4 ΔEx14 variant seemed to have a slightly greater effect on decreasing doubling time (Figure 3.8F, right). This suggested that changes in doubling times were not due to structural changes to the RECQL4 protein as a result of the Mut-2 mutation but rather due to decreased overall RECQL4 protein levels.

One striking observation from maintaining the Mut-2 clones in culture has been that despite the low levels of RECQL4 expression seen on western blot (Figure 2.3A-C), these cells continue to proliferate at a rate and with kinetics that do not drastically differ from that of parental HEK293 (Figure 3.3). This indicated that, despite a requirement for RECQL4 in cell proliferation, the levels of RECQL4 necessary for this function may actually be very low, confirming similar observations reported by others (Abe et al., 2011; Lu et al., 2016; Park et al., 2006).

3.4.2 Sensitivity profile of Mut-2 clones to DNA damaging compounds pointed to DNA DSB repair defect

The role of RECQL4 in DNA damage repair have been proposed and explored since its first discovery and subsequent identification as the gene mutated in the progeroid Type II RTS (Croteau et al., 2012; Kitao et al., 1998, 1999). However, efforts to study how *RECQL4* mutations affected DNA damage repair in the context of Type II RTS had, up to now, yielded inconsistent results, possibly due to limitations of the models or patient samples used (discussed in Chapter 2) (Jin et al., 2008).

The Mut-2 clones generated in this study presented viable models to study the particular effects of a clinically relevant and prevalent RTS *RECQL4* mutation while overcoming some of the limitations present in models previously used (discussed in Chapter 1 Section 1.6 and Chapter 2 Introduction). Therefore, these Mut-2 clones were tested against a panel of different classes of DNA damaging agents in the expectation that the sensitivity pattern could inform further mechanistic exploration of DNA damage repair in these clones (Figure 3.4). Summarised below in tabular form is the overall sensitivity profile of the Mut-2 clones to the six classes of compounds used and the DNA damage repair pathways implicated (as discussed previously in Chapter 3 Section 3.1.1):

Table 3.2 Sensitivities of the Mut-2 clones to different classes of DNA damaging agents

Compound class	Compounds Tested	Sensitivity	Repair Pathways Activated
Replication stress inducers	Hydroxyurea, aphidicolin	-	S-phase checkpoint, replication fork stabilisation
Radiomimetic	Neocarzinostatin, bleomycin	-	DNA DSB repair (NHEJ, HR, MMEJ)
DNA alkylator	Methyl methanesulfonate, busulfan	+	Base excision repair, mismatch repair, HR
DNA crosslinker	Cisplatin, cyclophosphamide, mitomycin C	+/-	FA pathway, Nucleotide excision repair, HR
Topoisomerase inhibitor	Camptothecin, topotecan, etoposide	+	Top1: HR Top2: DNA DSB repair (NHEJ, HR, MMEJ)
PARP inhibitor	Olaparib, veliparib	+/-	HR

Based on the results above, three sets of DNA damage repair pathways stood out: base excision repair (BER), nucleotide excision repair (NER), and DNA DSB repair. RECQL4 has been

reported to function in all three repair processes (Fan and Luo, 2008; Schurman et al., 2009; Singh et al., 2010). Among these three, the activation of DNA DSB repair pathways was common to all compounds to which the Mut-2 clones showed increased sensitivity and presented the most promising candidate for further study.

3.4.3 Etoposide treatment pointed to compromised replication-associated DNA DSB repair in Mut-2 clones

The effects of etoposide, a compound to which the Mut-2 clones were particularly sensitive, were studied in greater detail using flow cytometry (Figure 3.5 and Figure 3.6). ETP has been reported to generate DNA DSBs in a cell cycle independent manner and thus the repair pathways it activates should be dependent on the cell cycle status of the cell (Aparicio et al., 2016; Karanam et al., 2012; Quennet et al., 2010; Zhao et al., 2012). However, consistent with a previous report, ETP treatment of the Mut-2 clones in this study caused cell cycle arrest at what appeared to be the G2/M phase (Figure 3.5A) (Schonn et al., 2010). Further staining for phospho-histone H3, a specific marker for mitosis, showed that ETP-arrested cells had not entered M-phase and were likely arrested in late-S/G2 (Figure 3.5C) (Gurley et al., 1978; Juan et al., 1998). This suggested that HR, the repair pathway known to be most active during S/G2, might be preferentially activated in response to ETP-induced damage which would be in line with the repair pathways activated by other compounds to which the Mut-2 clones were sensitive (see table above) (Johnson and Jasin, 2000; Karanam et al., 2012).

In terms of the response of the Mut-2 clones to DNA damage, all ETP treated cells showed increased levels of γH2AX, a marker specific for DNA DSBs, as would be expected and comparable to levels seen in parental HEK293 (Figure 3.5B) (Rogakou et al., 1998, 1999). When the ETP-treated cells were allowed to recover over a period of 8 hours, relative to parental HEK293, the Mut-2 clones exhibited delayed cell cycle re-entry and progression through G2/M

phase as measured by total DNA content (Figure 3.6A and B). Furthermore, this delay was correlated with reduced resolution of γH2AX signalling, suggesting that the Mut-2 clones did not repair ETP-induced DNA DSBs as efficiently as parental HEK293 which was consistent with the drug sensitivity results above (Figure 3.4E and Figure 3.6C). Overall, these findings in ETP treated cells implicated compromised repair of DNA DSBs during replication, which is predominantly HR, in the Mut-2 clones.

3.4.4 Mut-2 clones showed decreased DNA DSB repair by HR and MMEJ but not NHEJ

Based on the drug sensitivity results above, the DNA DSB repair pathways appeared to be the most promising candidate for further investigation in the Mut-2 clones. GFP reporter assays, commonly used in studies of DNA damage repair, were performed to further probe the function of the three main DNA DSB repair pathways—HR, NHEJ, and MMEJ (Figure 3.2) (Kostyrko and Mermod, 2016; Pierce et al., 1999; Seluanov et al., 2010).

The results of the GFP reporter assays showed that, of the three pathways (HR, NHEJ, and MMEJ) tested, the Mut-2 clones showed decreased repair function in HR and MMEJ but not in NHEJ (Figure 3.7B). This result was in line with predictions above based on the drug sensitivity profile of the Mut-2 clones, which suggested increased sensitivity to compounds that activated the HR repair pathway. The defect in HR repair, in particular, was also consistent with phenotypes reported by others in cells in which RECQL4 expression was knocked down via siRNA treatment (Lu et al., 2016). Furthermore, because HR and MMEJ are known to share common early steps which have been reported to involve RECQL4 function, concurrent defects in HR and MMEJ in the Mut-2 clones were consistent with such models (Lu et al., 2016; Truong et al., 2013).

3.4.5 Reconstitution of RECQL4 expression in Mut-2 clones

To confirm that the phenotypes seen thus far in the Mut-2 clones were due to the effects of the *RECQL4* Mut-2 mutation, either wild-type RECQL4 or the RECQL4 ΔEx14 variant was overexpressed in the Mut-2 clones. Overexpression of the specific variant in each set of cells was confirmed by western blot and transcript-specific TaqMan RT-qPCR (Figure 3.8A and B). The sensitivities of these RECQL4 overexpressing cells to a small selection of the compounds used previously (HU, MMS, and ETP) were investigated (Figure 3.8C-E).

Unexpectedly, Mut-2 cells expressing both wild-type RECQL4 and the RECQL4 ΔEx14 variant showed increased resistance to MMS and ETP when compared with corresponding parental HEK293 and empty vector controls, seemingly suggesting that the structural changes to RECQL4 due to the Mut-2 mutation were not the cause of the sensitivity profile of the original Mut-2 clones (Figure 3.8D and E). However, the behaviour of these cells when treated with HU provided a clue to an alternate explanation. Both sets of cells also showed increased resistance, particularly cells overexpressing the RECQL4 ΔEx14 variant (Figure 3.8C). Since the original drug screens did not implicate a defect in DNA damage repair mechanisms activated by HU treatment, this pointed to a possible confounding factor in the RECQL4 reconstitution drug sensitivity experiment (Figure 3.4A).

Since the Incucyte proliferation assay's readout was confluency as a proxy for cell growth, results of the assay could have been affected by overexpression of RECQL4, which might have increased the proliferation rate of these cells due to RECQL4's role in DNA replication. To test this, the population doubling times of the RECQL4 overexpressing cells were calculated and did in fact decrease relative to corresponding parental HEK293 controls when compared with empty vector transduced cells. In particular, overexpression of the RECQL4 ΔEx14 variant had an especially strong positive effect on growth rate (Figure 3.8F).

Based on this observation, an alternate explanation could be proposed in which the increased growth rate of these RECQL4 overexpressing Mut-2 cells effectively masked their DNA damage repair defects, leading to the appearance of the “rescue” effect.

To overcome this issue, a second set of cells was generated that again overexpressed the same two forms of RECQL4, but this time without the GFP marker present in the overexpression constructs used previously (ΔGFP). These cells could then be used for GFP reporter assays to directly test the function of their DNA DSB repair pathways. Overexpression of the two RECQL4 forms was again confirmed via western blot and transcript-specific TaqMan RT-qPCR (Figure 3.9A and B).

This time, the GFP reporter assays showed that overexpression of wild-type RECQL4 alone increased the rate of HR repair in the Mut-2 cells but not the corresponding parental HEK293 or empty vector controls (Figure 3.9C, left). No rescue effect was seen in either the NHEJ or the MMEJ reporter assays or in cells overexpressing the RECQL4 ΔEx14 variant (Figure 3.9C). This result was strong evidence that the HR repair defect found previously in Mut-2 clones (Figure 3.9B left) was due to structural changes arising from the *RECQL4* Mut-2 mutation and not due to concurrent changes in RECQL4 protein levels.

Interestingly, the defect in MMEJ previously seen in the Mut-2 clones was not rescued by overexpression of either forms of RECQL4 (Figure 3.9B, right and Figure 3.9C, right). While this was not unexpected for the RECQL4 ΔEx14 variant, it was surprising that wild-type RECQL4 overexpression did not rescue MMEJ deficiency. It has been reported that during S/G2 phases when HR is active it is preferentially used in favour of MMEJ and may in fact suppress the activity of the MMEJ pathway (Jasin and Rothstein, 2013; Sfeir and Symington, 2015; Truong et al., 2014). Since the data showed that HR repair rates were increased due to overexpression

of wild-type RECQL4, it was possible that in these cells, increased HR rates acted to suppress MMEJ and masked any possible rescue effects.

3.4.6 Mut-2 clones did not exhibit impaired RAD51 foci formation

RECQL4 had previously been reported to mediate the recruitment of CtIP to as well as promote resection of DSB ends, important early steps shared by both HR and MMEJ (Lu et al., 2016; Truong et al., 2013). RNAi-mediated knockdown of RECQL4 expression resulted in impaired CtIP recruitment, reduced break end resection, and decreased HR function. Additionally, re-expression of a helicase-dead RECQL4 mutant failed to rescue the reduced break end resection and the HR deficiency in spite of restoration of CtIP interaction. These findings led Lu and colleagues to propose a model in which RECQL4 played multiple essential roles in early DSB end resection through both protein interactions as well as its helicase function. (Lu et al., 2016).

Given the predicted detrimental effect of the Mut-2 mutation on RECQL4 helicase function (Figure 2.9), as well as findings of HR and MMEJ deficiency in the Mut-2 clones from the GFP reporter assays (Figure 3.7), data from this study of the Mut-2 clones appeared to be consistent with the aforementioned model of RECQL4 function. Furthermore, if the early resection steps in the Mut-2 clones were compromised then downstream HR steps were also expected to be similarly affected.

The recruitment of RAD51 to resected ssDNA at the break ends to form nucleoprotein filaments for strand invasion is a known essential step downstream of the proposed function of RECQL4 in the HR pathway. The formation of RAD51 foci is itself also a commonly used marker of HR pathway activity (Cruz et al., 2018; Gachechiladze et al., 2017; San Filippo et al., 2008). To test whether the HR deficiency observed in the Mut-2 clones conformed with predictions from the Lu, *et al.* model, the formation of RAD51 foci in the Mut-2 clones was

investigated post ETP treatment (Figure 3.10). Unexpectedly, all Mut-2 clones upregulated RAD51 foci formation to levels comparable to parental HEK293 post ETP treatment (Figure 3.10A and B). Given that these Mut-2 clones did in fact show defects in HR repair (see discussion below), this observation called into question the hypothesis that the Mut-2 mutation negatively impacted HR by disrupting RECQL4's proposed function in the early resection steps of HR. Instead, this finding is suggestive of an alternate model where the *RECQL4* Mut-2 mutation disrupted as yet undefined functions of RECQL4 downstream of RAD51 nucleoprotein filament formation in HR.

3.4.7 Final summary

The result presented in this chapter demonstrated that *RECQL4* Mut-2 mutation was responsible for decreased HR repair capacity in Mut-2 clones. This effect was not due to decreased overall RECQL4 protein levels in these cells but rather, due to the structural effects of the Mut-2 mutation on the RECQL4 protein. Furthermore, data suggested that the effects of the Mut-2 mutation on RECQL4 function in the HR pathway may be exerted at a later (and yet undefined) step than current models propose (Lu et al., 2016).

Chapter 4 Final Discussion

4.1 Mut-2 clones are novel models for *RECQL4* Mut-2 mutation

Since the discovery of RECQL4 as a member of the RecQ helicase family in humans and recognition of its role in human disease, much effort has gone into studying the mechanisms of RECQL4 dysfunction in Type II RTS (Jin et al., 2008; Kitao et al., 1998, 1999a, 1999b; Lindor et al., 2000). These efforts have long been hampered by a dearth of suitable and clinically relevant models, be they RTS patient samples, animal models, or engineered cell lines, leading to inconsistent results (Castillo-Tandazo et al., 2019; Jin et al., 2008; Kohzaki et al., 2012; Siitonen et al., 2008).

This study presented the generation of cell line models for a prevalent *RECQL4* RTS patient mutation—the c.2269C>T "Mut-2" mutation. These models compared favourably to similar RTS patient cells in terms of RECQL4 protein expression levels. Furthermore, new data has shown, for the first time, that rather than the protein truncation that was predicted, the major effect of the Mut-2 mutation was to upregulate alternative splicing of RECQL4 which is predicted to produce a helicase-dead hypomorphic protein variant. Further work is needed to confirm whether this phenomenon is also present in RTS patients carrying the Mut-2 mutation.

Interestingly, while both the truncation of RECQL4 (as Mut-2 was predicted to do) and the generation of a hypomorphic protein in which the ATPase domain was disrupted (as the alternative splicing does) would be expected to abolish helicase function, only the latter preserves the C-terminal regions reported to be critical for protein stability (Kaiser et al., 2017). Therefore, it is tempting to speculate that the preference observed in the majority of the Mut-2 clones for upregulating alternative splicing of *RECQL4* may be due to possible energy and resource cost advantages that arise from producing a potentially more stable protein,

especially for a protein with an essential function such as RECQL4 (Abe et al., 2011; Matsuno et al., 2006; Sangrithi et al., 2005). On the other hand, observations from the study show that the alternatively spliced form of RECQL4 is expressed at a much lower level in the Mut-2 clones than is wild-type RECQL4 in the parental HEK293. This is in spite of the fact that the alternatively spliced form of RECQL4 is nearly identical to wild-type RECQL4 with the exception of the in-frame 66aa deletion in the ATPase domain. This finding hints at more complex mechanisms regulating RECQL4 protein abundance than currently understood and merits further study.

Another interesting observation is that the distribution of *RECQL4* mutations along gene seems to follow a bimodal distribution with one cluster of mutations around the exon 8-9 region and another cluster in the exon 14-15 region (Figure 1.4). Given the findings in this study regarding alternative splicing at the exon 14-15 junction, it is possible that this may represent a major mutational process in *RECQL4* in Type II RTS. Indeed, the alternative splicing observed in this study was first reported in samples from RTS patients carrying a very similar mutation located close by (c.2272C>T) (Colombo et al., 2014). Therefore, it is plausible that the clustering of mutation observed in the exon 14-15 region of *RECQL4* may represent a major structure-function principle in Type II RTS and present an avenue for the application of the findings in this study to a broader set of RTS patients.

Finally, next generation sequencing revealed that the Mut-2 clones were functionally hemizygous, which while not entirely achieving the original aim of generating homozygous mutant cells line, nevertheless, still resulted in viable models for downstream functional studies.

4.2 Functional characterisation of Mut-2 clones

4.2.1 Mut-2 clones exhibited surprisingly normal growth phenotypes

RECQL4 is unique within the RecQ helicase family for its essential function in DNA replication and thus cell proliferation (Abe et al., 2011; Matsuno et al., 2006; Sangrithi et al., 2005). Furthermore, the vast majority of *RECQL4* mutations found in Type II RTS patients spare the critical N-terminal region responsible for those essential functions (Figure 1.4). Therefore, given its retention, one would expect that cells containing *RECQL4* mutations would express the remaining portions of RECQL4 at near-normal levels. So, it was both surprising and illuminating to observe in the course of this study that the Mut-2 clones were able to maintain near normal viability despite the greatly reduced levels of RECQL4 protein expression, a phenomenon which was hinted at by observations of RECQL4 levels in patient cells as well as from work by others (Abe et al., 2011; De et al., 2012; Gupta et al., 2014; Petkovic et al., 2005; Werner et al., 2006; Yin et al., 2004; Yokoyama et al., 2019). If indeed the essential functions of RECQL4 require very little protein abundance, then this raises the question of whether the same is also true for its other functions such as DNA damage repair and the extent to which these functions are affected by RECQL4 protein abundance.

4.2.2 Drug sensitivity profile of Mut-2 clones uncovered replication-specific DNA DSB repair defect

Despite expectations of RECQL4's function in DNA damage repair, previous studies of sensitivities of RTS patient cells and other models containing mutant RECQL4 to various DNA damaging agents had yielded inconsistent results (Castillo-Tandazo et al., 2019; Jin et al., 2008; Kitao et al., 1998; Kohzaki et al., 2012). This study characterised the sensitivity profile of the Mut-2 clones to a panel of different classes of DNA damaging agents and took an in-depth look at the effects of one compound to which they were particularly sensitive. The results

strongly implicated DNA DSB repair, in particular, HR as being affected by *RECQL4* Mut-2 mutation.

Further direct functional assays of DNA DSB repair confirmed that both HR and MMEJ were compromised in the Mut-2 clones. Reconstitution experiments showed that the defect in HR was due to structural changes caused by the Mut-2 mutation on the RECQL4 protein rather than due to changes in RECQL4 protein abundance. This provided strong evidence that deficiency in HR in the context of Type II RTS was a result of disruption of the RECQL4 helicase function. These findings propose a model in which RECQL4 helicase activity—independent of the roles played by other portions of the protein—play an important role in replication-specific DNA DSB repair, complementing RECQL4's other S-phase specific functions.

Unexpectedly however, data from this study also showed that RAD51 foci formation was unaffected in Mut-2 clones. This observation stood in contrast to predictions based on the existing model of RECQL4 function in DNA resection during the early stages of HR (Lu et al., 2016). Further studies will be necessary to answer important questions in several areas raised by this finding.

First, the nature of the DNA resection defect previously reported should be further characterised in the context of *RECQL4* disruption. Are the Mut-2 clones in the current study similarly deficient in DNA resection after DNA DSB induction compared with parental HEK293? If so, is the extent of this deficiency comparable to those reported by others in RECQL4-depleted cells and cells expressing helicase-dead RECQL4 mutants (Lu et al., 2016)? If no deficiency is found, could the reported DNA resection deficiency be a cell line specific phenomenon? Do other models of Type II RTS such as patient cells or mouse models also show deficient DNA resection?

Second, the link between any DNA resection deficiencies observed above and downstream HR activity needs to be positively established. What is the effect of *RECQL4*-deficiency mediated resection defect on RAD51 foci formation? What is the magnitude of this effect? To what extent is RECQL4 function necessary for downstream HR steps? Are similar effects also seen in Type II RTS patient cells?

Finally, it is clear that the current model of RECQL4 function does not account for the possibility of RECQL4 participating in multiple steps in HR (Lu et al., 2016). RECQL4 has been shown to bind to Holliday junctions as a substrate (Sedlackova et al., 2015). In addition, interaction between RECQL4 and BLM, another protein that also acts on Holliday junctions, has also been reported, especially after treatment of cells with ionising radiation (Bizard and Hickson, 2014; Sharma et al., 2006; Singh et al., 2012). These findings and the data from this study support the hypothesis that additional new roles exist for RECQL4 in later steps of HR, possibly during the resolution of the double Holliday junction. The Mut-2 clones generated in this study are useful models for studies to isolate these functions.

In summary, while multiple studies—including this one—have shown defects in HR/replication-associated DNA DSB repair upon *RECQL4* disruption, the precise ways in which *RECQL4* disruption impacts these processes remain to be elucidated.

4.3 Limitations of the Mut-2 clones as models of RTS

Despite the utility of the Mut-2 clones in the study of this particular *RECQL4* mutation, there are important limitations and caveats to their usefulness as a model of RTS. First and foremost, these Mut-2 clones were generated from HEK293, which while convenient to manipulate and study, cannot be considered to be normal cells either genetically or functionally (Stepanenko and Dmitrenko, 2015). As tools for the study of basic processes such

as DNA damage repair, HEK293s may be acceptable and widely used, however, care must be taken when interpreting results (Lu et al., 2016; Singh et al., 2010).

A second limitation concerns the use of CRISPR/Cas9 to study *RECQL4* mutations. As discussed previously (Chapter 2 Section 2.4.1), HDR is essential to precise CRISPR/Cas9-mediated gene editing (Liu et al., 2019; Ran et al., 2013; Ryu et al., 2019). The CRISPR/Cas9 editing of *RECQL4* to knock-in the Mut-2 mutation in this study resulted in significant errors in the repair of the Cas9-induced DNA DSBs. Future work using this approach should incorporate measures to suppress error-prone repair such as that arising from NHEJ and/or to enhance HDR efficiency (Liu et al., 2019). Such measures could include NHEJ inhibition via SCR-7, a chemical inhibitor of DNA ligase 4, or siRNA-mediated knockdown of the Ku-complex components or DNA ligase 4 (Chu et al., 2015; Findlay et al., 2018; Li et al., 2018). Similarly, measures to directly stimulate HDR activity such as using RS-1, a chemical RAD51 enhancer, should also be considered, perhaps even in combination with NHEJ suppression (Pinder et al., 2015; Song et al., 2016).

Finally, a third limitation of this model system, in the context of my particular broad interest in the mechanisms underlying the aetiology of osteosarcoma, is the obvious fact that these HEK293-based models are ill-suited for studying the specificity for elevated risk of osteosarcoma in Type II RTS. Such tissue/lineage-specific effects will likely require animal-based models rather than cell line-based approaches.

4.4 Future directions

There are several potential lines of inquiry which can arise from this study. For instance, more work is needed to define the potentially multiple roles of RECQL4 in HR discussed above (Section 4.2.2). In particular, what are the precise protein interactions and steps affected by the *RECQL4* Mut-2 mutation? One avenue of approach briefly touched upon in the discussion

above is based on data from this study implicating RECQL4 in HR downstream of RAD51 nucleoprotein filament formation. Evidence from other studies already suggests that Holliday junction resolution is a potential step on which RECQL4 may act (Bizard and Hickson, 2014; Sedlackova et al., 2015; Sharma et al., 2006; Singh et al., 2012). The Mut-2 clones generated in this study are excellent models to study whether *RECQL4* disruption affects Holliday junction resolution. For example, one possible prediction of RECQL4 potentially functioning in this process is that the balance of the end products from the dissolution of the Holliday junctions could be altered in the Mut-2 clones, possibly towards aberrant crossover products. This can be studied both by assaying for rates of sister-chromatid exchange in the Mut-2 clones as well as by sequencing the end repair products of the GFP reporter assays. Aberrant Holliday junction resolution could lead to large scale structural rearrangements as well as increased genomic instability. If shown to be present in the Mut-2 clones, can such genomic instability be detected in cells that have undergone extended periods of cell culture versus those from earlier passages? Such an observation, if shown to be a consequence of *RECQL4* disruption, could be an explanation for some of the phenotypes seen in Type II RTS.

Another area of interest is the potential functions of RECQL4 in other DNA damage repair pathways. RECQL4 has been previously reported to interact with components of NHEJ, BER, and NER (Fan and Luo, 2008; Schurman et al., 2009; Shamanna et al., 2014). Furthermore, data from this study indicated possible defects in additional DNA damage repair pathways such as BER as a result of *RECQL4* mutations. With these findings in mind, is BER compromised in the Mut-2 clones or are findings such as their increased MMS sensitivity due to their known HR deficiency? To address this, studies should be done to assess BER-mediated removal of nucleotide adducts in Mut-2 clones arrested in G1. In addition, if a BER-specific defect exists in the Mut-2 clones, is it due to decreased RECQL4 protein abundance or disruption of its

helicase function? For this, BER repair efficiencies in G1 arrested cells could be compared for the Mut-2 clones reconstituted with wild-type and ΔEx14 forms of RECQL4 that were generated in this study. Finally, current understanding of the roles of RECQL4 in BER does not indicate a requirement for helicase function. If this is supported by the results of the above studies implicating protein abundance in BER-specific defects, then it may be speculated that decreased protein abundance and disruption of RECQL4 helicase function in Type II RTS may interact synergistically to impair different aspects of the cellular response to damage from agents such as MMS. Increased accumulation of nucleotide adducts due to BER deficiency could be compounded by their conversion to DSBs during replication whose repair is then impaired by HR deficiency. This model could be tested by again comparing the response of the different sets of RECQL4 overexpression Mut-2 clones generated in this study, but without the G1 arrest.

A broader question regarding the role of RECQL4 in other DNA damage repair pathways is whether the spectrum of *RECQL4* mutations found in Type II RTS patients results in differing effects on individual repair pathways and whether structure-function relationships could be elucidated that predict such effects based on patient genotype. Such questions could be answered by replicating the approaches used in this study on a larger panel of *RECQL4* mutations.

Finally, it may be useful to attempt to generate cell line models of *RECQL4* RTS mutations in normal mesenchymal cells such as mesenchymal stem cells. This would allow for the study of the effects of *RECQL4* mutations in the context of osteoblastic differentiation and may yield insights into questions such as what role RECQL4 plays in osteogenesis, how disruption of *RECQL4* leads to the skeletal phenotypes seen in Type II RTS, and whether or how that leads to the predisposition for osteosarcoma in Type II RTS. Such studies could also

be invaluable in uncovering the mechanisms and processes involved in the pathogenesis of sporadic osteosarcoma.

References

Abe, T., Yoshimura, A., Hosono, Y., Tada, S., Seki, M., and Enomoto, T. (2011). The N-terminal region of RECQL4 lacking the helicase domain is both essential and sufficient for the viability of vertebrate cells: Role of the N-terminal region of RECQL4 in cells. Biochim. Biophys. Acta - Mol. Cell Res. *1813*, 473–479.

Ahn, B., Kang, D., Kim, H., and Wei, Q. (2004). Repair of mitomycin C cross-linked DNA in mammalian cells measured by a host cell reactivation assay. Mol. Cells *18*, 249–255.

Ajeawung, N.F., Nguyen, T.T.M., Lu, L., Kucharski, T.J., Rousseau, J., Molidperee, S., Atienza, J., Gamache, I., Jin, W., Plon, S.E., et al. (2019). Mutations in ANAPC1, Encoding a Scaffold Subunit of the Anaphase-Promoting Complex, Cause Rothmund-Thomson Syndrome Type 1. Am. J. Hum. Genet. *105*, 625–630.

Aparicio, T., Baer, R., Gottesman, M., and Gautier, J. (2016). MRN, CtIP, and BRCA1 mediate repair of topoisomerase II–DNA adducts. J. Cell Biol. *212*, 399–408.

Baller, F. (1950). Radiusaplasie und Inzucht. Z Menschl Vererb Konstitutionsl *29*, 782–790.

Baranovskiy, A.G., Babayeva, N.D., Suwa, Y., Gu, J., Pavlov, Y.I., and Tahirov, T.H. (2014). Structural basis for inhibition of DNA replication by aphidicolin. Nucleic Acids Res. *42*, 14013–14021.

Bass, P.D., Gubler, D.A., Judd, T.C., and Williams, R.M. (2013). Mitomycinoid Alkaloids: Mechanism of Action, Biosynthesis, Total Syntheses, and Synthetic Approaches. Chem. Rev. *113*, 6816–6863.

Basu, A., and Krishnamurthy, S. (2010). Cellular Responses to Cisplatin-Induced DNA Damage. J. Nucleic Acids *2010*, 201367.

Beghini, A., Castorina, P., Roversi, G., Modiano, P., and Larizza, L. (2003). RNA processing

defects of the helicase geneRECQL4 in a compound heterozygous Rothmund-Thomson patient. Am. J. Med. Genet. *120A*, 395–399.

Bennardo, N., Cheng, A., Huang, N., and Stark, J.M. (2008). Alternative-NHEJ Is a Mechanistically Distinct Pathway of Mammalian Chromosome Break Repair. PLOS Genet. *4*, e1000110.

Beranek, D.T. (1990). Distribution of methyl and ethyl adducts following alkylation with monofunctional alkylating agents. Mutat. Res. Mol. Mech. Mutagen. *231*, 11–30.

Bernstein, D.A., Zittel, M.C., and Keck, J.L. (2003). High-resolution structure of the E. coli RecQ helicase catalytic core. EMBO J. *22*, 4910 LP – 4921.

Bernstein, K.A., Gangloff, S., and Rothstein, R. (2010). The RecQ DNA Helicases in DNA Repair. Annu. Rev. Genet. *44*, 393–417.

Bétous, R., Mason, A.C., Rambo, R.P., Bansbach, C.E., Badu-Nkansah, A., Sirbu, B.M., Eichman, B.F., and Cortez, D. (2012). SMARCAL1 catalyzes fork regression and Holliday junction migration to maintain genome stability during DNA replication. Genes Dev. *26*, 151–162.

Bizard, A.H., and Hickson, I.D. (2014). The Dissolution of Double Holliday Junctions. Cold Spring Harb. Perspect. Biol. *6*.

Borst, P., Rottenberg, S., and Jonkers, J. (2008). How do real tumors become resistant to cisplatin? Cell Cycle *7*, 1353–1359.

Bryant, H.E., Petermann, E., Schultz, N., Jemth, A.-S., Loseva, O., Issaeva, N., Johansson, F., Fernandez, S., McGlynn, P., and Helleday, T. (2009). PARP is activated at stalled forks to mediate Mre11-dependent replication restart and recombination. EMBO J. *28*, 2601–2615.

Burger, R.M., Peisach, J., and Horwitz, S.B. (1978). Effect of light and oxygen on neocarzinostatin stability and DNA-cleaving activity. J. Biol. Chem. *253*, 4830–4832.

Burks, L.M., Yin, J., and Plon, S.E. (2007). Nuclear import and retention domains in the amino

terminus of RECQL4. Gene *391*, 26–38.

Bylund, L., Kytölä, S., Lui, W.-O., Larsson, C., and Weber, G. (2004). Analysis of the cytogenetic stability of the human embryonal kidney cell line 293 by cytogenetic and STR profiling approaches. Cytogenet. Genome Res. *106*, 28–32.

Caldecott, K.W. (2008). Single-strand break repair and genetic disease. Nat. Rev. Genet. *9*, 619–631.

Cannan, W.J., and Pederson, D.S. (2016). Mechanisms and Consequences of Double-Strand DNA Break Formation in Chromatin. J. Cell. Physiol. *231*, 3–14.

Capp, C., Wu, J., and Hsieh, T. (2009). Drosophila RecQ4 Has a 3′-5′ DNA Helicase Activity That Is Essential for Viability. J. Biol. Chem. *284*, 30845–30852.

Casorelli, I., Bossa, C., and Bignami, M. (2012). DNA Damage and Repair in Human Cancer: Molecular Mechanisms and Contribution to Therapy-Related Leukemias. Int. J. Environ. Res. Public Health *9*.

Castillo-Tandazo, W., Smeets, M.F., Murphy, V., Liu, R., Hodson, C., Heierhorst, J., Deans, A.J., and Walkley, C.R. (2019). ATP-dependent helicase activity is dispensable for the physiological functions of Recql4. PLOS Genet. *15*, e1008266.

Ceccaldi, R., Liu, J.C., Amunugama, R., Hajdu, I., Primack, B., Petalcorin, M.I.R., O'Connor, K.W., Konstantinopoulos, P.A., Elledge, S.J., Boulton, S.J., et al. (2015). Homologous-recombination-deficient tumours are dependent on Polθ-mediated repair. Nature *518*, 258–262.

Chaganti, R.S.K., Schonberg, S., and German, J. (1974). A Manyfold Increase in Sister Chromatid Exchanges in Bloom's Syndrome Lymphocytes. Proc. Natl. Acad. Sci. *71*, 4508 LP – 4512.

Champoux, J.J. (1978). Mechanism of the reaction catalyzed by the DNA untwisting enzyme:

Attachment of the enzyme to 3'-terminus of the nicked DNA. J. Mol. Biol. *118*, 441–446.

Chapman, J.R., Taylor, M.R.G., and Boulton, S.J. (2012). Playing the End Game: DNA Double-Strand Break Repair Pathway Choice. Mol. Cell *47*, 497–510.

Chen, H., Lisby, M., and Symington, L.S. (2013). RPA Coordinates DNA End Resection and Prevents Formation of DNA Hairpins. Mol. Cell *50*, 589–600.

Chen, X., Schulz-Trieglaff, O., Shaw, R., Barnes, B., Schlesinger, F., Källberg, M., Cox, A.J., Kruglyak, S., and Saunders, C.T. (2015). Manta: rapid detection of structural variants and indels for germline and cancer sequencing applications. Bioinformatics *32*, 1220–1222.

Chi, Z., Nie, L., Peng, Z., Yang, Q., Yang, K., Tao, J., Mi, Y., Fang, X., Balajee, A.S., and Zhao, Y. (2012). RecQL4 cytoplasmic localization: Implications in mitochondrial DNA oxidative damage repair. Int. J. Biochem. Cell Biol. *44*, 1942–1951.

Cho, S.W., Kim, S., Kim, J.M., and Kim, J.-S. (2013). Targeted genome engineering in human cells with the Cas9 RNA-guided endonuclease. Nat. Biotechnol. *31*, 230–232.

Chu, V.T., Weber, T., Wefers, B., Wurst, W., Sander, S., Rajewsky, K., and Kühn, R. (2015). Increasing the efficiency of homology-directed repair for CRISPR-Cas9-induced precise gene editing in mammalian cells. Nat. Biotechnol. *33*, 543–548.

Cingolani, P., Platts, A., Wang, L.L., Coon, M., Nguyen, T., Wang, L., Land, S.J., Lu, X., and Ruden, D.M. (2012). A program for annotating and predicting the effects of single nucleotide polymorphisms, SnpEff. Fly (Austin). *6*, 80–92.

Colombo, E.A., Fontana, L., Roversi, G., Negri, G., Castiglia, D., Paradisi, M., Zambruno, G., and Larizza, L. (2014). Novel physiological RECQL4 alternative transcript disclosed by molecular characterisation of Rothmund-Thomson Syndrome sibs with mild phenotype. Eur J Hum Genet *22*, 1298–1304.

Cong, L., Ran, F.A., Cox, D., Lin, S., Barretto, R., Habib, N., Hsu, P.D., Wu, X., Jiang, W., Marraffini,

L.A., et al. (2013). Multiplex Genome Engineering Using CRISPR/Cas Systems. Science (80-.). *339*, 819–823.

Cortez, D. (2015). Preventing replication fork collapse to maintain genome integrity. DNA Repair (Amst). *32*, 149–157.

Croteau, D.L., Singh, D.K., Hoh Ferrarelli, L., Lu, H., and Bohr, V.A. (2012a). RECQL4 in genomic instability and aging. Trends Genet. *28*, 624–631.

Croteau, D.L., Rossi, M.L., Ross, J., Dawut, L., Dunn, C., Kulikowicz, T., and Bohr, V.A. (2012b). RAPADILINO RECQL4 mutant protein lacks helicase and ATPase activity. Biochim. Biophys. Acta - Mol. Basis Dis. *1822*, 1727–1734.

Croteau, D.L., Popuri, V., Opresko, P.L., and Bohr, V.A. (2014). Human RecQ Helicases in DNA Repair, Recombination, and Replication. Annu. Rev. Biochem. *83*, 519–552.

Cruz, C., Castroviejo-Bermejo, M., Gutiérrez-Enríquez, S., Llop-Guevara, A., Ibrahim, Y.H., Gris-Oliver, A., Bonache, S., Morancho, B., Bruna, A., Rueda, O.M., et al. (2018). RAD51 foci as a functional biomarker of homologous recombination repair and PARP inhibitor resistance in germline BRCA-mutated breast cancer. Ann. Oncol. *29*, 1203–1210.

D'Andrea, A.D. (2018). Mechanisms of PARP inhibitor sensitivity and resistance. DNA Repair (Amst). *71*, 172–176.

D'Andrea, A.D., and Haseltine, W.A. (1978). Sequence specific cleavage of DNA by the antitumor antibiotics neocarzinostatin and bleomycin. Proc. Natl. Acad. Sci. *75*, 3608 LP – 3612.

De, S., Kumari, J., Mudgal, R., Modi, P., Gupta, S., Futami, K., Goto, H., Lindor, N.M., Furuichi, Y., Mohanty, D., et al. (2012). RECQL4 is essential for the transport of p53 to mitochondria in normal human cells in the absence of exogenous stress. J. Cell Sci. *125*, 2509–2522.

Deans, A.J., and West, S.C. (2011). DNA interstrand crosslink repair and cancer. Nat. Rev.

Cancer *11*, 467–480.

Dedon, P.C., and Goldberg, I.H. (1992). Free-radical mechanisms involved in the formation of sequence-dependent bistranded DNA lesions by the antitumor antibiotics bleomycin, neocarzinostatin, and calicheamicin. Chem. Res. Toxicol. *5*, 311–332.

DePristo, M.A., Banks, E., Poplin, R., Garimella, K. V, Maguire, J.R., Hartl, C., Philippakis, A.A., del Angel, G., Rivas, M.A., Hanna, M., et al. (2011). A framework for variation discovery and genotyping using next-generation DNA sequencing data. Nat. Genet. *43*, 491–498.

Dobin, A., Davis, C.A., Schlesinger, F., Drenkow, J., Zaleski, C., Jha, S., Batut, P., Chaisson, M., and Gingeras, T.R. (2012). STAR: ultrafast universal RNA-seq aligner. Bioinformatics *29*, 15–21.

Drabløs, F., Feyzi, E., Aas, P.A., Vaagbø, C.B., Kavli, B., Bratlie, M.S., Peña-Diaz, J., Otterlei, M., Slupphaug, G., and Krokan, H.E. (2004). Alkylation damage in DNA and RNA—repair mechanisms and medical significance. DNA Repair (Amst). *3*, 1389–1407.

Ellis, N.A., Groden, J., Ye, T.-Z., Straughen, J., Lennon, D.J., Ciocci, S., Proytcheva, M., and German, J. (1995). The Bloom's syndrome gene product is homologous to RecQ helicases. Cell *83*, 655–666.

Fairman-Williams, M.E., Guenther, U.-P., and Jankowsky, E. (2010). SF1 and SF2 helicases: family matters. Curr. Opin. Struct. Biol. *20*, 313–324.

Fan, W., and Luo, J. (2008). RecQ4 Facilitates UV Light-induced DNA Damage Repair through Interaction with Nucleotide Excision Repair Factor Xeroderma Pigmentosum Group A (XPA). J. Biol. Chem. *283*, 29037–29044.

Ferrarelli, L.K., Popuri, V., Ghosh, A.K., Tadokoro, T., Canugovi, C., Hsu, J.K., Croteau, D.L., and Bohr, V.A. (2013). The RECQL4 protein, deficient in Rothmund–Thomson syndrome is active on telomeric D-loops containing DNA metabolism blocking lesions. DNA Repair (Amst). *12*,

518–528.

Fichtinger-Schepman, A.M.J., Van der Veer, J.L., Den Hartog, J.H.J., Lohman, P.H.M., and Reedijk, J. (1985). Adducts of the antitumor drug cis-diamminedichloroplatinum(II) with DNA: formation, identification, and quantitation. Biochemistry *24*, 707–713.

Findlay, G.M., Daza, R.M., Martin, B., Zhang, M.D., Leith, A.P., Gasperini, M., Janizek, J.D., Huang, X., Starita, L.M., and Shendure, J. (2018). Accurate classification of BRCA1 variants with saturation genome editing. Nature *562*, 217–222.

Fisher, A.E.O., Hochegger, H., Takeda, S., and Caldecott, K.W. (2007). Poly(ADP-Ribose) Polymerase 1 Accelerates Single-Strand Break Repair in Concert with Poly(ADP-Ribose) Glycohydrolase. Mol. Cell. Biol. *27*, 5597 LP – 5605.

Gachechiladze, M., Škarda, J., Soltermann, A., and Joerger, M. (2017). RAD51 as a potential surrogate marker for DNA repair capacity in solid malignancies. Int. J. Cancer *141*, 1286–1294.

German, J. (1969). Bloom's syndrome. I. Genetical and clinical observations in the first twenty-seven patients. Am. J. Hum. Genet. *21*, 196–227.

German, J., Archibald, R., and Bloom, D. (1965). Chromosomal Breakage in a Rare and Probably Genetically Determined Syndrome of Man. Science (80-.). *148*, 506 LP – 507.

Gerold, M. (1959). Healing of a fracture in an unusual case of congenital anomaly of the upper extremities. Zentralbl Chir *84*, 831–834.

Ghosh, A.K., Rossi, M.L., Singh, D.K., Dunn, C., Ramamoorthy, M., Croteau, D.L., Liu, Y., and Bohr, V.A. (2012). RECQL4, the Protein Mutated in Rothmund-Thomson Syndrome, Functions in Telomere Maintenance. J. Biol. Chem. *287*, 196–209.

Gorbalenya, A.E., Koonin, E. V, Donchenko, A.P., and Blinov, V.M. (1989). Two related superfamilies of putative helicases involved in replication, recombination, repair and

expression of DNA and RNA genomes. Nucleic Acids Res. *17*, 4713–4730.

Gottschalk, U., Garnett, M.C., Ward, R.K., Maibücher, A., and Köhnlein, W. (1991). The drug consists of an apoprotein and a non covalently associated chromophorethat is very sensitive to light and heat.5) The primary structure of the apoprotein has been elucidated and revised,6) and the. J. Antibiot. (Tokyo). *44*, 1148–1154.

Graeser, M., McCarthy, A., Lord, C.J., Savage, K., Hills, M., Salter, J., Orr, N., Parton, M., Smith, I.E., Reis-Filho, J.S., et al. (2010). A Marker of Homologous Recombination Predicts Pathologic Complete Response to Neoadjuvant Chemotherapy in Primary Breast Cancer. Clin. Cancer Res. *16*, 6159 LP – 6168.

Grant, S.G., Wenger, S.L., Latimer, J.J., Thull, D., and Burke, L.W. (2000). Analysis of genomic instability using multiple assays in a patient with Rothmund–Thomson syndrome. Clin. Genet. *58*, 209–215.

Gupta, S., De, S., Srivastava, V., Hussain, M., Kumari, J., Muniyappa, K., and Sengupta, S. (2014). RECQL4 and p53 potentiate the activity of polymerase γ and maintain the integrity of the human mitochondrial genome. Carcinog. *35*, 34–45.

Gurley, L.R., D'Anna, J.A., Barham, S.S., Deaven, L.L., and Tobey, R.A. (1978). Histone Phosphorylation and Chromatin Structure during Mitosis in Chinese Hamster Cells. Eur. J. Biochem. *84*, 1–15.

Haas, B.J., Dobin, A., Stransky, N., Li, B., Yang, X., Tickle, T., Bankapur, A., Ganote, C., Doak, T.G., Pochet, N., et al. (2017). STAR-Fusion: Fast and Accurate Fusion Transcript Detection from RNA-Seq. BioRxiv 120295.

Hande, K.R. (1998). Etoposide: four decades of development of a topoisomerase II inhibitor. Eur. J. Cancer *34*, 1514–1521.

Harmon, F.G., and Kowalczykowski, S.C. (2001). Biochemical Characterization of the DNA

Helicase Activity of the Escherichia coli RecQ Helicase. J. Biol. Chem. *276*, 232–243.

Harrow, J., Frankish, A., Gonzalez, J.M., Tapanari, E., Diekhans, M., Kokocinski, F., Aken, B.L., Barrell, D., Zadissa, A., Searle, S., et al. (2012). GENCODE: The reference human genome annotation for The ENCODE Project. Genome Res. *22*, 1760–1774.

Hecht, S.M. (2000). Bleomycin: New Perspectives on the Mechanism of Action. J. Nat. Prod. *63*, 158–168.

Higgins, N.P., Kato, K., and Strauss, B. (1976). A model for replication repair in mammalian cells. J. Mol. Biol. *101*, 417–425.

Hoehn, H., Bryant, E.M., Au, K., Norwood, T.H., Boman, H., and Martin, G.M. (1975). Variegated translocation mosaicism in human skin fibroblast cultures. Cytogenet. Genome Res. *15*, 282–298.

Hoki, Y., Araki, R., Fujimori, A., Ohhata, T., Koseki, H., Fukumura, R., Nakamura, M., Takahashi, H., Noda, Y., Kito, S., et al. (2003). Growth retardation and skin abnormalities of the Recql4 -deficient mouse. Hum. Mol. Genet. *12*, 2293–2299.

Hsieh, P., and Zhang, Y. (2017). The Devil is in the details for DNA mismatch repair. Proc. Natl. Acad. Sci. *114*, 3552 LP – 3554.

Huang, Y., and Li, L. (2013). DNA crosslinking damage and cancer - a tale of friend and foe. Transl. Cancer Res. Vol 2, No 3 (June 2013) Transl. Cancer Res. (DNA Damage Repair).

Hug, N., Longman, D., and Cáceres, J.F. (2016). Mechanism and regulation of the nonsense-mediated decay pathway. Nucleic Acids Res. *44*, 1483–1495.

Ichikawa, K., Noda, T., and Furuichi, Y. (2002). Preparation of the gene targeted knockout mice for human premature aging diseases, Werner syndrome, and Rothmund-Thomson syndrome caused by the mutation of DNA helicases. Folia Pharmacol. Jpn. *119*, 219–226.

Ikenaga, M., Ichikawa-Ryo, H., and Kondo, S. (1975). The major cause of inactivation and

mutation by 4-Nitroquinoline 1-Oxide in Escherichia coli: Excisable 4NQO-purine adducts. J. Mol. Biol. *92*, 341–356.

Im, J.-S., Ki, S.-H., Farina, A., Jung, D.-S., Hurwitz, J., and Lee, J.-K. (2009). Assembly of the Cdc45-Mcm2–7-GINS complex in human cells requires the Ctf4/And-1, RecQL4, and Mcm10 proteins. Proc. Natl. Acad. Sci. *106*, 15628–15632.

Im, J.-S., Park, S.-Y., Cho, W.-H., Bae, S.-H., Hurwitz, J., and Lee, J.-K. (2015). RecQL4 is required for the association of Mcm10 and Ctf4 with replication origins in human cells AU - Im, Jun-Sub. Cell Cycle *14*, 1001–1009.

Ishihara, S., Kotomura, N., Yamamoto, N., and Ochiai, H. (2017). Ligation-mediated PCR with a back-to-back adapter reduces amplification bias resulting from variations in GC content. Anal. Biochem. *531*, 37–44.

Iwamoto, T., Hiraku, Y., Oikawa, S., Mizutani, H., Kojima, M., and Kawanishi, S. (2004). DNA intrastrand cross-link at the 5'-GA-3' sequence formed by busulfan and its role in the cytotoxic effect. Cancer Sci. *95*, 454–458.

Jasin, M., and Rothstein, R. (2013). Repair of Strand Breaks by Homologous Recombination. Cold Spring Harb. Perspect. Biol. *5*.

Jin, W., Liu, H., Zhang, Y., Otta, S.K., Plon, S.E., and Wang, L.L. (2008). Sensitivity of RECQL4-deficient fibroblasts from Rothmund–Thomson syndrome patients to genotoxic agents. Hum. Genet. *123*, 643–653.

Jinek, M., East, A., Cheng, A., Lin, S., Ma, E., and Doudna, J. (2013). RNA-programmed genome editing in human cells. Elife *2*, e00471.

Johnson, R.D., and Jasin, M. (2000). Sister chromatid gene conversion is a prominent double-strand break repair pathway in mammalian cells. EMBO J. *19*, 3398 LP – 3407.

Johzuka, K., and Ogawa, H. (1995). Interaction of Mre11 and Rad50: two proteins required for

DNA repair and meiosis-specific double-strand break formation in Saccharomyces cerevisiae. Genetics *139*, 1521 LP – 1532.

Juan, G., Traganos, F., James, W.M., Ray, J.M., Roberge, M., Sauve, D.M., Anderson, H., and Darzynkiewicz, Z. (1998). Histone H3 phosphorylation and expression of cyclins A and B1 measured in individual cells during their progression through G2 and mitosis. Cytometry *32*, 71–77.

Kääriäinen, H., Ryöppy, S., and Norio, R. (1989). RAPADILINO syndrome with radial and patellar aplasia/hypoplasia as main manifestations. Am. J. Med. Genet. *33*, 346–351.

Kaiser, S., Sauer, F., and Kisker, C. (2017). The structural and functional characterization of human RecQ4 reveals insights into its helicase mechanism. Nat. Commun. *8*, 15907.

Kamimura, Y., Masumoto, H., Sugino, A., and Araki, H. (1998). Sld2, Which Interacts with Dpb11 in Saccharomyces cerevisiae, Is Required for Chromosomal DNA Replication. Mol. Cell. Biol. *18*, 6102 LP – 6109.

Karanam, K., Kafri, R., Loewer, A., and Lahav, G. (2012). Quantitative Live Cell Imaging Reveals a Gradual Shift between DNA Repair Mechanisms and a Maximal Use of HR in Mid S Phase. Mol. Cell *47*, 320–329.

Kawabe, T., Tsuyama, N., Kitao, S., Nishikawa, K., Shimamoto, A., Shiratori, M., Matsumoto, T., Anno, K., Sato, T., Mitsui, Y., et al. (2000). Differential regulation of human RecQ family helicases in cell transformation and cell cycle. Oncogene *19*, 4764.

Keller, H., Kiosze, K., Sachsenweger, J., Haumann, S., Ohlenschläger, O., Nuutinen, T., Syväoja, J.E., Görlach, M., Grosse, F., and Pospiech, H. (2014). The intrinsically disordered amino-terminal region of human RecQL4: multiple DNA-binding domains confer annealing, strand exchange and G4 DNA binding. Nucleic Acids Res.

Kitao, S., Ohsugi, I., Ichikawa, K., Goto, M., Furuichi, Y., and Shimamoto, A. (1998). Cloning of

Two New Human Helicase Genes of the RecQ Family: Biological Significance of Multiple Species in Higher Eukaryotes. Genomics *54*, 443–452.

Kitao, S., Shimamoto, A., Goto, M., Miller, R.W., Smithson, W.A., Lindor, N.M., and Furuichi, Y. (1999a). Mutations in RECQL4 cause a subset of cases of Rothmund-Thomson syndrome. Nat Genet *22*, 82–84.

Kitao, S., Lindor, N.M., Shiratori, M., Furuichi, Y., and Shimamoto, A. (1999b). Rothmund–Thomson Syndrome Responsible Gene, RECQL4: Genomic Structure and Products. Genomics *61*, 268–276.

Kohzaki, M., Chiourea, M., Versini, G., Adachi, N., Takeda, S., Gagos, S., and Halazonetis, T.D. (2012). The helicase domain and C-terminus of human RecQL4 facilitate replication elongation on DNA templates damaged by ionizing radiation. Carcinogenesis *33*, 1203–1210.

Kolinjivadi, A.M., Sannino, V., De Antoni, A., Zadorozhny, K., Kilkenny, M., Técher, H., Baldi, G., Shen, R., Ciccia, A., Pellegrini, L., et al. (2017). Smarcal1-Mediated Fork Reversal Triggers Mre11-Dependent Degradation of Nascent DNA in the Absence of Brca2 and Stable Rad51 Nucleofilaments. Mol. Cell *67*, 867-881.e7.

Kondo, N., Takahashi, A., Ono, K., and Ohnishi, T. (2010). DNA Damage Induced by Alkylating Agents and Repair Pathways. J. Nucleic Acids *2010*, 543531.

Kosicki, M., Tomberg, K., and Bradley, A. (2018). Repair of double-strand breaks induced by CRISPR–Cas9 leads to large deletions and complex rearrangements. Nat. Biotechnol. *36*, 765–771.

Koster, D.A., Palle, K., Bot, E.S.M., Bjornsti, M.-A., and Dekker, N.H. (2007). Antitumour drugs impede DNA uncoiling by topoisomerase I. Nature *448*, 213–217.

Köster, J., and Rahmann, S. (2012). Snakemake—a scalable bioinformatics workflow engine.

Bioinformatics *28*, 2520–2522.

Kostyrko, K., and Mermod, N. (2016). Assays for DNA double-strand break repair by microhomology-based end-joining repair mechanisms. Nucleic Acids Res. *44*, e56–e56.

Krakoff, I.H., Brown, N.C., and Reichard, P. (1968). Inhibition of Ribonucleoside Diphosphate Reductase by Hydroxyurea. Cancer Res. *28*, 1559 LP – 1565.

Krogh, B.O., and Symington, L.S. (2004). Recombination Proteins in Yeast. Annu. Rev. Genet. *38*, 233–271.

Krokan, H.E., and Bjørås, M. (2013). Base Excision Repair. Cold Spring Harb. Perspect. Biol. *5*.

Krokan, H., Wist, E., and Krokan, R.H. (1981). Aphidicolin inhibits DNA synthesis by DNA polymerase α and isolated nuclei by a similar mechanism. Nucleic Acids Res. *9*, 4709–4719.

Larizza, L., Roversi, G., and Volpi, L. (2010). Rothmund-Thomson syndrome. Orphanet J. Rare Dis. *5*, 2.

Lee, S.-H., Singh, I., Tisdale, S., Abdel-Wahab, O., Leslie, C.S., and Mayr, C. (2018). Widespread intronic polyadenylation inactivates tumour suppressor genes in leukaemia. Nature.

Li, G.-M. (2008). Mechanisms and functions of DNA mismatch repair. Cell Res. *18*, 85–98.

Li, H., and Durbin, R. (2009). Fast and accurate short read alignment with Burrows–Wheeler transform. Bioinformatics *25*, 1754–1760.

Li, G., Liu, D., Zhang, X., Quan, R., Zhong, C., Mo, J., Huang, Y., Wang, H., Ruan, X., Xu, Z., et al. (2018). Suppressing Ku70/Ku80 expression elevates homology-directed repair efficiency in primary fibroblasts. Int. J. Biochem. Cell Biol. *99*, 154–160.

Liao, H., Ji, F., Helleday, T., and Ying, S. (2018). Mechanisms for stalled replication fork stabilization: new targets for synthetic lethality strategies in cancer treatments. EMBO Rep. *19*, e46263.

Lieber, M.R. (2010). The mechanism of double-strand DNA break repair by the

nonhomologous DNA end-joining pathway. Annu Rev Biochem *79*.

Lieber, M.R., Ma, Y., Pannicke, U., and Schwarz, K. (2003). Mechanism and regulation of human non-homologous DNA end-joining. Nat. Rev. Mol. Cell Biol. *4*, 712.

Lin, Y.-C., Boone, M., Meuris, L., Lemmens, I., Van Roy, N., Soete, A., Reumers, J., Moisse, M., Plaisance, S., Drmanac, R., et al. (2014). Genome dynamics of the human embryonic kidney 293 lineage in response to cell biology manipulations. Nat. Commun. *5*, 4767.

Lindor, N.M., Furuichi, Y., Kitao, S., Shimamoto, A., Arndt, C., and Jalal, S. (2000). Rothmund-Thomson syndrome due to RECQ4 helicase mutations: Report and clinical and molecular comparisons with Bloom syndrome and Werner syndrome. Am. J. Med. Genet. *90*, 223–228.

Liu, M., Rehman, S., Tang, X., Gu, K., Fan, Q., Chen, D., and Ma, W. (2019). Methodologies for Improving HDR Efficiency. Front. Genet. *9*, 691.

Liu, X., Jian, X., and Boerwinkle, E. (2013). dbNSFP v2.0: A Database of Human Non-synonymous SNVs and Their Functional Predictions and Annotations. Hum. Mutat. *34*, E2393–E2402.

Loenn, U., and Loenn, S. (1988). Extensive regions of single-stranded DNA in aphidicolin-treated melanoma cells. Biochemistry *27*, 566–570.

Lu, H., Fang, E.F., Sykora, P., Kulikowicz, T., Zhang, Y., Becker, K.G., Croteau, D.L., and Bohr, V.A. (2014a). Senescence induced by RECQL4 dysfunction contributes to Rothmund–Thomson syndrome features in mice. Cell Death &Amp; Dis. *5*, e1226.

Lu, H., Shamanna, R.A., Keijzers, G., Anand, R., Rasmussen, L.J., Cejka, P., Croteau, D.L., and Bohr, V.A. (2016). RECQL4 Promotes DNA End Resection in Repair of DNA Double-Strand Breaks. Cell Rep. *16*, 161–173.

Lu, H., Shamanna, R.A., de Freitas, J.K., Okur, M., Khadka, P., Kulikowicz, T., Holland, P.P., Tian,

J., Croteau, D.L., Davis, A.J., et al. (2017). Cell cycle-dependent phosphorylation regulates RECQL4 pathway choice and ubiquitination in DNA double-strand break repair. Nat. Commun. *8*, 2039.

Lu, L., Jin, W., Liu, H., and Wang, L.L. (2014b). RECQ DNA Helicases and Osteosarcoma. In Current Advances in Osteosarcoma, M.D. Kleinerman Eugenie S., ed. (Springer International Publishing), pp. 129–145.

Lu, L., Harutyunyan, K., Jin, W., Wu, J., Yang, T., Chen, Y., Joeng, K.S., Bae, Y., Tao, J., Dawson, B.C., et al. (2015). RECQL4 Regulates p53 Function In Vivo During Skeletogenesis. J. Bone Miner. Res. *30*, 1077–1089.

Lundin, C., North, M., Erixon, K., Walters, K., Jenssen, D., Goldman, A.S.H., and Helleday, T. (2005). Methyl methanesulfonate (MMS) produces heat-labile DNA damage but no detectable in vivo DNA double-strand breaks. Nucleic Acids Res. *33*, 3799–3811.

Macris, M.A., Krejci, L., Bussen, W., Shimamoto, A., and Sung, P. (2006). Biochemical characterization of the RECQ4 protein, mutated in Rothmund-Thomson syndrome. DNA Repair (Amst). *5*, 172–180.

Maeda, H., and Takeshita, J. (1975). Degradation of Neocarzinostatin by Blood Sera In Vitro and Its Inhibition by Diisopropyl Fluorophosphate and N-Ethylmaleimide. GANN Japanese J. Cancer Res. *66*, 523–527.

Van Maldergem, L., Siitonen, H.A., Jalkh, N., Chouery, E., De Roy, M., Delague, V., Muenke, M., Jabs, E.W., Cai, J., Wang, L.L., et al. (2006). Revisiting the craniosynostosis-radial ray hypoplasia association: Baller-Gerold syndrome caused by mutations in the RECQL4 gene. J. Med. Genet. *43*, 148 LP – 152.

Mali, P., Yang, L., Esvelt, K.M., Aach, J., Guell, M., DiCarlo, J.E., Norville, J.E., and Church, G.M. (2013). RNA-Guided Human Genome Engineering via Cas9. Science (80-.). *339*, 823 LP –

826.

Mann, M.B., Hodges, C.A., Barnes, E., Vogel, H., Hassold, T.J., and Luo, G. (2005). Defective sister-chromatid cohesion, aneuploidy and cancer predisposition in a mouse model of type II Rothmund–Thomson syndrome. Hum. Mol. Genet. *14*, 813–825.

Manthei, K.A., Hill, M.C., Burke, J.E., Butcher, S.E., and Keck, J.L. (2015). Structural mechanisms of DNA binding and unwinding in bacterial RecQ helicases. Proc. Natl. Acad. Sci. *112*, 4292 LP – 4297.

Matsuno, K., Kumano, M., Kubota, Y., Hashimoto, Y., and Takisawa, H. (2006). The N-Terminal Noncatalytic Region of Xenopus RecQ4 Is Required for Chromatin Binding of DNA Polymerase α in the Initiation of DNA Replication. Mol. Cell. Biol. *26*, 4843–4852.

McHugh, P.J., Sones, W.R., and Hartley, J.A. (2000). Repair of Intermediate Structures Produced at DNA Interstrand Cross-Links in Saccharomyces cerevisiae. Mol. Cell. Biol. *20*, 3425 LP – 3433.

McKenna, A., Hanna, M., Banks, E., Sivachenko, A., Cibulskis, K., Kernytsky, A., Garimella, K., Altshuler, D., Gabriel, S., Daly, M., et al. (2010). The Genome Analysis Toolkit: A MapReduce framework for analyzing next-generation DNA sequencing data. Genome Res. *20*, 1297–1303.

McNeill, D.R., Lam, W., DeWeese, T.L., Cheng, Y.-C., and Wilson, D.M. (2009). Impairment of APE1 Function Enhances Cellular Sensitivity to Clinically Relevant Alkylators and Antimetabolites. Mol. Cancer Res. *7*, 897 LP – 906.

Mijic, S., Zellweger, R., Chappidi, N., Berti, M., Jacobs, K., Mutreja, K., Ursich, S., Ray Chaudhuri, A., Nussenzweig, A., Janscak, P., et al. (2017). Replication fork reversal triggers fork degradation in BRCA2-defective cells. Nat. Commun. *8*, 859.

Mo, D., Zhao, Y., and Balajee, A.S. (2018). Human RecQL4 helicase plays multifaceted roles in

the genomic stability of normal and cancer cells. Cancer Lett. *413*, 1–10.

Mojumdar, A., De March, M., Marino, F., and Onesti, S. (2017). The Human RecQ4 Helicase Contains a Functional RecQ C-terminal Region (RQC) That Is Essential for Activity. J. Biol. Chem. *292*, 4176–4184.

Moldovan, G.-L., and D'Andrea, A.D. (2009). How the Fanconi Anemia Pathway Guards the Genome. Annu. Rev. Genet. *43*, 223–249.

Moynahan, M.E., Cui, T.Y., and Jasin, M. (2001). Homology-directed DNA Repair, Mitomycin-C Resistance, and Chromosome Stability Is Restored with Correction of a Brca1 Mutation. Cancer Res. *61*, 4842 LP – 4850.

Murai, J., Huang, S.N., Das, B.B., Renaud, A., Zhang, Y., Doroshow, J.H., Ji, J., Takeda, S., and Pommier, Y. (2012). Trapping of PARP1 and PARP2 by Clinical PARP Inhibitors. Cancer Res. *72*, 5588 LP – 5599.

Napier, M.A., Holmquist, B., Strydom, D.J., and Goldberg, I.H. (1979). Neocarzinostatin: Spectral characterization and separation of a non-protein chromophore. Biochem. Biophys. Res. Commun. *89*, 635–642.

Ng, A.J.M., Walia, M.K., Smeets, M.F., Mutsaers, A.J., Sims, N.A., Purton, L.E., Walsh, N.C., Martin, T.J., and Walkley, C.R. (2015). The DNA Helicase Recql4 Is Required for Normal Osteoblast Expansion and Osteosarcoma Formation. PLoS Genet *11*, e1005160.

Nik-Zainal, S., Davies, H., Staaf, J., Ramakrishna, M., Glodzik, D., Zou, X., Martincorena, I., Alexandrov, L.B., Martin, S., Wedge, D.C., et al. (2016). Landscape of somatic mutations in 560 breast cancer whole-genome sequences. Nature *534*, 47–54.

Nikolova, T., Ensminger, M., Löbrich, M., and Kaina, B. (2010). Homologous recombination protects mammalian cells from replication-associated DNA double-strand breaks arising in response to methyl methanesulfonate. DNA Repair (Amst). *9*, 1050–1063.

Ohlenschläger, O., Kuhnert, A., Schneider, A., Haumann, S., Bellstedt, P., Keller, H., Saluz, H.P., Hortschansky, P., Hänel, F., Grosse, F., et al. (2012). The N-terminus of the human RecQL4 helicase is a homeodomain-like DNA interaction motif. Nucleic Acids Res. *40*, 8309–8324.

Ohtsuki, K., and Ishida, N. (1980). The Biological Effect of a Nonprotein Component Removed from Neocarzinostatin (NCS). J. Antibiot. (Tokyo). *33*, 744–750.

Opresko, P.L., Cheng, W.-H., and Bohr, V.A. (2004). Junction of RecQ Helicase Biochemistry and Human Disease. J. Biol. Chem. *279*, 18099–18102.

Park, S.-J., Lee, Y.-J., Beck, B.D., and Lee, S.-H. (2006). A Positive Involvement of RecQL4 in UV-Induced S-Phase Arrest. DNA Cell Biol. *25*, 696–703.

Patro, R., Duggal, G., Love, M.I., Irizarry, R.A., and Kingsford, C. (2017). Salmon provides fast and bias-aware quantification of transcript expression. Nat. Methods *14*, 417–419.

Pepe, A., and West, S.C. (2013). Substrate specificity of the MUS81-EME2 structure selective endonuclease. Nucleic Acids Res. *42*, 3833–3845.

Petermann, E., Orta, M.L., Issaeva, N., Schultz, N., and Helleday, T. (2010a). Hydroxyurea-stalled replication forks become progressively inactivated and require two different RAD51-mediated pathways for restart and repair. Mol. Cell *37*, 492–502.

Petermann, E., Woodcock, M., and Helleday, T. (2010b). Chk1 promotes replication fork progression by controlling replication initiation. Proc. Natl. Acad. Sci. *107*, 16090 LP – 16095.

Petkovic, M., Dietschy, T., Freire, R., Jiao, R., and Stagljar, I. (2005). The human Rothmund-Thomson syndrome gene product, RECQL4, localizes to distinct nuclear foci that coincide with proteins involved in the maintenance of genome stability. J. Cell Sci. *118*, 4261–4269.

Pierce, A.J., Johnson, R.D., Thompson, L.H., and Jasin, M. (1999). XRCC3 promotes homology-directed repair of DNA damage in mammalian cells. Genes Dev. *13*, 2633–2638.

Pike, A.C.W., Shrestha, B., Popuri, V., Burgess-Brown, N., Muzzolini, L., Costantini, S., Vindigni,

A., and Gileadi, O. (2009). Structure of the human RECQ1 helicase reveals a putative strand-separation pin. Proc. Natl. Acad. Sci. *106*, 1039 LP – 1044.

Pinder, J., Salsman, J., and Dellaire, G. (2015). Nuclear domain 'knock-in' screen for the evaluation and identification of small molecule enhancers of CRISPR-based genome editing. Nucleic Acids Res. *43*, 9379–9392.

Ponti, M., Souhami, R.L., Fox, B.W., and Hartley, J.A. (1991). DNA interstrand crosslinking and sequence selectivity of dimethanesulphonates. Br. J. Cancer *63*, 743–747.

Povirk, L.F., Han, Y.H., and Steighner, R.J. (1989). Structure of bleomycin-induced DNA double-strand breaks: predominance of blunt ends and single-base 5' extensions. Biochemistry *28*, 5808–5814.

Puranam, K.L., and Blackshear, P.J. (1994). Cloning and characterization of RECQL, a potential human homologue of the Escherichia coli DNA helicase RecQ. J. Biol. Chem. *269*, 29838–29845.

Quennet, V., Beucher, A., Barton, O., Takeda, S., and Löbrich, M. (2010). CtIP and MRN promote non-homologous end-joining of etoposide-induced DNA double-strand breaks in G1. Nucleic Acids Res. *39*, 2144–2152.

Ran, F.A., Hsu, P.D., Wright, J., Agarwala, V., Scott, D.A., and Zhang, F. (2013). Genome engineering using the CRISPR-Cas9 system. Nat. Protoc. *8*, 2281.

Rausch, T., Zichner, T., Schlattl, A., Stütz, A.M., Benes, V., and Korbel, J.O. (2012). DELLY: structural variant discovery by integrated paired-end and split-read analysis. Bioinformatics *28*, i333–i339.

Reichard, P. (1988). Interactions Between Deoxyribonucleotide and DNA Synthesis. Annu. Rev. Biochem. *57*, 349–374.

Richardson, C., Moynahan, M.E., and Jasin, M. (1998). Double-strand break repair by

interchromosomal recombination: suppression of chromosomal translocations. Genes Dev. *12*, 3831–3842.

Robinson, J.T., Thorvaldsdóttir, H., Winckler, W., Guttman, M., Lander, E.S., Getz, G., and Mesirov, J.P. (2011). Integrative genomics viewer. Nat. Biotechnol. *29*, 24–26.

Robinson, J.T., Thorvaldsdóttir, H., Wenger, A.M., Zehir, A., and Mesirov, J.P. (2017). Variant Review with the Integrative Genomics Viewer. Cancer Res. *77*, e31 LP-e34.

Rocha, C.R.R., Silva, M.M., Quinet, A., Cabral-Neto, J.B., and Menck, C.F.M. (2018). DNA repair pathways and cisplatin resistance: an intimate relationship. Clinics *73*, e478s.

Rogakou, E.P., Pilch, D.R., Orr, A.H., Ivanova, V.S., and Bonner, W.M. (1998). DNA Double-stranded Breaks Induce Histone H2AX Phosphorylation on Serine 139. J. Biol. Chem. *273*, 5858–5868.

Rogakou, E.P., Boon, C., Redon, C., and Bonner, W.M. (1999). Megabase Chromatin Domains Involved in DNA Double-Strand Breaks in Vivo. J. Cell Biol. *146*, 905–916.

Rossi, M.L., Ghosh, A.K., Kulikowicz, T., Croteau, D.L., and Bohr, V.A. (2010). Conserved helicase domain of human RecQ4 is required for strand annealing-independent DNA unwinding. DNA Repair (Amst). *9*, 796–804.

Ryu, S.-M., Hur, J.W., and Kim, K. (2019). Evolution of CRISPR towards accurate and efficient mammal genome engineering. BMB Rep. *52*, 475–481.

Saleh-Gohari, N., and Helleday, T. (2004). Conservative homologous recombination preferentially repairs DNA double-strand breaks in the S phase of the cell cycle in human cells. Nucleic Acids Res. *32*, 3683–3688.

Saleh-Gohari, N., Bryant, H.E., Schultz, N., Parker, K.M., Cassel, T.N., and Helleday, T. (2005). Spontaneous Homologous Recombination Is Induced by Collapsed Replication Forks That Are Caused by Endogenous DNA Single-Strand Breaks. Mol. Cell. Biol. *25*, 7158 LP – 7169.

Salk, D., Au, K., Hoehn, H., and Martin, G.M. (1981a). Cytogenetics of Werner's syndrome cultured skin fibroblasts: variegated translocation mosaicism. Cytogenet. Genome Res. *30*, 92–107.

Salk, D., Au, K., Hoehn, H., Stenchever, M.R., and Martin, G.M. (1981b). Evidence of clonal attenuation, clonal succession, and clonal expansion in mass cultures of aging Werner's syndrome skin fibroblasts. Cytogenet. Genome Res. *30*, 108–117.

Samanta, S., and Karmakar, P. (2012). Recruitment of HRDC domain of WRN and BLM to the sites of DNA damage induced by mitomycin C and methyl methanesulfonate. Cell Biol. Int. *36*, 873–881.

San Filippo, J., Sung, P., and Klein, H. (2008). Mechanism of Eukaryotic Homologous Recombination. Annu. Rev. Biochem. *77*, 229–257.

Sangrithi, M.N., Bernal, J.A., Madine, M., Philpott, A., Lee, J., Dunphy, W.G., and Venkitaraman, A.R. (2005). Initiation of DNA replication requires the RECQL4 protein mutated in Rothmund-Thomson syndrome. Cell *121*, 887–898.

Saunders, C.T., Wong, W.S.W., Swamy, S., Becq, J., Murray, L.J., and Cheetham, R.K. (2012). Strelka: accurate somatic small-variant calling from sequenced tumor–normal sample pairs. Bioinformatics *28*, 1811–1817.

Schärer, O.D. (2013). Nucleotide Excision Repair in Eukaryotes. Cold Spring Harb. Perspect. Biol. *5*.

Schlacher, K., Christ, N., Siaud, N., Egashira, A., Wu, H., and Jasin, M. (2011). Double-Strand Break Repair-Independent Role for BRCA2 in Blocking Stalled Replication Fork Degradation by MRE11. Cell *145*, 529–542.

Schonn, I., Hennesen, J., and Dartsch, D.C. (2010). Cellular responses to etoposide: cell death despite cell cycle arrest and repair of DNA damage. Apoptosis *15*, 162–172.

Schurman, S.H., Hedayati, M., Wang, Z., Singh, D.K., Speina, E., Zhang, Y., Becker, K., Macris, M., Sung, P., Wilson David M., I.I.I., et al. (2009). Direct and indirect roles of RECQL4 in modulating base excision repair capacity. Hum. Mol. Genet. *18*, 3470–3483.

Sedlackova, H., Cechova, B., Mlcouskova, J., and Krejci, L. (2015). RECQ4 selectively recognizes Holliday junctions. DNA Repair (Amst). *30*, 80–89.

Seki, M., Miyazawa, H., Tada, S., Yanagisawa, J., Yamaoka, T., Hoshino, S., Ozawa, K., Eki, T., Nogami, M., and Okumura, K. (1994). Molecular cloning of cDNA encoding human DNA helicase Q1 which has homology to Escherichia coli Rec Q helicase and localization of the gene at chromosome 12p12. Nucleic Acids Res. *22*, 4566–4573.

Seluanov, A., Mao, Z., and Gorbunova, V. (2010). Analysis of DNA Double-strand Break (DSB) Repair in Mammalian Cells. e2002.

Setlow, R.B., and Setlow, J.K. (1972). Effects of Radiation on Polynucleotides. Annu. Rev. Biophys. Bioeng. *1*, 293–346.

Sfeir, A., and Symington, L.S. (2015). Microhomology-Mediated End Joining: A Back-up Survival Mechanism or Dedicated Pathway? Trends Biochem Sci *40*, 701–714.

Shamanna, R.A., Singh, D.K., Lu, H., Mirey, G., Keijzers, G., Salles, B., Croteau, D.L., and Bohr, V.A. (2014). RECQ helicase RECQL4 participates in non-homologous end joining and interacts with the Ku complex. Carcinogenesis *35*, 2415–2424.

Sharma, S., Doherty, K.M., and Brosh, R.M. (2006). Mechanisms of RecQ helicases in pathways of DNA metabolism and maintenance of genomic stability. Biochem. J. *398*, 319 LP – 337.

Shechter, D., Costanzo, V., and Gautier, J. (2004). ATR and ATM regulate the timing of DNA replication origin firing. Nat. Cell Biol. *6*, 648–655.

Shiloh, Y., Schans, G.P. van der, Lohman, P.H.M.L., and Becker, Y. (1983). Induction and repair of DNA damage in normal and ataxiatelangiectasia skin fibroblasts treated with

neocarzinostatin. Carcinogenesis *4*, 917–921.

Shinya, A., Nishigori, C., Moriwaki, S., Takebe, H., Kubota, M., Ogino, A., and Imamura, S. (1993). A Case of Rothmund-Thomson Syndrome With Reduced DNA Repair Capacity. Arch. Dermatol. *129*, 332–336.

Siitonen, H.A., Kopra, O., Kääriäinen, H., Haravuori, H., Winter, R.M., Säämänen, A.-M., Peltonen, L., and Kestilä, M. (2003). Molecular defect of RAPADILINO syndrome expands the phenotype spectrum of RECQL diseases. Hum. Mol. Genet. *12*, 2837–2844.

Siitonen, H.A., Sotkasiira, J., Biervliet, M., Benmansour, A., Capri, Y., Cormier-Daire, V., Crandall, B., Hannula-Jouppi, K., Hennekam, R., Herzog, D., et al. (2008). The mutation spectrum in RECQL4 diseases. Eur J Hum Genet *17*, 151–158.

Singh, D.K., Karmakar, P., Aamann, M., Schurman, S.H., May, A., Croteau, D.L., Burks, L., Plon, S.E., and Bohr, V.A. (2010). The involvement of human RECQL4 in DNA double-strand break repair. Aging Cell *9*, 358–371.

Singh, D.K., Popuri, V., Kulikowicz, T., Shevelev, I., Ghosh, A.K., Ramamoorthy, M., Rossi, M.L., Janscak, P., Croteau, D.L., and Bohr, V.A. (2012). The human RecQ helicases BLM and RECQL4 cooperate to preserve genome stability. Nucleic Acids Res. *40*, 6632–6648.

Smeets, M.F., DeLuca, E., Wall, M., Quach, J.M., Chalk, A.M., Deans, A.J., Heierhorst, J., Purton, L.E., Izon, D.J., and Walkley, C.R. (2014). The Rothmund-Thomson syndrome helicase RECQL4 is essential for hematopoiesis. J. Clin. Invest. *124*, 3551–3565.

Smith, P.J., and Paterson, M.C. (1981). Abnormal Responses to Mid-Ultraviolet Light of Cultured Fibroblasts from Patients with Disorders Featuring Sunlight Sensitivity. Cancer Res. *41*, 511–518.

Sogo, J.M., Lopes, M., and Foiani, M. (2002). Fork Reversal and ssDNA Accumulation at Stalled Replication Forks Owing to Checkpoint Defects. Sci. *297*, 599–602.

Song, J., Yang, D., Xu, J., Zhu, T., Chen, Y.E., and Zhang, J. (2016). RS-1 enhances CRISPR/Cas9- and TALEN-mediated knock-in efficiency. Nat. Commun. *7*, 10548.

Spivak, G. (2015). Nucleotide excision repair in humans. DNA Repair (Amst). *36*, 13–18.

Stepanenko, A.A., and Dmitrenko, V. V (2015). HEK293 in cell biology and cancer research: phenotype, karyotype, tumorigenicity, and stress-induced genome-phenotype evolution. Gene *569*, 182–190.

Ström, C.E., Johansson, F., Uhlén, M., Szigyarto, C.A.-K., Erixon, K., and Helleday, T. (2010). Poly (ADP-ribose) polymerase (PARP) is not involved in base excision repair but PARP inhibition traps a single-strand intermediate. Nucleic Acids Res. *39*, 3166–3175.

Suzuki, T., Kohno, T., and Ishimi, Y. (2009). DNA Helicase Activity in Purified Human RECQL4 Protein. J. Biochem. *146*, 327–335.

Syljuåsen, R.G., Sørensen, C.S., Hansen, L.T., Fugger, K., Lundin, C., Johansson, F., Helleday, T., Sehested, M., Lukas, J., and Bartek, J. (2005). Inhibition of Human Chk1 Causes Increased Initiation of DNA Replication, Phosphorylation of ATR Targets, and DNA Breakage. Mol. Cell. Biol. *25*, 3553 LP – 3562.

Symington, L.S., and Gautier, J. (2011). Double-strand break end resection and repair pathway choice. Annu Rev Genet *45*.

Thangavel, S., Berti, M., Levikova, M., Pinto, C., Gomathinayagam, S., Vujanovic, M., Zellweger, R., Moore, H., Lee, E.H., Hendrickson, E.A., et al. (2015). DNA2 drives processing and restart of reversed replication forks in human cells. J. Cell Biol. *208*, 545–562.

Thompson, L.H., and Hinz, J.M. (2009). Cellular and molecular consequences of defective Fanconi anemia proteins in replication-coupled DNA repair: Mechanistic insights. Mutat. Res. Mol. Mech. Mutagen. *668*, 54–72.

Thorvaldsdóttir, H., Robinson, J.T., and Mesirov, J.P. (2012). Integrative Genomics Viewer

(IGV): high-performance genomics data visualization and exploration. Brief. Bioinform. *14*, 178–192.

Toledo, L.I., Altmeyer, M., Rask, M.-B., Lukas, C., Larsen, D.H., Povlsen, L.K., Bekker-Jensen, S., Mailand, N., Bartek, J., and Lukas, J. (2013). ATR Prohibits Replication Catastrophe by Preventing Global Exhaustion of RPA. Cell *155*, 1088–1103.

Tripathi, K., Mani, C., Clark, D.W., and Palle, K. (2016). Rad18 is required for functional interactions between FANCD2, BRCA2, and Rad51 to repair DNA topoisomerase 1-poisons induced lesions and promote fork recovery. Oncotarget; Vol 7, No 11.

Truong, L.N., Li, Y., Shi, L.Z., Hwang, P.Y.-H., He, J., Wang, H., Razavian, N., Berns, M.W., and Wu, X. (2013). Microhomology-mediated End Joining and Homologous Recombination share the initial end resection step to repair DNA double-strand breaks in mammalian cells. Proc. Natl. Acad. Sci. U. S. A. *110*, 7720–7725.

Truong, L.N., Li, Y., Sun, E., Ang, K., Hwang, P.Y.-H., and Wu, X. (2014). Homologous Recombination is a Primary Pathway to Repair DNA Double-Strand Breaks Generated During DNA Rereplication. J. Biol. Chem.

Tsubouchi, H., and Ogawa, H. (1998). A Novel mre11 Mutation Impairs Processing of Double-Strand Breaks of DNA during Both Mitosis and Meiosis. Mol. Cell. Biol. *18*, 260 LP – 268.

Vasseur, F., Delaporte, E., Zabot, M., Sturque, M., Barrut, D., Savary, J., Thomas, L., and Thomas, P. (1999). Excision repair defect in Rothmund Thomson syndrome. Acta Derm Venereol *79*, 150–152.

Vennos, E.M., and James, W.D. (1995). Rothmund-Thomson Syndrome. Dermatol. Clin. *13*, 143–150.

Vennos, E.M., Collins, M., and James, W.D. (1992). Rothmund-Thomson syndrome: Review of

the world literature. J. Am. Acad. Dermatol. *27*, 750–762.

Vesela, E., Chroma, K., Turi, Z., and Mistrik, M. (2017). Common Chemical Inductors of Replication Stress: Focus on Cell-Based Studies. Biomolecules *7*.

Vierstraete, J., Willaert, A., Vermassen, P., Coucke, P.J., Vral, A., and Claes, K.B.M. (2017). Accurate quantification of homologous recombination in zebrafish: brca2 deficiency as a paradigm. Sci. Rep. *7*, 16518.

Vijayalaxmi, Evans, H.J., Ray, J.H., and German, J. (1983). Bloom's syndrome: evidence for an increased mutation frequency in vivo. Science (80-.). *221*, 851 LP – 853.

Wang, H., and Xu, X. (2017). Microhomology-mediated end joining: new players join the team. Cell {&} Biosci. *7*, 6.

Wang, K., Li, M., and Hakonarson, H. (2010). ANNOVAR: functional annotation of genetic variants from high-throughput sequencing data. Nucleic Acids Res. *38*, e164–e164.

Wang, L.L., Levy, M.L., Lewis, R.A., Chintagumpala, M.M., Lev, D., Rogers, M., and Plon, S.E. (2001). Clinical manifestations in a cohort of 41 Rothmund-Thomson syndrome patients. Am. J. Med. Genet. *102*, 11–17.

Wang, L.L., Worley, K., Gannavarapu, A., Chintagumpala, M.M., Levy, M.L., and Plon, S.E. (2002). Intron-size constraint as a mutational mechanism in Rothmund-Thomson syndrome. Am. J. Hum. Genet. *71*, 165—167.

Wang, L.L., Gannavarapu, A., Kozinetz, C.A., Levy, M.L., Lewis, R.A., Chintagumpala, M.M., Ruiz-Maldanado, R., Contreras-Ruiz, J., Cunniff, C., Erickson, R.P., et al. (2003). Association Between Osteosarcoma and Deleterious Mutations in the RECQL4 Gene in Rothmund–Thomson Syndrome. J. Natl. Cancer Inst. *95*, 669–674.

Weng, M., Zheng, Y., Jasti, V.P., Champeil, E., Tomasz, M., Wang, Y., Basu, A.K., and Tang, M. (2010). Repair of mitomycin C mono- and interstrand cross-linked DNA adducts by UvrABC:

a new model. Nucleic Acids Res. *38*, 6976–6984.

Werner, S.R., Prahalad, A.K., Yang, J., and Hock, J.M. (2006). RECQL4-deficient cells are hypersensitive to oxidative stress/damage: Insights for osteosarcoma prevalence and heterogeneity in Rothmund-Thomson syndrome. Biochem. Biophys. Res. Commun. *345*, 403–409.

Wiedenheft, B., Sternberg, S.H., and Doudna, J.A. (2012). RNA-guided genetic silencing systems in bacteria and archaea. Nature *482*, 331–338.

Wold, M.S., and Kelly, T. (1988). Purification and characterization of replication protein A, a cellular protein required for in vitro replication of simian virus 40 DNA. Proc. Natl. Acad. Sci. *85*, 2523 LP – 2527.

Woo, L.L., Futami, K., Shimamoto, A., Furuichi, Y., and Frank, K.M. (2006). The Rothmund-Thomson gene product RECQL4 localizes to the nucleolus in response to oxidative stress. Exp. Cell Res. *312*, 3443–3457.

Wyatt, M.D., and Pittman, D.L. (2006). Methylating Agents and DNA Repair Responses: Methylated Bases and Sources of Strand Breaks. Chem. Res. Toxicol. *19*, 1580–1594.

Xu, X., and Liu, Y. (2009). Dual DNA unwinding activities of the Rothmund–Thomson syndrome protein, RECQ4. EMBO J. *28*, 568 LP – 577.

Xu, X., Rochette, P.J., Feyissa, E.A., Su, T. V, and Liu, Y. (2009a). MCM10 mediates RECQ4 association with MCM2-7 helicase complex during DNA replication. EMBO J. *28*, 3005–3014.

Xu, Y., Lei, Z., Huang, H., Dui, W., Liang, X., Ma, J., and Jiao, R. (2009b). dRecQ4 Is Required for DNA Synthesis and Essential for Cell Proliferation in Drosophila. PLoS One *4*, e6107.

Yin, J., Kwon, Y.T., Varshavsky, A., and Wang, W. (2004). RECQL4, mutated in the Rothmund–Thomson and RAPADILINO syndromes, interacts with ubiquitin ligases UBR1 and UBR2 of the N-end rule pathway. Hum. Mol. Genet. *13*, 2421–2430.

Ying, S., Hamdy, F.C., and Helleday, T. (2012). Mre11-Dependent Degradation of Stalled DNA Replication Forks Is Prevented by BRCA2 and PARP1. Cancer Res. *72*, 2814 LP – 2821.

Yokoyama, H., Moreno-Andres, D., Astrinidis, S.A., Hao, Y., Weberruss, M., Schellhaus, A.K., Lue, H., Haramoto, Y., Gruss, O.J., and Antonin, W. (2019). Chromosome alignment maintenance requires the MAP RECQL4, mutated in the Rothmund–Thomson syndrome. Life Sci. Alliance *2*, e201800120.

Yu, C.-E., Oshima, J., Fu, Y.-H., Wijsman, E.M., Hisama, F., Alisch, R., Matthews, S., Nakura, J., Miki, T., Ouais, S., et al. (1996). Positional Cloning of the Werner's Syndrome Gene. Science (80-.). *272*, 258 LP – 262.

Zellweger, R., Dalcher, D., Mutreja, K., Berti, M., Schmid, J.A., Herrador, R., Vindigni, A., and Lopes, M. (2015). Rad51-mediated replication fork reversal is a global response to genotoxic treatments in human cells. J. Cell Biol. *208*, 563–579.

Zhao, H., Rybak, P., Dobrucki, J., Traganos, F., and Darzynkiewicz, Z. (2012). Relationship of DNA damage signaling to DNA replication following treatment with DNA topoisomerase inhibitors camptothecin/topotecan, mitoxantrone, or etoposide. Cytom. Part A *81A*, 45–51.

Zou, L., and Elledge, S.J. (2003). Sensing DNA Damage Through ATRIP Recognition of RPA-ssDNA Complexes. Science (80-.). *300*, 1542 LP – 1548.